THE UNIVERSITY OF QUEENSLAND

AUSTRALIA

Understanding and Controlling the Structure of Thin Polymer Films used in Photolithography

Md Mahbub Alam

BSc, MSc

A thesis submitted for the degree of Doctor of Philosophy at

The University of Queensland in 2018

Australian Institute for Bioengineering and Nanotechnology (AIBN)

Abstract

Line edge roughness (LER) is one of the major impediments to the semiconductor industry achieving the desired device performance and satisfying the goals set by International Technology Roadmap for Semiconductor (ITRS). LER is defined as any sort of unwanted roughness in semiconductor features, and among many other factors, structural heterogeneity of the photoresist materials is one of the sources of LER in photolithographic devices. This gives the motivation to study a new class of copolymer named 'gradient copolymer', which is unique in terms of the copolymer chain structure. The copolymer composition of gradient copolymers changes from one end of the chain to the other gradually, while the copolymer composition is on average constant along the chains for conventional statistical copolymers. In contrast, block copolymers show an abrupt switch in the polymer composition. In this study, statistical, block and gradient copolymers have been synthesized for two different monomer pairs (styrene – acrylonitrile and hydroxystyrene – t-butyl acrylate) using reversible addition-fragmentation chain transfer (RAFT) and conventional radical polymerization (CvRP) method, and their surface properties extensively studied.

The kinetics of copolymerization of styrene (St) and acrylonitrile (AN) by RAFT method was studied in detail. Reactivity ratios of St and AN were determined for nine different feed compositions for RAFT, and the effect of solvent on reactivity ratios was discussed based on the bootstrap model. Batch polymerization of styrene (St) and acrylonitrile (AN) yielded statistical and spontaneous gradient copolymers depending on the monomer feed ratio, and the chain structures were confirmed from the change in the copolymer composition. St- and AN-centered triad distributions were determined using quantitative ^{13}C NMR. Using the continuous feeding approach, forced gradient St-AN copolymers were prepared, and St-block-AN copolymers synthesized by the chain extension method. Statistical, gradient and block copolymers have also been synthesized for the acetoxystyrene – t-butyl acrylate monomer system. The statistical and gradient structures were confirmed from the change in the composition since this pair does not provide any well resolved peaks for different triad sequences in ^{13}C NMR. Hydroxystyrene – t-butyl acrylate (HOST-tBA) copolymers were prepared by selective hydrolysis of 4-acetoxystyrene – t-butyl acrylate (AOST-tBA) copolymers.

The properties of the both copolymer systems were found to be strongly dependent on the copolymer structure. A unique broad glass transition was observed for the gradient copolymers, which is different from behaviour of the statistical and block copolymers. Surface properties of St-AN statistical, gradient and block copolymer thin films were found to be very different due to the

differences in their structure. X-ray photoelectron spectroscopy (XPS) and surface free energy studies suggest strong phase segregation for the block copolymer and the statistical copolymers do not show any phase segregation. However, the extent of phase segregation in gradient copolymer thin films was found to be intermediate of those of block and statistical copolymer thin films. However, the effect of structural differences on thin film properties was not as significant for the HOST-tBA system. Grazing angle attenuated total reflectance Fourier transform infra-red (GATR-FTIR) studies provided detailed information on extent of hydrogen bonding in the HOST-tBA copolymer thin films. The proportion of 'free' and hydrogen bonded carbonyl groups was quantified from the IR spectra and found to be in good agreement with the structure of HOST-tBA statistical, gradient and block copolymers.

Overall, the study provided important information on the effect of chain sequence distribution on the properties of thin polymeric films. The implications for lithographic applications is discussed.

Declaration by author

This thesis is composed of my original work, and contains no material previously published or written by another person except where due reference has been made in the text. I have clearly stated the contribution by others to jointly-authored works that I have included in my thesis.

I have clearly stated the contribution of others to my thesis as a whole, including statistical assistance, survey design, data analysis, significant technical procedures, professional editorial advice, financial support and any other original research work used or reported in my thesis. The content of my thesis is the result of work I have carried out since the commencement of my higher degree by research candidature and does not include a substantial part of work that has been submitted to qualify for the award of any other degree or diploma in any university or other tertiary institution. I have clearly stated which parts of my thesis, if any, have been submitted to qualify for another award.

I acknowledge that an electronic copy of my thesis must be lodged with the University Library and, subject to the policy and procedures of The University of Queensland, the thesis be made available for research and study in accordance with the Copyright Act 1968 unless a period of embargo has been approved by the Dean of the Graduate School.

I acknowledge that copyright of all material contained in my thesis resides with the copyright holder(s) of that material. Where appropriate I have obtained copyright permission from the copyright holder to reproduce material in this thesis and have sought permission from co-authors for any jointly authored works included in the thesis.

Publications during candidature

Peer-Reviewed Papers:

1. Alam, M. M.; Peng, H.; Jack, K. S.; Hill, D. J. T; Whittaker, A. K. Reactivity Ratios and Sequence Distribution Characterization by Quantitative ^{13}C NMR for RAFT Synthesis of Styrene-Acrylonitrile Copolymers, *Journal of Polymer Science, Part A*: *Polymer Chemistry* 2017, 55, 919-927

Conference Presentations:

1. Alam, M. M.; Guo, Y.; Peng, H.; Jack, K. S.; Whittaker, A. K. Effect of Compositional Heterogeneity of Gradient Copolymers on Line Edge Roughness, *35th Australasian Polymer Symposium, Gold Coast, QLD, Australia*, 2015

2. Alam, M. M.; Peng, H.; Jack, K. S.; Whittaker, A. K. Synthesis of Gradient Copolymers by RAFT process and Their Applications in Photolithography, AIBN Student Conference, Brisbane, 2015

Publications included in this thesis

1. Alam, M. M.; Peng, H.; Jack, K. S.; Hill, D. J. T; Whittaker, A. K. Reactivity Ratios and Sequence Distribution Characterization by Quantitative ^{13}C NMR for RAFT Synthesis of Styrene-Acrylonitrile Copolymers, *Journal of polymer science, Part A*: *Polymer Chemistry* 2017, 55, 919-927 – incorporated as part of Chapter 2.

Contributor	Statement of contribution
Alam, M. M.	Conception and design 40% Analysis and interpretation 45% Drafting and production 50%
Peng, H.	Conception and design 5% Analysis and interpretation 5% Drafting and production 5%
Jack, K. S.	Conception and design 5% Analysis and interpretation 10% Drafting and production 5%
Hill, D. J. T.	Conception and design 20% Analysis and interpretation 20% Drafting and production 20
Whittaker, A. K.	Conception and design 30% Analysis and interpretation 20% Drafting and production 20%

Contributions by others to the thesis

Prof. Andrew K. Whittaker	Conception, design, characterization, analysis and critical revision of the work contained within this thesis
A/Prof. Kevin S. Jack	Conception, design, characterization, analysis and critical revision of the work contained within this thesis
Dr Hui Peng	Characterization, analysis and critical revision of the work contained within this thesis
Dr David Hill	Conception, design, characterization, analysis and critical revision of the work contained within this thesis
Dr Barry Wood	XPS studies of polymer thin films

Statement of parts of the thesis submitted to qualify for the award of another degree

None

Research Involving Human or Animal Subjects

No animal or human subjects were involved in this research

Acknowledgements

The journey of my PhD study was full of hurdles, but I was fortunate to overcome all those with the support of so many helping hands. I would like acknowledge all of them for their generous contributions.

First of all, I would like to express my sincere gratitude to my advisors, Prof. Andrew K. Whittaker, A/Prof. Kevin S. Jack and Dr Hui Peng for their valuable guidance, continuous support, motivation and patience throughout my whole PhD journey. Their immense knowledge and vast experience in the field of polymer science was always inspiring to learn more to be a better academic researcher.

I would like to extend my gratitude to the veteran scientist Dr David J. T. Hill for sharing his ideas, for his help in designing my project and in analysing the data. It was always a pleasure to learn from him, to discuss about ideas and results.

I would like to thank Prof. Ian Gentle and Dr James Blinco for being the assessors of my PhD program. Their comments during each of the milestones guided me towards the successful ending of my PhD project.

I would like to thank Dr Barry Wood, the Scientific Manager from Centre for Microscopy and Microanalysis (CMM), for providing me the training on x-ray photoelectron spectroscopy (XPS) and for his help with the XPS characterization of my polymer samples. I would like to acknowledge the contribution of Australian National Fabrication Facility (ANFF) and CMM for providing the access to all the specialised equipment. I want to thank Dr Javaid Khan for size exclusion chromatography (SEC) training; Dr Wael Al Abdulla his help in using the spin coater; Dr Elena Taran for providing the training on atomic force microscopy (AFM); Mr. Kai-Yu Liu for the training on Filmtek measurements and Dr Sandra Camarero-Espinosa for the training on contact angle measurements.

My thank goes to Dr Yi Guo for his guidance, support and training during the early days of my PhD journey. I would also like to thank all the members of Polymer Chemistry Group for their friendly help and support. Special thanks to Dr Cheng Zhang, Dr Ao Chen, Dr Yun Huang, Mr. Samuel Richardson, Mr. Lewis Chambers, Mr. Zhen Jiang in particular for the input of their ideas and expertise on my experiments and results. I would like to thank Ms. Katarzyna Kępa for her help in contact angle measurements.

I would like to acknowledge the University of Queensland and Australian Institute for Bioengineering and Nanotechnology for the generous financial support (UQI and AIBN Top-up). I appreciate the contribution of the research higher degree (RHD) officers for providing the administrative supports.

Finally, my passionate thank goes to my dearest wife Khandakar Josia Nishat, who provided the unconditional love, support and motivation, both at good and bad times throughout my PhD journey. I would also like to thank my parents and family members, without their support I would not have come this far.

Financial support

This research was supported by University of Queensland International (UQI) Scholarship, Hui Peng's University of Queensland Postdoctoral Research Fellowship for Women, the Australian Research Council (CE140100036, DP130103774, and LE140100087) and the Asian Office of Aerospace Research and Development (AOARD).

Keywords

line edge roughness (LER), RAFT polymerization, gradient copolymer, reactivity ratios, glass transition temperature, thin films, x-ray photoelectron spectroscopy (XPS), contact angle measurement, surface free energy.

Australian and New Zealand Standard Research Classifications (ANZSRC)

ANZSRC code: 030306, Synthesis of Materials, 50%
ANZSRC code: 030301, Chemical Characterisation of Materials, 50%

Fields of Research (FoR) Classification

FoR code: 0303, Macromolecular and Materials Chemistry, 100%

Table of Contents

List of Figures

List of Tables

List of abbreviations

AA acrylic acid
AIBN azobisisobutyronitrile
AIC aerial image contrast
AFM atomic force microscopy
AGET activators generated by electron transfer
AN acrylonitrile
AS 4-acetoxystyrene
ATRP atom transfer radical polymerization
BMA butyl methacrylate
3BrHT 3-(6-Bromohexyl) thiophene
CCD chemical composition distribution
CD critical dimension
$CDCl_3$ deuterated chloroform
CMC critical micelle concentration
CPDB 2-cyano-2-propyl benzodithioate
CRP controlled radical polymerization
CSD copolymer sequence distribution
CvRP conventional radical polymerization
DLS dynamic light scattering
DMA dynamic mechanical analyses
DMAA N,N-dimethylacrylamide
DMAc N,N-dimethylacetamide
DMAEMA 2-(dimethylamino) ethyl methacrylate
DMF N,N-dimethylformamide
DMSO dimethyl sulfoxide
DSA directed self-assembly
DSC differential scanning calorimetry
DUV deep ultra-violet
EOVE 2-ethoxyethyl vinyl ether
EUV extreme ultra-violet
FBA 2,2,3,4,4,4-hexafluoro butyl acrylate
FMA 2,2,3,4,4,4-hexafluorobutyl methacrylate
FRES forward recoil spectroscopy
HEMA 2-hydroxyethyl methacrylate
HOVE 2-hydroxyethyl vinyl ether
3HT 3-hexylthiophene
HFBMA 2,2,3,3,4,4-heptafluorobutyl methacrylate
HOST hydroxystyrene
HPLC high performance liquid chromatography
iBRA isobornyl acrylate
ITRS international technology roadmap for semiconductor
LER line edge roughness
LG linear gradient
LWR line width roughness

MA methyl acrylate
MAA methacrylic acid
MC Monte Carlo
MiPrOx 2-methyl- or 2-isopropyl-2-oxazoline
MMA methyl methacrylate
MMFS model-based monomer feeding strategy
MOS metal-oxide-semiconductor
MOVE 2-methoxyethyl vinyl ether
MPC 2-methacryloyloxyethyl phosphorylcholine
MSt 4-methyl styrene
nBA n-butyl acrylate
nBMA n-butyl methacrylate
NMP nitroxide mediated polymerization
NMR – nuclear magnetic resonance
nPrOx 2-n-propyl-2-oxazoline
OEGMA oligoethylene glycol methyl ether methacrylate
PAN poly(acrylonitrile)
PABTC propanoic acidyl butyl trithiocarbonate
PCBM phenyl-C61-butyric acid methyl ester
PEB post-exposure bake
PHOST polyhydroxystyrene
PMMA poly(methyl methacrylate)
RAFT reversible addition-fragmentation chain transfer
ROMP ring-opening metathesis polymerization
RRP resist reflow processing
SANS small-angle neutron scattering
SAXS small-angle X-ray scattering
SCF self-consistent field
SEC size exclusion chromatography
SiMM Si containing methyl methacrylate
SMC simplified Monte Carlo
St styrene
tBA tert-butyl acrylate
T_{CP} cloud point temperature
TEM transmission electron microscopy
TFEMA 2,2,2-trifluoroethyl methacrylate
TFOA 3,3,4,4,5,5,6,6,7,7,8,8,8-tridecafluorooctyl acrylate
T_g glass transition temperature
THF tetrahydrofuran
TGA thermogravimetric analysis
TMAH tetramethylammonium hydroxide
TMSEMA 2-(trimethylsiloxy)ethyl methacrylate
TRI triblock copolymer
4VP 4-vinylpyridine
WC water content

Chapter 1: Introduction

1.1 Line Edge Roughness (LER)

In microelectronics technology, semiconductor feature size continues to decrease and is moving down to sub-20 nm scales so as to produce high energy-efficient and high-density data storage devices. As the device size enters into the sub-100 nm range, Line Edge Roughness (LER) or line width roughness (LWR) does not scale accordingly and has become a major problem in realization of small feature sizes. LER is any unwanted roughness in the semiconductor feature, on the order of several nanometres and has adverse effects on device performance [1]. In early technologies, the ratio of LER to the device dimension was very low and did not have any significant effect on device performance. However, as the devices are becoming smaller and roughness of the devices remains almost unchanged, the ratio of LER to the device dimension increases and this affects the performance of the device [2]. Therefore, LER puts a limit in effectively achieving minimum feature size and maximum circuit density. Extensive studies have been made to identify the sources of LER and to suggest methods of remediation of LER, to achieve the goals set by International Technology Roadmap for Semiconductor (ITRS) [3-12].

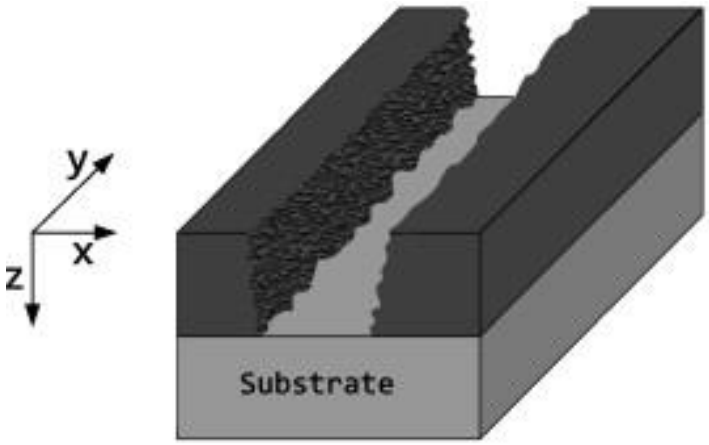

Figure-1.1: 3D model of resist LER generated by simplified Monte Carlo simulation (SMC) method [3]. The X-Y plane corresponds to the resist surface, the Z-axis is along the resist depth dimension which shows surface roughness. Just to check.

1.1.1 The Sources of LER

Since photolithography involves a complicated series of steps, it is difficult to assign a particular step or factor as the overriding source of LER. In the last couple of decades, a number of studies have attempted to isolate and describe the factors affecting resist LER in photolithography. It has been reported that almost all the materials and process parameters involved in photolithography affect LER [5]. Some of the factors found to be affecting the roughness include polymer structure, molecular weight and molecular weight dispersity [13-15], acid diffusion [16, 17], development time and developer concentration [18, 19], the quality of aerial image contrast [5, 20, 21], roughness transferred from the patterning tool [22, 23], the types of resist materials [8, 24].

Several studies have been reported on the effect of molecular weight and molecular weight distribution of polymer molecules on LER [13-15, 25]. The surface roughness was found to increase with molecular weight due to the larger size of aggregates protruding from the surface as a result of development process [13]. Therefore, it was expected that LER for low molecular weight resists would be smaller than that of high molecular weight resist, assuming that the size of a single polymer molecule determines the LER. Yamaguchi and co-workers [13, 14] investigated the effect of resist molecular weight on LER and found results contrary to the expectations. In their study, they have quantified LER from AFM images of the feature sidewalls for resists with four different molecular weights and molecular weight dispersity. LER changes with various extents of defocus depended on the resist molecular weight and larger LER was found for low molecular weight resists than a high molecular weight resist. Kozawa and co-workers [15] also studied the dependence of the resist molecular weight on LER at three exposure dose ranging from 10 to 30 mJ cm^{-2}, and in each case LER was found to be decreasing with increase in molecular weight.

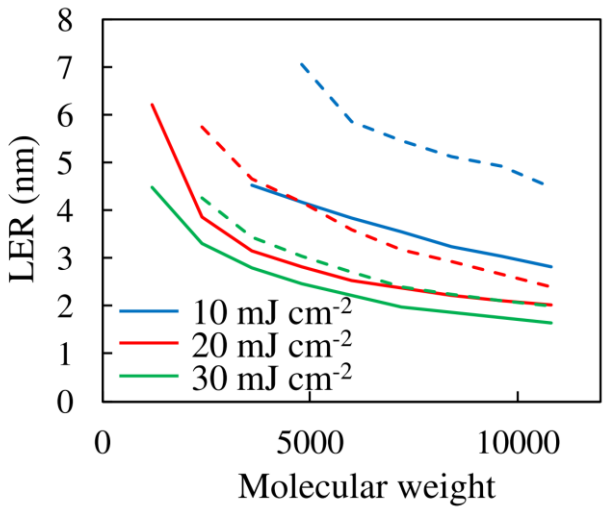

Figure-1.2: Molecular weight dependence of LER. The solid lines were calculated by assuming the monodisperse polymer as an initial condition. The dashed lines were calculated by assuming the randomly protected polymer as an initial condition. The protection ratio was 30% [15].

The intrinsic edge roughness of the mask was found to be one of the sources of LER, which can be transferred to the resist features [22, 26]. The sidewall roughness of a mask contributing to the overall LER measured with Atomic Force Microscopy (AFM) was found to be in between 2.7 to 3.0 nm rms, though the value depends on particular masks [22].

Sanchez et al. [20] studied the influence of aerial image contrast (AIC) on photoresists LER for a diverse set of high contrast photoresist materials by varying AIC in a systematic manner (Figure-1.3). All the resist materials possess very low LER at the maximum AIC (100%), and as the AIC decreased, in all cases the magnitude of LER increased. This result also identified the resist composition as a significant factor governing the behaviour of LER with the change of AIC. However, at maximum AIC, the magnitude of LER is nearly independent of the resist material composition. Shin and co-workers [21] have also discussed the correlation of LER with aerial image modulation for different lithography and found higher aerial image contrast leading to lower LER, though there is a threshold. They also reported LER of the photoresist UV6 to be more sensitive to aerial image modulation than PMMA.

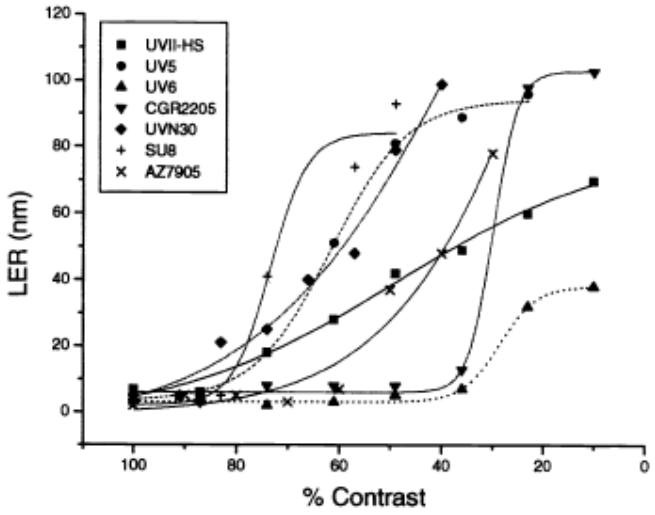

Figure-1.3: LER as a function of decreasing contrast for a diverse set of photoresist materials [20]. LER increases with decreasing image contrast depending on the composition of resist materials.

Shot noise is another source of LER which can be observed in both DUV and EUV lithography [27-29]. Studies suggest that the shot noise generated LER decreases as the number of photons absorbed at the line edge increases. An analytical model for the influence of shot noise based on Poisson statistics predicts the relation between LER and the dose required to produce features in a particular resist (E_{size}) is LER $\propto E_{size}^{-1/2}$. Plots for LER against E_{size} at both wavelengths give straight lines; the resists requiring low doses have poor LER, whereas the resists requiring high doses have good LER.

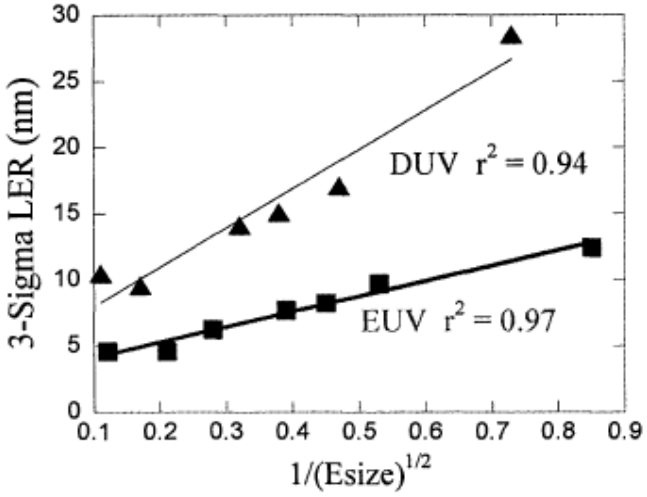

Figure-1.4: LER vs. $(E_{size})^{-1/2}$ for DUV and EUV exposure [27]. Resists requiring low doses have poor LER, whereas better LER is shown by the resists requiring high doses.

The extent of acid diffusion is also a potential contributor to the overall LER of photoresists [16, 30, 31]. Photo acids are generated in the exposed regions of the photoresist during illumination through a mask. At the high temperatures of the post-exposure bake (PEB), the acid catalyzes deprotection of the blocking groups and the polymer becomes soluble in regions of high acid concentration. In regions of low acid concentration, the remaining blocking groups render the polymer insoluble. These two extremes cause variation in solubility in the boundary regions, which determines the shape of the resist feature after development [31].

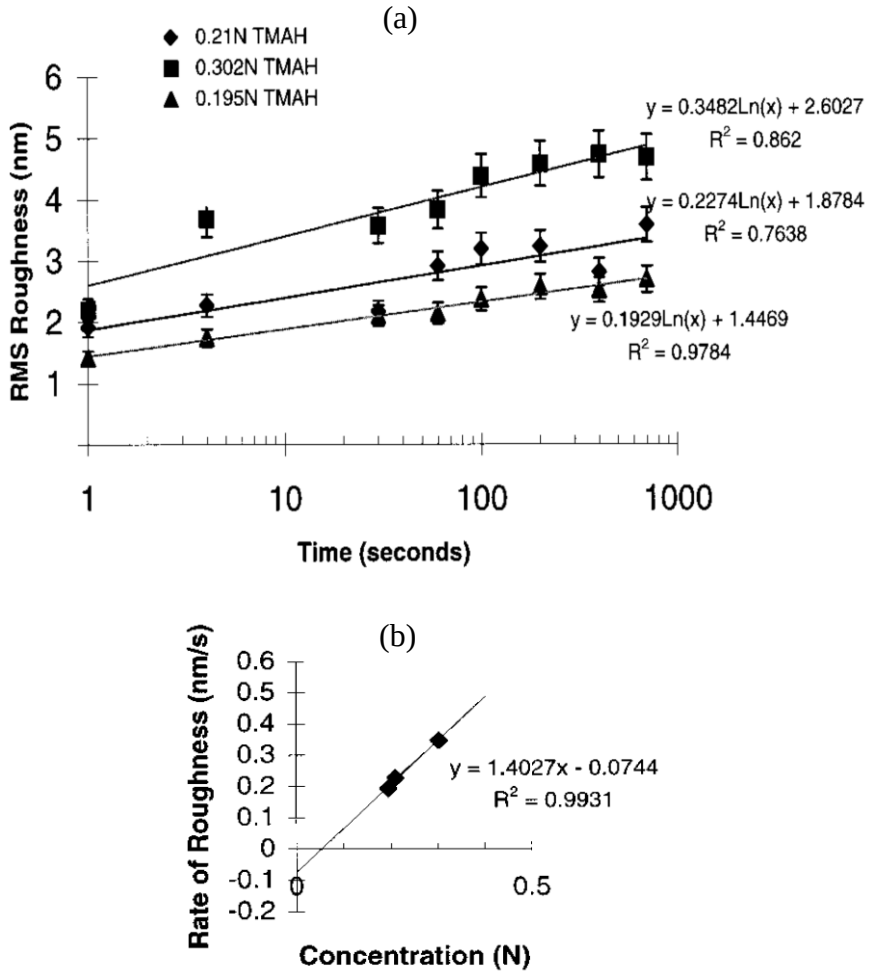

Figure-1.5: (a) Effect of time in the developing solution on LER for three different developer strengths, (b) rate of increase of roughness as a function of developer concentration [19].

The contribution of the development process to LER [18, 19] has been found to be on the order of 2-3 nm, depending on the development time and developer concentration (Figure-1.5). It is apparent that the concentration of the developer has a more profound effect on the line edge roughness than the development time.

An important source of resist LER is the inhomogeneity of the chemical compounds which determines the solubility of the resist. Qinghuang et al.[8] studied the material origins of LER in a positive-tone chemically-amplified resist by designing experiments to mimic the composition and morphology of the resists in the line edge regions. They synthesized copolymers and terpolymers with different pre-determined levels of de-protection and revealed that the resist in the line edge region consists of a mixture of the protected and de-protected polymers rather than a uniform, one component material. Blends of incompatible protected and de-protected polymer parts form two separate phases and thus cause LER after development due to compositional heterogeneity.

The surface roughness varies within a short range with the variation in protected polymer content before development process. After developing with a dilute aqueous TMAH developer, the roughness was significantly increased. The surface roughness after development process increased first, reached a maximum value and then decreased with further increase in content of protected polymer in the blend.

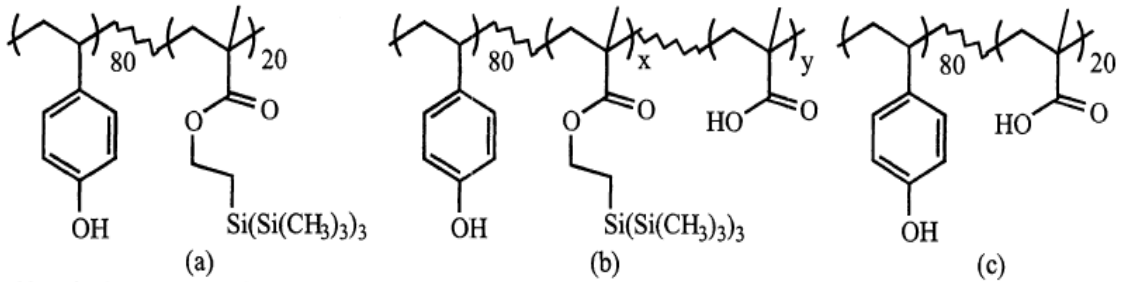

Figure-1.6: Chemical structures of (a) protected, (b) partially protected, and (c) completely deprotected 248 nm bilayer copolymers and terpolymers of p-hydroxystyrene (HOST), Si containing methyl methacrylate (SiMM) and methacrylic acid (MA) [8].

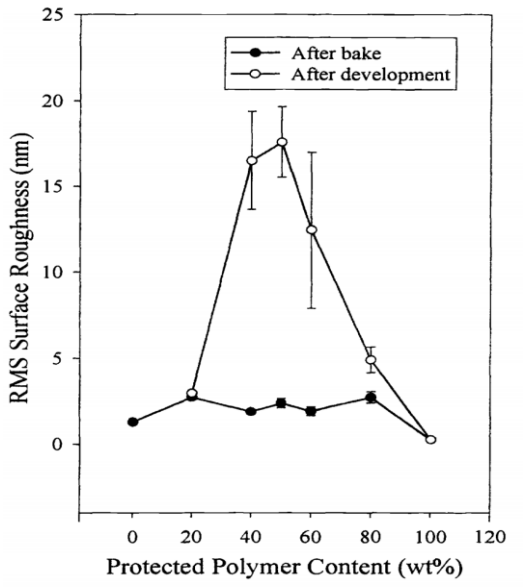

Figure-1.7: Surface roughness as a function of the protected polymer content in the 248 nm bilayer resist [8]. The roughness changes with the change in the protection level before and after development process to different extents.

Kozawa et al. [4, 15] studied the effect of deprotonation efficiency of protected units and the protected unit ratio on LER. They reported that, LER can be expressed as:

$$LER = \frac{0.68\ \sigma_n}{dm/dx}$$

where σ_n, m, and dm/dx represent the normalized standard deviation of the number of the protected units connected to a polymer molecule, the normalized protected unit concentration, and the chemical gradient, respectively. They suggested that enhancement of the chemical gradient at the boundary between lines and spaces is an essential strategy to reduce LER [32].

The factors affecting the formation of LER can be divided into three categories (initial acid distribution, catalytic chain reaction, and development and rinse) as summarized in Table-1.1.

Table-1.1: The major contributors to the Line Edge Roughness [5].

Initial acid distribution
Aerial image including reflection from substrate and flare
Acid concentration
Exposure dose
Acid generation efficiency
Shot noise
Specific to EB and EUV
Reaction of acid generator with low energy electron (~ 0eV)
Catalytic chain reaction (acid diffusion and reaction)
Pre-baking and post-exposure bake conditions (temperature and period)
Diffusion constant of acid and base quencher
Glass transition temperature of polymer
Size of acid counter anion and base quencher
Residual solvent
Base quencher concentration
Activation energy for catalytic reaction and diffusion
Development and rinse
Development time
Temperature of developer
Strength and molecular size of solvents
Rinse
Molecular weight
Molecular dispersion
Rigidity of polymer structure
Polymer aggregation
Crystallization

1.1.2 Effect of LER on device performance

LER has been considered as a key limiting factor in sub-100 nm device performance as it degrades both the pattern fidelity and critical dimension control [7]. It was found that the effect of LER on device performance was more prominent in smaller devices.

A number of studies have been carried out to investigate the effect of LER on device performances [33-38]. LER is a significant source of channel length variation and thus causes the threshold voltage (V_{th}), leakage current (I_{off}), and trans-conductance of the metal-oxide-semiconductor (MOS) to be affected [37]. An increase in LER from 5.7 to 11.4 nm increases the threshold voltage (from 5.25 to 17.3 mV), as well as the leakage current (from 12.34 to 202.5 nA/μm) in an 80 nm nominal gate length device [39]. This kind of dramatic change in leakage current will cause significant power consumption of transistors. Diaz et al. experimentally showed that a reduction of LER from 9.3 to 6.5 nm translated into 1.5 times improvement in leakage current [36].

Ban and co-workers [40] investigated the device saturation current variation and the leakage current variation with the amount of LER in 45 nm and 32 nm inverter standard cells and found that, the deviation between upper bound and lower bound is highly increased as LER increases, while there was slight increase in average values. The leakage current suffers more critically than that of the saturation current with a change of LER as shown in Figure-1.8.

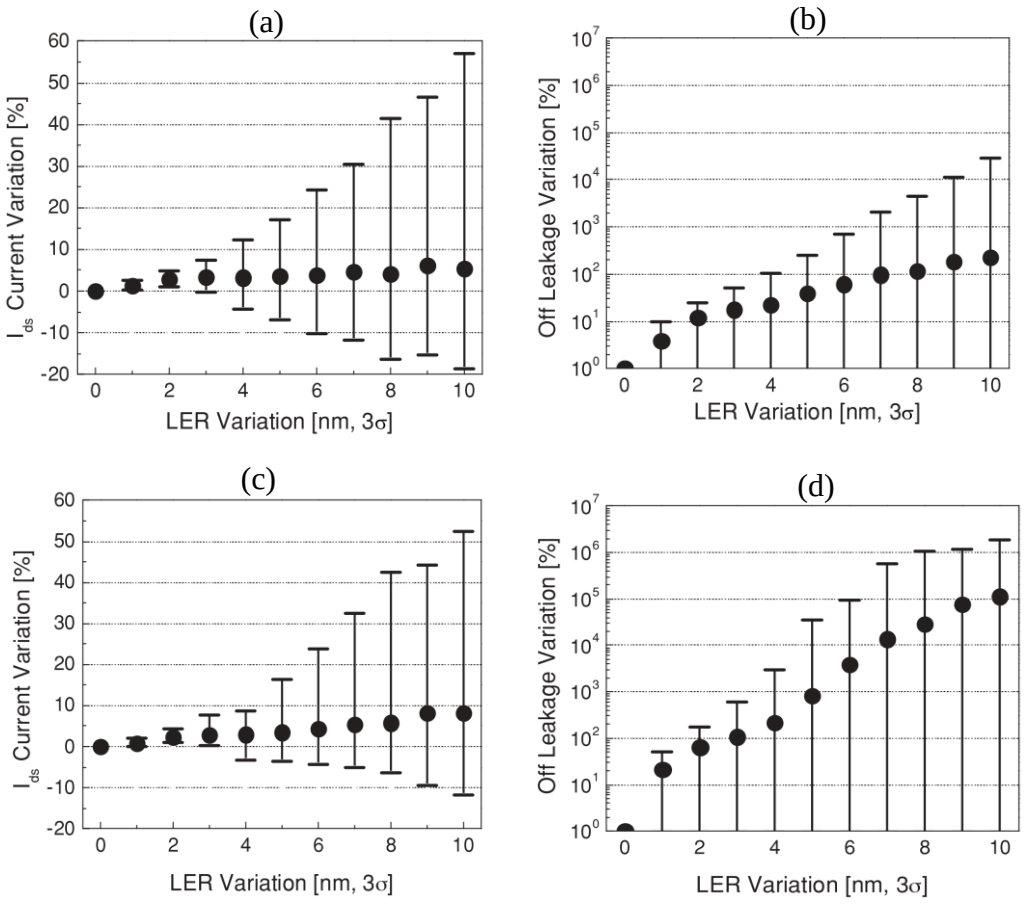

Figure-1.8: The change in current variation and off leakage variation with LER for 45 nm [(a) and (b)] and 32 nm [(c) and (d)] inverter standard cells. The black circled dot represents the average of the variation, and the small bars show the upper and lower bounds of the variation.

1.1.3 Reported Methods for the Remediation of LER

LER has become a critical problem to address in order to keep up with the trend of shrinking semiconductor device sizes. Since the resist LER can be affected by many different sources in the different steps throughout the process as discussed earlier, efforts needs to be made at each step to minimize LER.

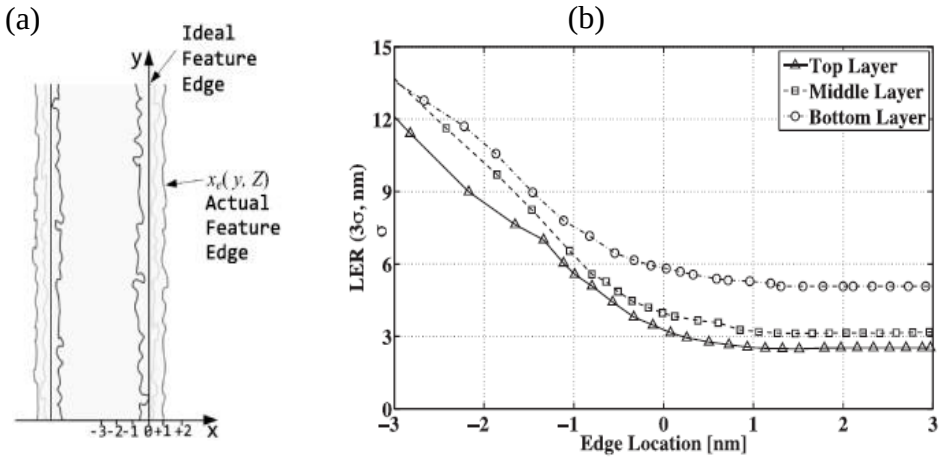

Figure-1.9: (a) LER in resist pattern along the inside and outside edge, and (b) layer dependency of LER on PHOST film. For all different layer, the LER decreases as the edge location varies from the inside to the outside with respect to the ideal edge of the resist pattern [3].

A computational approach to develop an effective method to minimize LER was taken using the fact that the spatial distribution of exposure affects solubility behaviour differently in different regions [3]. Two different methods named ‘shape control’ and ‘shape and dose control’ have been proposed to reduce LER. The LER varies with the edge location from the inside to the outside of a feature. This is due to the fluctuation of exposure from the exposed to the unexposed area and it is possible to reduce LER by shrinking the exposure area of the feature size according to the shape control method.

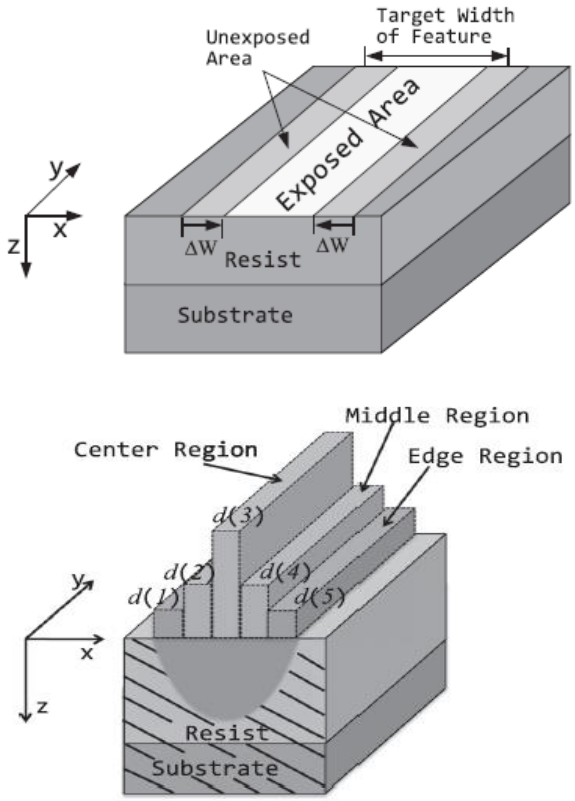

Figure-1.10: In 'shape control', the feature area to be exposed is shrunk from the feature boundary inward (top), and spatial distribution of dose depending on the different regions of the feature in the 'shape and dose control' method (bottom) [3].

According to their study, a higher dose helps to reduce the fluctuation of exposure leading to a lower LER. Therefore, further reduction of LER may be achieved by controlling the spatial distribution of dose within a feature in addition to the shape control. It has been reported that a 'shape and dose control' method provides a better option as it utilizes both shape adjustment and spatial dose control to find a better balance without increasing the total dose. Using an extensive simulation, the effectiveness of the methods was verified for polyhydroxystyrene (PHOST) and poly(methyl methacrylate) (PMMA) resists.

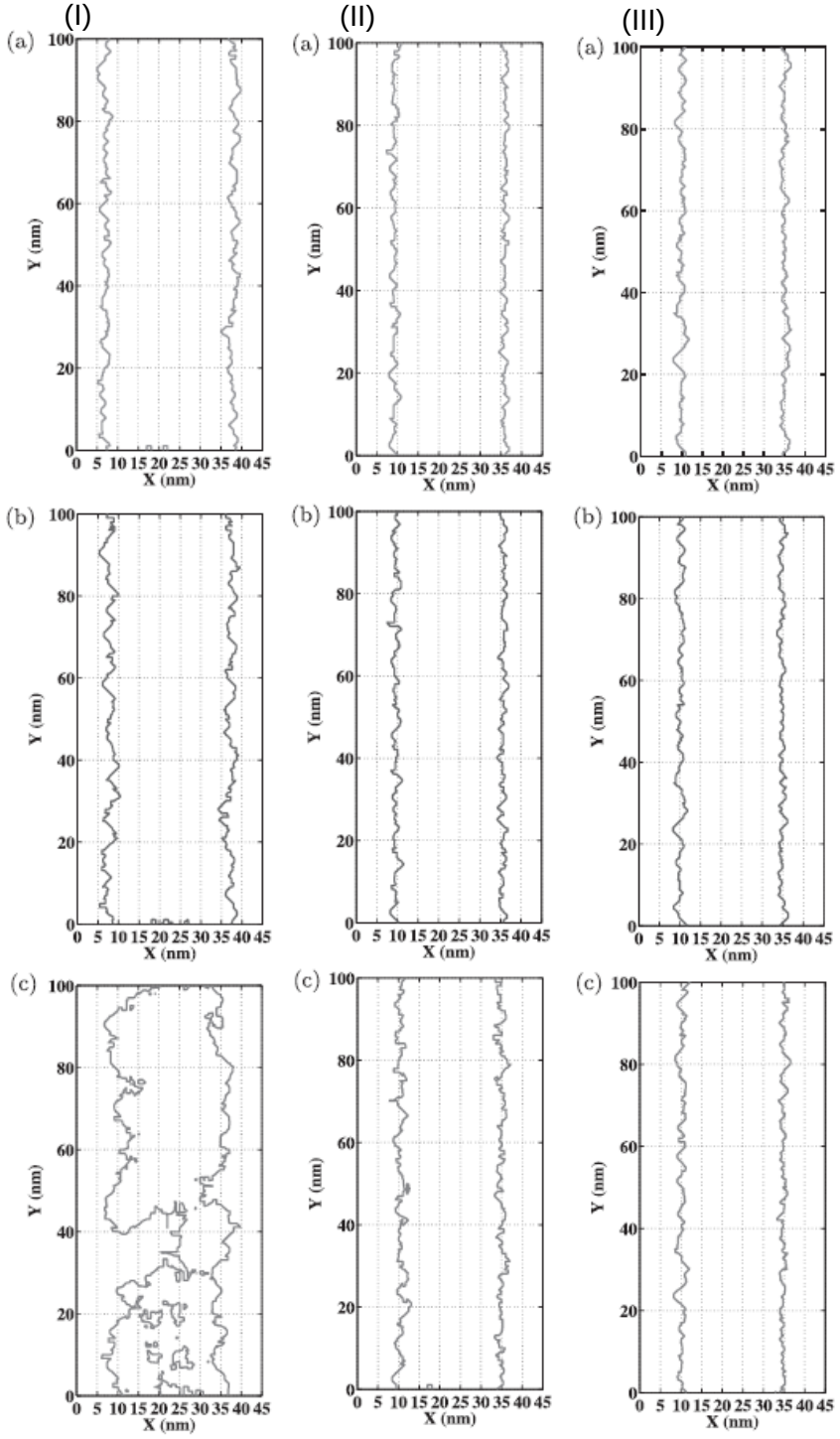

Figure-1.11: Contour of remaining resist profile at (a) top, (b) middle, and (c) bottom layers (I) without 'shape control' and 'shape and dose control' methods, (II) with 'shape control' method, and (III) with 'shape and dose control' method for PHOST film on Si. Resist thickness: 300 nm, beam energy: 50 keV, beam diameter: 3 nm, and exposing interval: 1 nm, feature size: 25 nm [3].

Oh et al. proposed a method named resist reflow processing (RRP) to reduce roughness [9]. In their method, a developed resist is baked at a temperature above the glass transition temperature and the roughness of the pattern can be reduced by flowing the resist over the pattern. Using this technique, they reported a reduction of LER from ~6 nm to ~1 nm for 22 nm CD devices.

(a)

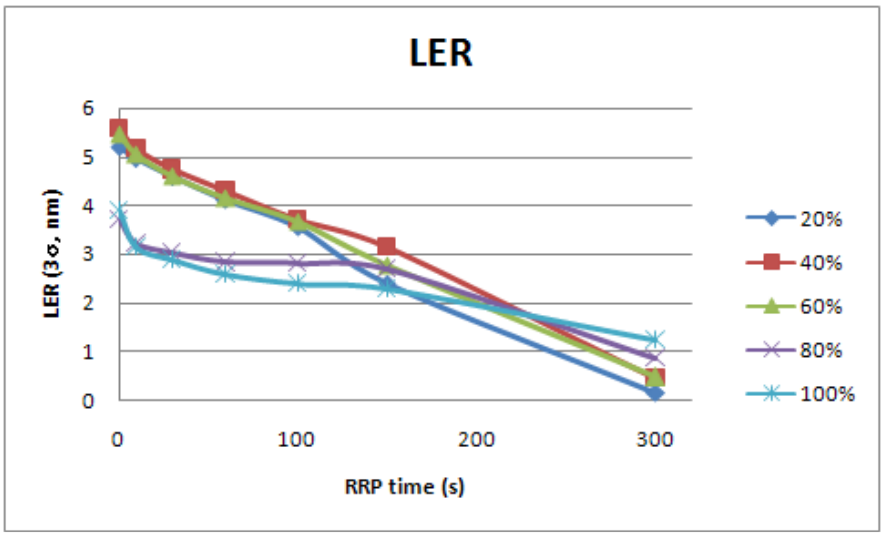

(b) (c)

Figure-1.12: (a) The reduction of LER and LWR with RRP time for t-Boc polymer resists with different percentage of protected groups, before (b) and after (c) 300 s of RRP. The roughness of the pattern is significantly decreased by RRP process [9].

In another systematic approach, Bolten et al. combined efficient proximity effect correction (PEC) with multi-pass grey scale exposure in electron beam lithography to reduce LER [10, 41]. In multi-pass gray scale exposure technique, each feature is exposed for n times with roughly 1/n of the

nominal dose each pass which can reduce LER and thereby enhance device performance. This novel strategy was claimed to reduce LER by ~25% and LWR (Line Width Roughness; the variation about the mean of the distance between edges on adjacent features) by ~40%.

Ruzic et al. focused on improving long spatial-length LER rather than focusing on molecular-scale LER [42]. They used broad ion beams at grazing incidence along the features to heal the LER after lithography using Ne and Ar beams with beam energy, length of time and angular dependence as variables. An increased sputtering rate at higher angles of incidence was shown by the Stopping and Range of Ions in Matter (SRIM/TRIM) simulations method. It has been found to reduce LER from 9.8 ± 0.67 nm to 5.5 ± 0.86 for 45 nm critical dimensions using an Ar beam at 500 eV for 6 s at 85º angle of incidence.

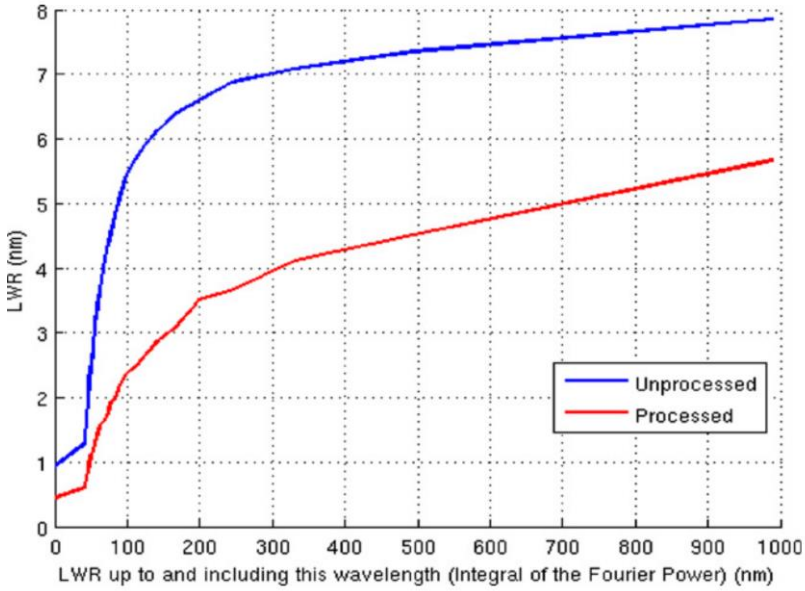

Figure-1.13: Fourier graph of the LWR up to and including the wavelength of 980 nm for the unprocessed and processed samples [42].The samples were processed with a 500 eV Ne beam at an 85º angle of incidence. For both the processed and unprocessed samples, LWR increases with wavelength, though the values for unprocessed samples are higher than the processed samples.

Use of directed self-assembly (DSA) of block copolymer is another approach to healing LER [11, 12]. It has been shown that the highly ordered patterns of immiscible blocks formed by DSA depending on the relative volume fraction of each block, the total molecular weight, and the degree of immiscibility, have smaller LER than the lithographic features that were used to guide them [43].

All of the above discussed approaches, and others, have been reported to minimize the resist LER by varying the conditions and applying new methods to some extent. Since photolithography involves a number of steps, and as discussed in earlier sections of this chapter, LER depends on a number of variables. In addition to optimize those variables, few post-photolithographic treatment such as resist reflow processing [9], or applying broad ion beams at grazing incidence along the features [42]. Despite this, further improvements and optimizations are still needed to achieve the ITRS goals of LER < 10% of the critical dimension.

Both Qinghuang et al. [8] and Kozawa et al. [4, 15, 44] in many of their studies suggested that compositional heterogeneity of the resist materials in the line edge region is one of the main sources of LER. By using a series of deprotected, partially protected, and protected copolymers and terpolymers, LER was found to be strongly dependent on the level of deprotection on the resist materials. Therefore, the heterogeneity of the resist materials which determines the solubility in the line edge region is an important source of LER. However, this particular source of LER is somewhat understudied, and therefore proper understanding of the relation of resist materials structure and LER could provide potential solution.

Apart from the conventional statistical copolymers with constant average copolymer compositions, and block copolymers with a well-defined change in copolymer composition, a less studied type of copolymers architecture, the gradient copolymers have recently attracted significant attention due to their unique structure. The comparison of the properties of the statistical and block copolymers to those of the gradient copolymers could be an important source of understanding the correlation between the resist materials structure and LER. In the following chapter, synthesis, properties and applications of the gradient copolymers are discussed in details.

1.2 Gradient Copolymers

1.2.1 Introduction to Gradient Copolymers

Polymer chain microstructure plays an important role in determining materials properties of polymer products [45]. Extensive theoretical and experimental investigations have suggested that, beside the overall copolymer composition, the distribution of monomer units along the polymer chains can be an important microstructural parameter for fine-tuning nanomorphologies, and thus physical and functional properties of polymeric materials [46-51].

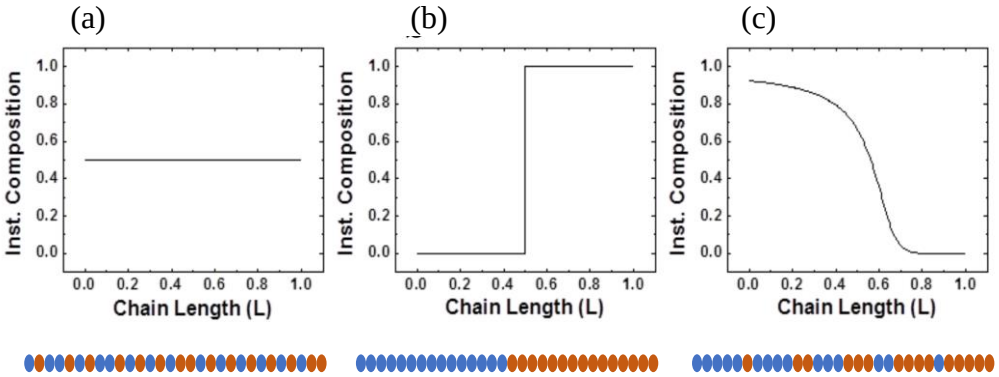

Figure-1.14: Illustration of the instantaneous copolymer composition and typical monomer distribution for (a) a statistical copolymer, (b) a diblock copolymer, and (c) a gradient copolymer [52, 53].

The recent development of advanced radical polymerization techniques provides the researcher with significant control over polymer properties, by controlling physiochemical characteristics such as molecular weight, chain architecture, and sequence chemistry [54-57]. A less-studied class of copolymers named ‘gradient copolymers’, with unique chain microstructure, has recently attracted significant attention [50, 58-63]. As the name implies, gradient copolymers exhibit a gradual change in composition from predominantly one monomer to the second monomer along the copolymer chain [64-67] as illustrated in Figure-1.14. Such a sequence distribution is markedly different from statistical and block copolymers. For example statistical (often mistakenly referred to as random) copolymers have a constant average composition along the polymer chain, once a sufficient number of monomer units are incorporated. Whereas block copolymers exhibit an abrupt change in chemical composition at the point where one block was chain extended by reaction with a second monomer [68, 69]. Another type of copolymer termed as ‘tapered block copolymer’ was introduced by Kraus et al. [70, 71] and Hashimoto et al. [72-74] which has a gradual transition between two

monomer blocks. With the gradual transition, these copolymers can be considered as the primitive form of today's gradient copolymers. Hashimoto et al. [74] simulated the composition of St-butadiene (Bu) system to extend the tapered region through the entire chain length, and the sinusoidal copolymer composition directly corresponded to the concept of gradient copolymer [75]. The gradual change in composition along the chains of gradient copolymers results in less intra-chain and inter-chain repulsion, leading to a much wider range of local environments, unique interfacial behaviour and thermal properties, compared to statistical and diblock copolymers [47, 76-81].

Gradient copolymers are predicted by theory to undergo microphase separation similar to block copolymers, however the morphologies formed may be different and reflect the precise differences in their microstructures [48, 76, 82, 83]. The continuous change in composition along the polymer chains in the gradient copolymer leads to the formation of many separate microphase domains with different compositions, as supported by theoretical simulations and experimental data [76, 84, 85]. Gradient copolymers are also expected to possess unique thermal properties, particularly a broad glass transition temperature (T_g) in situations where the corresponding homopolymers have very different glass temperatures [48, 50, 75, 81, 86]. Gradient copolymers with their unique chain structures, have applications in many fields, such as compatibilizers of immiscible polymer blends [49, 60, 61, 87-89], stabilizers of emulsions or dispersions [90], thermoplastic elastomers [91, 92], damping materials [81, 86] and multi-shape memory materials [93].

Amphiphilic gradient copolymers represent a new class of responsive polymers, in which average properties of the monomers change from hydrophilic to hydrophobic gradually along the molecular chains, and consequently exhibit unique properties in aqueous or mixed solvents [94-106]. Amphiphilic gradient copolymers were found to self-assemble in solutions and can be made to respond to environmental triggers such as changes in pH [107-110], temperature [63, 103, 111], the nature of solvents [112, 113]. Consequently such copolymers have vast potential application in the biomedical and pharmaceutical fields [49, 60, 61, 87, 88, 114-116]. These and other properties are discussed in detail in the following sections of this review.

1.2.2 Synthesis of Gradient Copolymers

The synthesis of gradient copolymers with continuous change in composition from one end of the chain to the other requires simultaneous initiation and uniform growth of all propagating chains in the polymerization process [52]. Controlled radical polymerization (CRP) techniques are therefore

widely used to prepare gradient copolymers [64, 101, 102, 113, 117, 118]. Well-defined gradient copolymers have been synthesized using CRP techniques such as NMP (nitroxide mediated polymerization) [68, 81, 119-124], ATRP (atom transfer radical polymerization) [80, 125-129] and RAFT (reversible addition-fragmentation chain transfer polymerization) [101, 102, 107, 130-132].

Gradient copolymers are prepared either by exploiting a natural or spontaneous gradient in composition, or by producing a forced gradient. Spontaneous gradient copolymers are prepared by the batch technique, and relies on differences in the copolymerization reactivity ratios [107, 133-135]. Example pairs of monomers which form spontaneous gradients include styrene (St)/acrylic acid (AA) [136], tert-butyl acrylate (tBA)/octadecyl methacrylate (ODMA) [137], St/methyl methacrylate (MMA) [138], n-butyl acrylate (nBA)/n-butyl methacrylate (nBMA) [135] and St/tBA [139]. In such polymerizations, one monomer is consumed more rapidly than the other resulting in segments rich in that monomer and preferential depletion of the monomer in the reaction mixture. As the polymerization proceeds, the second, more slowly reacting monomer is incorporated to a greater extent by virtue of depletion of the first monomer. The resulting polymer chains will have various chemical composition distributions (CCDs) depending on the monomer reactivity ratios and initial feed composition [140]. Figure-1.15 shows the calculated cumulative and instantaneous compositions of styrene in styrene-n-butyl acrylate copolymers (r_{St} = 0.8, r_{nBA} = 0.2) at different initial monomer feed ratios. The gradient in composition was more apparent in the plots of instantaneous composition, and strength of the gradient was reported to be significantly dependent on the monomer feed ratio [80].

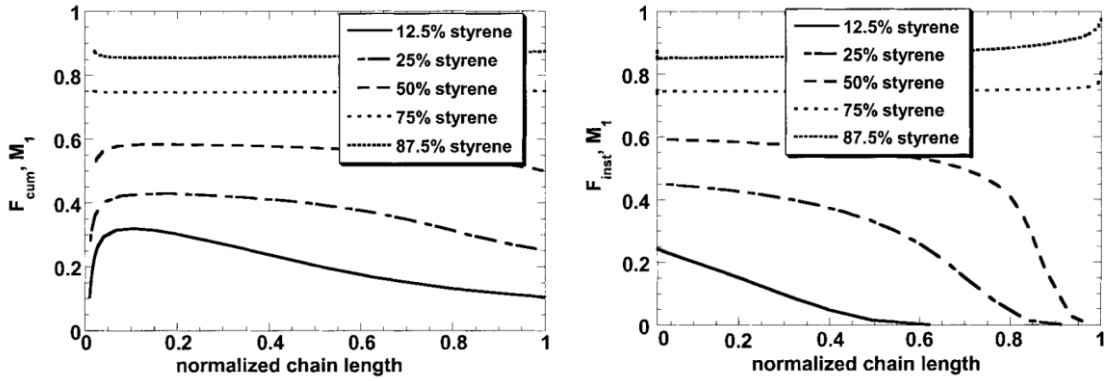

Figure-1.15: F_{cum} (left) and F_{inst} (right) of M_1 (styrene) for a simulated living batch copolymerization of styrene and n-butyl acrylate with reactivity ratios r_{St} = 0.8 and r_{nBA} = 0.2 with different monomer feed ratios. $[M]_0$ = 10 M; $[I]_0$ = 0.1 M. The rate constants for initiation for both monomers are assumed to be equal [80].

Oleszko-Torbus et al. synthesized a series of thermoresponsive statistical copolymers based on 2-n-propyl-2-oxazoline (nPrOx) and 2-ethyl-2-oxazoline (EOx), and gradient copolymers of nProOx with 2-methyl- or 2-isopropyl-2-oxazoline (MiPrOx) by living cationic ring opening polymerization [141, 142] and exploiting differences in the monomer reactivity ratios. Kim and Choi [143] used ring-opening metathesis polymerization (ROMP) to synthesize dendronized gradient copolymers of endo-tricycle[4.2.2.0]deca-3,9-diene (TD) monomers via a macromolecular approach, and demonstrated gradient profile of single chains using AFM.

Whilst the simplicity of the batch approach to synthesis of gradient copolymers makes this method very attractive, there are a very limited number of monomer combinations with sufficiently different reactivity ratios to produce copolymer chains with desired architectures [143]. In the batch process, the reactivity ratios of the monomer pair strongly limits the details of the composition gradients that are to be formed [144].

The second approach used to create gradient in the copolymer structures is known as 'forced gradient', and is a semi-batch technique. In forced gradient copolymerization, a second monomer is continuously added to the polymerization mixture during the reaction so as to change the instantaneous monomer compositions, as illustrated in Figure-1.16. The addition of the second monomer leads to an increase in its content in the monomer feed, and thus results in a gradual increase in the composition of this monomer in the copolymer [117, 145]. The majority of gradient copolymers are made by this technique due to the flexibility and freedom it gives to design the copolymer compositions and gradient [52, 64, 78, 132, 146, 147]. For example, it has been experimentally and theoretically demonstrated that, through optimized feeding in a semi-batch reactor, copolymers with uniform composition or linear gradient in composition can be successfully designed and prepared [64, 132, 148-152].

Nitroxide mediated polymerization (NMP) has been used extensively to synthesize gradient copolymers. Billon and co-workers [123] performed the polymerization of St and MA (r_{St} = 0.89, r_{MA} = 0.22) in a batch process to prepare gradients in the copolymer structure. Both the batch and semi-batch approaches were used to synthesize gradient copolymers of St and AA in dioxane at 120 °C [108, 153]. They also prepared in semi-batch NMP, gradient copolymers of N,N-dimethylacrylamide (DMAA) /nBA [154, 155], St/nBA [156] and octadecyl acrylate (ODA)/methyl acrylate (MA) [157]. Torkelson and co-workers reported the synthesis of St/4-acytoxystyrene (AS) [61, 87, 158], (St/MMA) [159], St/4-methyl styrene (MSt) [122], St/tBA [50, 85, 160], St/nBA [85, 161], St/4-vinylpyridine (VP) [85, 162] and St/nBMA [85] gradient copolymers using the same

technique. Charleux et al. [90, 136] used the batch NMP technique to produce St/AA gradient copolymers and confirmed good control over the copolymer molecular weight and molecular weight distribution.

The ATRP methods has been used extensively by Matyjaszewski and co-workers to synthesize a series of gradient copolymers of St/nBA [80], St/acrylonitrile (AN) [80], nBA/isobornyl acrylate (iBRA) [77], MMA/nBA [163] and 2-(dimethylamino) ethyl methacrylate (DMAEMA)/nBMA [164]. ATRP has also been reported for creating composition gradients in MMA/2-(trimethylsiloxy) ethyl methacrylate (TMSEMA) [127, 165], tBA/2,2,3,3,4,4-heptafluorobutyl methacrylate (HFBMA) [128] and St/nBA [166] copolymers. Gradient copolymer grafts based on styrene and α-tert-butoxy-ω-vinylbenzyl-polyglycidol were prepared by surface-initiated AGET ATRP by Basinska and co-workers [167]. Zhou et al. [126] reported the facile synthesis of MMA/tBA gradient copolymers using Cu(0) and conventional ATRP ligands as catalysts in N,N-dimethylformamide (DMF) solvent using the semi-batch technique. Using the same method, Kim et al. [168] synthesized amphiphilic gradient copolymers of oligoethylene glycol methyl ether methacrylate (OEGMA) and St, whilst D'hooge and co-workers [169] generated linear gradient copolymers of MMA/nBA by the fed-batch ATRP technique.

The RAFT method has been similarly broadly used to create gradients in copolymer structures by both the batch and semi-batch technique. Zhang and co-workers prepared fluorinated gradient copolymers of OEGMA and 3,3,4,4,5,5,6,6,7,7,8,8,8-tridecafluorooctyl acrylate (TFOA) [170], and a series of copolymers of fluorinated methyl acrylate (FMA) and BMA [52] via semibatch RAFT miniemulsion polymerization. Chen et al. [113] synthesized fluorinated amphiphilic gradient copolymers of AA and 2,2,2-trifluoroethyl methacrylate (TFEMA) using the RAFT semi-batch approach., whilst Zhen et al. [171] prepared gradient copolymers of St/MMA using multi-shot RAFT copolymerization. Guo and co-workers [117, 172] used the same method to produce gradient structure of St/nBA copolymers. In this method, the polymer is prepared as a series of sequential blocks and the average composition of each block is continuously changed from one chain end to the other. At the end of the polymerization, a kind of 'many block' copolymer results [117].

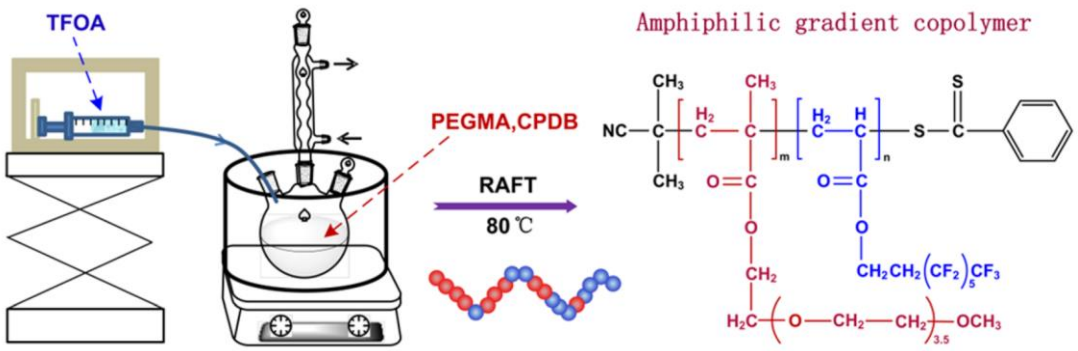

Figure-1.16: A schematic diagram of the synthesis of amphiphilic gradient copolymer of OEGMA and TFOA using the RAFT semi-batch approach [170].

In addition to the above monomer feeding approach with constant addition rate, gradient copolymers can also be prepared using a step-increasing constant addition strategy [88, 173]. In the synthesis of St/MMA gradient copolymers [88], styrene was initially fed into the batch reactor. MMA was then added at a constant rate of 10 mL/h for 3 h, followed by addition at 15 mL/h for additional 3 h and then at 20 mL/h for the last 3 h. With increased rate of addition of MMA, the mole fraction of MMA in the reactor increased rapidly, resulting in gradient St/MMA copolymers with increasing MMA composition. Torkelson and his group have exploited the monomer feeding strategy to prepare a series of St/nBA gradient copolymers [51, 85, 161, 162, 174, 175].

Polymerization in solution often results in CRP with better control, however the rate of reaction may be slowed due to dilution of reactants. Enhanced rates of polymerization can be achieved using emulsion or miniemulsion CRP. In these methods, the propagating radicals experience a segregation effect within the particles [145]. Using the constant monomer feeding semi-batch strategy for miniemulsion ATRP with activators generated by electron transfer (AGET), Matyjaszewski and co-workers [146] synthesized a series of gradient nBA/tBA, nBMA/MMA, and nBA/St copolymers. They reported that the form of the gradient along the backbone of the copolymers was influenced by the molar ratio of the monomers, the reactivity ratios of the comonomers as well as the rate of monomer addition. The preparation of copolymers of BMA/dodecafluoroheptyl (DFMA) [176], MMA/St [138], and St/Butadiene (Bu) [177] via RAFT miniemulsion copolymerization with continuous and constant monomer addition has also been reported. Luo et al. [178] produced a series of triblock St/nBA/St thermoplastic elastomers using the same approach. Chen et al. [102] synthesized AA/TFEMA gradient copolymers in RAFT emulsion system employing the same monomer feeding strategy. Charleux and co-workers [179] studied NMP miniemulsion polymerization of nBA and St in a batch process to create a gradient in the copolymer composition.

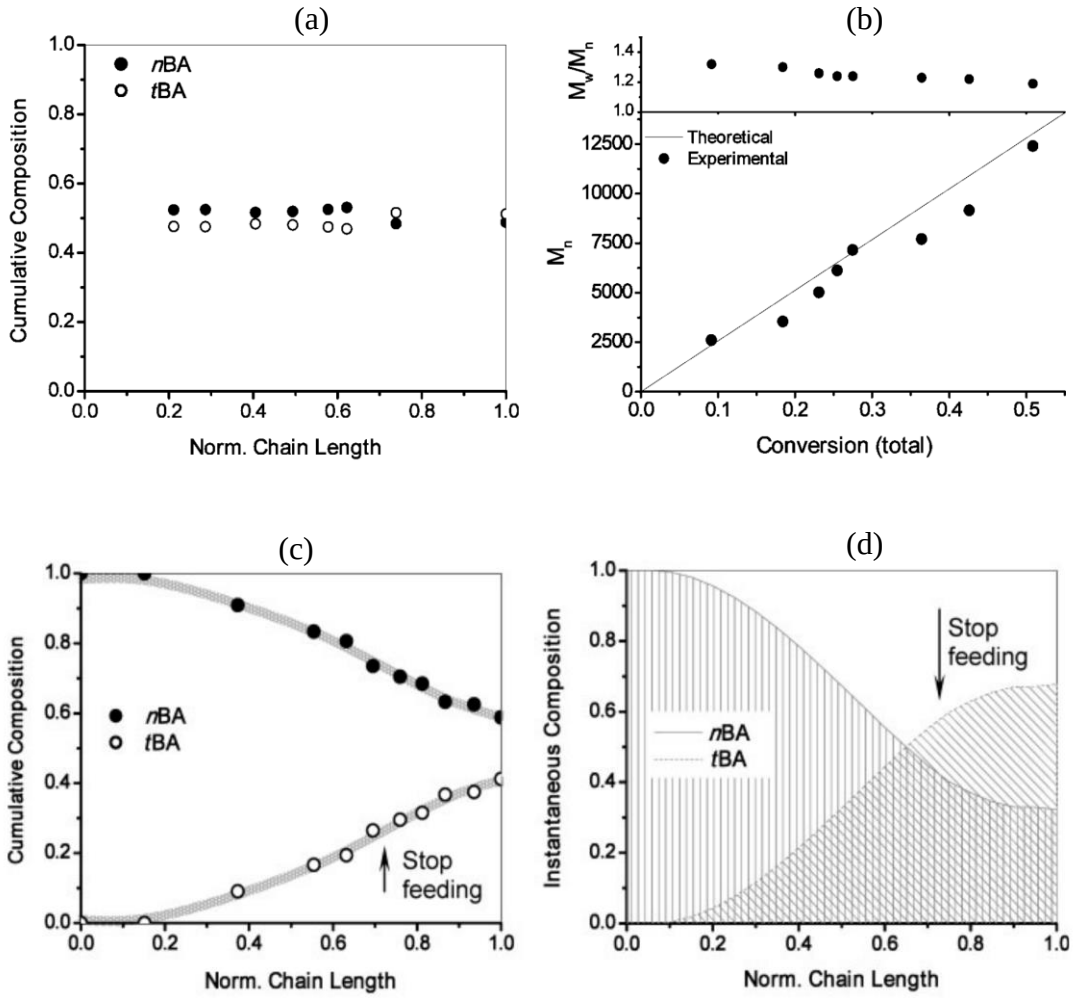

Figure-1.17: Cumulative compositions and the evolution of molecular weight of nBA/tBA copolymer in batch ((a), (b)) AGET ATRP for copolymerization in miniemulsion. (c) and (d) show the cumulative and instantaneous composition of nBA and tBA in the forced copolymer with tBA feeding rate of 0.01 mL/min for 200 minutes. The molecular weight was determined by SEC based on linear polystyrene standards. The normalized chain length was calculated as the ratio of the molecular weight at time t to the final molecular weight [146].

The composition profile for the copolymerization of nBA with tBA was studied in both batch and fed-batch modes [146]. This monomer pair was found to produce statistical copolymers, with both monomers being incorporated into the copolymer chains at similar rates due to their comparable reactivity ratios. However, in the forced copolymerization method using continuous feeding of tBA, both the cumulative and instantaneous composition of tBA increased as shown in Figure-1.17, resulting in nBA/tBA gradient copolymers. The rate of feeding of tBA could be optimized to achieve a smooth gradient in copolymer composition.

Despite the success of these studies, the constant monomer feeding approach is insufficiently versatile for precision production of polymer chains with designed chemical composition distributions (CCDs), such as gradient copolymers with specific comonomer composition profiles along the chain backbone [145]. Therefore, based on the understanding of polymerization mechanism, a kinetic model was developed [127, 180-185] to allow production of copolymers with predesigned CCDs, a so-called model-based monomer feeding strategy (MMFS). MMFS was first exploited by Zhu and co-workers [64, 109, 132, 150-152, 186], and has been demonstrated as an effective technology for precision production of polymer chains. Broadbelt [148, 149, 187, 188] used Monte Carlo (MC) simulations to predict the copolymer sequence distribution (CSD) in the NMP copolymerization of St/MMA, and employed the model to control the CSD in a semi-batch copolymerization. Schork and co-workers [189-191] developed a kinetic model using the method of moments and studied the CSD in RAFT copolymerization under semi-batch operation.

In most reported studies, the gradient in the copolymer structure has been characterized by the change in the copolymer composition determined by ^{1}H NMR spectroscopy. However, as detailed in Chapter 3 of this thesis, the gradient structure is better characterized by considering the change in the triad distributions as demonstrated for the synthesis of St/AN gradient copolymers in a RAFT batch process [133]. As shown in Figure-1.18, for an initial styrene feed composition of 60%, the triad fractions are almost constant throughout the whole chain, while for styrene feed compositions of 20 and 80%, the proportions of styrene-centred and acrylonitrile-centred triads change with conversion, though the former shows a comparatively sharper change, indicating a stronger gradient in composition. Such a study provides a more detailed understanding of the sequence distribution of this gradient copolymer system.

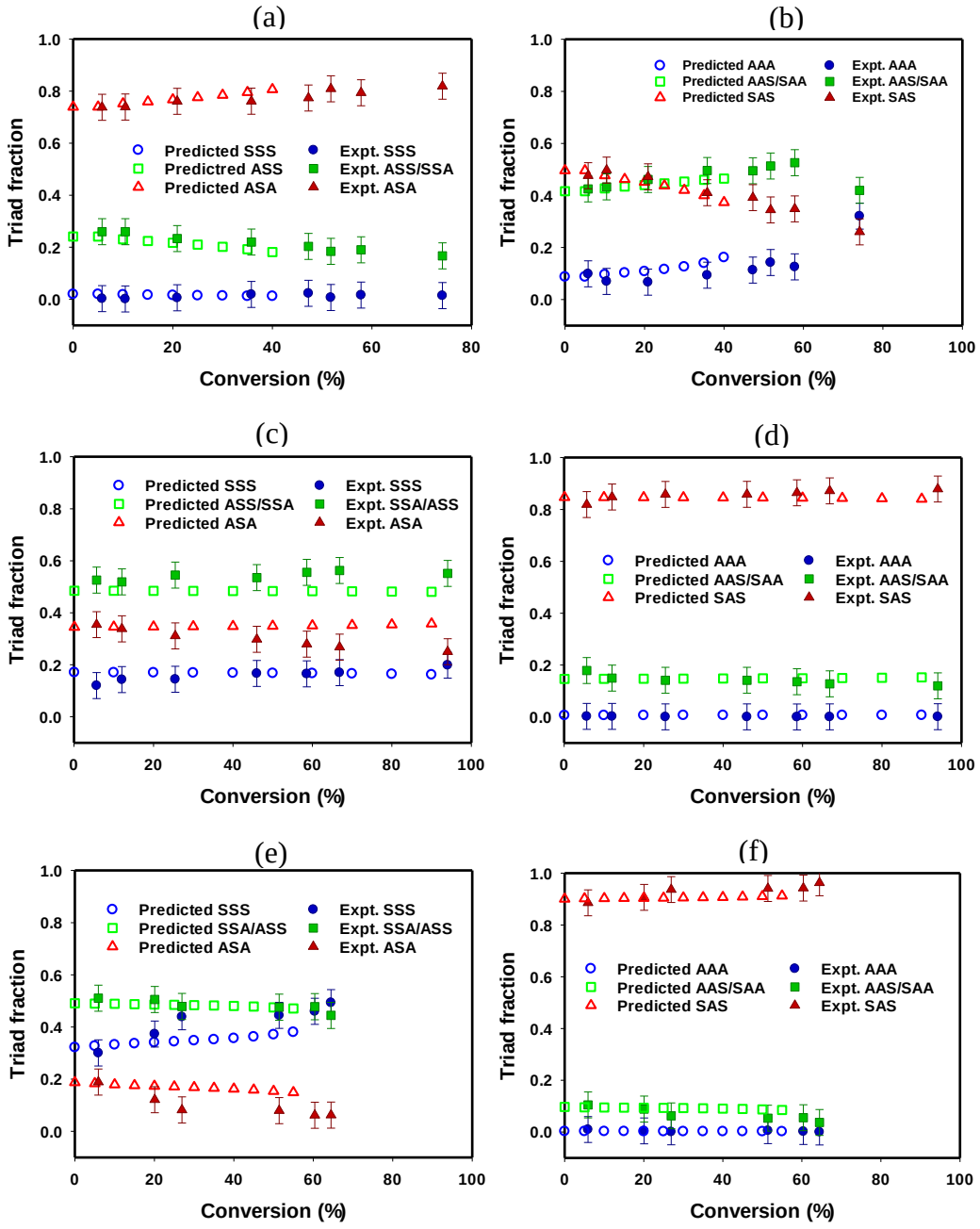

Figure-1.18: The experimental styrene centred and acrylonitrile centred triad distributions for 20% [(a), (b)]; 60% [(c), (d)], and 80% [(e), (f)] styrene feed composition characterized by ^{13}C NMR compared with predicted data [133].

Table-1.2: A summary of CRP techniques used to synthesize various monomer pairs either by the batch or semi-batch method.

Monomer pair	CRP technique	Batch/ semi-batch	References
N,N-dimethylacrylamide/n-butyl acrylate	NMP	Semi-batch	[154, 155]
Styrene/n-butyl acrylate	NMP	Semi-batch	[85, 156, 161]
Styrene/n-butyl acrylate	ATRP	Batch	[80]
Styrene/n-butyl acrylate	ATRP	Semi-batch	[166]
Styrene/n-butyl acrylate	RAFT	Semi-batch	[117, 172]
Octadecyl acrylate/methyl acrylate	NMP	Semi-batch	[157]
n-Butyl acrylate/methyl methacrylate	NMP	Semi-batch	[192]
Styrene/4-acetoxystyrene	NMP	Semi-batch	[61, 87, 158]
Styrene/4-hydroxystyrene	NMP	Semi-batch	[158]
Styrene/methyl methacrylate	NMP	Semi-batch	[159]
Styrene/methyl methacrylate	RAFT	Semi-batch	[171]
Styrene/4-methyl styrene	NMP	Semi-batch	[122]
Styrene/t-butyl acrylate	NMP	Semi-batch	[50, 85, 160]
Styrene/4-vinyl pyridine	NMP	Semi-batch	[85, 162]
Styrene/n-butyl methacrylate	NMP	Semi-batch	[85]
Styrene/acrylic acid	NMP	Batch	[108]
Styrene/acrylic acid	RAFT	Batch	[107]
Styrene/acrylic acid	NMP	Semi-batch	[108, 153]
Styrene/acrylonitrile	ATRP	Semi-batch	[80]
Styrene/acrylonitrile	RAFT	Batch	[133]
Isobornyl acrylate/n-butyl acrylate	ATRP	Semi-batch	[77]
2-(Dimethylamino) ethyl methacrylate/n-butylmethacrylate	ATRP	Semi-batch	[164]
Methyl methacrylate/2-(trimethylsiloxy) ethyl methacrylate	ATRP	Semi-batch	[127, 165]
t-Butyl acrylate/2,2,3,3,4,4-heptafluorobutyl methacrylate	ATRP	Semi-batch	[128]
Methyl methacrylate/t-butyl acrylate	ATRP	Semi-batch	[126]

Monomer pair	**CRP technique**	**Batch/ semi-batch**	**References**
Poly (ethylene glycol) methyl ether methacrylate (OEGMA)/Styrene	ATRP	Semi-batch	[168]
Methyl methacrylate/n-butyl acrylate	ATRP	Semi-batch	[169]
2-Hydroxyethyl metharylate/tBA	ATRP	Batch	[129]
Methyl methacrylate/2-hydroxyethyl methacrylate	ATRP	Semi-batch	[127]
Poly (ethylene glycol) methyl ether methacrylate/ 3,3,4,4,5,5,6,6,7,7,8,8,8-tridecafluorooctyl acrylate	RAFT	Semi-batch	[170]
Fluorinated methyl acrylate/butyl methacrylate	RAFT	Semi-batch	[52]
Acrylic acid/2,2,2-trifluoroethyl methacrylate	RAFT	Semi-batch	[102, 113]
2-Methacryloyloxyethyl phosphorycholine/2,2,2-trifluoroethyl methacrylate	RAFT	Semi-batch	[193]
Styrene/butyl acrylate	RAFT	Semi-batch	[64, 132]
Styrene/2,2,3,4,4,4-hexafluorobutyl acrylate	RAFT	Semi-batch	[131]
2-n-Propyl-2-oxazoline/2-ethyl-2-oxazoline	ROMP	Batch	[141, 142]
2-n-Propyl-2-oxazoline/2-methyl- or 2-isopropyl-2-oxazoline	ROMP	Batch	[141]

1.2.3 Properties of Gradient Copolymers

Gradient copolymers, which exhibit a gradual change in their composition from one end of the chain to the other, are of particular interest because they exhibit unique properties compared with their statistical, alternating and block copolymer counterparts [194]. The properties of a copolymer are not only determined by the monomer type and composition but is also strongly associated with the distribution of different monomer units along the polymer chains [64, 117]. It is obvious to state that an A-B diblock or A-B-A triblock copolymer will have profoundly different properties compared with statistical A-co-B copolymers of the same overall composition [195, 196]. Both theoretical and experimental investigations have suggested that the composition distribution along chain can be an important microstructural parameter for fine-tuning nanomorphologies and thus influencing physical and functional properties of polymer materials [47, 51, 64, 75, 81]. For example, there have been numerous studies [47, 49, 76, 82, 83, 197-201] of interfacial properties, self-assembly morphologies and the conformations of gradient polymer brushes using self-consistent field theory. The most important properties of the gradient copolymers are discussed below.

1.2.3.1 Interfacial Behaviour and Blending Properties

The phase behaviour of the gradient copolymers and their interfacial activities have been intensively studied by a number of groups [47-49, 51, 60, 61, 82, 83, 160, 162, 202-206]. Shull and co-workers used the self-consistent field (SCF) theory to study the interfacial behaviour of gradient copolymers, and introduced a gradient parameter, λ which describes the length of the composition gradient relative to the entire length of the copolymer [48, 82]. For AB copolymers, when $\lambda = 0$, the copolymer is a conventional block copolymer consisting of separate blocks of A and B units. When $\lambda = 1$, the composition varies smoothly along the chain from pure A to pure B. The random phase approximation (RPA) was used to calculate the scattering function analytically and find the location of the critical order-disorder transition for the gradient copolymer as a function of the gradient parameter.

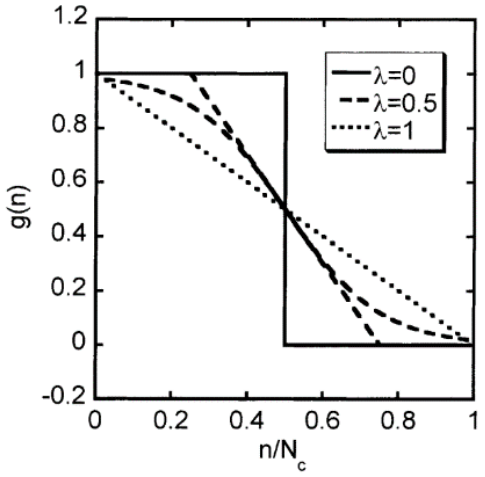

Figure-1.19: Definition of the gradient parameter λ [82].

By combining the SCF and RPA techniques, these authors examined the phase segregation behaviour of four symmetric A-B copolymers: a block copolymer, two linear gradient copolymers, and a tanh gradient copolymer [48]. They found that, for a fixed value of χN (χ = Flory Huggins interaction parameter, N = degree of polymerization), increasing the width of the composition gradient along the chain decreases the lamellar repeat length, which makes phase separation more difficult for gradient copolymers than that of a block copolymer. The order-disorder transition for block copolymers, known to occur at (χN) = 10.495, was reported to be raised to 29.25 for a melt of fully tapered gradient copolymers (λ = 1) [48].

This team also experimentally examined interfacial segregation of diblock, gradient, and statistical copolymers at the interface of immiscible polymer blends using forward recoil spectroscopy (FRES) [47]. Block copolymers (λ = 0) were suggested as more effective compatibilizers than statistical copolymers, acting as surfactants by localizing at the interface and lowering the interfacial tension [207].

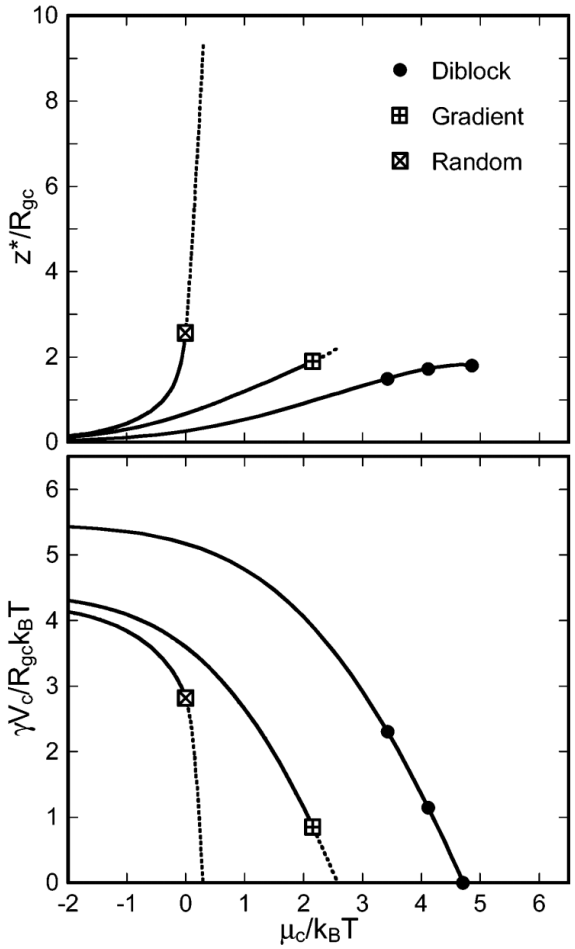

Figure-1.20: Interfacial excess (top) and interfacial energy (bottom) as a function of copolymer chemical potential for the diblock, gradient, and statistical copolymers. The circles are the results of the mean field fits to the FRES data for the diblock copolymer, and the solid lines are calculated by mean-field theory using the value of χ determined for the block copolymer samples, $\chi = 0.036$. The squares correspond to the coexistence points for the statistical and gradient copolymers, and the dotted lines are extensions of the theory to the point where the interfacial energy is zero [47].

The interfacial excess, z^* is defined as the excess volume fraction of copolymer at the interface with respect to the volume fraction of copolymer in the bulk, and $\gamma V_c/R_{gc}k_BT$ is the normalized interfacial energy where γ is the interfacial energy, and V_c is the volume of the copolymer, R_{gc} is the radius of gyration. The experimental and computation results supported interfacial properties for diblock, gradient and statistical copolymers varying from formation of a monolayer of diblock copolymers to a wetting layer for the statistical copolymer. The gradient copolymer with $\lambda = 1$ exhibits intermediate behaviour, forming a monolayer with low interfacial energy at the interface but with larger interfacial excess and interfacial width than the monolayer formed by the diblock copolymer [47].

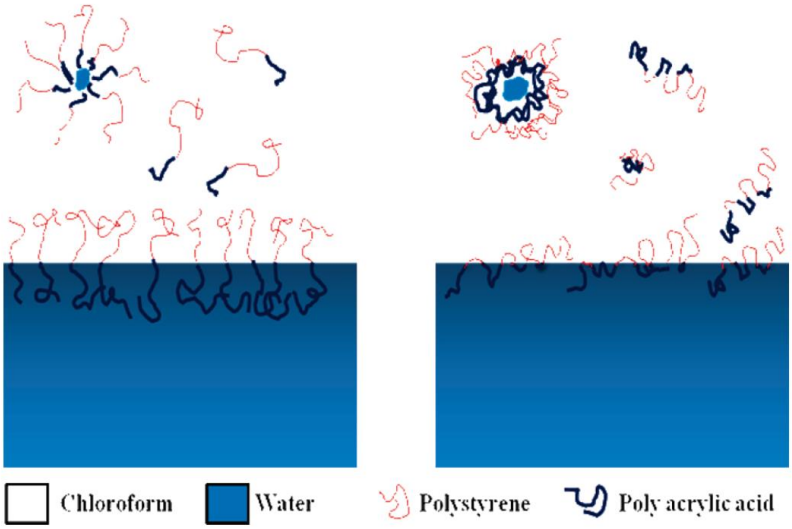

Figure-1.21: Schematic representations of the chloroform/water interface in the presence of diblock copolymer (left) and gradient copolymer (right) [150].

Drop shape analysis was used to investigate the interfacial tension of styrene/acrylic gradient and block copolymers at the liquid/liquid interface [160]. Figure-1.21 illustrates the nature of absorbed layers formed for diblock and gradient copolymers. The block copolymer exhibits a single junction at the interface of the oil and water, while gradient copolymers adopt a parallel structure as a result of multiple junction points along the chains. The overall properties of the interfacial layer depend on the geometric distribution of the copolymer chains, which is further dependent on the sequence distribution along the backbone of the gradient copolymers [160].

Wang and co-workers [49] also studied the effect of gradient on the phase behaviour of ternary homopolymer/gradient copolymer blends using RPA and SCF theory and found that the composition profile of the gradient copolymers has a significant effect on the critical behaviour of the blends. The microphase structure of the blends, including the breadth and distribution of the copolymer layers, the width of the interface region, and the distribution of homopolymers are strongly dependent on the gradient distributions. Therefore, by designing the copolymer composition profile, the interfacial properties of immiscible homopolymer blends could be fine-tuned.

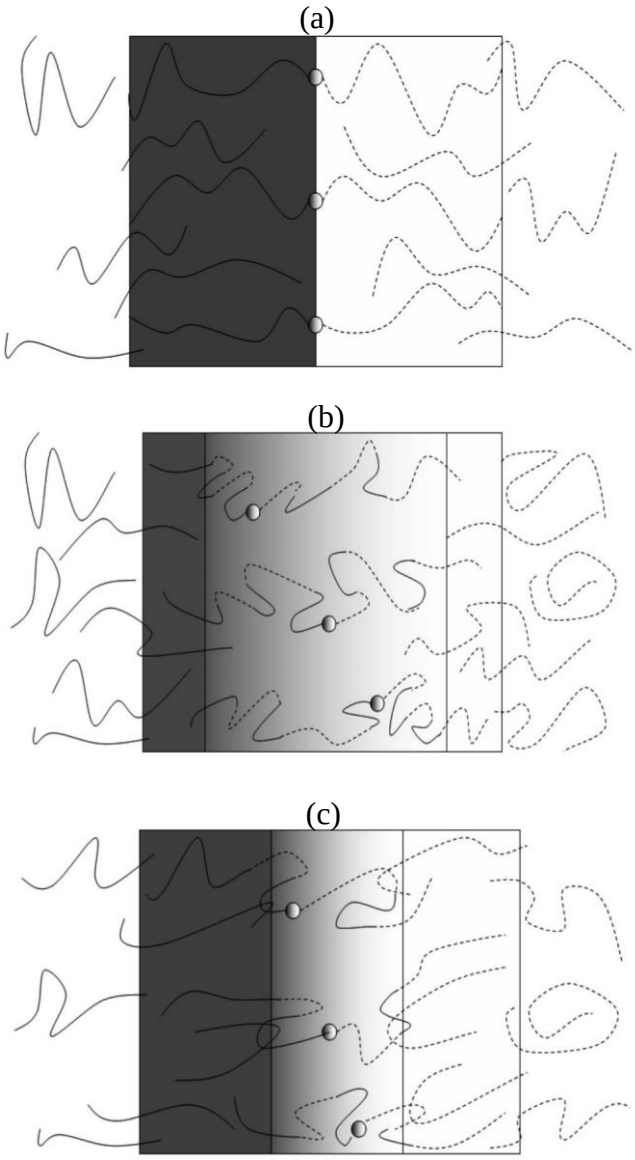

Figure-1.22: Schematic illustration of microstructures formed by blends involving copolymers with (a) steep (b) smooth and (c) intermediate gradient distributions. Circles denotes the positions of the middle section in gradient copolymer chains. Solid and dashed lines denote the chain sections composed of A and B, respectively. The darkness of the background represents the A monomer fraction in the copolymer layer [49].

Torkelson and co-worker [60, 61, 87, 88] produced a series of gradient copolymers, and showed that macrophase separated polymer/polymer blends can be rendered thermally stable by including a gradient copolymer as an additive. The gradient copolymer localizing at the interface lowers the interfacial tension, and as a result, suppresses the phase separation process. Wang et al. [131] reported compatibility of St/fluorobutyl acrylate (FBA) blends was improved after adding gradient

St/F_6BA copolymer. The copolymer molecular weight and the proportion of added gradient copolymer significantly influenced the extent of compatibilization.

Gradient copolymers were also found to modulate and suppress phase separation in polymer/polymer and polymer/fullerene blends, and shown to improve long-term thermal stability of photovoltaic devices as additives, though at the expense of reducing the filling factor [208]. Physical blends of polymers of 3-hexylthiophene (3HT) and 3-(6-bromohexyl) thiophene (3BrHT) showed extensive micron-scale phase separation as found by atomic force microscopy (AFM) and transmission electron microscopy (TEM) studies [209]. Addition of gradient copolymer to the blend resulted in a dramatic reduction in the domain size, and the size decreased further as the amount of the gradient copolymer increased. In comparison, statistical and block copolymers were less effective in promoting mixing, which suggests gradient copolymers are effective compatibilizers for incompatible homopolymer blends (Figure-1.23) [209]. This result was further supported by photoluminescence (PL) data. The blend containing P3HT/phenyl-C61-butyric acid methyl ester (PCBM) and 10 wt% gradient copolymer additive exhibited marked PL quenching even after prolonged thermal annealing, which suggests that gradient copolymers are effective compatibilizers and would improve the thermal stability of the corresponding bulk heterojunction-based solar cells [210].

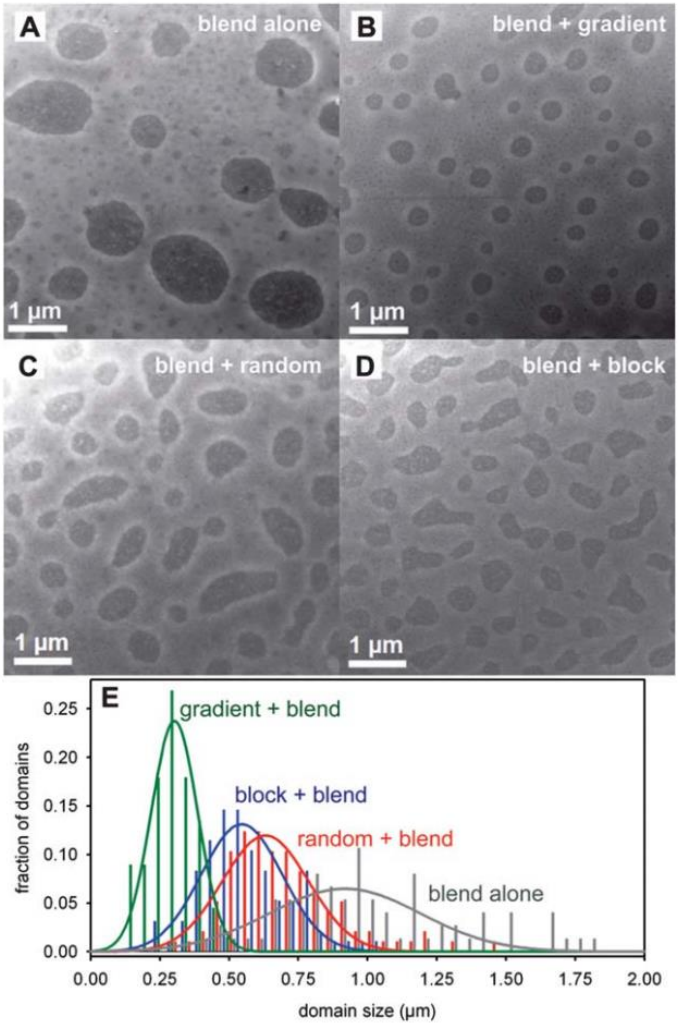

Figure-1.23: STEM images of the 1:1 (v/v) P3HT-P3BrHT blend (A) without copolymer additive, (B) with 20 wt% gradient copolymer, (C) with 20 wt% statistical copolymer, (D) with 20 wt% block copolymer. (E) Histogram of the domain size distributions [209].

Microscopy especially electron microscopy, has played a fundamental role in the study of phase segregation in block copolymers. Scanning electron microscopy (SEM) [211, 212], atomic force microscopy (AFM) [213, 214] and transmission electron microscopy (TEM) [215-217] have been extensively used in determining the boundaries between different morphologies in block copolymers. However, there are few reports on imaging of gradient copolymers, due to the low contrast offered by the continuous variation in the composition. Torkelson et al. [162] studied the surface patterns of St/nBA gradient and block copolymers formed in thin films using three different types of microscopic analysis (Figure-1.24). Patterns typical of phase-segregated block copolymer domains could be clearly seen using each of the techniques. In the gradient copolymers films, SEM micrographs appeared uniform, whereas the AFM images show some level of topography and diffused patterns could be seen in the TEM micrographs, suggestive of short-range phase

segregation. However, annealing proved to be a useful means of directly demonstrating the phase segregation properties of gradient copolymers. One of three gradient copolymer pairs showed no pattern development, but the other two showed the emergence of island/hole patterns similar to those observed in block copolymers, which coarsened and then disappeared on annealing [162]. For example, as given in Figure-1.25, patterns are formed as a result of annealing at 130 ºC for St-block-nBA copolymers, while no such patterning can be seen for St-grad-nBA copolymers.

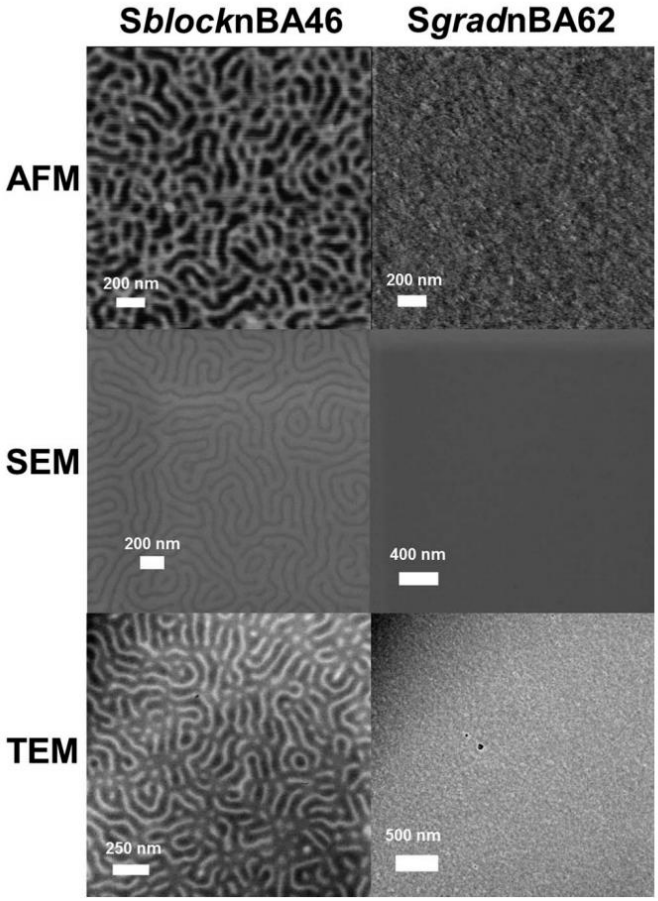

Figure-1.24: Representative micrographs of St-block-nBA46 and St-grad-nBA62 taken using AFM, SEM and TEM [162].

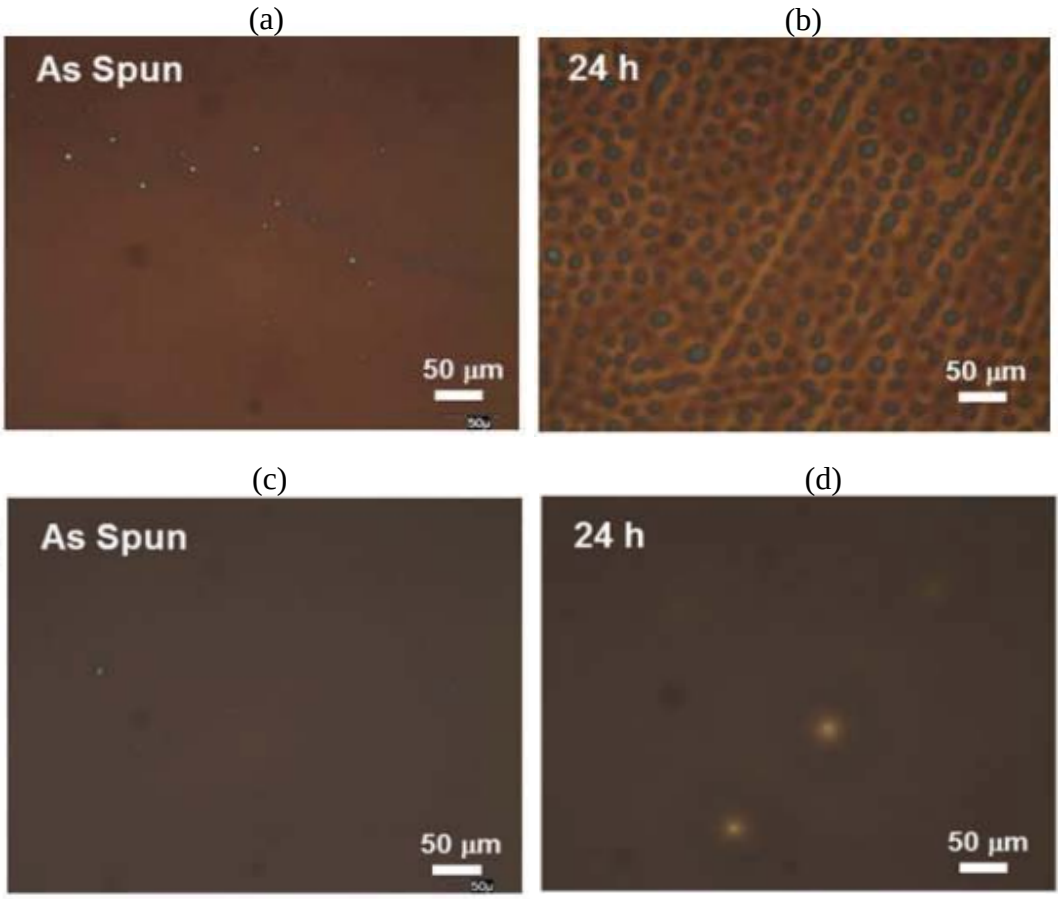

Figure-1.25: Optical micrographs of(a) as spun, (b) 24 hours annealed St-block-nBA copolymer thin films; and (c) as spun, (d) 24 hours annealed St-grad-nBA copolymer thin films.

Guo and co-workers studied the morphology of St/nBA copolymers using AFM, and reported that the block copolymers shows clear boundaries between the blocks. However, no evident boundaries could be seen for the gradient copolymers, due to much weaker phase separation, and instead indistinct boundaries were observed [117]. Figure-1.26 shows the high resolution AFM images of gradient and block dendronized copolymers prepared from these same two monomers [143]. Accurate imaging was possible because both dendronized polymers were large enough to show clear AFM images, and the size difference between two dendrons was sufficiently large to differentiate their microstructures. The gradient copolymer showed a smooth and gradual change in both height and thickness, without any interfacial boundary. Whereas the diblock copolymer contained a clear boundary, showing abrupt changes in both height and thickness.

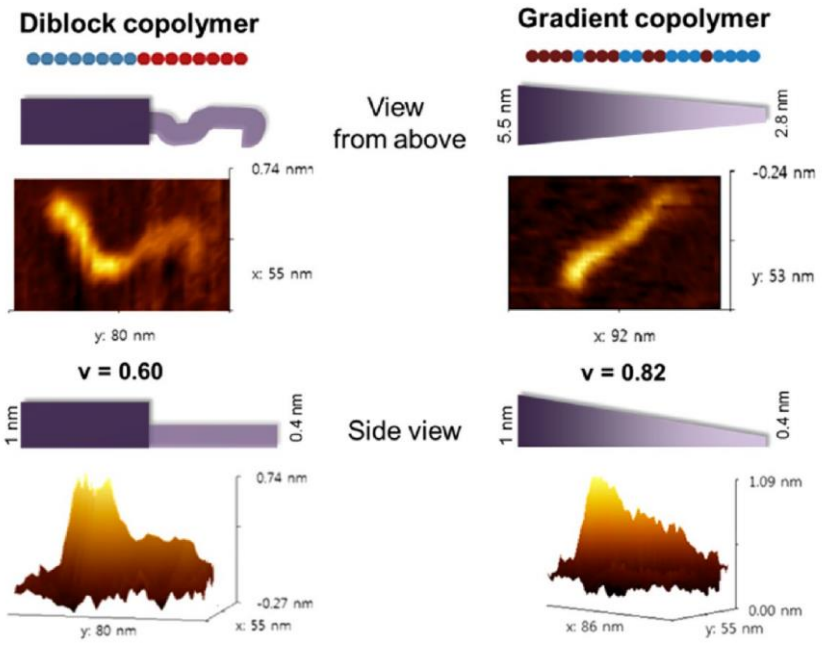

Figure-1.26: AFM image of single chain of dendronized block (left) and gradient (right) copolymers showing variation in height along the chain from above and the side view. [143].

1.2.3.2 Thermal Properties

Both differential scanning calorimetry (DSC) [50, 64, 65, 77, 80, 81, 85, 86, 154, 218] and dynamic mechanical analysis (DMA) [75, 77, 80, 154, 156] studies of gradient copolymer systems have revealed extremely broad glass transition (T_g) regions, indicating contributions from chain segments with a wide range of compositions. The broad glass temperatures of gradient copolymers differ markedly from those of the analogous statistical copolymers, which show a single T_g, and the block copolymers which usually show two sharp and distinct glass transition temperatures [50, 75, 81, 85].

Torkelson and co-workers studied the thermal behaviour of a range of gradient copolymers, including St/MSt, St/AS, St/HOST, St/AA, St/nBA, St/tBA, St/BMA, and compared their properties with those of the corresponding block and statistical copolymers [50, 81, 85, 122, 158, 174]. Conventional thermal analysis did not reveal any significant differences in the T_g of statistical and gradient copolymers of St/MSt due to the close proximity of the transitions of the homopolymers (T_g between 100 °C to 110 °C) [122].

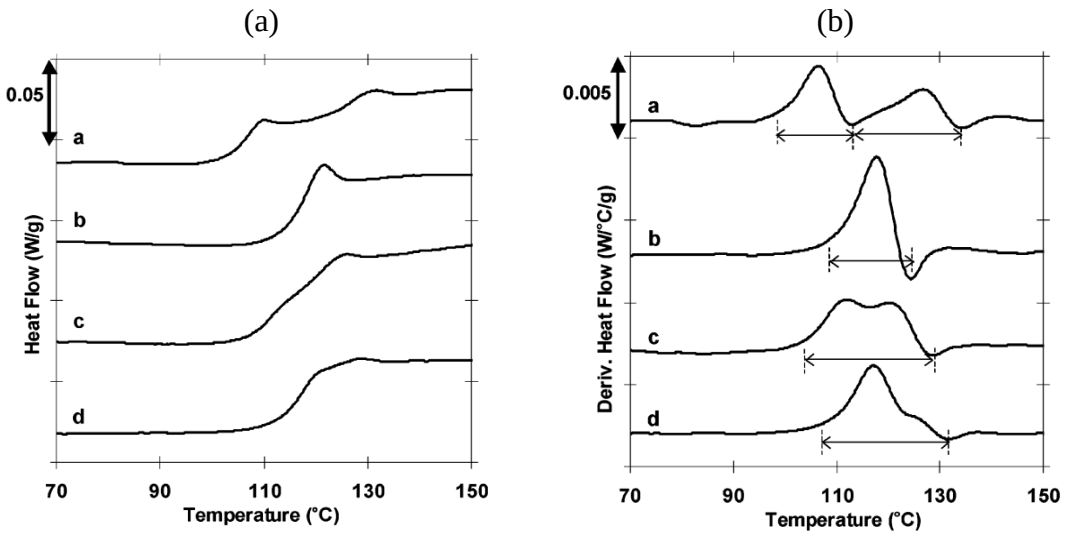

Figure-1.27: The DSC heating curves (a) and first derivatives of the heating curves (b) for [**a**] block, [**b**] statistical and, two different gradient [**c,d**] copolymer of St and AS [81].

However, for copolymers containing monomers where homopolymers have significantly different glass temperatures (St/AS; St/HOST), the DSC heating curves were markedly different for statistical, block and gradient copolymers (Figure-1.27) [81]. A single, narrow T_g was observed for each statistical copolymer, consistent with a single phase of limited compositional nano-heterogeneity. Two narrow transitions were evident for each block copolymer, consistent with well-developed nanophases containing nearly pure St or nearly pure AS or HOST units. However, the gradient copolymers exhibited unusually broad glass transitions (breadth ~65-80 °C), dependent on the degree of the gradient in the copolymer structures. These authors also found similar behaviour for St/AA copolymers [50]. These results are in agreement with predictions by Lefebvre et al. [48] for gradient copolymers with a sinusoidally varying composition. Recent work by Torkelson et al. has indicated that the T_g and breadth of the glass transition can be tuned through the choice of monomer pairs and copolymer compositions [85]. Chain and sequence lengths are also other factors which can influence the glass transition [49, 77, 81].

Matyjaszewski et al. [77] synthesized well defined statistical, block and gradient copolymers of isobornyl acrylate (iBRA) and nBA, and investigated the thermomechanical behaviour using differential scanning calorimetry (DSC) and dynamic mechanical analyses (DMA). While statistical copolymers showed a single T_g, block copolymers showed two distinct transitions and the DSC thermograms for the gradient copolymer indicated a single, but very broad glass transition.

Zhang et al. [52] found that the T_g of gradient copolymers of fluorinated methacrylate and butyl methacrylate were distinctly different than those of the statistical copolymers with similar copolymer compositions. For statistical copolymers, there was a clear T_g in the range of 30-34 °C, while the gradient copolymers showed a broad T_g ranging from 20 °C to 50 °C. Similar results were also reported Guo and co-workers [117, 172].

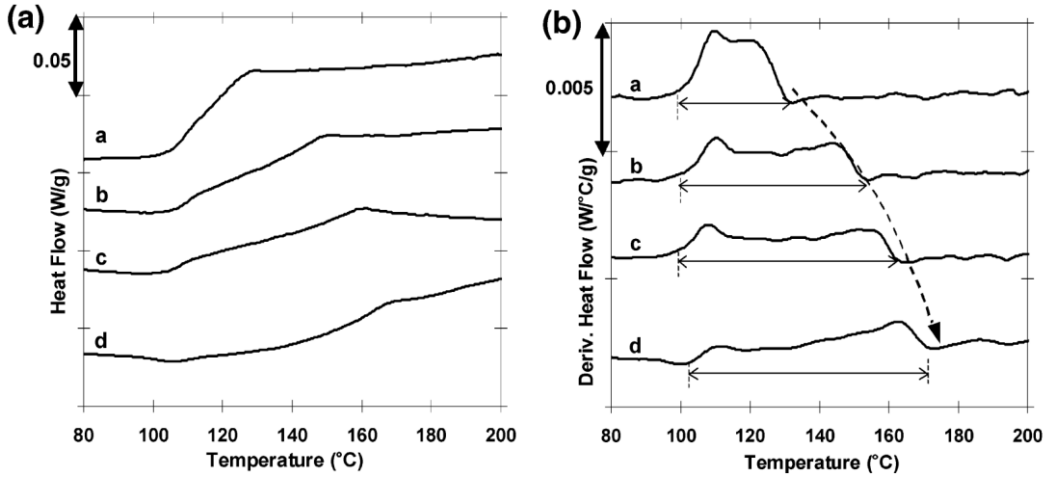

Figure-1.28: DSC heating curves (a) and the first derivatives of DSC heating curves (b) for aliquot samples (taken during gradient copolymerization and then hydrolysed) and the final St-grad-HOST sample. Arrows in (b) indicate the breadth of the T_g. The broken arrow in (b) is drawn to indicate the increase in T_e as the gradient copolymerization proceeds [81].

Figure-1.28 shows how closely the breadth of the T_g is dependent on the length of gradient in the copolymer structure. Samples were collected from a semi-batch reaction system, considered to be 'partial' gradient copolymers, and were hydrolysed before measuring the glass transition. The breadth of the T_g was found to increase as a result of gradual incorporation of HOST into the copolymer.

1.2.3.3 Micellization and Solution Properties

Extensive studies of the association behaviour of gradient copolymers in selective solvents have been reported over the past few years [98, 99, 105, 164, 204, 219-226]. A significant finding was that gradient copolymers have higher solubility than the corresponding diblock copolymers leading to significantly higher values of the CMC [173, 222, 227]. Monte Carlo (MC) simulations have been employed to study the self-assembly of gradient copolymers, which differs with respect to the steepness of the gradient of the local composition along the chain [225]. It was demonstrated that the association behaviour does not depend solely on the net composition of the copolymers, but also

on the sequence of monomer units [228]. In contrast to the diblock copolymers, which form well-defined spherical micelles in selective solvents, gradient copolymers often associate into aggregates with ill-defined shapes and a wide size distribution [108, 225].

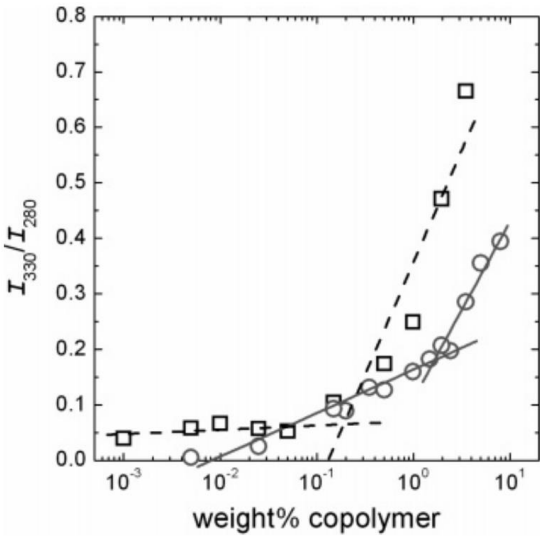

Figure-1.29: Concentration dependence of I_{330}/I_{280} for copolymer present in PMMA; St-*b*-MMA (squares, dashed lines); St-grad-MMA (circles, solid lines). CMCs are estimated from the intersections of the fits to low and high concentration data; block copolymer CMC = 0.2 wt %, and gradient copolymer CMC = 2 wt % [173].

Using SCF theory, Shull [82] predicted that gradient copolymers should exhibit a substantially higher CMC than those of block copolymers of similar molecular weight and composition, and this was later experimentally confirmed by Torkelson and co-workers [173] for St/MMA copolymers. Figure-1.29 shows measurement of the CMCs of copolymers via plots of the ratio of fluorescence intensity at 330nm to that at 280nm (I_{330}/I_{280}) as a function of logarithmic copolymer concentration in PMMA. The ratio I_{330}/I_{280} increases sharply as the concentration of block copolymer exceeds 0.2 wt%, whereas, the gradient copolymer shows a slight concentration dependence below 2 wt%. However, above 2 wt%, I_{330}/I_{280} increases dramatically, and the intersection of the linear fits to low and high concentration data leads to an estimated CMC of the gradient copolymer of 2 wt%, an order of magnitude larger than the CMC for the block copolymer. The higher CMC values associated with the gradient copolymers means that, on addition to an immiscible blend, gradient copolymers are less likely than block copolymers to be trapped in micelles and thus are able to affect the interfacial activity of the blend more effectively than block copolymers [159].

Pandav and co-workers [204] studied the phase separation behaviour of amphiphilic gradient copolymers using kinetic MC simulations, and found that the copolymer chains collapse under poor solvent conditions to form micelle-like aggregates. They also reported that the critical temperature for the transition exhibits a linear dependence on the gradient strength of the copolymer. This is in good agreement with the results reported by Gallow et al. [223].

An interesting observation is that the core region of spherical micelles formed by gradient copolymers can expand or shrink under the influence of environmental stimuli, such as temperature [94, 112, 153], pH [95, 109, 110, 128] and changes in solvents [94, 104, 221]. Such stimuli-responsive behaviour was examined by Seno et al. [221] for gradient, block and statistical copolymers of 2-ethoxyethyl vinyl ether (EOVE) and 2-hydroxyethyl vinyl ether (HOVE). They found that, the temperature stimulus or the solvent stimulus resulted in shrinking of the micellar corona and an expansion of the micellar core in EOVE-HOVE gradient copolymer micelles, but block and statistical copolymer micelles did not undergo these changes in size.

Okabe et al. [63, 103, 111] studied the solution behaviour of block and gradient copolymers of EOVE and 2-methoxyethyl vinyl ether (MOVE). The dimension of block copolymer micelles was not sensitive to changes in temperature, because of the distinctive differences in hydrophilicity of the core and shell. However, and increase in temperature resulted in an increase in size of the micellar core and a contraction of the micellar shell for the EOVE-MOVE gradient copolymer micelles. These phenomena were explained as being due to a “reel-in” process, shown schematically in Figure-1.30 [63]. The gradient copolymers form micelles with a diffuse interface, and the hydrophobic interactions between the core segments are weaker than within the block copolymer micelles. With an increase in temperature, the contribution from the hydrophobic interactions dominates the hydrophobic hydration effect of MOVE segments, akin to reeling in of a fishing wire, resulting in formation of smaller micelles with larger cores than those formed at lower temperatures.

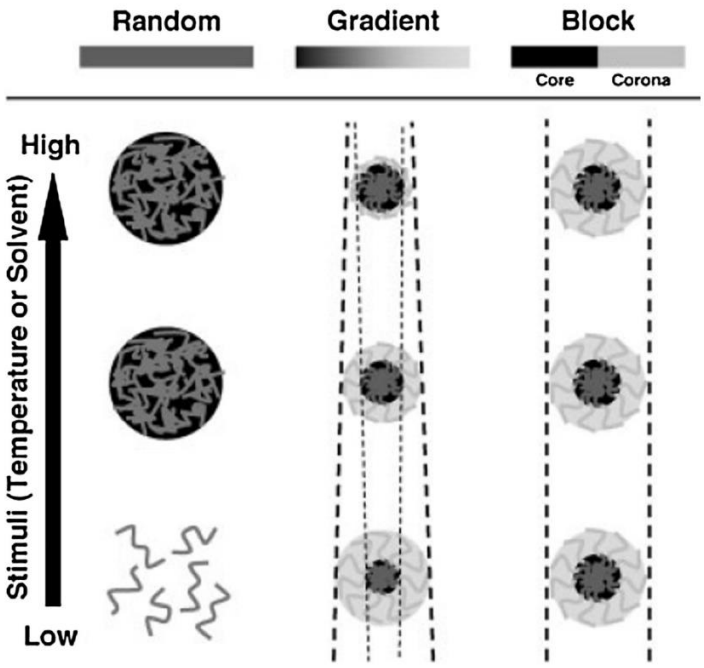

Figure-1.30: Schematic illustration of micellization behaviour in solutions of stimuli-responsive gradient, block and statistical copolymers [221].

A number of other studies of the micellization of gradient copolymers reported similar behaviour of gradient copolymers [95, 98, 128, 229, 230]. Borisov and co-workers observed 'kinetically frozen' micelles for block copolymers of AA/St incapable of rearrangement on variation in environment, while gradient copolymers of the same monomers micelles redissolve completely when the pH was increased [95, 229]. Similar shrinkage of micelles caused by changes in pH was demonstrated by Luo et al. in the methyl acrylic acid (MAA)/MMA gradient copolymer system [109].

Borisova and co-workers [108] used small-angle neutron scattering (SANS) to examine the behaviour of St/AA copolymers in aqueous solution. The SANS data exhibited a correlation peak pointing to the formation of micelles with repulsive coronae. TEM images showed that the micelles had an approximately spherical shape and exhibited a wide size distribution. They claimed to prove that, in contrast to 'frozen' aggregates formed by PAA-b-PS copolymers in aqueous media, the micelles of PAA-block-(PAA-grad-PS) amphiphilic copolymers exhibit 'dynamic' pH-responsive properties, i.e. they can reversibly change their aggregation number upon a variation in the pH or ionic strength of the solution [108]. As a result of the presence of both hydrophobic styrene and pH-sensitive acrylic acid comonomer units in the terminal gradient blocks, the block-gradient copolymers were capable of reversible association into nano-scale aggregates (micelles) in aqueous solution. By combining dynamic light scattering (DLS) and SANS methods, they proved that a

decrease in the pH of the solution below a certain threshold led to formation of the nano-scale aggregates, which disassembled upon a subsequent increase in pH.

Zheng et al. [230] studied the micellization behaviour of St/MMA gradient copolymers in binary acetone-water mixtures. Three different kinds of transitions were observed sequentially in response to an increase in water content (WC), namely a unimer-to-micelle transition, a 'star-like' micelle to 'crew-cut' micelle transition resulting from shrinkage of the micelles, and a morphological transition from spherical micelles to cylindrical micelles and to vesicles (Figure-1.31). Changes in the solvent quality induced the gradual collapse of the gradient copolymer chains and a change in the proportion of solvated chains and collapsed chains; the details of the interactions determined the type of the transition in the system. As a result, three kind of transitions have been observed from a single gradient copolymer micelle system regulated by solvent quality [230]. Chen et al. [128] and Pispas and co-workers [98] also reported similar structures for gradient copolymer micelles.

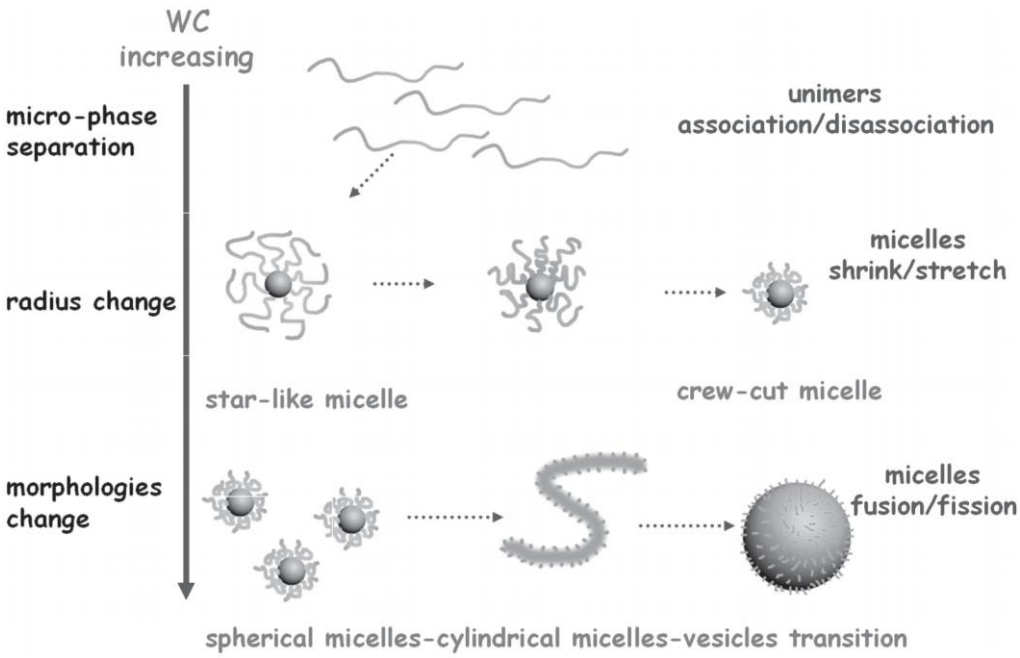

Figure-1.31: Schematic illustration of the overall transitions of the gradient copolymer micellar system via increasing the water content in acetone–water mixtures: unimers to micelles transition; star-like micelles to crew-cut micelles transition; and morphological transition from spherical micelles to cylindrical micelles to vesicles [230].

Huang and co-workers [112] reported that the temperature-induced shrinkage/ stretching of St/MMA gradient copolymer micelles was totally reversible after several heating–cooling cycles between 288 K and 303 K, indicating that this process is thermodynamically controlled. Based on the model and experimental analysis, it was proposed that temperature responsiveness is an intrinsic and universal property of gradient copolymer micelles, and originates from the gradient structure [112].

Kravchenko et al. [231] performed computer simulations to reveal the difference in internal structures of micelles formed by gradient copolymers and equivalent diblock copolymers in a selective solvent. In contrast to the diblock copolymer micelles, segregation of the different groups in the gradient copolymer micelles is less pronounced even in a strongly selective solvent. The sensitivity of the size of the gradient copolymer micelles to a change in the solvent quality is provided by the presence of insoluble units in the corona. A decrease in solvent quality drives solvophobic groups into the core of the micelle, and induces aggregation of other insoluble groups in the corona. As a result, the corona becomes less swollen and the total size of the micelle decreases as shown in Figure-1.32.

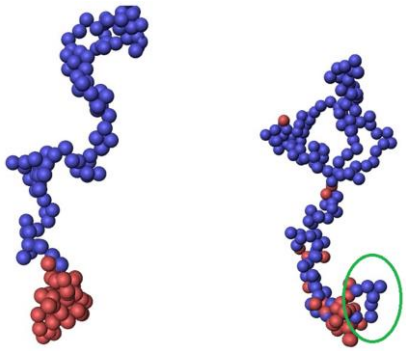

Figure-1.32: Typical conformations of diblock copolymers (left) and exponential gradient copolymers (right) in their corresponding micelles. The green circle depicts a loop formed by the soluble block near the core-shell interface [231].

Rebaut and co-workers [227] studied the solubility of gradient copolymers in supercritical CO_2, and compared these with the analogous block copolymers. Cloud point measurements showed that the gradient copolymers were soluble under milder conditions of pressure and temperature than the block copolymers. Similar to observations in aqueous solutions, the block copolymers form ‘frozen’ aggregates in $scCO_2$, whereas the gradient copolymers form ‘dynamic’ aggregates which are environmentally sensitive [222].

Natalia and co-workers measured the lower critical solution properties of solutions of EOx/nPrOx statistical and gradient copolymers as a function of temperature during heating and cooling cycles [141]. As shown in Figure-1.33, at 5 mg/mL concentration, the hysteresis of the phase transition for the statistical copolymer was negligible, while for the gradient copolymer a pronounced hysteresis was observed regardless of the copolymer composition. The hysteresis was more pronounced for the gradient copolymer of MOx/nPrOx, and the difference in T_{CP} between heating and cooling runs was reported to be equal to 7-9 °C.

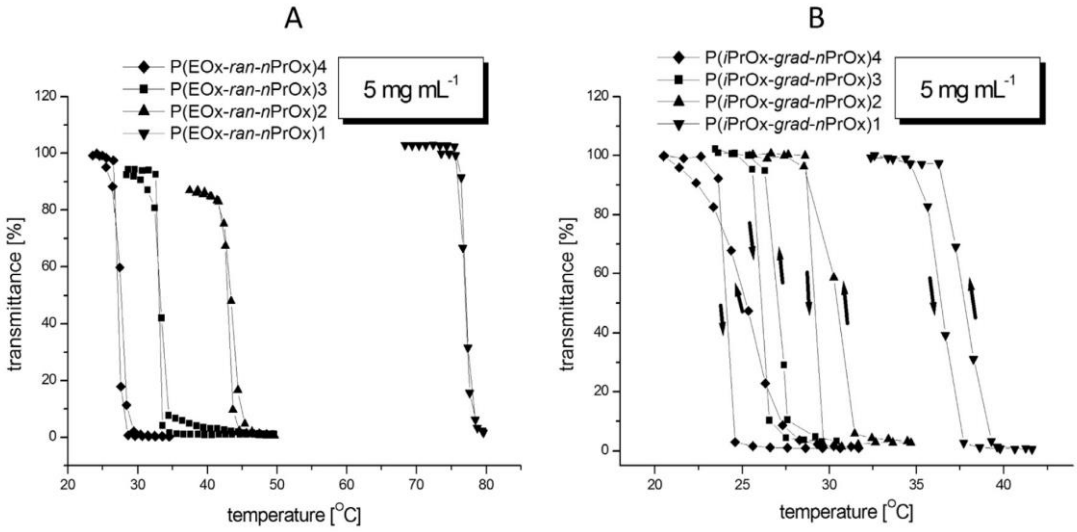

Figure-1.33: Transmittance curves during heating and cooling of 5 mg/mL aqueous solution of EOx/nPrOx (A) statistical and (B) gradient copolymers [141].

1.2.3.4 Mechanical and other Properties

Gradient copolymers also possess unique mechanical properties compared with block and statistical copolymers. Zaremski and co-workers [232] reported that gradient copolymers of styrene-methyl acrylate possessed a lower elastic modulus, higher elongation at break and higher tensile strength compared to statistical copolymers of the same composition. This is in accordance with the results reported by Michler and co-workers [233], in which a St/butadiene tapered copolymer exhibited much superior tensile properties than the corresponding neat block copolymer. Similar results have been reported by Guo et al. [172] for St/nBA copolymers, and the observations were ascribed to reduction in the stress concentration resulting from the gradual change in local modulus within different types of nanodomains and the smaller nanodomains of the gradient copolymers. The mechanical properties of the gradient copolymers were more sensitive to temperature than their

block copolymer counterparts [172]. As shown in Figure-1.34, the diblock copolymer broke at only 6% elongation, like a brittle plastic, in contrast to the linear gradient copolymer, which behaved like an elastomer with an elongation at break over 300% [172].

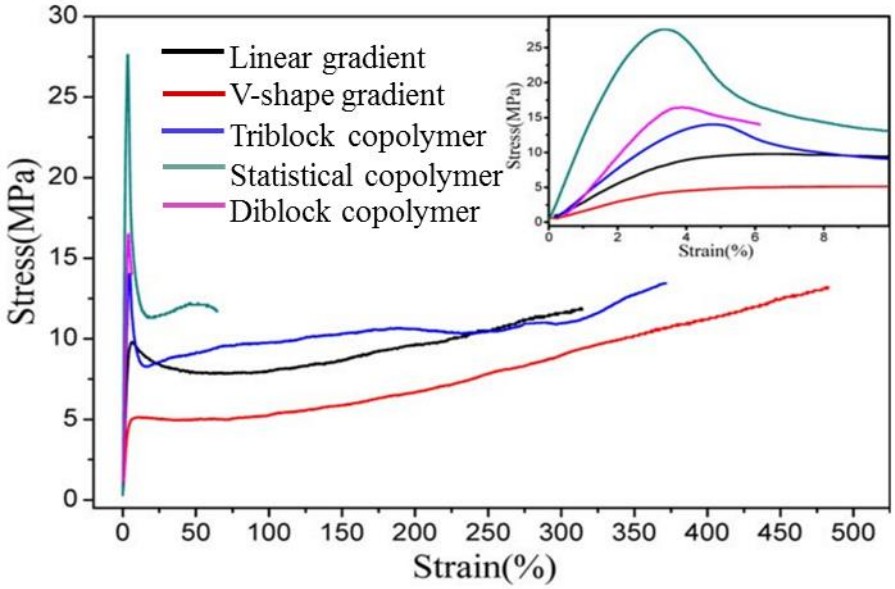

Figure-1.34: Tensile tests of statistical, linear and V-shape gradient, diblock and triblock St/nBA copolymers at 25 °C. The inset enlarges the small strain portion to show the yield (figure adapted from [172]).

Zheng et al. [171] measured the conductivity of gel polymer electrolytes prepared from different copolymers with a range of contents of electrolytes. The gradient copolymers exhibited remarkably higher ion conductivity than the block and statistical copolymers for the same uptake of the liquid electrolyte, and the differences in behaviour clearly resulted from the differences in their copolymer chain structures. It was proposed that in a film, continuous ionic conducting pathways are formed by connecting polar conductive domains, which are always circuitous. If strong phase separation and distinctive domain boundaries exist, the nonpolar domains may isolate some polar domains, form numerous dead ends, and intersect the polar pathways [234-236]. In comparison, the gradient copolymer based gel polymer electrolyte had no sharp domain boundaries in morphology because of the gradient chain structure (Figure-1.35). Therefore, highly connected conducting pathways were formed, eliminating or minimizing the interruptions of the conducting domains, and significantly facilitating fast and efficient Li ion transport.

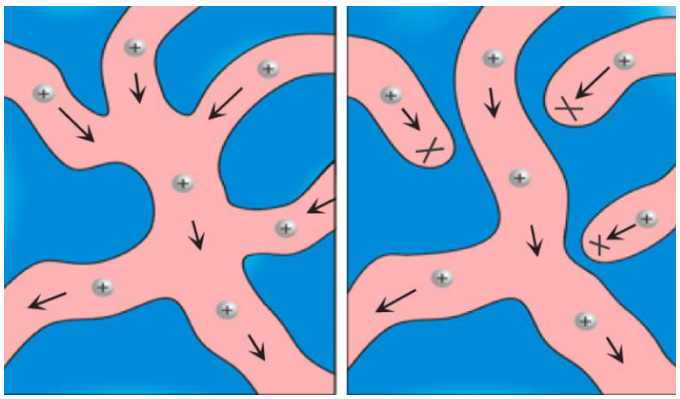

Figure-1.35: Proposed continuous conducting pathways for gradient copolymers, and pathways with dead ends for block copolymers [171].

1.2.4 An Overview of the Applications of Gradient Copolymers

The uniqueness in the structure of the gradient copolymers gives them a number of unique properties, and as a result gradient copolymers have immense potential in a number of applications. A very attractive aspect of gradient copolymers is that their properties can be optimized by fine-tuning the copolymer structure. One of the most common application is as compatibilizers for immiscible polymer blends [49, 60, 61, 87-89]. Multiple reports have experimentally shown the impact of the incorporation of gradient copolymers on mixing in otherwise immiscible homopolymer blends. Other applications reported for gradient copolymers include as stabilizers of emulsions or dispersions [90], as thermoplastic elastomers [91, 92], and multi-shape memory materials [93]. Gradient copolymers with broad glass transition behaviour can be designed to yield materials with excellent damping behaviour [81, 86].

Amphiphilic fluorinated gradient copolymers with optimized hydrophilicity and low surface energy segments exhibit excellent antifouling performance [170]. Besides the well-known application of such amphiphilic structures as detergents and stabilizers, the micelles formed by self-assembly of amphiphilic gradient copolymers in aqueous medium can be used as micellar catalysis and in drug delivery [197, 237] and amphiphilic gradient copolymers have also been used to fabricate nano-carriers in biocompatible media [94]. Stable spherical nanostructures formed by gradient copolymers of 2-methyl-2-oxazoline and 2-phenyl-2-oxazoline (MPOx) are capable of delivering DNA chains [115], and the stable MPOx/DNA complexes demonstrate potential in broad applications in the biomedical field.

Zheng et al. [171] evaluated a series of statistical, block and gradient St-co-MA copolymers as polymer electrolytes. They found that the gradient copolymers yielded the highest lithium ion conductivity (10^{-3} S cm^{-1}), of the three architectures studied, by providing continuous ion conductive pathways. It is proposed, therefore, that gradient copolymers could be a much better replacement for the commonly used statistical copolymer gel electrolytes.

1.2.5 Summary of Gradient Copolymers

The field of conventional radical polymerization has experienced enormous development over the past two-three decades. In particular, the invention of controlled radical polymerization techniques such as ATRP, NMP, RAFT provide the freedom to design and prepare homo and copolymers with precise control over molecular weight, molecular weight dispersity, and the distribution of monomer units in the copolymer chains, for a wide range of monomer pairs. These advances in the polymerization techniques have allowed the introduction of 'gradient copolymers', a novel class of copolymers with unique structure compared with conventional statistical and block copolymers. Theory tells us that the properties of copolymers are strongly dependent on not only their compositions, but also on the distribution of monomer units along the copolymer chains. This has been confirmed by comparison of interfacial properties, thermal properties and micellization properties of gradient copolymers with those of statistical and block copolymers. Microscopic analyses suggest no evident phase boundaries are formed in gradient copolymers due to weak phase segregation, in contrast with equivalent block copolymers. The uniqueness in the properties of the gradient copolymers owing to their unique structures are also visible in their thermal properties. Gradient copolymers show a broad glass temperature due to the drift in composition along the chain, while block copolymers generally possess two transitions, and statistical copolymers show a single sharp T_g. Gradient copolymers also demonstrate unique self-assembly behaviour in solution. Micelles of gradient copolymers can be designed to be sensitive to the changes in temperature, pH and solvent quality. Gradient copolymers have wide practical application, for example as compatibilizers for immiscible polymer blends, as stabilizers of emulsions or dispersions, as multi-shape memory materials, and also in the biomedical field. With their unique structures and properties, gradient copolymers possess immense potential to be applied in many other different polymer-based applications.

1.3 Summary

Among many others, the type of resist materials is one of the important sources of LER in photolithographic devices. The heterogeneity of the resist materials in the line edge region forms different phases which leads to LER. On the other hand, it has been proved that the properties of copolymers are directly dependent on not only the composition, but also on the monomer distribution in the copolymer chains. The gradient copolymers exhibit unique interfacial, thermal, and solution properties than those of the conventional statistical and block copolymers owing to their unique chain structures.

In this thesis, two different monomer pairs have been chosen for the synthesis of statistical, block and gradient copolymers, and to study the dependence of their properties on chain structures. Styrene-Acrylonitrile (St-AN) copolymer system was chosen due to their ability to produce natural gradients in their structures. The significant difference of the reactivity ratios of St and AN produces gradient copolymers at specific monomer feed ratios. Also, due to the completely resolved triad peaks, the change in the triad distributions in the St-AN copolymer structure was possible to prove. The second monomer pair studied in this thesis was Acetoxystyrene – t-butyl acrylate (AOST-tBA). This pair was chosen in particular to mimic one of the commercial photoresists, TER60.

The aim this study is to prepare gradient copolymers (either spontaneous or forced) with compositional gradient in the chain structures, in addition to the conventional statistical and block copolymers by RAFT and CvRP methods for St-AN and AOST-tBA systems. The properties of the copolymers in bulk as well as on the thin films will be studied to understand the relation between the properties and the chain structures of the copolymers. The focus of this study was to preparing copolymers with well-defined structures and understanding properties. The study of LER was not possible due to limited time frame.

1.4 References

[1] Constantoudis V, Kokkoris G, Gogolides E, Pargon E, Martin M. Effects of resist sidewall morphology on line-edge roughness reduction and transfer during etching: is the resist sidewall after development isotropic or anisotropic? MOEMS. 2010;9:041209--11.

[2] Peters AJ, Lawson RA, Ludovice PJ, Henderson CL. Effects of block copolymer polydispersity and χN on pattern line edge roughness and line width roughness from directed self-assembly of diblock copolymers. Proc SPIE. 2013;8680:1-8.

[3] Zhao X, Lee S-Y, Choi J, Lee S-H, Shin I-K, Jeon C-U. Minimization of line edge roughness and critical dimension error in electron-beam lithography. J Vac Sci Technol, B: Nanotechnol Microelectron: Mater, Process, Meas, Phenom. 2014;32:1-13.
[4] Kozawa T, Santillan JJ, Itani T. Effects of deprotonation efficiency of protected units on line edge roughness and stochastic defect generation in chemically amplified resist processes for 11 nm node of extreme ultraviolet lithography. Jpn J Appl Phys. 2014;53:116504/1-/5, 5 pp.
[5] Kozawa T, Tagawa S, Santillan JJ, Toriumi M, Itani T. Image contrast slope and line edge roughness of chemically amplified resists for postoptical lithography. J Vac Sci Technol, B: Microelectron Nanometer Struct--Process, Meas, Phenom. 2007;25:2295-300.
[6] Sanchez MI, Hinsberg WD, Houle FA, Hoffnagle JA, Ito H, Nguyen C. Aerial image contrast using interferometric lithography: effect on line-edge roughness. Proc SPIE-Advances in Resist Technology and Processing XVI. 1999;3678:160-71.
[7] Lin Q, Black CT, Detavernier C, Gignac L, Guarini K, Herbst B, et al. Does line-edge roughness matter?: FEOL and BEOL perspectives. Proc SPIE-Int Soc Opt Eng. 2003;5039:1076-85.
[8] Lin Q, Sooriyakumaran R, Huang W-S. Toward controlled resist line-edge roughness: material origin of line-edge roughness in chemically amplified positive-tone resists. Proc SPIE-Int Soc Opt Eng. 2000;3999:230-9.
[9] Cho IW, Kim H, Hong J-Y, Oh H-K, Kim SW. Reduction of line width and edge roughness by using a resist reflow process for extreme ultraviolet lithography. J Korean Phys Soc. 2010;56:1767-71.
[10] Bolten J, Wahlbrink T, Koo N, Kurz H, Stammberger S, Hofmann U, et al. Improved CD control and line edge roughness in E-beam lithography through combining proximity effect correction with gray scale techniques. Microelectron Eng. 2010;87:1041-3.
[11] Chuang Y-M, Cheng H-H, Jack K, Whittaker A, Blakey I. Healing LER using directed self assembly: treatment of EUVL resists with aqueous solutions of block copolymers. Proc SPIE. 2013;8680:1-10.
[12] Stoykovich MP, Daoulas KC, Muller M, Kang H, de Pablo JJ, Nealey PF. Remediation of Line Edge Roughness in Chemical Nanopatterns by the Directed Assembly of Overlying Block Copolymer Films. Macromolecules. 2010;43:2334-42.
[13] Yamaguchi T, Yamazaki K, Namatsu H. Influence of molecular weight of resist polymers on surface roughness and line-edge roughness. Journal of Vacuum Science and Technology B. 2004;22:2604-10.
[14] Yamaguchi T, Yamazaki K, Namatsu H. Molecular weight effect on line-edge roughness. Proc SPIE-Advances in Resist Technology and Processing XX. 2003;5039:1212-9.
[15] Kozawa T, Santillan JJ, Itani T. Effect of molecular weight and protection ratio on line edge roughness and stochastic defect generation in chemically amplified resist processes of extreme ultraviolet lithography. Jpn J Appl Phys. 2014;53:084002/1-/6, 6 pp.

[16] Yoshimura T, Nakayama Y, Okazaki S. Acid-diffusion effect on nanofabrication in chemical amplification resist. J Vac Sci Technol, B. 1992;10:2615-19.
[17] Stewart MD, Schmid GM, Goldfarb DL, Angelopoulos M, Willson CG. Diffusion-induced line-edge roughness. Proc SPIE-Advances in Resist Technology and Processing XX. 2003;5039:415-22.
[18] Tsiartas PC, Flanagin LW, Henderson CL, Hinsberg WD, Sanchez IC, Willson CG. Mechanism of Phenolic Polymer Dissolution. Macromolecules. 1997;30:4656-64.
[19] Reynolds GW, Taylor JW. Factors contributing to sidewall roughness in a positive-tone, chemically amplified resist exposed by x-ray lithography. J Vac Sci Technol, B. 1999;17:334-44.
[20] Sanchez MI, Hinsberg WD, Houle FA, Hoffnagle JA, Ito H, Nguyen CV. Aerial image contrast using interferometric lithography: effect on line-edge roughness. 1999;3678:160-71.
[21] Shin J, Han G, Ma Y, Moloni K, Cerrina F. Resist line edge roughness and aerial image contrast. J Vac Sci Technol, B. 2001;19:2890-5.
[22] Reynolds GW, Taylor JW, Brooks CJ. Direct measurement of x-ray mask sidewall roughness and its contribution to the overall sidewall roughness of chemically amplified resist features. J Vac Sci Technol, B. 1999;17:3420-5.
[23] Fuller SE, Young M. Photomask-edge-roughness characterization using an atomic force microscope. Proc SPIE-Metrology, Inspection, and Process Control for Microlithography XII. 1998;3332:433-40.
[24] Patsis GP, Constantoudis V, Gogolides E. Material origins of line-edge roughness: Monte Carlo simulations and scaling analysis. Proc SPIE-Int Soc Opt Eng. 2004;5376:773-81.
[25] Shiraishi H, Yoshimura T, Sakamizu T, Ueno T, Okazaki S. Nanometer-scale imaging characteristics of novolak resin-based chemical amplification negative resist systems and molecular weight distribution effects of the resin matrix. J Vac Sci Technol, B. 1994;12:3895-9.
[26] Fuller SE, Young M. Photomask-edge-roughness characterization using an atomic force microscope. 1998;3332:433-40.
[27] Brainard RL, Trefonas P, Lammers JH, Cutler CA, Mackevich JF, Trefonas A, et al. Shot noise, LER, and quantum efficiency of EUV photoresists. Proc SPIE-Int Soc Opt Eng. 2004;5374:74-85.
[28] Rau N, Stratton F, Fields C, Ogawa T, Neureuther A, Kubena R, et al. Shot-noise and edge roughness effects in resists patterned at 10 nm exposure. J Vac Sci Technol, B. 1998;16:3784-8.
[29] Bhattarai S, Chao W, Neurether AR, Neaulleau PP. Comparative analysis of shot noise in EUV and E-beam lithography. Proc SPIE. 2014;9048:90481H/1-H/11.
[30] Stewart MD, Schmid GM, Goldfarb DL, Angelopoulos M, Willson CG. Diffusion-induced line-edge roughness. 2003;5039:415-22.
[31] Schmid GM, Stewart MD, Singh VK, Willson CG. Spatial distribution of reaction products in positive tone chemically amplified resists. Journal of Vacuum Science and Technology B. 2002;20:185-90.

[32] Itani T, Kozawa T. Resist materials and processes for extreme ultraviolet lithography. Jpn J Appl Phys. 2013;52:010002/1-/14.
[33] Ban Y, Sundareswaran S, Panda R, Pan DZ. Electrical impact of line-edge roughness on sub-45 nm node standard cell. Proc SPIE. 2009;7275:727518/1-/10.
[34] Yamaguchi A, Ichinose K, Shimamoto S, Fukuda H, Tsuchiya R, Ohnishi K, et al. Metrology of LER: influence of line-edge roughness (LER) on transistor performance. Proc SPIE-Int Soc Opt Eng. 2004;5375:468-76.
[35] Shibata K, Izumi N, Tsujita K. Influence of line-edge roughness on MOSFET devices with sub-50-nm gates. Proc SPIE-Int Soc Opt Eng. 2004;5375:865-73.
[36] Diaz CH, Hun-Jan T, Yao-Ching K, Yen A, Young K. An experimentally validated analytical model for gate line-edge roughness (LER) effects on technology scaling. Electron Device Letters, IEEE. 2001;22:287-9.
[37] Kim H-W, Lee J-Y, Shin J, Woo S-G, Cho H-K, Moon J-T. Experimental investigation of the impact of LWR on sub-100-nm device performance. IEEE Trans Electron Devices. 2004;51:1984-8.
[38] Patsis GP, Constantoudis V, Gogolides E. Integrated simulation of line-edge roughness (LER) effects on sub-65 nm transistor operation: from lithography simulation, to LER metrology, to device operation. Proc SPIE-Int Soc Opt Eng. 2006;6151:61513J/1-J/11.
[39] Oldiges P, Lin Q, Petrillo K, Sanchez M, Meikei I, Hargrove M. Modeling line edge roughness effects in sub 100 nanometer gate length devices. Simulation of Semiconductor Processes and Devices, 2000 SISPAD 2000 2000 International Conference on. 2000:131-4.
[40] Ban Y, Sundareswaran S, Pan DZ. Electrical impact of line-edge roughness on sub-45-nm node standard cells. MOEMS. 2010;9:041206--10.
[41] Bolten J, Wahlbrink T, Schmidt M, Gottlob HDB, Kurz H. Implementation of electron beam grey scale lithography and proximity effect correction for silicon nanowire device fabrication. Microelectron Eng. 2011;88:1910-2.
[42] Struck CRM, Flauta R, Neumann MJ, Kim KN, Raju R, Bristol RL, et al. Grazing incidence broad ion beams for reducing line-edge roughness. J Micromech Microeng. 2010;20:075038/1-/6.
[43] Cheng JY, Sanders DP, Truong HD, Harrer S, Friz A, Holmes S, et al. Simple and Versatile Methods To Integrate Directed Self-Assembly with Optical Lithography Using a Polarity-Switched Photoresist. ACS Nano. 2010;4:4815-23.
[44] Kozawa T, Santillan JJ, Itani T. Analysis of stochastic effect in line-and-space resist patterns fabricated by extreme ultraviolet lithography. Appl Phys Express. 2013;6:026502/1-/4.
[45] Barner-Kowollik C, Editor. Handbook of RAFT Polymerization. Weinheim, Germany: Wiley-VCH; 2008.
[46] Khokhlov AR, Berezkin AV, Khalatur PG. Computer modeling of radical copolymerization under unusual conditions. J Polym Sci, Part A: Polym Chem. 2004;42:5339-53.

[47] Lefebvre MD, Dettmer CM, McSwain RL, Xu C, Davila JR, Composto RJ, et al. Effect of Sequence Distribution on Copolymer Interfacial Activity. Macromolecules. 2005;38:10494-502.
[48] Lefebvre MD, Olvera de la Cruz M, Shull KR. Phase Segregation in Gradient Copolymer Melts. Macromolecules. 2004;37:1118-23.
[49] Wang R, Li W, Luo Y, Li B-G, Shi A-C, Zhu S. Phase Behavior of Ternary Homopolymer/Gradient Copolymer Blends. Macromolecules (Washington, DC, U S). 2009;42:2275-85.
[50] Wong CLH, Kim J, Torkelson JM. Breadth of glass transition temperature in styrene/acrylic acid block, random, and gradient copolymers: unusual sequence distribution effects. J Polym Sci, Part B: Polym Phys. 2007;45:2842-9.
[51] Mok MM, Ellison CJ, Torkelson JM. Effect of Gradient Sequencing on Copolymer Order-Disorder Transitions: Phase Behavior of Styrene/n-Butyl Acrylate Block and Gradient Copolymers. Macromolecules (Washington, DC, U S). 2011;44:6220-6.
[52] Zhang G, Zhang Q, Wang Q, Zhan X, Chen F. Synthesis and properties of gradient copolymers of butyl methacrylate and fluorinated acrylate via RAFT miniemulsion copolymerizations. J Appl Polym Sci. 2016;133:n/a.
[53] Gallow KC. Synthesis of gradient copolymers and their properties in dilute solution and the melt: Princeton University; 2013.
[54] Bates FS, Fredrickson GH. Block copolymer thermodynamics: theory and experiment. Annu Rev Phys Chem. 1990;41:525-57.
[55] Krejchi MT, Atkins EDT, Waddon AJ, Fournier MJ, Mason TL, Tirrell DA. Chemical sequence control of β-sheet assembly in macromolecular crystals of periodic polypeptides. Science (Washington, D C). 1994;265:1427-32.
[56] Yu SM, Conticello VP, Zhang G, Kayser C, Fournier MJ, Mason TL, et al. Smectic ordering in solutions and films of a rod-like polymer owing to monodispersity of chain length. Nature (London). 1997;389:167-70.
[57] Fasolka MJ, Mayes AM. Block copolymer thin films: physics and applications. Annu Rev Mater Res. 2001;31:323-55.
[58] Matyjaszewski K, Tsarevsky NV. Nanostructured functional materials prepared by atom transfer radical polymerization. Nat Chem. 2009;1:276-88.
[59] Patten TE, Matyjaszewski K. Atom-transfer radical polymerization and the synthesis of polymeric materials. Adv Mater (Weinheim, Ger). 1998;10:901-15.
[60] Kim J, Gray MK, Zhou H, Nguyen ST, Torkelson JM. Polymer Blend Compatibilization by Gradient Copolymer Addition during Melt Processing: Stabilization of Dispersed Phase to Static Coarsening. Macromolecules. 2005;38:1037-40.
[61] Kim J, Sandoval RW, Dettmer CM, Nguyen ST, Torkelson JM. Compatibilized polymer blends with nanoscale or sub-micron dispersed phases achieved by hydrogen-bonding effects: Block copolymer vs blocky gradient copolymer addition. Polymer. 2008;49:2686-97.

[62] Malik R, Hall CK, Genzer J. Effect of copolymer compatibilizer sequence on the dynamics of phase separation of immiscible binary homopolymer blends. Soft Matter. 2011;7:10620-30.
[63] Okabe S, Seno K-i, Kanaoka S, Aoshima S, Shibayama M. Micellization Study on Block and Gradient Copolymer Aqueous Solutions by DLS and SANS. Macromolecules. 2006;39:1592-7.
[64] Sun X, Luo Y, Wang R, Li B-G, Zhu S. Semibatch RAFT polymerization for producing ST/BA copolymers with controlled gradient composition profiles. AIChE J. 2008;54:1073-87.
[65] Paris R, De La Fuente JL. Glass transition temperature of allyl methacrylate-n-butyl acrylate gradient copolymers in dependence on chemical composition and molecular weight. J Polym Sci, Part B: Polym Phys. 2007;45:1845-55.
[66] Tonnar J, Lacroix-Desmazes P. One-pot surfactant-free functional latexes by controlled radical polymerization in ab initio emulsion. Soft Matter. 2008;4:1255-60.
[67] Park J-S, Kataoka K. Comprehensive and Accurate Control of Thermosensitivity of Poly(2-alkyl-2-oxazoline)s via Well-Defined Gradient or Random Copolymerization. Macromolecules (Washington, DC, U S). 2007;40:3599-609.
[68] Phan TNT, Maiez-Tribut S, Pascault J-P, Bonnet A, Gerard P, Guerret O, et al. Synthesis and Characterizations of Block Copolymer of Poly(n-butyl acrylate) and Gradient Poly(methyl methacrylate-co-N,N-dimethyl acrylamide) Made via Nitroxide-Mediated Controlled Radical Polymerization. Macromolecules (Washington, DC, U S). 2007;40:4516-23.
[69] Vidts KRM, Dervaux B, Du Prez FE. Block, blocky gradient and random copolymers of 2-ethylhexyl acrylate and acrylic acid by atom transfer radical polymerization. Polymer. 2006;47:6028-37.
[70] Kraus G, Childers CW, Gruver JT. Properties of random and block copolymers of butadiene and styrene. I. Dynamic properties and glass-transition temperatures. J Appl Polym Sci. 1967;11:1581-91.
[71] Kraus G, Rollmann KW. Effects of monomer sequence on the viscoelastic behavior of random copolymers of butadiene and styrene. Angew Makromol Chem. 1971;16/17:271-96.
[72] Tsukahara Y, Nakamura N, Hashimoto T, Kawai H, Nagaya T, Sugimura Y, et al. Structure and properties of tapered block polymers of styrene and isoprene. Polym J (Tokyo). 1980;12:455-66.
[73] Hashimoto T, Tsukahara Y, Kawai H. Structure and properties of tapered block polymers of styrene and isoprene. II. Dynamic mechanical responses and their structural interpretations. Polym J (Tokyo). 1983;15:699-711.
[74] Hashimoto T, Tsukahara Y, Tachi K, Kawai H. Structure and properties of tapered block polymers. 4. "Domain-boundary mixing" and "mixing-in-domain" effects on microdomain morphology and linear dynamic mechanical response. Macromolecules. 1983;16:648-57.
[75] Mok MM, Kim J, Torkelson JM. Gradient copolymers with broad glass transition temperature regions: Design of purely interphase compositions for damping applications. Journal of Polymer Science Part B: Polymer Physics. 2008;46:48-58.

[76] Jiang R, Jin Q, Li B, Ding D, Wickham RA, Shi A-C. Phase Behavior of Gradient Copolymers. Macromolecules. 2008;41:5457-65.
[77] Jakubowski W, Juhari A, Best A, Koynov K, Pakula T, Matyjaszewski K. Comparison of thermomechanical properties of statistical, gradient and block copolymers of isobornyl acrylate and n-butyl acrylate with various acrylate homopolymers. Polymer. 2008;49:1567-78.
[78] Fu C, Yang B, Zhu C, Wang S, Zhang Y, Wei Y, et al. Synthesis of gradient copolymers by concurrent enzymatic monomer transformation and RAFT polymerization. Polym Chem. 2013;4:5720-5.
[79] Matyjaszewski K, Shipp DA, McMurtry GP, Gaynor SG, Pakula T. Simple and effective one-pot synthesis of (meth)acrylic block copolymers through atom transfer radical polymerization. J Polym Sci, Part A: Polym Chem. 2000;38:2023-31.
[80] Matyjaszewski K, Ziegler MJ, Arehart SV, Greszta D, Pakula T. Gradient copolymers by atom transfer radical copolymerization. J Phys Org Chem. 2000;13:775-86.
[81] Kim J, Mok MM, Sandoval RW, Woo DJ, Torkelson JM. Uniquely Broad Glass Transition Temperatures of Gradient Copolymers Relative to Random and Block Copolymers Containing Repulsive Comonomers. Macromolecules. 2006;39:6152-60.
[82] Shull KR. Interfacial Activity of Gradient Copolymers. Macromolecules. 2002;35:8631-9.
[83] Aksimentiev A, Holyst R. Phase behavior of gradient copolymers. J Chem Phys. 1999;111:2329-39.
[84] Slimani MZ, Moreno AJ, Rossi G, Colmenero J. Dynamic Heterogeneity in Random and Gradient Copolymers: A Computational Investigation. Macromolecules (Washington, DC, U S). 2013;46:5066-79.
[85] Mok MM, Kim J, Wong CLH, Marrou SR, Woo DJ, Dettmer CM, et al. Glass Transition Breadths and Composition Profiles of Weakly, Moderately, and Strongly Segregating Gradient Copolymers: Experimental Results and Calculations from Self-Consistent Mean-Field Theory. Macromolecules (Washington, DC, U S). 2009;42:7863-76.
[86] Buzin AI, Pyda M, Costanzo P, Matyjaszewski K, Wunderlich B. Calorimetric study of block-copolymers of poly(n-butyl acrylate) and gradient poly(n-butyl acrylate-co-methyl methacrylate). Polymer. 2002;43:5563-9.
[87] Kim J, Zhou H, Nguyen ST, Torkelson JM. Synthesis and application of styrene/4-hydroxy styrene gradient copolymers made by controlled radical polymerization: Compatibilization of immiscible polymer blends via hydrogen-bonding effects. Polymer. 2006;47:5799-809.
[88] Tao Y, Kim J, Torkelson JM. Achievement of quasi-nanostructured polymer blends by solid-state shear pulverization and compatibilization by gradient copolymer addition. Polymer. 2006;47:6773-81.
[89] Sun D, Cho J. Ring gradient copolymers as amphiphiles in their ternary blends with two linear homopolymers. Polymer. 2015;66:192-200.

[90] Lefay C, Save M, Charleux B, Magnet S. Miniemulsion Polymerization Stabilized by a Well-Defined, Amphiphilic Gradient Poly(styrene-co-acrylic acid) Copolymer. Australian Journal of Chemistry. 2006;59:544-8.
[91] Jouenne S, González-León JA, Ruzette A-V, Lodefier P, Tencé-Girault S, Leibler L. Styrene/Butadiene Gradient Block Copolymers: Molecular and Mesoscopic Structures. Macromolecules. 2007;40:2432-42.
[92] Hodrokoukes P, Floudas G, Pispas S, Hadjichristidis N. Microphase Separation in Normal and Inverse Tapered Block Copolymers of Polystyrene and Polyisoprene. 1. Phase State. Macromolecules. 2001;34:650-7.
[93] Luo Y, Guo Y, Gao X, Li B-G, Xie T. A General Approach Towards Thermoplastic Multishape-Memory Polymers via Sequence Structure Design. Adv Mater (Weinheim, Ger). 2013;25:743-8.
[94] Chen Y, Chen H, Feng M, Dong Y. Amphiphilic gradient copolymers: Synthesis, self-assembly, and applications. Eur Polym J. 2016;85:489-98.
[95] Cernochova Z, Bogomolova A, Borisova OV, Filippov SK, Cernoch P, Billon L, et al. Thermodynamics of the multi-stage self-assembly of pH-sensitive gradient copolymers in aqueous solutions. Soft Matter. 2016;12:6788-98.
[96] Beginn U. Gradient copolymers. Colloid Polym Sci. 2008;286:1465-74.
[97] Pippa N, Kaditi E, Pispas S, Demetzos C. Gradient block copolymer structures as drug nanocarriers. Adv Sci, Eng Med. 2014;6:642-8.
[98] Milonaki Y, Kaditi E, Pispas S, Demetzos C. Amphiphilic gradient copolymers of 2-methyl- and 2-phenyl-2-oxazoline: self-organization in aqueous media and drug encapsulation. J Polym Sci, Part A: Polym Chem. 2012;50:1226-37.
[99] Hoogenboom R, Lambermont-Thijs HML, Jochems MJHC, Hoeppener S, Guerlain C, Fustin C-A, et al. A schizophrenic gradient copolymer: switching and reversing poly(2-oxazoline) micelles based on UCST and subtle solvent changes. Soft Matter. 2009;5:3590-2.
[100] Jiang R, Wang Z, Yin Y, Li B, Shi A-C. Effects of compositional polydispersity on gradient copolymer melts. J Chem Phys. 2013;138:074906/1-/10.
[101] Steinhauer W, Hoogenboom R, Keul H, Moeller M. Block and Gradient Copolymers of 2-Hydroxyethyl Acrylate and 2-Methoxyethyl Acrylate via RAFT: Polymerization Kinetics, Thermoresponsive Properties, and Micellization. Macromolecules (Washington, DC, U S). 2013;46:1447-60.
[102] Chen Y, Luo W, Wang Y, Sun C, Han M, Zhang C. Synthesis and self-assembly of amphiphilic gradient copolymer via RAFT emulsifier-free emulsion polymerization. J Colloid Interface Sci. 2012;369:46-51.
[103] Okabe S, Seno K-i, Kanaoka S, Aoshima S, Shibayama M. Small-angle neutron scattering study on block and gradient copolymer aqueous solutions. Polymer. 2006;47:7572-9.
[104] Hoogenboom R, Thijs HML, Wouters D, Hoeppener S, Schubert US. Solvent Responsive Micelles Based on Block and Gradient Copoly(2-oxazoline)s. Macromolecules. 2008;41:1581-3.

[105] Bloksma MM, Hoeppener S, D'Haese C, Kempe K, Mansfeld U, Paulus RM, et al. Self-assembly of chiral block and gradient copolymers. Soft Matter. 2012;8:165-72.
[106] Glassner M, Lava K, Rosa VR, Hoogenboom R. Tuning the LCST of poly(2-cyclopropyl-2-oxazoline) via gradient copolymerization with 2-ethyl-2-oxazoline. J Polym Sci, Part A: Polym Chem. 2014;52:3118-22.
[107] Harrisson S, Ercole F, Muir BW. Living spontaneous gradient copolymers of acrylic acid and styrene: one-pot synthesis of pH-responsive amphiphiles. Polym Chem. 2010;1:326-32.
[108] Borisova O, Billon L, Zaremski M, Grassl B, Bakaeva Z, Lapp A, et al. Synthesis and pH- and salinity-controlled self-assembly of novel amphiphilic block-gradient copolymers of styrene and acrylic acid. Soft Matter. 2012;8:7649-59.
[109] Zhao Y, Luo Y-W, Li B-G, Zhu S. pH Responsivity and Micelle Formation of Gradient Copolymers of Methacrylic Acid and Methyl Methacrylate in Aqueous Solution. Langmuir. 2011;27:11306-15.
[110] Li J-J, Zhou Y-N, Luo Z-H. Synthesis and pH-responsive micellization of brush copolymers poly(methyl methacrylate-co-2-(2-bromoisobutyryloxy)ethyl methacrylate-graft-acrylic acid): role of composition profile. Soft Matter. 2012;8:11051-61.
[111] Okabe S, Fuse C, Sugihara S, Aoshima S, Shibayama M. Structural transition in block and gradient copolymer aqueous solutions. Physica B: Condensed Matter. 2006;385–386, Part 1:756-8.
[112] Zheng C, Huang H, He T. Gradient Structure-Induced Temperature Responsiveness in Styrene/Methyl Methacrylate Gradient Copolymers Micelles. Macromol Rapid Commun. 2014;35:309-16.
[113] Chen Y, Zhang Y, Wang Y, Sun C, Zhang C. Synthesis, characterization, and self-assembly of amphiphilic fluorinated gradient copolymer. J Appl Polym Sci. 2013;127:1485-92.
[114] Suarez P, Rojo L, Gonzalez-Gomez A, Roman JS. Self-assembling gradient copolymers of vinylimidazol and (acrylic)ibuprofen with anti-inflammatory and zinc chelating properties. Macromol Biosci. 2013;13:1174-84.
[115] Vlassi E, Pispas S. Solution Behavior of Hydrolyzed Gradient Methyl/Phenyl Oxazoline Copolymers and Complexation with DNA. Macromolecular Chemistry and Physics. 2015;216:873-83.
[116] Pippa N, Merkouraki M, Pispas S, Demetzos C. DPPC:MPOx chimeric advanced Drug Delivery nano Systems (chi-aDDnSs): Physicochemical and structural characterization, stability and drug release studies. International Journal of Pharmaceutics. 2013;450:1-10.
[117] Guo Y, Zhang J, Xie P, Gao X, Luo Y. Tailor-made compositional gradient copolymer by a many-shot RAFT emulsion polymerization method. Polym Chem. 2014;5:3363-71.
[118] Kalugin DI, Zaremski MY, Golubev VB, Garina ES. Synthesis of gradient copolymers of styrene and tert-butyl acrylate by pseudoliving radical polymerization mediated by the reversible inhibitor TEMPO. Polym Sci, Ser B. 2011;53:307-12.

[119] Grubbs RB. Nitroxide-Mediated Radical Polymerization: Limitations and Versatility. Polym Rev (Philadelphia, PA, U S). 2011;51:104-37.
[120] Borisova OV, Billon L, Zaremski MY, Borisov OV. Synthesis of amphiphilic block-gradient copolymers of styrene and acrylic acid by Nitroxide Mediated Polymerization. Polym Sci, Ser C. 2015;57:86-93.
[121] Mignard E, Leblanc T, Bertin D, Guerret O, Reed WF. Online Monitoring of Controlled Radical Polymerization: Nitroxide-Mediated Gradient Copolymerization. Macromolecules. 2004;37:966-75.
[122] Gray MK, Zhou H, Nguyen ST, Torkelson JM. Differences in enthalpy recovery of gradient and random copolymers of similar overall composition: styrene/4-methylstyrene copolymers made by nitroxide-mediated controlled radical polymerization. Polymer. 2004;45:4777-86.
[123] Karaky K, Pere E, Pouchan C, Garay H, Khoukh A, Francois J, et al. Gradient or statistical copolymers by batch nitroxide mediated polymerization: effect of styrene/methyl acrylate feed. New J Chem. 2006;30:698-705.
[124] Nicolas J, Guillaneuf Y, Lefay C, Bertin D, Gigmes D, Charleux B. Nitroxide-mediated polymerization. Prog Polym Sci. 2013;38:63-235.
[125] Matyjaszewski K, Xia J. Atom transfer radical polymerization. Chem Rev. 2001;101:2921-90.
[126] Zhou Y-N, Luo Z-H. Facile synthesis of gradient copolymers via semi-batch copper(0)-mediated living radical copolymerization at ambient temperature. Polym Chem. 2013;4:76-84.
[127] Zhou Y-N, Li J-J, Luo Z-H. Synthesis of gradient copolymers with simultaneously tailor-made chain composition distribution and glass transition temperature by semibatch ATRP: From modeling to application. J Polym Sci, Part A: Polym Chem. 2012;50:3052-66.
[128] Chen J, Li J-J, Luo Z-H. Synthesis, surface property, micellization and pH responsivity of fluorinated gradient copolymers. J Polym Sci, Part A: Polym Chem. 2013;51:1107-17.
[129] He J, Wang Y, Lin Q, Chen L, Zhou X. Synthesis and Characterization of Functional Gradient Copolymers of 2-Hydroxyethyl Methacrylate and tert-Butyl Acrylate by Atom Transfer Radical Polymerization. J Macromol Sci, Part A: Pure Appl Chem. 2009;46:405-11.
[130] Moad G, Rizzardo E, Thang SH. Living Radical Polymerization by the RAFT Process. Aust J Chem. 2005;58:379-410.
[131] Wang H, Zhou H, Chen Y, Zhang C. Synthesis of fluorinated gradient copolymers by RAFT emulsifier-free emulsion polymerization and their compatibilization in copolymer blends. Colloid Polym Sci. 2014;292:2803-9.
[132] Sun X, Luo Y, Wang R, Li B-G, Liu B, Zhu S. Programmed Synthesis of Copolymer with Controlled Chain Composition Distribution via Semibatch RAFT Copolymerization. Macromolecules. 2007;40:849-59.
[133] Alam MM, Peng H, Jack KS, Hill DJT, Whittaker AK. Reactivity Ratios and Sequence Distribution Characterization by Quantitative 13C NMR for RAFT Synthesis of Styrene-Acrylonitrile Copolymers. Journal of Polymer Science Part A: Polymer Chemistry. 2017;55:919-27.

[134] Ritz P, Latalova P, Kriz J, Genzer J, Vlcek P. Statistical copolymers of 2-(trimethylsilyloxy)ethyl methacrylate and methyl methacrylate synthesized by ATRP. J Polym Sci, Part A: Polym Chem. 2008;46:1919-23.
[135] Min KE, Li M, Matyjaszewski K. Preparation of gradient copolymers via ATRP using a simultaneous reverse and normal initiation process. I. spontaneous gradient. J Polym Sci, Part A: Polym Chem. 2005;43:3616-22.
[136] Lefay C, Charleux B, Save M, Chassenieux C, Guerret O, Magnet S. Amphiphilic gradient poly(styrene-co-acrylic acid) copolymer prepared via nitroxide-mediated solution polymerization. Synthesis, characterization in aqueous solution and evaluation as emulsion polymerization stabilizer. Polymer. 2006;47:1935-45.
[137] Qin S, Saget J, Pyun J, Jia S, Kowalewski T, Matyjaszewski K. Synthesis of Block, Statistical, and Gradient Copolymers from Octadecyl (Meth)acrylates Using Atom Transfer Radical Polymerization. Macromolecules. 2003;36:8969-77.
[138] Luo Y, Liu X. Reversible addition-fragmentation transfer (RAFT) copolymerization of methyl methacrylate and styrene in miniemulsion. J Polym Sci, Part A: Polym Chem. 2004;42:6248-58.
[139] Kalugin D, Borisova O, Zaremski M, Garina E, Kolesov D, Bulgakov B, et al. Styrene/alkylacrylate copolymers: Relationship between molecular structure and properties. European Polymer Journal. 2014;60:213-21.
[140] Barner-Kowollik C, Editor. Handbook of RAFT Polymerization: Wiley-VCH Verlag GmbH & Co. KGaA; 2008.
[141] Oleszko-Torbus N, Utrata-Wesolek A, Walach W, Dworak A. Solution behavior of thermoresponsive random and gradient copolymers of 2-n-propyl-2-oxazoline. Eur Polym J. 2017;88:613-22.
[142] Dworak A, Utrata-Wesolek A, Oleszko N, Walach W, Trzebicka B, Aniol J, et al. Poly(2-substituted-2-oxazoline) surfaces for dermal fibroblasts adhesion and detachment. J Mater Sci: Mater Med. 2014;25:1149-63.
[143] Kim KO, Choi T-L. Synthesis of Dendronized Polymers via Macromonomer Approach by Living ROMP and Their Characterization: From Rod-Like Homopolymers to Block and Gradient Copolymers. Macromolecules. 2013;46:5905-14.
[144] Matyjaszewski K. Controlled/Living Radical Polymerization: Progress in ATRP, NMP, and RAFT. Controlled/Living Radical Polymerization Progress in ATRP, NMP, and RAFT; ACS Symposium Series 768. New Orleans: American Chemical Society; 2000. p. 484.
[145] Li X, Liang S, Wang W-J, Li B-G, Luo Y, Zhu S. Model-Based Production of Polymer Chains Having Precisely Designed End-to-End Gradient Copolymer Composition and Chain Topology Distributions in Controlled Radical Polymerization, A Review. Macromol React Eng. 2015;9:409-17.
[146] Min K, Oh JK, Matyjaszewski K. Preparation of gradient copolymers via ATRP in miniemulsion. II. Forced gradient. J Polym Sci, Part A: Polym Chem. 2007;45:1413-23.

[147] Zhang J, Li J, Huang L, Liu Z. Gradient copolymers of styrene-methyl acrylate and styrene-acrylic acid by organostibine-mediated controlled/living radical polymerization and their glass transition behaviors. Polym Chem. 2013;4:4639-47.
[148] Wang L, Broadbelt LJ. Factors Affecting the Formation of the Monomer Sequence along Styrene/Methyl Methacrylate Gradient Copolymer Chains. Macromolecules (Washington, DC, U S). 2009;42:8118-28.
[149] Wang L, Broadbelt LJ. Model-Based Design for Preparing Styrene/Methyl Methacrylate Structural Gradient Copolymers. Macromol Theory Simul. 2011;20:191-204.
[150] Wang R, Luo Y, Li B, Sun X, Zhu S. Design and control of copolymer composition distribution in living radical polymerization using semi-batch feeding policies: A model simulation. Macromol Theory Simul. 2006;15:356-68.
[151] Wang R, Luo Y, Li B-G, Zhu S. Control of gradient copolymer composition in ATRP using semibatch feeding policy. AIChE J. 2007;53:174-86.
[152] Zhao Y, Luo Y-W, Ye C, Li B-G, Zhu S. Model-based design and synthesis of gradient MMA/tBMA copolymers by computer-programmed semibatch atom transfer radical copolymerization. Journal of Polymer Science Part A: Polymer Chemistry. 2009;47:69-79.
[153] Borisova OV, Billon L, Cernochova Z, Lapp A, Stepanek P, Borisov OV. Effect of Temperature on Self-Assembly of Amphiphilic Block-Gradient Copolymers of Styrene and Acrylic Acid. Macromolecular Symposia. 2015;348:25-32.
[154] Karaky K, Billon L, Pouchan C, Desbrieres J. Amphiphilic Gradient Copolymers Shape Composition Influence on the Surface/Bulk Properties. Macromolecules. 2007;40:458-64.
[155] Karaky K, Derail C, Reiter G, Billon L. Tuning the surface/bulk properties by the control of the amphiphilic profile in gradient copolymer. Macromol Symp. 2008;267:31-40.
[156] Karaky K, Pere E, Pouchan C, Desbrieres J, Derail C, Billon L. Effect of the synthetic methodology on molecular architecture: from statistical to gradient copolymers. Soft Matter. 2006;2:770-8.
[157] Karaky K, Clisson G, Reiter G, Billon L. Semicrystalline macromolecular design by nitroxide-mediated polymerization. Macromol Chem Phys. 2008;209:715-22.
[158] Gray MK, Zhou H, Nguyen ST, Torkelson JM. Synthesis and glass transition behavior of high molecular weight styrene/4-acetoxystyrene and styrene/4-hydroxystyrene gradient copolymers made via nitroxide-mediated controlled radical polymerization. Macromolecules. 2004;37:5586-95.
[159] Sandoval RW, Williams DE, Kim J, Roth CB, Torkelson JM. Critical micelle concentrations of block and gradient copolymers in homopolymer: effects of sequence distribution, composition, and molecular weight. J Polym Sci, Part B: Polym Phys. 2008;46:2672-82.
[160] Yuan W, Mok MM, Kim J-K, Wong CLH, Dettmer CM, Nguyen S-BT, et al. Behavior of gradient copolymers at liquid/liquid interfaces. Langmuir. 2010;26:3261-7.

[161] Mok MM, Masser KA, Runt J, Torkelson JM. Dielectric Relaxation Spectroscopy of Gradient Copolymers and Block Copolymers: Comparison of Breadths in Relaxation Time for Systems with Increasing Interphase. Macromolecules (Washington, DC, U S). 2010;43:5740-8.
[162] Mok MM, Torkelson JM. Imaging of phase segregation in gradient copolymers: Island and hole surface topography. J Polym Sci, Part B: Polym Phys. 2012;50:189-97.
[163] Ziegler MJ, Matyjaszewski K. Atom transfer radical copolymerization of methyl methacrylate and n-butyl acrylate. Macromolecules. 2001;34:415-24.
[164] Lee SB, Russell AJ, Matyjaszewski K. ATRP synthesis of amphiphilic random, gradient, and block copolymers of 2-(dimethylamino)ethyl methacrylate and n-butyl methacrylate in aqueous media. Biomacromolecules. 2003;4:1386-93.
[165] Li J-J, Luo Z-H. Case Study to Bridge the Gap between Chemistry and Chemical Product Engineering: From Molecules to Products Based on Brush Copolymers Having Different Backbone Composition Profiles. Ind Eng Chem Res. 2014;53:1900-8.
[166] Fu Y, Cunningham MF, Hutchinson RA. Semibatch atom transfer radical copolymerization of styrene and butyl acrylate. Macromol Symp. 2007;259:151-63.
[167] Gosecka M, Pietrasik J, Decorse P, Glebocki B, Chehimi MM, Slomkowski S, et al. Gradient Poly(styrene-co-polyglycidol) Grafts via Silicon Surface-Initiated AGET ATRP. Langmuir. 2015;31:4853-61.
[168] Kim B-S, Lee H-K, Jeong S, Lee J-O, Paik H-j. Amphiphilic gradient copolymer of [poly(ethylene glycol) methyl ether] methacrylate and styrene via atom transfer radical polymerization. Macromolecular Research. 2011;19:1257-63.
[169] D'hooge RD, Van Steenberge HP, Reyniers M-F, Marin BG. Fed-Batch Control and Visualization of Monomer Sequences of Individual ICAR ATRP Gradient Copolymer Chains. Polymers. 2014;6:1074-95.
[170] Zhang G, Jiang J, Zhang Q, Gao F, Zhan X, Chen F. Ultralow Oil-Fouling Heterogeneous Poly(ether sulfone) Ultrafiltration Membrane via Blending with Novel Amphiphilic Fluorinated Gradient Copolymers. Langmuir. 2016;32:1380-8.
[171] Zheng Z, Gao X, Luo Y, Zhu S. Employing Gradient Copolymer To Achieve Gel Polymer Electrolytes with High Ionic Conductivity. Macromolecules (Washington, DC, U S). 2016;49:2179-88.
[172] Guo Y, Gao X, Luo Y. Mechanical properties of gradient copolymers of styrene and n-butyl acrylate. J Polym Sci, Part B: Polym Phys. 2015;53:860-8.
[173] Wong CLH, Kim J, Roth CB, Torkelson JM. Comparison of Critical Micelle Concentrations of Gradient Copolymer and Block Copolymer in Homopolymer: Novel Characterization by Intrinsic Fluorescence. Macromolecules (Washington, DC, U S). 2007;40:5631-3.
[174] Mok MM, Pujari S, Burghardt WR, Dettmer CM, Nguyen ST, Ellison CJ, et al. Microphase Separation and Shear Alignment of Gradient Copolymers: Melt Rheology and Small-Angle X-Ray Scattering Analysis. Macromolecules (Washington, DC, U S). 2008;41:5818-29.

[175] Kim J, Torkelson JM. Gradient copolymers: exploiting the synthesis, characterization and application of a new class of copolymer materials. Polym Prepr (Am Chem Soc, Div Polym Chem). 2007;48:221-2.
[176] Zhang Q, Zhan X, Chen F, Shi Y, Wang Q. Block copolymers of dodecafluoroheptyl methacrylate and butyl methacrylate by RAFT miniemulsion polymerization. J Polym Sci, Part A: Polym Chem. 2007;45:1585-94.
[177] Wang ZX, Zhang QH, Yu YT, Zhan XL, Chen FQ, Xiong JH. Synthesis of polystyrene-styrene/butadiene diblock copolymers via reversible addition-fragmentation chain transfer miniemulsion polymerization. Chin Chem Lett. 2010;21:1497-500.
[178] Luo Y, Wang X, Zhu Y, Li B-G, Zhu S. Polystyrene-block-poly(n-butyl acrylate)-block-polystyrene Triblock Copolymer Thermoplastic Elastomer Synthesized via RAFT Emulsion Polymerization. Macromolecules (Washington, DC, U S). 2010;43:7472-81.
[179] Farcet C, Charleux B, Pirri R. Nitroxide-mediated miniemulsion polymerization of n-butyl acrylate: synthesis of controlled homopolymers and gradient copolymers with styrene. Macromol Symp. 2002;182:249-60.
[180] Zhang M, Ray WH. Modeling of "living" free-radical polymerization processes. Part I. Batch, semibatch, and continuous tank reactors. J Appl Polym Sci. 2002;86:1630-62.
[181] Al-Harthi M, Soares JBP, Simon LC. Mathematical modeling of atom-transfer radical copolymerization. Macromol React Eng. 2007;1:468-79.
[182] Al-Harthi MA, Masihullah JK, Abbasi SH, Soares JBP. Dynamic Monte Carlo Simulation of ATRP in a Batch Reactor. Macromol Theory Simul. 2009;18:307-16.
[183] Wang W, Zhou Y-N, Luo Z-H. Modeling of the Atom Transfer Radical Copolymerization Processes of Methyl Methacrylate and 2-(Trimethylsilyl) Ethyl Methacrylate under Batch, Semibatch, and Continuous Feeding: A Chemical Reactor Engineering Viewpoint. Ind Eng Chem Res. 2014;53:11873-83.
[184] Zapata-Gonzalez I, Hutchinson RA, Matyjaszewski K, Saldivar-Guerra E, Ortiz-Cisneros J. Copolymer composition deviations from Mayo-Lewis conventional free radical behavior in nitroxide mediated copolymerization. Macromol Theory Simul. 2014;23:245-65.
[185] Fortunatti C, Sarmoria C, Brandolin A, Asteasuain M. Theoretical Analysis of Nitroxide-Mediated Copolymerization of Styrene and α-Methyl-Styrene under Different Operating Policies and Reactor Designs. Macromol React Eng. 2014;8:260-81.
[186] Li X, Wang W-J, Weng F, Li B-G, Zhu S. Targeting Copolymer Composition Distribution via Model-Based Monomer Feeding Policy in Semibatch RAFT Mini-Emulsion Copolymerization of Styrene and Butyl Acrylate. Ind Eng Chem Res. 2014;53:7321-32.
[187] Wang L, Broadbelt LJ. Explicit Sequence of Styrene/Methyl Methacrylate Gradient Copolymers Synthesized by Forced Gradient Copolymerization with Nitroxide-Mediated Controlled Radical Polymerization. Macromolecules (Washington, DC, U S). 2009;42:7961-8.

[188] Wang L, Broadbelt LJ. Kinetics of Segment Formation in Nitroxide-Mediated Controlled Radical Polymerization: Comparison with Classic Theory. Macromolecules (Washington, DC, U S). 2010;43:2228-35.
[189] Zargar A, Schork FJ. Copolymer sequence distributions in controlled radical polymerization. Macromol React Eng. 2009;3:118-30.
[190] Zargar A, Schork FJ. Design of Copolymer Molecular Architecture via Design of Continuous Reactor Systems for Controlled Radical Polymerization. Ind Eng Chem Res. 2009;48:4245-53.
[191] Ye Y, Schork FJ. Modeling and Control of Sequence Length Distribution for Controlled Radical (RAFT) Copolymerization. Ind Eng Chem Res. 2009;48:10827-39.
[192] Cherifi N, Issoulie A, Khoukh A, Benaboura A, Save M, Derail C, et al. Synthetic methodology effect on the microstructure and thermal properties of poly(n-butyl acrylate-co-methyl methacrylate) synthesized by nitroxide mediated polymerization. Polym Chem. 2011;2:1769-77.
[193] Inoue Y, Watanabe J, Takai M, Yusa S-I, Ishihara K. Synthesis of sequence-controlled copolymers from extremely polar and apolar monomers by living radical polymerization and their phase-separated structures. J Polym Sci, Part A: Polym Chem. 2005;43:6073-83.
[194] Palermo EF, McNeil AJ. Gradient sequence π-conjugated copolymers. ACS Symp Ser. 2014;1170:287-99.
[195] Matyjaszewski K. Architecturally complex polymers with controlled heterogeneity. Science (Washington, DC, U S). 2011;333:1104-5.
[196] Palermo EF, McNeil AJ. Impact of Copolymer Sequence on Solid-State Properties for Random, Gradient and Block Copolymers containing Thiophene and Selenophene. Macromolecules (Washington, DC, U S). 2012;45:5948-55.
[197] Tito NB, Milner ST, Lipson JEG. Self-assembly of lamellar microphases in linear gradient copolymer melts. Macromolecules (Washington, DC, U S). 2010;43:10612-20.
[198] Pakula T. Copolymers with controlled distribution of comonomers along the chain. Part 1. Structure, thermodynamics, and dynamic properties of gradient copolymers. Computer simulation. Macromol Theory Simul. 1996;5:987-1006.
[199] Sun D, Guo H. Monte Carlo Studies on the Interfacial Properties and Interfacial Structures of Ternary Symmetric Blends with Gradient Copolymers. J Phys Chem B. 2012;116:9512-22.
[200] Van Steenberge PHM, D'Hooge DR, Wang Y, Zhong M, Reyniers M-F, Konkolewicz D, et al. Linear Gradient Quality of ATRP Copolymers. Macromolecules (Washington, DC, U S). 2012;45:8519-31.
[201] Tito NB, Milner ST, Lipson JEG. Ball-of-Yarn Conformation of a Linear Gradient Copolymer in a Homopolymer Melt. Macromolecules (Washington, DC, U S). 2012;45:7607-20.
[202] Sigle JL, Clough A, Zhou J, White JL. Controlling Macroscopic Properties by Tailoring Nanoscopic Interfaces in Tapered Copolymers. Macromolecules (Washington, DC, U S). 2015;48:5714-22.

[203] Clough A, Sigle JL, Tapash A, Gill L, Patil NV, Zhou J, et al. Component-Specific Heterogeneity and Differential Phase Partitioning in Gradient Copolymers Revealed by Solids NMR. Macromolecules. 2014;47:2625-31.
[204] Pandav G, Pryamitsyn V, Gallow KC, Loo Y-L, Genzer J, Ganesan V. Phase behavior of gradient copolymer solutions: a Monte Carlo simulation study. Soft Matter. 2012;8:6471-82.
[205] Matyjaszewski K, Greszta D, Pakula T. Thermal properties of gradient copolymers and their compatibilizing ability. Polym Prepr (Am Chem Soc, Div Polym Chem). 1997;38:707-8.
[206] Greszta D, Matyjaszewski K, Pakula T. Gradient copolymers of styrene and acrylonitrile via atom transfer radical polymerization. Polym Prepr (Am Chem Soc, Div Polym Chem). 1997;38:709-10.
[207] Lyatskaya Y, Gersappe D, Gross NA, Balazs AC. Designing Compatibilizers to Reduce Interfacial Tension in Polymer Blends. J Phys Chem. 1996;100:1449-58.
[208] Palermo EF, Darling SB, McNeil AJ. [small pi]-Conjugated gradient copolymers suppress phase separation and improve stability in bulk heterojunction solar cells. Journal of Materials Chemistry C. 2014;2:3401-6.
[209] Palermo EF, van der Laan HL, McNeil AJ. Impact of π-conjugated gradient sequence copolymers on polymer blend morphology. Polym Chem. 2013;4:4606-11.
[210] Palermo EF, Darling SB, McNeil AJ. π-Conjugated gradient copolymers suppress phase separation and improve stability in bulk heterojunction solar cells. J Mater Chem C. 2014;2:3401-6.
[211] Vezie DL, Thomas EL, Adams WW. Low-voltage, high-resolution scanning electron microscopy: a new characterization technique for polymer morphology. Polymer. 1995;36:1761-79.
[212] Kim SO, Solak HH, Stoykovich MP, Ferrier NJ, de Pablo JJ, Nealey PF. Epitaxial self-assembly of block copolymers on lithographically defined nanopatterned substrates. Nature (London, U K). 2003;424:411-4.
[213] van Dijk MA, van den Berg R. Ordering Phenomena in Thin Block Copolymer Films Studied Using Atomic Force Microscopy. Macromolecules. 1995;28:6773-8.
[214] Peng J, Xuan Y, Wang H, Yang Y, Li B, Han Y. Solvent-induced microphase separation in diblock copolymer thin films with reversibly switchable morphology. J Chem Phys. 2004;120:11163-70.
[215] Heck B, Arends P, Ganter M, Kressler J, Stuehn B. SAXS and TEM Studies on Poly(styrene)-block-poly(ethene-co-but-1-ene)-block-poly(styrene) in Bulk and at Various Interfaces. Macromolecules. 1997;30:4559-66.
[216] Taube C, Garcia MF, Schmidt-Naake G, Fischer H. Synthesis, characterization, and thermal properties of block copolymers containing poly(styrene-co-4-vinylpyridine) and poly(styrene-co-butyl acrylate) by controlled radical polymerization. Macromol Chem Phys. 2002;203:2665-73.
[217] Park I, Park S, Park H-W, Chang T, Yang H, Ryu CY. Unexpected Hexagonally Perforated Layer Morphology of PS-b-PMMA Block Copolymer in Supported Thin Film. Macromolecules. 2006;39:315-8.

[218] Zhao R, Shea KJ. Gradient Methylidene-Ethylidene Copolymer via C1 Polymerization: an Ersatz Gradient Ethylene-Propylene Copolymer. ACS Macro Lett. 2015;4:584-7.
[219] Park J-S, Kataoka K. Precise Control of Lower Critical Solution Temperature of Thermosensitive Poly(2-isopropyl-2-oxazoline) via Gradient Copolymerization with 2-Ethyl-2-oxazoline as a Hydrophilic Comonomer. Macromolecules. 2006;39:6622-30.
[220] Huber S, Jordan R. Modulation of the lower critical solution temperature of 2-Alkyl-2-oxazoline copolymers. Colloid Polym Sci. 2008;286:395-402.
[221] Seno K-I, Tsujimoto I, Kanaoka S, Aoshima S. Synthesis of various stimuli-responsive gradient copolymers by living cationic polymerization and their thermally or solvent induced association behavior. J Polym Sci, Part A: Polym Chem. 2008;46:6444-54.
[222] Ribaut T, Oberdisse J, Annighofer B, Stoychev I, Fournel B, Sarrade S, et al. SANS study of the self-organization of gradient copolymers with ligand groups in supercritical CO2. Soft Matter. 2009;5:4962-70.
[223] Gallow KC, Jhon YK, Tang W, Genzer J, Loo Y-L. Cloud point suppression in dilute solutions of model gradient copolymers with prespecified composition profiles. J Polym Sci, Part B: Polym Phys. 2011;49:629-37.
[224] Merlet-Lacroix N, Di Cola E, Cloitre M. Swelling and rheology of thermoresponsive gradient copolymer micelles. Soft Matter. 2010;6:984-93.
[225] Kuldova J, Kosovan P, Limpouchova Z, Prochazka K. Computer Study of the Association Behavior of Gradient Copolymers: Analysis of Simulation Results Based on a New Algorithm for Recognition and Classification of Aggregates. Macromol Theory Simul. 2013;22:61-70.
[226] Hodrokoukes P, Pispas S, Hadjichristidis N. Controlling Micellar Properties of Styrene/Isoprene Copolymers by Altering the Monomer Arrangement along the Chain. Macromolecules. 2002;35:834-40.
[227] Ribaut T, Oberdisse J, Annighofer B, Fournel B, Sarrade S, Haller H, et al. Solubility and Self-Assembly of Amphiphilic Gradient and Block Copolymers in Supercritical CO2. J Phys Chem B. 2011;115:836-43.
[228] Kuldova J, Kosovan P, Limpouchova Z, Prochazka K, Borisov OV. Self-association of copolymers with various composition profiles. Collect Czech Chem Commun. 2010;75:493-505.
[229] Borisov OV, Zhulina EB, Leermakers FAM, Muller AHE. Self-assembled structures of amphiphilic ionic block copolymers: theory, self-consistent field modeling and experiment. Adv Polym Sci. 2011;241:57-129.
[230] Zheng C, Huang H, He T. Micellization of St/MMA Gradient Copolymers: A General Picture of Structural Transitions in Gradient Copolymer Micelles. Macromol Rapid Commun. 2013;34:1654-61.
[231] Kravchenko VS, Potemkin II. Micelles of Gradient vs Diblock Copolymers: Difference in the Internal Structure and Properties. J Phys Chem B. 2016;120:12211-7.

[232] Zaremski MY, Kalugin DI, Golubev VB. Gradient copolymers: Synthesis, structure, and properties. Polymer Science Series A. 2009;51:103-22.
[233] Adhikari R, Michler GH, Lebek W, Goerlitz S, Weidisch R, Knoll K. Morphology and micromechanical deformation behavior of SB-block copolymers. II. Influence of molecular architecture of asymmetric star block copolymers. J Appl Polym Sci. 2002;85:701-13.
[234] Thomas EL, Anderson DM, Henkee CS, Hoffman D. Periodic area-minimizing surfaces in block copolymers. Nature (London). 1988;334:598-601.
[235] Jinnai H, Sawa K, Nishi T. Direct Observation of Twisted Grain Boundary in a Block Copolymer Lamellar Nanostructure. Macromolecules. 2006;39:5815-9.
[236] Jinnai H, Yasuda K, Nishi T. Three-dimensional observations of grain boundary morphologies in a cylinder-forming block copolymer. Macromol Symp. 2006;245/246:170-4.
[237] Vagner J, Handl HL, Gillies RJ, Hruby VJ. Novel targeting strategy based on multimeric ligands for drug delivery and molecular imaging: homooligomers of α-MSH. Bioorg Med Chem Lett. 2004;14:211-5.

Chapter 2: Synthesis of Styrene-Acrylonitrile Copolymers

2.1 Introduction

Styrene-acrylonitrile (St-AN) copolymers are found in a wide range of industrial applications, due to their outstanding chemical, thermal, mechanical and optical properties and their easy processability [238, 239]. Therefore, this monomer pair has been one of the most studied from the early days of polymer science [240-242]. Prior to the introduction of controlled radical polymerization, CvRP was used to synthesize St-AN copolymers and a number of scientists have studied the kinetics of St-AN copolymerization both in bulk [243-246] and in a variety of solvents [243, 247-250] as well as in heterogeneous systems such as aqueous emulsions [241, 251] or micro-emulsions [252, 253]. Several authors have suggested that the reactivity ratios of the styrene and acrylonitrile monomers are affected to some extent by the medium of the reaction. The interaction of acrylonitrile with the solvent, which is termed 'preferential solvation', was reported as the reason for the change in the reactivity ratios with the reaction medium [249, 254]. The effect of solvent on the copolymerization of monomers of very different polarity has been further reported to be explained based on the bootstrap model [243, 255-259]. The bootstrap model explains the solvent effect by postulating a difference in the monomer concentration around the growing chain and in the free solvent.

RAFT has been found to be suitable for the homopolymerization of both acrylonitrile [260-262] and styrene [263-265] monomers, and Chernikova et al. [266] have reported the synthesis of St-AN copolymers with controlled molecular weight and low molecular weight dispersity ($Đ_M$) using RAFT. St-AN copolymers with varying molecular weight were also successfully synthesized by the RAFT emulsion copolymerization, as reported by Huang and colleagues [267]. Fan et al. [268] reported that the reactivity ratios for St-AN copolymers prepared by the RAFT method were higher than those of CvRP and suggested that this was due to the presence of the RAFT end groups showing a preferential affinity towards one monomer over the other. A difference in the reactivity ratios was also reported for reverse ATRP of St-AN copolymers, [269] although Tsarevsky et al. [270] reported that the reactivity ratios match those observed in the CvRP process. Despite these studies, the effect of solvent on both the reactivity ratios and the copolymer triad distributions of the St-AN system have not been studied previously for controlled radical polymerizations.

In this chapter, the reactivity ratios of styrene and acrylonitrile have been obtained by an analysis of the sequence distributions for nine different comonomer feed ratios using the RAFT method in bulk. Based on the Mayo-Lewis plot for the St-AN copolymer system, four different feed compositions were selected for the study of kinetics of high-conversion St-AN copolymer synthesis by both the RAFT and CvRP batch polymerizations. For each feed compositions, the copolymer compositions as well as the St and AN centred triad fractions were characterized using ^{1}H NMR and quantitative ^{13}C NMR, and the experimental data were compared with the predicted data. In addition to the batch St-AN copolymers, RAFT polymerization was also used to synthesize forced gradient copolymers by employing the continuous feeding approach for the azeotrope feed compositions. Using PSt as the macro-RAFT agent, PSt-block-PAN copolymers were synthesized by the chain extension method.

2.2 Materials

Both styrene (St) and acrylonitrile (AN) monomers were purchased from Sigma-Aldrich, and passed through a basic alumina column to remove the inhibitor prior to polymerization reactions. Azobisisobutyronitrile (AIBN) initiator was purchased from Sigma-Aldrich, and purified by recrystallizing in methanol followed by drying in a vacuum oven at room temperature. The RAFT agent 2-cyano-2-propyl benzodithioate (CPDB) was used as purchased from Sigma-Aldrich and propanoic acidyl butyl trithiocarbonate (PABTC) was synthesized as described in the literature [271]. Solvent 1,4-dioxane was purchased from Ajax Finechem and N,N-dimethylformamide (DMF) was purchased from Merck Millipore.

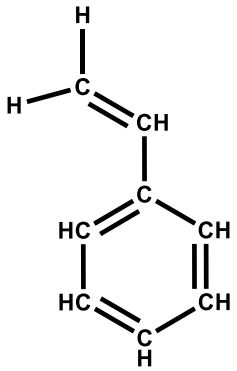

Styrene

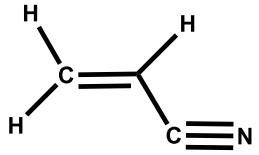

Acrylonitrile

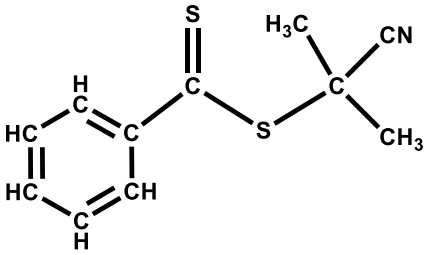

2-Cyano-2-propyl benzodithioate (CPDB)

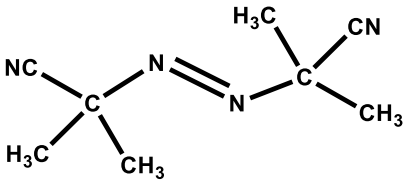

Azobisisobutyronitrile (AIBN)

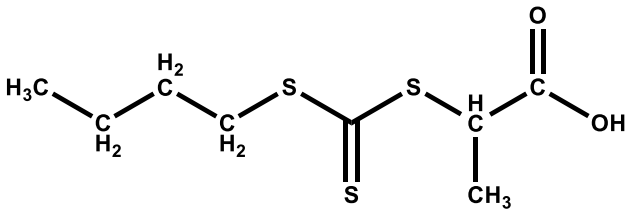

Propionic acidyl butyl trithiocarbonate (PABTC)

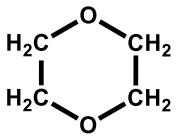

1,4-Dioxane

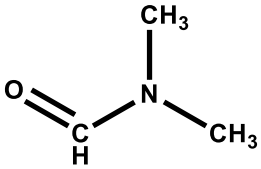

N,N-dimethylformamide

Figure-2.1: Materials used for the synthesis of St-AN copolymers.

2.3 Characterization Techniques

2.3.1 Size Exclusion Chromatography (SEC)

Size exclusion chromatography (SEC) is one of the fundamental characterization techniques in polymer chemistry which gives the molecular weight and molecular weight distributions of the polymer. In this study, two different SEC systems have been used for polymers and copolymers characterization. One of them is a Waters GPC 1515 pump system with Ultra Violet and Differential Refractive Index detectors. HPLC-grade Tetrahydrofuran (THF) was used as eluent at a flow rate of 1 mL min^{-1} at 40 °C. The samples with a known concentration (1.0 mg mL^{-1}) were dissolved in THF and filtered through a polytetrafluoroethylene (PTFE) 0.45 micron 13 mm filter before measurement. Molecular weight and molecular weight dispersity of polymer were determined with respect to polystyrene (PS) standards.

The second SEC used in this project is a Polymer Laboratories GPC 50 Plus equipped with a dual angle laser-light scattering detector, viscometer and differential refractive index detector. HPLC grade N,N-dimethylacetamide (DMAc, containing 0.03% LiCl) was used as the eluent at a flow rate of 1.0 mL min^{-1} and the temperature was held constant at 50 °C. The system allows for the determination of the absolute molecular weight of the polymers. Empirical values of *dn*/*dc* were determined from the slopes of the refractive index vs concentration for St-AN copolymers (dn/dc values are given in section 2.5.3.3).

2.3.2 Nuclear Magnetic Resonance (NMR)

NMR was used to study the kinetics of polymerization, to study the polymer structure, and to study the copolymer compositions. In this study, both proton (^{1}H) and quantitative carbon (^{13}C) NMR spectroscopy were utlized using a Bruker Avance 400 MHz spectrometer. In most of the cases, deuterated chloroform ($CDCl_3$) was used as solvent, and deuterated dimethyl sulfoxide (DMSO-d_6) was used for the samples those were found to be insoluble (produced non-transparent liquid) in $CDCl_3$. A 10 wt% polymer solution was used for characterization with quantitative ^{13}C NMR. The delay time and scan number of the samples were adjusted for quantitative ^{13}C NMR based on the types of polymer samples, detail parameters are noted in the later sections for individual samples.

2.4 Determination of reactivity ratios for St-AN copolymerization

The kinetics of the polymerization of styrene and acrylonitrile monomers have been studied extensively in different reaction mediums and polymerization techniques. Klumperman and co-workers [257] investigated the CvRP of St and AN in bulk and in the solvents toluene, butanone and N,N'-dimethylformamide. They reported a small but noticeable effect of solvent on the kinetics of St-AN copolymerization. Hill et al. [243] also found a similar solvent effect on the St-AN polymerization in bulk as well as in acetonitrile and toluene. In addition to the solvent effect, the reactivity ratios are also reported to be dependent on the polymerization temperatures [272].

In this study, the reactivity ratios of the RAFT polymerization of St-AN were determined using nine different monomer feed compositions ranging from 10:90 to 90:10 St:AN mole ratios. The polymerization reactions were carried out at 80 ºC in bulk, with a 2:1 RAFT to initiator ratio. The reaction concentrations for the reactivity ratios determination are given in Table-2.1. A small amount of dioxane was added to each reaction mixture to use as a reference peak in ^{1}H NMR to aid in determination of the reaction conversion. The dioxane peak in the ^{1}H NMR spectrum is well separated (3.71 ppm in $CDCl_3$) from the monomer peaks, and therefore could be used as the reference to monitor the changes in the intensities of the monomer peaks during the course of the polymerization.

Table-2.1: Reaction concentrations for the synthesis of St-AN copolymers with different feed compositions to determine the reactivity ratios of St and AN. The number at the end of the names of the St-AN copolymers represent the styrene fraction in the initial monomer mixture.

Designation	Feed compositions St:AN	St (mole)	AN (mole)	CPDB (mmole)	AIBN (mmole)	Dioxane (mmole)
St-AN10	10:90	0.0116	0.1038	0.2099	0.1122	1.1591
St-AN20	20:80	0.0192	0.0769	0.2262	0.1128	2.2727
St-AN30	30:70	0.0259	0.0606	0.2439	0.1098	1.3296
St-AN40	40:60	0.0336	0.0478	0.2199	0.1098	1.2386
St-AN50	50:50	0.0384	0.0392	0.2358	0.1122	1.068
St-AN60	60:40	0.0385	0.0255	0.2262	0.1128	2.2727
St-AN70	70:30	0.0483	0.0209	0.2199	0.1140	1.1591
St-AN80	80:20	0.0481	0.0120	0.2262	0.1128	2.2727
St-AN90	90:10	0.0542	0.0061	0.2267	0.1098	1.1705

The reactions were quenched in an ice batch at certain times, and the crude reaction mixtures were characterized by ^{1}H NMR. The spectra of the crude copolymer solutions were compared to the spectra of the starting crude copolymer solutions, and using the dioxane peak as the reference, the conversion for each composition was determined from the change in the intensities of the monomer peaks. Figure-2.2 shows the ^{1}H NMR spectrum for the crude reaction mixture for St-AN20 copolymer before the start of the reaction. The reference (dioxane) peak is highlighted in the red box. The conversion of St to polymer was calculated by comparing the dioxane peak to the St proton peak '**a**' and the AN conversion was calculated by comparing the dioxane peak to the AN proton peak '**f**', both highlighted in green boxes. The overall conversion were calculated from the individual monomer conversion using the feed ratios. The copolymer conversion were kept under 10% to enable accurate determination of the monomer reactivity ratios.

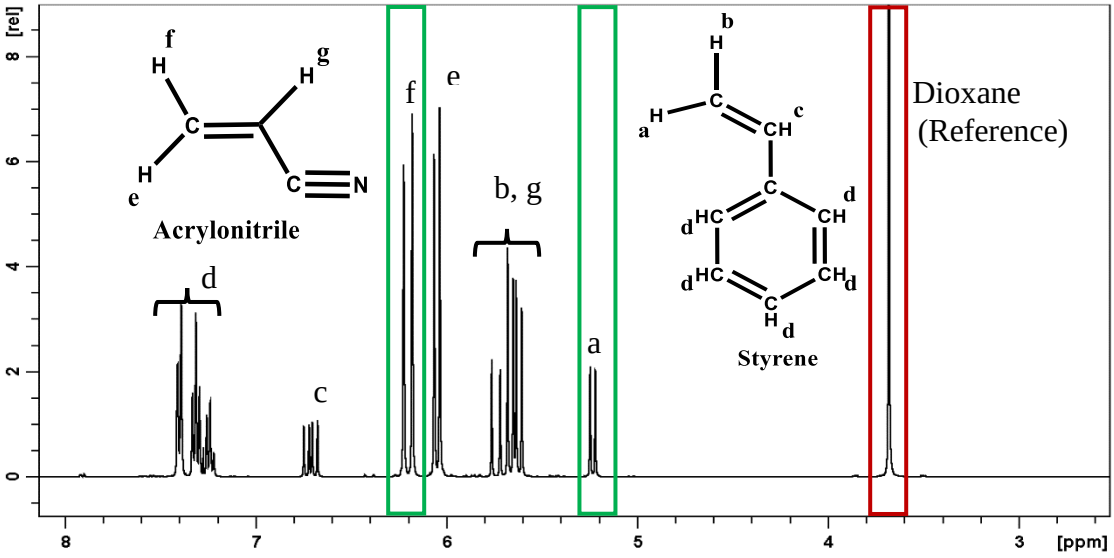

Figure-2.2: ^{1}H NMR spectrum of the initial reaction mixture for St-AN20 showing the peaks assigned to the protons of each monomer and the reference solvent dioxane.

The copolymers were precipitated by adding drop-wise to a mixture of methanol and water. For very low conversion (less than 5%), n-hexane was found to be a better solvent for precipitating the St-AN copolymers. The precipitated copolymers were then filtered and dried in a vacuum oven for 48 hours at room temperature to a constant weight. The molecular weight and molecular weight dispersity of the resultant copolymers were characterized by SEC using THF as the eluent. The copolymer compositions and triad distributions were also characterized by both ^{1}H NMR and quantitative ^{13}C NMR using $CDCl_3$ as the NMR solvent (delay time: 1 s, scans: 16). For quantitative ^{13}C NMR, a 10 wt% solution of the copolymer was prepared, and the data were acquired with a 5 s delay time, and 2048 scans. NMR measurements using different delay times confirmed that 5 s was sufficiently long to ensure full relaxation of the ^{13}C spins. Figure-2.5 shows

the comparison of the peak intensities of St-AN60 copolymer for three different delay times, and only one example is shown as the spectra were essentially identical for copolymers with other compositions as well.

Table-2.2: Copolymer conversion characterized by ^{1}H NMR, compositions characterized by ^{1}H and ^{13}C NMR, and molecular weight characterized by ^{1}H NMR and SEC for nine different feed compositions of St-AN copolymers.

Designation	**Conv. (%)**	f_{St}	F_{St} (^{1}H NMR)	F_{St} (^{13}C NMR)	M_n (^{1}H NMR) gmol^{-1}	M_n (SEC) gmol^{-1}	$Đ_M$ (SEC)
St-AN10	3.8	0.10	0.40	0.42	1400	1100	1.46
St-AN20	6.2	0.20	0.44	0.47	1600	1300	1.41
St-AN30	5.9	0.30	0.51	0.53	2800	2900	1.13
St-AN40	3.0	0.40	0.57	0.57	1600	1400	1.30
St-AN50	5.7	0.50	0.60	0.61	2200	1750	1.28
St-AN60	6.0	0.60	0.65	0.63	1600	1100	1.26
St-AN70	6.8	0.70	0.68	0.68	3200	3100	1.13
St-AN80	3.3	0.80	0.75	0.73	1500	1500	1.23
St-AN90	3.3	0.90	0.81	0.80	1400	1000	1.30

The number at the end of St-AN copolymer name represents the St feed composition in the copolymerization mixture

Conv. = conversion

f_{St} = St feed composition

F_{St} = St composition in the copolymer

M_n = Number-average molecular weight

$Đ_M$ = Molecular weight dispersity

The overall St-AN copolymer conversion calculated from the individual St and AN monomer conversion using ^{1}H NMR, as listed in Table-2.2 are found to be less than 7% for each monomer feed composition. The compositions of the purified copolymers were calculated by comparing the intensity of the peaks due to the aromatic protons of the St units (H_f) to those of the backbone protons of AN (H_c and H_d) (Figure-2.3). The RAFT agent CPDB also gives a well resolved peak for its aromatic protons (H_g) in ^{1}H NMR. Therefore, by comparing the intensity of the peak from the

RAFT end group to those of the copolymer, the molecular weight of the copolymers were calculated from ^{1}H NMR. Copolymer molecular weight (M_n) and molecular weight dispersity ($Đ_M$) have also been determined by SEC. The target molecular weight was sufficiently high (approx. 25,000), but for calculating reactivity ratios, the conversion has to be as low as possible, and therefore resulted in low molecular weight polymers. Unless it is mentioned to be characterized by the triple detector, the molecular weight of the copolymers mentioned in this thesis are actually apparent molecular weights with respect to PSt standard, which may lack the precision and accuracy due to the introduction of systematic error depending on the quality of the solvent for the analyte and the standard [273, 274]. Similarly, the apparent dispersity of the copolymers might be differ from the actual value due to the fact that THF is not as good for PAN as it is for PSt as solvent which especially affects the dispersity values for the St-AN copolymers with high AN content.

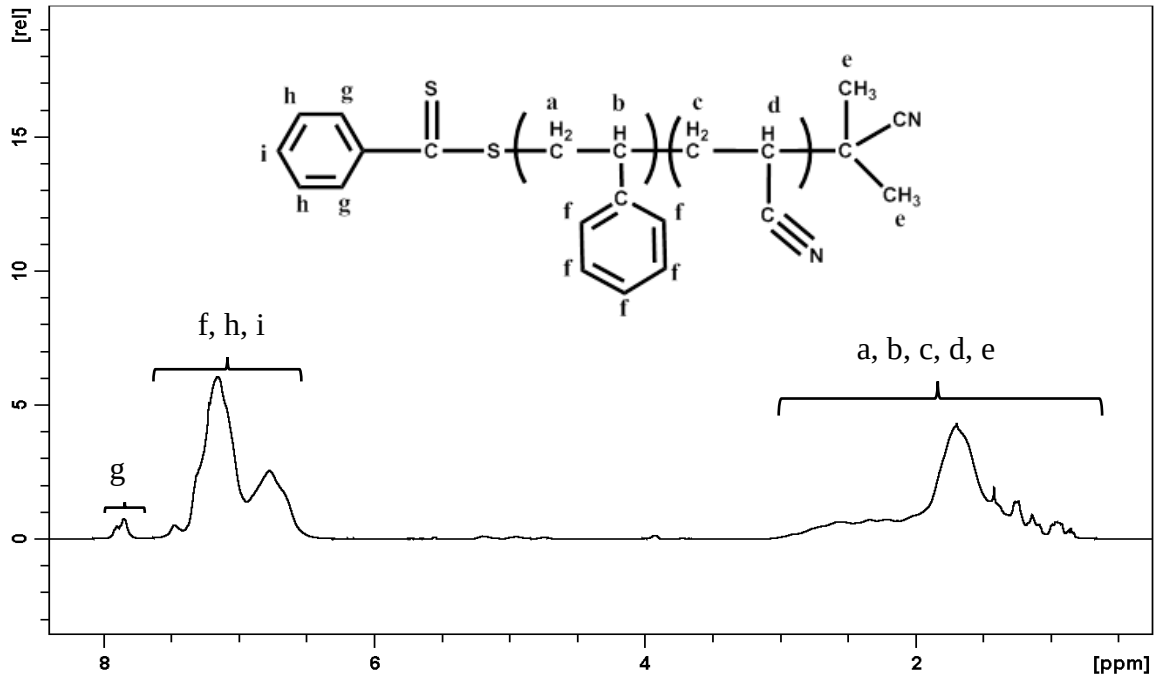

Figure-2.3: ^{1}H NMR spectrum of purified St-AN60 copolymer with peaks assigned for each proton in the copolymer and the RAFT end group. Due to high sample concentration (approximately 10 wt%), the chloroform-d peak is overlapped by the aromatic proton peaks from St.

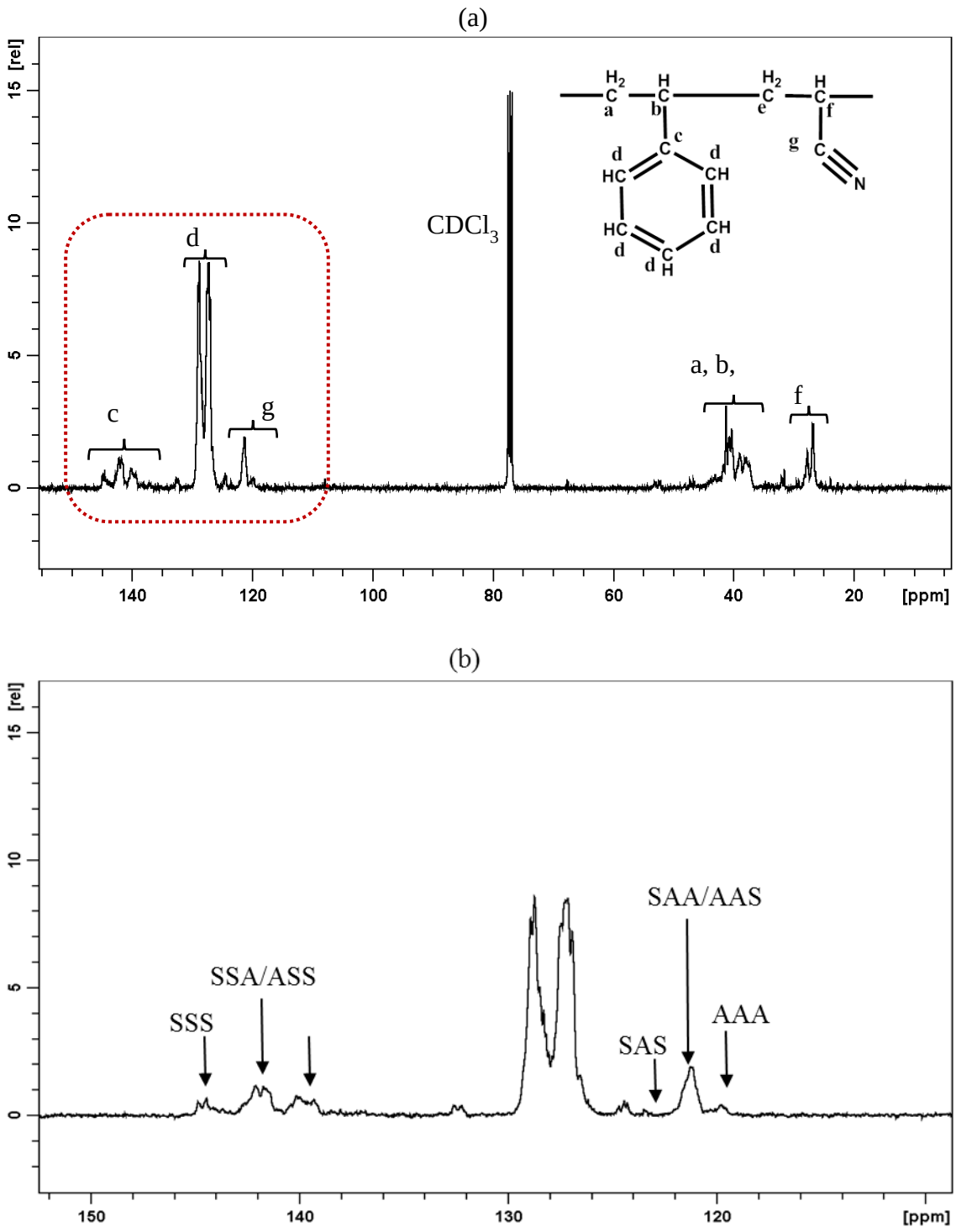

Figure-2.4: (a) ^{13}C NMR spectrum for St-AN60 copolymer at 6% conversion, with peaks assigned to each carbon in the copolymer; (b) the highlighted portion of 'a', showing the peaks for the styrene centred and acrylonitrile centred triads.

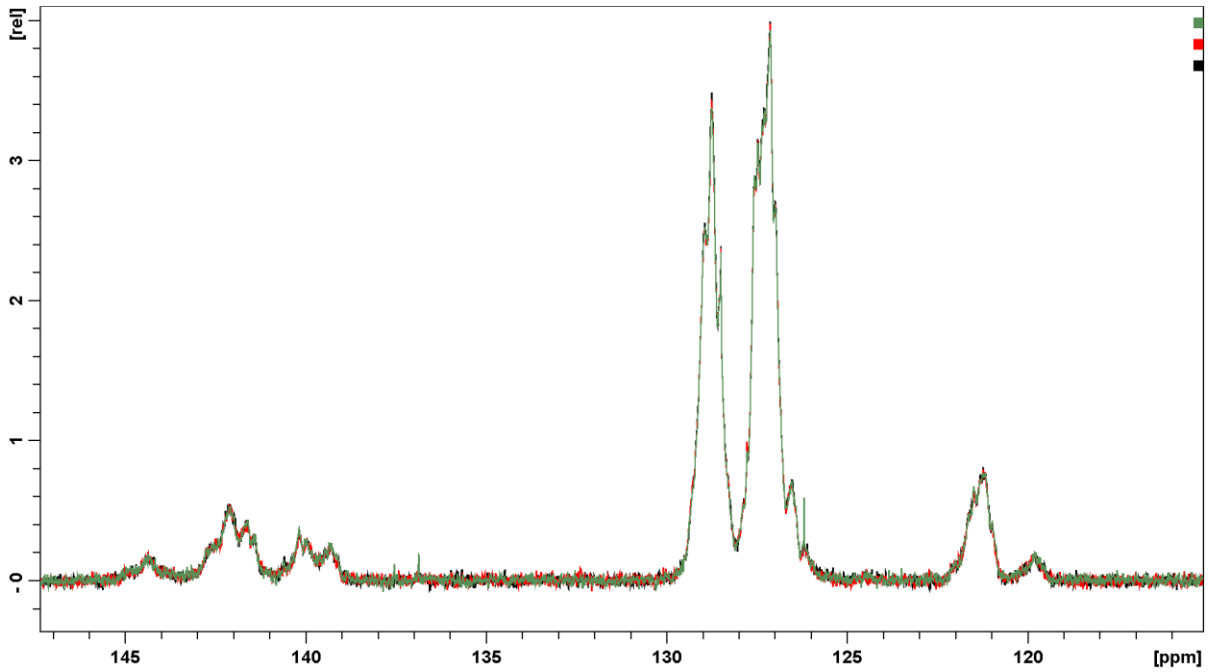

Figure-2.5: Comparison of St and AN centred peaks of St-AN60 copolymers for delay time 5 s (—), 10 s (—) and 15 s (—) with 2048 scans, showing no differences in peak heights.

Using ^{13}C NMR, the compositions were calculated by comparing intensities of peaks due to the aromatic carbons (C_d) from St units to the nitrile carbon (C_g) of AN units in Figure-2.4 (a). The variation in the sequence of the monomer units in a triad gives well resolved peaks [275-277], for both styrene and acrylonitrile centred triads, as can be seen in Figure-2.4 (b). These triad peaks have been used to quantify the individual triad fractions present in a copolymer for all different feed compositions. The structures of the St and AN centred triads are shown in Figure-2.6.

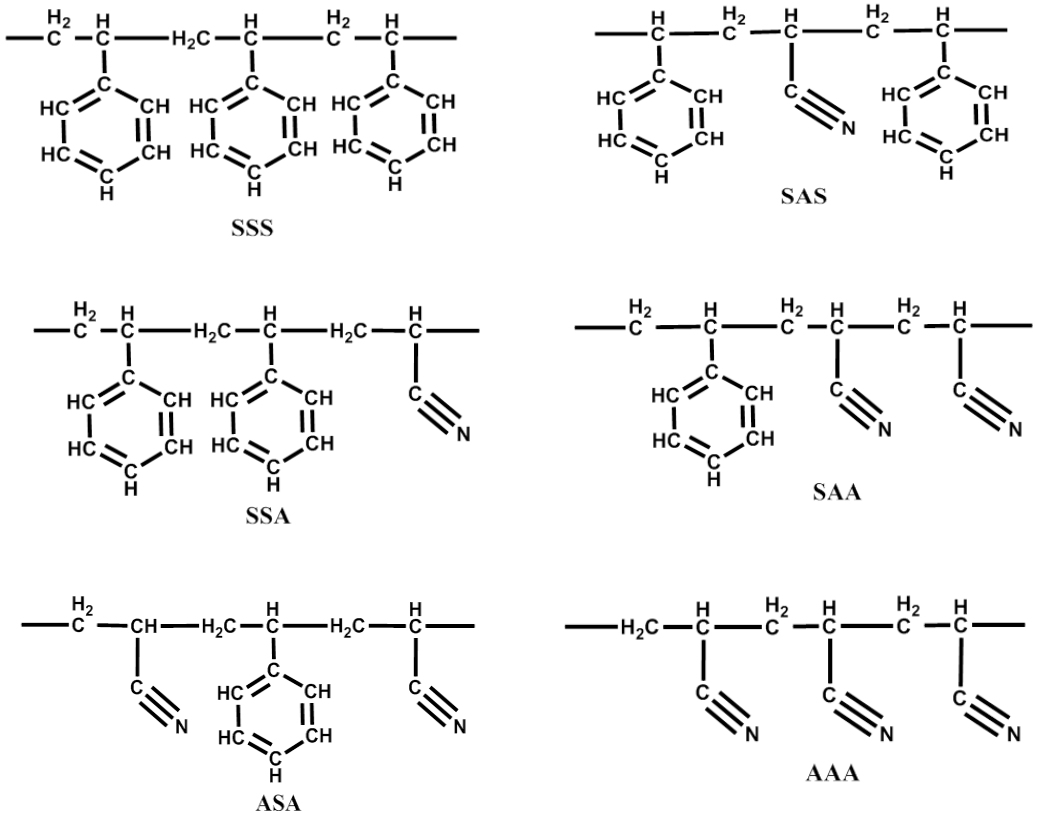

Figure-2.6: Structures of the styrene centred and acrylonitrile centred triads.

Table-2.3: Triad fractions obtained from ^{13}C NMR of the St-AN copolymers prepared at low conversion for nine different monomer feed compositions.

Designation	St-centred triad fractions			AN-centred triad fractions		
	F(SSS)	***F(SSA/ASS)***	***F(ASA)***	***F(SAS)***	***F(SAA/AAS)***	***F(AAA)***
St-AN10	0.000	0.164	0.836	0.279	0.560	0.161
St-AN20	0.011	0.260	0.729	0.478	0.456	0.066
St-AN30	0.024	0.336	0.640	0.600	0.366	0.033
St-AN40	0.048	0.431	0.521	0.714	0.267	0.018
St-AN50	0.078	0.507	0.415	0.780	0.211	0.009
St-AN60	0.134	0.554	0.311	0.845	0.152	0.004
St-AN70	0.197	0.572	0.231	0.881	0.100	0.019
St-AN80	0.292	0.532	0.176	0.898	0.096	0.006
St-AN90	0.402	0.486	0.112	0.925	0.075	0.000

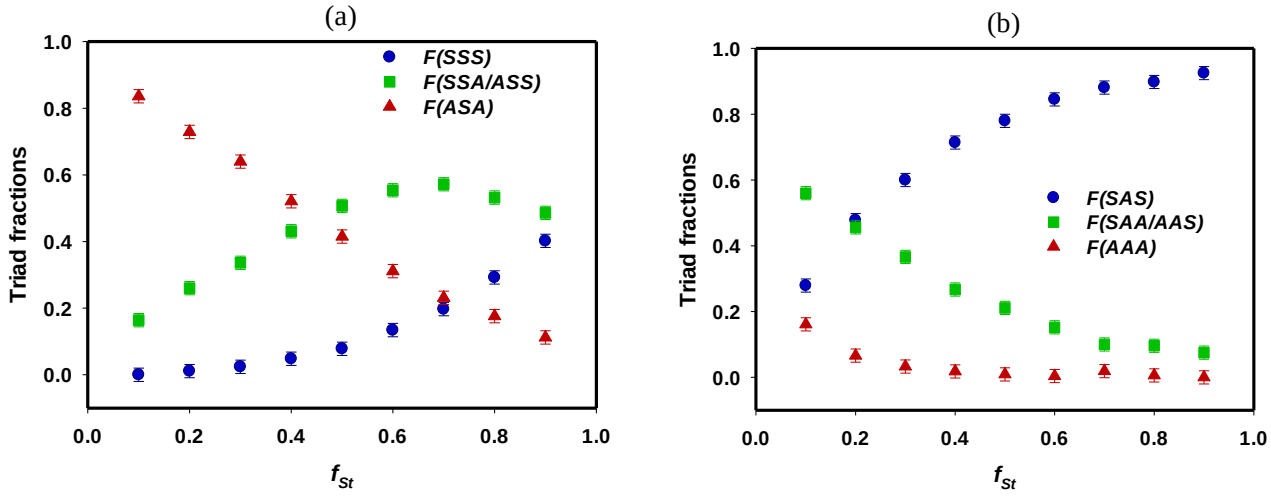

Figure-2.7: Change in (a) St-centred and (b) AN-centred triad fractions with St feed composition for St-AN copolymers with varying monomer feed compositions at low conversion (less than 10%).

The St and AN centred triads have been quantified from the quantitative ^{13}C NMR for each of the monomer feed ratios, and the triad fractions calculated which is given in Table-2.3 as well as plotted against the feed ratios in Figure-2.7. As expected, the fraction of all three St units in a triad (SSS) increases with the increase in the St in the monomer feed while triad fraction with all AN units (AAA) decreases.

The triad distributions in the copolymer chains at very low conversion can be used to determine the reactivity ratios of the monomers using the expressions based on the conditional probabilities [278].

$$r_{St} = \frac{f_{AN}}{f_{St}}\left(\frac{1}{P_{St-AN}} - 1\right) \quad \text{..... [1]}$$

$$r_{AN} = \frac{f_{St}}{f_{AN}}\left(\frac{1}{P_{AN-St}} - 1\right) \quad \text{..... [2]}$$

Where f_{St} and f_{AN} are the feed mole fraction compositions of styrene and acrylonitrile, respectively, and $P_{St\text{-}AN}$ and $P_{AN\text{-}St}$ are the conditional probabilities given by:

$$P_{St-AN} = \frac{[ASA]+[ASS]/2}{[ASA]+[ASS]+[SSS]} \quad \text{..... [3]}$$

$$P_{AN-St} = \frac{[SAS]+[AAS]/2}{[SAS]+[AAS]+[AAA]} \quad \text{..... [4]}$$

Here, $P_{St\text{-}AN}$ is the probability that an St-AN unit is formed as a result of a styrene growing chain end adding acrylonitrile, and $P_{AN\text{-}St}$ is the probability that an AN-St unit is formed as a result of an acrylonitrile growing chain end adding styrene. The parameters in the square brackets are the triad fractions calculated from the quantitative ^{13}C NMR spectra. Using equations [1] and [2], the reactivity ratios of styrene and acrylonitrile for all nine different feed compositions were calculated with the results shown in Table-2.4.

Table-2.4. Reactivity ratios for copolymerization of styrene and acrylonitrile for different feed compositions calculated from the triad distributions for the copolymerization in bulk at 80 ^{o}C.

f_{St}	**0.10**	**0.20**	**0.30**	**0.40**	**0.50**	**0.60**	**0.70**	**0.80**	**0.90**
r_{St}	0.805	0.658	0.553	0.536	0.497	0.469	0.400	0.315	0.202
r_{AN}	0.088	0.104	0.119	0.120	0.129	0.130	0.173	0.229	0.351
$r_{AN}r_{St}$	0.071	0.068	0.066	0.064	0.064	0.061	0.069	0.072	0.071

Table-2.4 shows that the reactivity ratios are not constant across the range of feed compositions and the reactivity ratio of styrene increases with a higher percentage of acrylonitrile in the monomer feed, while the opposite is true for the acrylonitrile reactivity ratio. The reactivity ratios are in good agreement with those reported previously for the bulk CvRP copolymerizations by Hill et al.[7] and Klumperman and Kraeger [257], as demonstrated in Figure-2.8. The latter workers have explained their observations in a range of solvents in terms of a bootstrap effect [257].

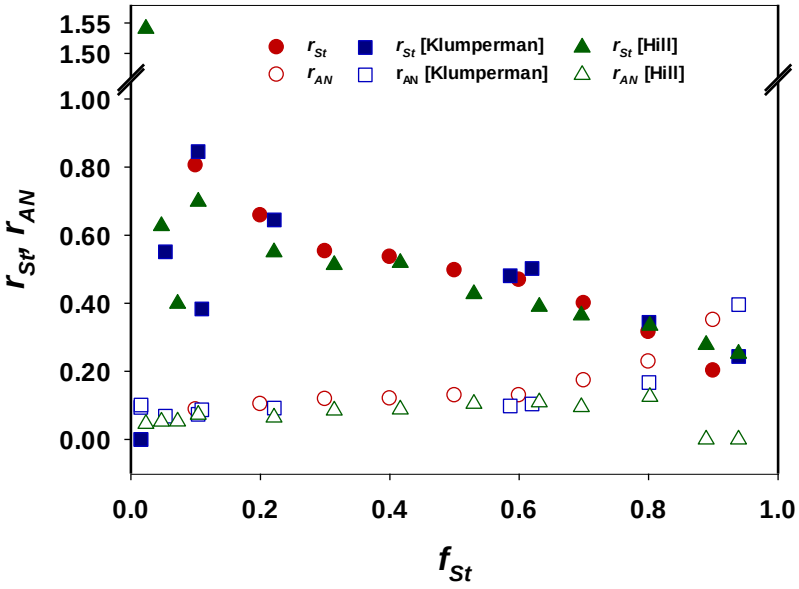

Figure-2.8: Reactivity ratios for copolymerization of styrene [●r_{St}] and acrylonitrile [○r_{AN}] found in this study versus the feed composition for the RAFT polymerization at 80 ºC. Also plotted are the reactivity ratios for CvRP reported by Klumperman et al. [257] [■r_{St}, □r_{AN}] and Hill et al.[7] [▲r_{St}, Δr_{AN}].

Several decades ago Harwood [256] explained how the polarity of the solvent can affect the reactivity ratios of mixtures of polar and non-polar monomers following studies of the copolymerizations of four different monomer pairs of different polarity. He proposed the so called 'bootstrap' model to explain his results. He postulated that the monomers could be partitioned between the solvent phase and a 'phase' surrounding the solvated copolymer which altered the concentration of the monomers in the vicinity of the propagating radical compared to that in the bulk solution (illustrated in Figure-2.9). The partitioning of monomers 1 and 2 can be described by their partition coefficients, K_1 and K_2, for the equilibria that exist between the two monomers in the domain of the growing polymer radicals and in the free solvent.

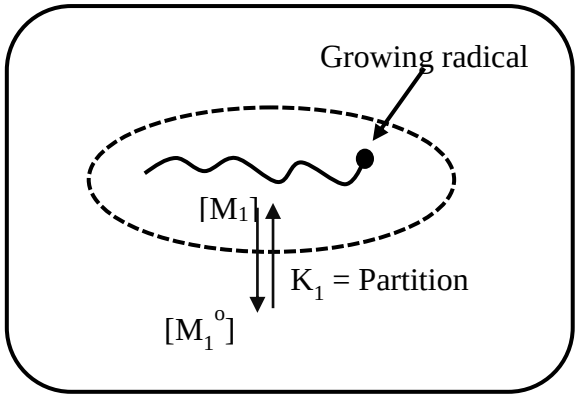

Figure-2.9: Illustration of partitioning of the monomers into the vicinity of the growing chain radical proposed by Harwood[20] for the bootstrap model.

From the bootstrap model it can be shown that there is a relationship between the reactivity ratios calculated using the terminal model copolymer equation and the reactivity ratios which would apply in the case of no partitioning taking place, r_{St}' and r_{AN}'. These relationships are:

$$r_1 = K\, r_1' \text{ and } r_2 = r_2' / K \quad \ldots\ldots\ldots\ldots [5]$$

where K is the ratio K_1/K_2.

Hence $r_1.r_2 = r_1'.r_2'$

Table-2.4 shows that the product of the reactivity ratios, $r_{(AN)}r_{(St)}$, remains approximately constant (0.067 +/- 0.007) across the feed composition range. This is strong evidence that a bootstrap effect occurs in the bulk copolymerization of styrene and acrylonitrile due to the different polarities of the growing copolymer and the unreacted bulk comonomer mixture. This is a consequence of the difference in compositions of growing copolymer chains and monomer reaction mixtures at most monomer feed ratios.

Harwood [256] proposed that the partition coefficients were independent of the comonomer composition, but to explain their observations for the styrene–acrylonitrile copolymerization Klumperman and Kraeger [257] suggested that there is a linear relationship between K and the copolymer composition, F_1. Klumperman and Kraeger described this dependency by Equation 6, in which A and B are solvent-dependent constants.

$$K = AF_1 + B \quad \ldots\ldots\ldots\ldots\ldots\ldots [6]$$

Klumperman and Kraeger [257] used the bulk copolymerization as a reference and defined that for the copolymerization in bulk A = 0 and B = 1. They then calculated the values of A and B for a range of solvents, and reported that as the solvent polarity increased A increased and B decreased in value. From the comparison of St-AN copolymerization in bulk and in three different solvents, they

revealed little but noticeable solvent effect due to penultimate unit effect which can be explained by qualitative description of bootstrap model. Hill et al. [246, 279] pointed out St and AN monomers as one of the major examples of copolymerization where penultimate unit model was obeyed. Therefore, the bootstrap model is applicable for both the penultimate unit model and terminal model which is also mathematically proved by Klumperman and O'Driscoll [280].

Hill et al. [243] earlier had reported a similar solvent effect on the reactivity ratios of St-AN copolymers by studying the copolymerization reactions in bulk, toluene, butanone and acetonitrile and they reported copolymer compositions and triad fraction data in the different solvents. They also attributed their observations of the reactivity ratios obtained assuming a terminal model to a bootstrap effect. From Figure-2.8, and according to the relationships in equation 5, the value of K must decrease as the value of f_{St} increases, by a factor of approximately four across the composition range. As the value of f_{St} increases, the polarity of the bulk comonomer mixture (the 'solvent') will decrease, and so will that of the copolymer that is formed. Therefore, as explained for the CvRP polymerization of St-AN copolymers, the solvent effect on the reactivity ratios of St and AN could also be explained based on the bootstrap model for RAFT method.

2.5 Synthesis of high-conversion St-AN copolymers by RAFT polymerization

2.5.1 Theoretical background

The Mayo-Lewis plot was generated to predict the copolymer composition for styrene-acrylonitrile monomer pair using the copolymer equation and their reactivity ratios. The difference between the reactivity ratios of St and AN results in significant deviation in the copolymer compositions from the ideal copolymerization at specific feed compositions. As Figure-2.10 shows, at 60% St feed compositions, the copolymer composition meets the ideal copolymerization plot at the azeotrope feed composition. Therefore, this particular feed composition should provide statistical copolymers with no change in the copolymer composition as monomer is consumed.

In contrast to this, for the St feed composition less than 60%, the predicted instantaneous copolymer composition of St is higher than the ideal copolymerization, and especially for 10% and 20% St feed composition the deviation is most significant. On the other hand, for St feed compositions greater than 60%, the Mayo-Lewis plot gives lower St compositions in the copolymer than the ideal copolymerization plot.

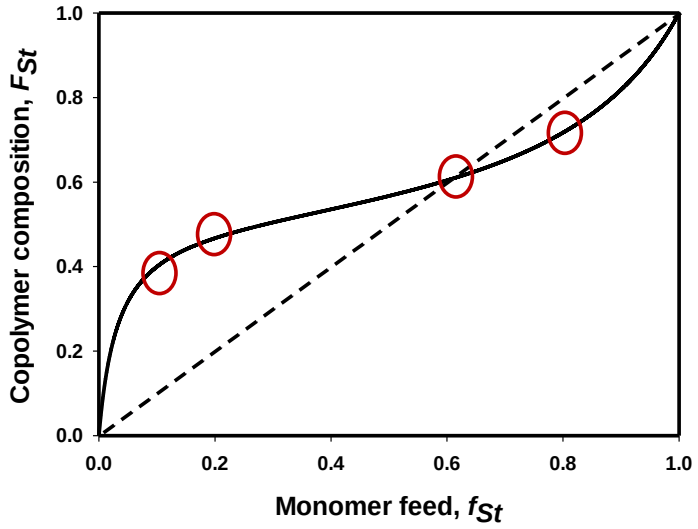

Figure-2.10: Mayo-Lewis plot for styrene – acrylonitrile copolymer showing the copolymer composition against the monomer feed composition using reactivity ratios, r_{St} = 0.394 and r_{AN} = 0.063 as reported by Hill et al. [243]. The red circles show the chosen St feed composition for high-conversion kinetics studies.

In summary, at St feed compositions other than 60%, the composition of the St-AN copolymer should change with conversion to produce a natural gradient in the copolymers chains (for RAFT polymerization where the individual chains remain alive during the full reaction). Based on the above predictions, 10% 20%, 60% and 80% St feed compositions have been chosen to study high-conversion copolymerization kinetics for the synthesis of St-AN statistical copolymers with and without composition drift.

A computer program REACT, developed by Hill and co-workers [281-283], has been used to predict the *instantaneous* copolymer compositions and triad distributions for all four monomer feed ratios using the terminal model. The data were predicted until 90% conversion with step size 0.01%. The St compositions and the triad distributions predicted using the REACT program are plotted against the copolymer conversion for four different St feed compositions (Figure-2.11 to Figure-2.14).

As expected, for 60% St feed, the azeotrope composition, the copolymer compositions and the triad distributions are essentially constant throughout the whole conversion range, and therefore produces St-AN statistical copolymers (Figure-2.12). The Mayo-Lewis plot shows very little deviation in St composition in the copolymer from the ideal copolymerization plot at 80% feed composition. This is reflected in the REACT predicted *instantaneous* composition and triad distribution plot (Figure-2.11). The copolymer composition of St increases slightly with the increase in the conversion, and the St composition reaches to 0.78 starting from an initial value of 0.68. There is also a noticeable change in the triad distributions, though the change in the St centred triads is more prominent than for the AN centred triads.

More pronounced changes are seen in the compositions and triad distributions with conversion for 10% and 20% St feed composition due to the significant deviation of the copolymer composition in the Mayo-Lewis plot for these feed compositions. The St composition in the copolymer goes from 0.45 to 0.22 at 90% conversion for 20% St feed (Figure-2.13), while the composition drift is even steeper for 10% St feed, reaching to F_{St} = 0.11 at 90% conversion starting from F_{St} = 0.38 (Figure-2.14). Both the St and AN centred triad distributions are also found to change significantly with increasing copolymer conversion. Therefore, for 10% and 20% St feed compositions, REACT predicts formation of St-AN copolymers with a strong gradient in the copolymer chains.

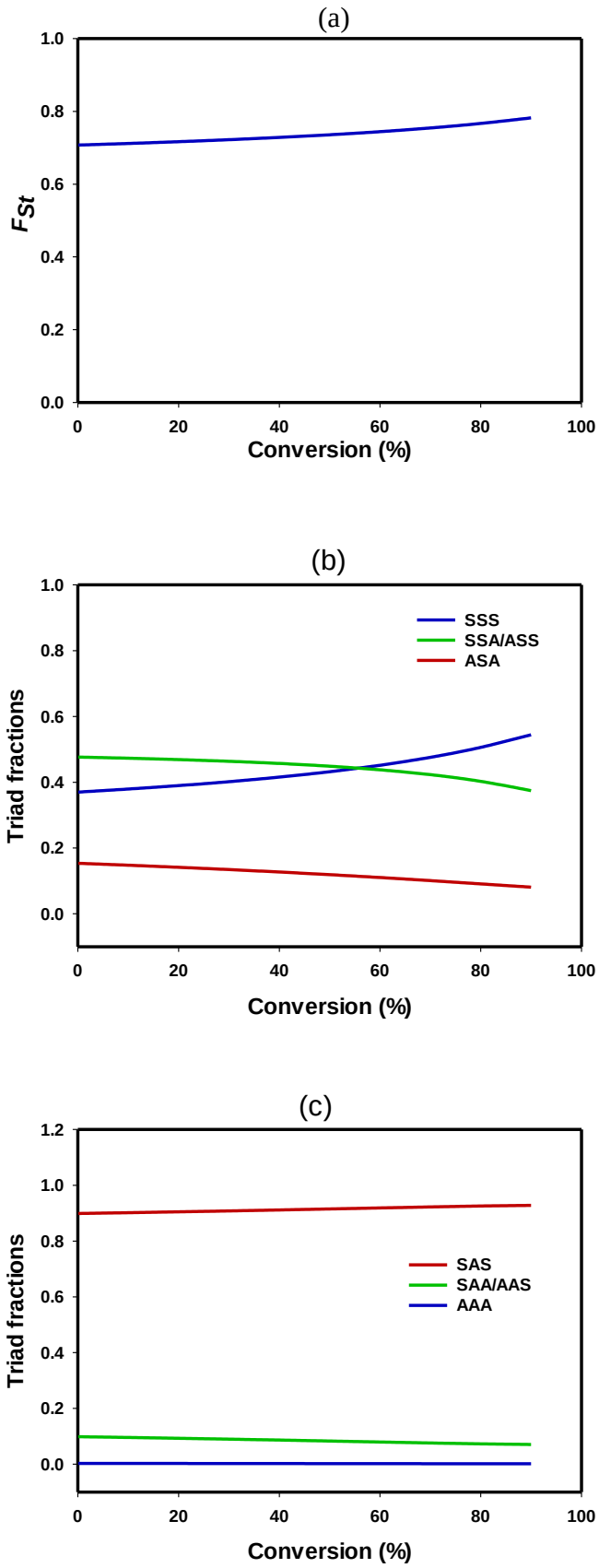

Figure-2.11: *Instantaneous* (a) St compositions in the copolymer, (b) St-centred triad distributions, and (c) AN-centred triad distributions, predicted by the REACT computer program for St-AN80 copolymer, using reactivity ratios r_{St} = 0.315 and r_{AN} = 0.229.

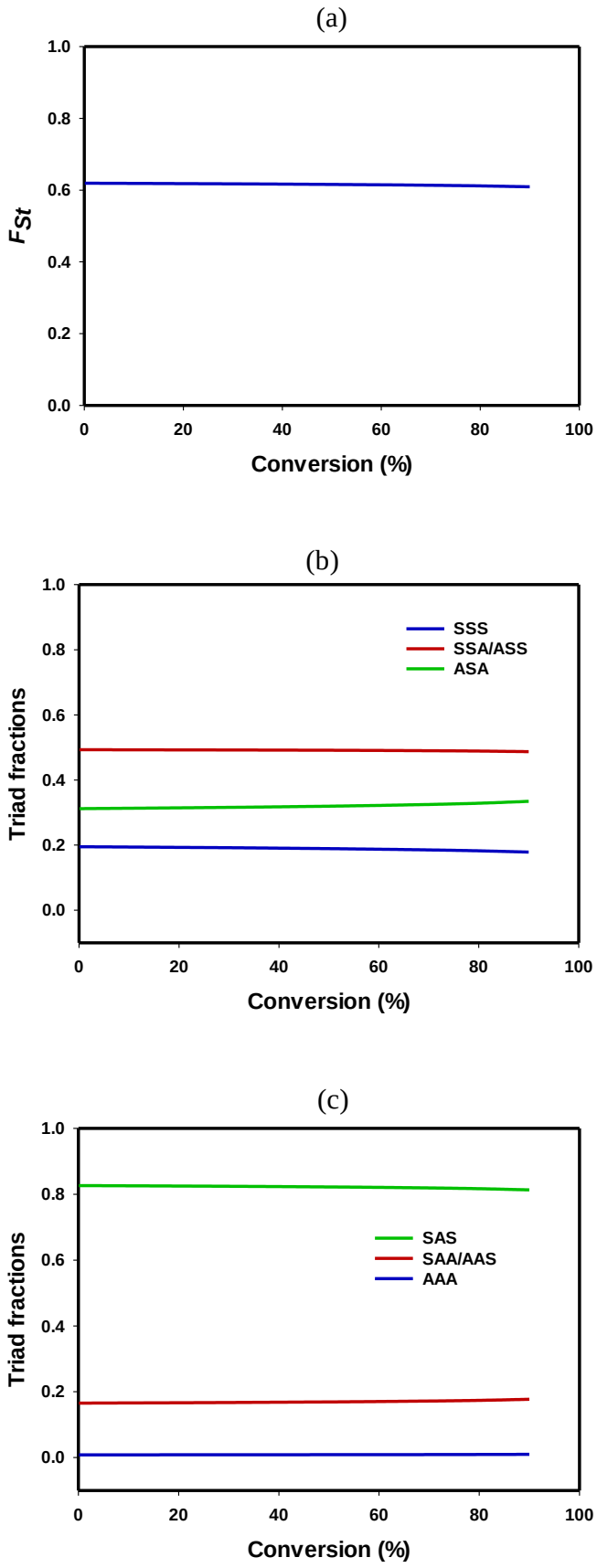

Figure-2.12: *Instantaneous* (a) St compositions in the copolymer, (b) St-centred triad distributions, and (c) AN-centred triad distributions, predicted by the REACT computer program for St-AN60 copolymer, using reactivity ratios r_{St} = 0.469 and r_{AN} = 0.130.

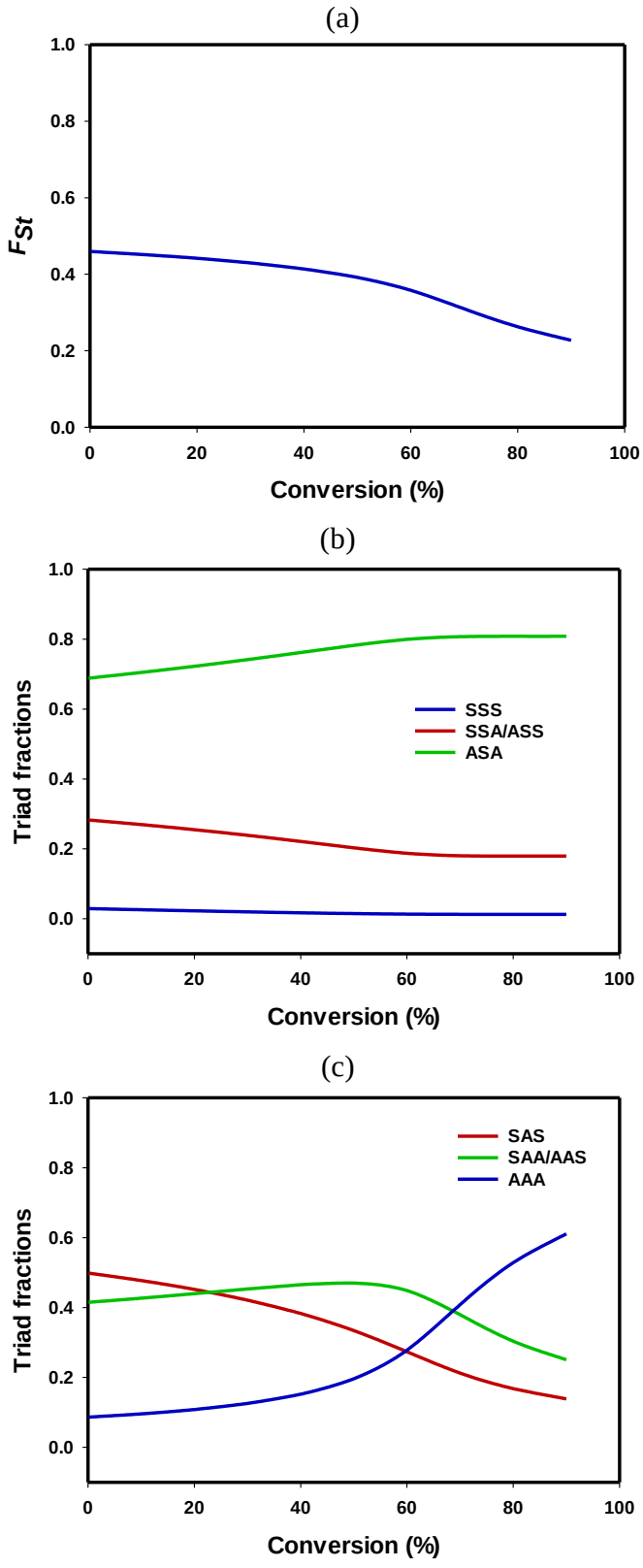

Figure-2.13: *Instantaneous* (a) St compositions in the copolymer, (b) St-centred triad distributions, and (c) AN-centred triad distributions, predicted by the REACT computer program for St-AN20 copolymer, using reactivity ratios r_{St} = 0.658 and r_{AN} = 0.104.

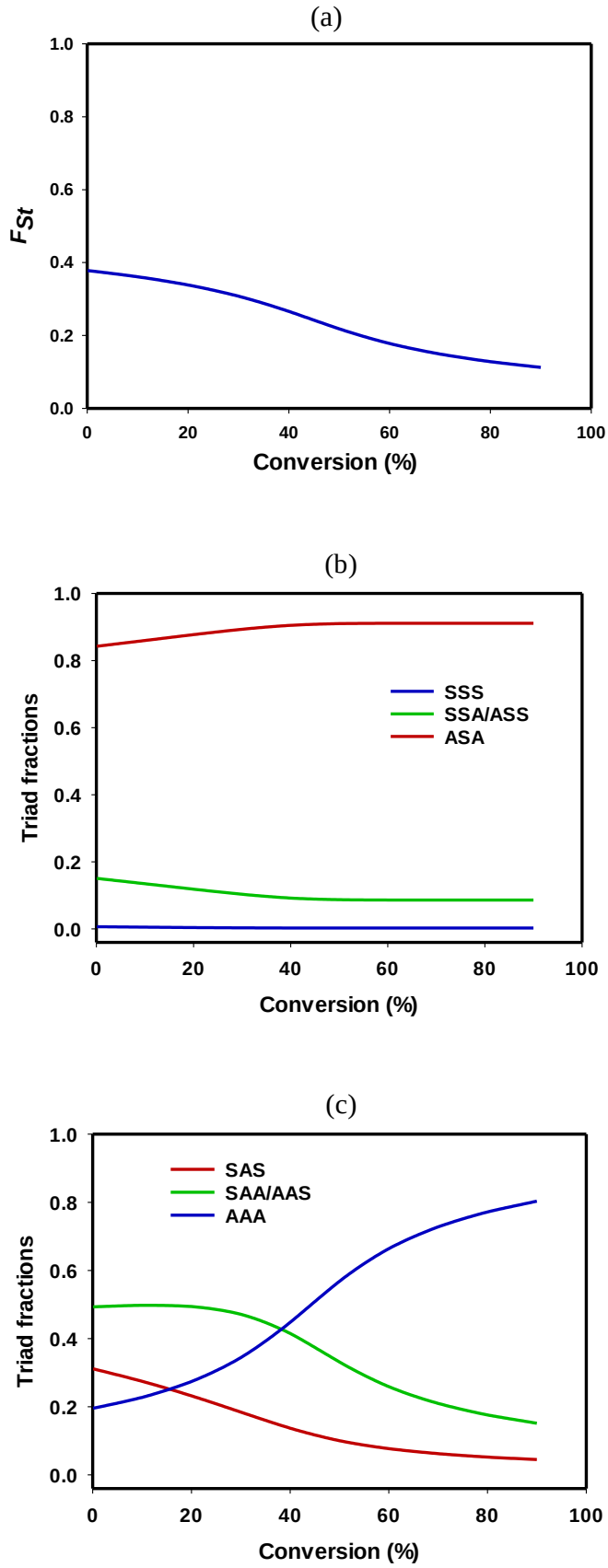

Figure-2.14: *Instantaneous* (a) St compositions in the copolymer, (b) St-centred triad distributions, and (c) AN-centred triad distributions, predicted by the REACT computer program for St-AN10 copolymer, using reactivity ratios r_{St} = 0.805 and r_{AN} = 0.088.

2.5.2 Synthesis of St-AN copolymers by RAFT method

For synthesizing high-conversion St-AN copolymers with the desired feed compositions, the reaction mixtures given in the Table-2.5 were added to a 50 mL round bottom flask for each composition. CPDB was used as the RAFT agent, and AIBN as initiator at 2:1 mole ratio for all four feed compositions. A small amount (~0.5 g) of solvent (dioxane or DMF) was added to the reaction mixture to use as reference for calculating the copolymer conversion from ^{1}H NMR. The flask was then sealed with a rubber septum and purged with N_2 for an hour to remove oxygen from the system. In a N_2 glove box, the reaction mixture from the flask was divided into six parts in 20 mL vials and each of the vials was sealed with a rubber septum. For each monomer feed composition, all six vials were allowed to react in an oil bath at 80 °C with continuous stirring. The vials were collected from the oil bath after at regular intervals and quenched in an ice bath to stop the polymerization. This process was followed for all four feed compositions to synthesize high-conversion St-AN copolymers.

Table-2.5: Reaction conditions for the synthesis of high-conversion St-AN80, St-AN60, St-AN20 and St-AN10 copolymers at 80 °C in bulk.

Designation	**St**	**AN**	**CPDB**	**AIBN**
St-AN80	18.022 g 0.173 mole	2.300 g 0.043 mole	0.201 g 0.909 mmole	0.076 g 0.463 mmole
St-AN60	15.008 g 0.144 mole	5.096 g 0.096 mole	0.198 g 0.896 mmole	0.075 g 0.457 mmole
St-AN20	6.130 g 0.059 mole	12.380 g 0.234 mole	0.178 g 0.805 mmole	0.070 g 0.427 mmole
St-AN10	3.520 g 0.034 mole	16.160 g 0.305 mole	0.198 g 0.896 mmole	0.074 g 0.451 mmole

2.5.3 Results and discussion

The conversion of St and AN monomer at any polymerization time was determined using ^{1}H NMR, from the changes in intensities of the monomer peaks with respect to the solvent as shown in Figure-2.2. The overall copolymer conversion were calculated from the individual monomer conversion and the feed compositions, as described in Section 3.3. The crude copolymer solutions were diluted by adding THF or DMF, and then precipitated in a methanol-water mixture. The process was repeated twice for complete removal of unreacted monomers and the purified copolymers were then dried in a vacuum oven at room temperature to a constant weight.

The molecular weight (M_n) and molecular weight dispersity ($Đ_M$) of the purified copolymers were characterized by SEC using THF as eluent for St-AN80 and St-AN60. Copolymers with high AN compositions are insoluble in THF and resulted in non-transparent liquid. Therefore DMAc was used as the eluent for St-AN20 and St-AN10 copolymers. Both ^{1}H and quantitative ^{13}C NMR were used to characterize the composition of styrene and acrylonitrile in the copolymers at different conversion, and the triad fractions of the copolymers were determined using the triad peaks in the quantitative ^{13}C NMR spectra. The results for each of the monomer feed compositions are described in the following sections.

2.5.3.1 St-AN80 copolymers

The conversion data shown in Table-2.6 for individual monomer and the overall copolymer conversion for St-AN80 shows a steady increase in the individual monomer and overall copolymer conversion with polymerization time, and reaches almost 65% in 20 hours. However, the individual rate of conversion of St was slower than that of AN monomer which agrees with the Mayo-Lewis plot for St-AN copolymer (Figure-2.10) showing lower instantaneous St copolymer composition.

Table-2.7 shows the molecular weight and molecular weight dispersity data characterized by SEC, and is plotted against copolymer conversion in Figure-2.15 (a). ^{1}H NMR of the purified copolymers has also been used to calculate the copolymer molecular weight as listed in Table-2.7, by comparing the intensity of peaks for St and AN unit protons in the copolymer to that of the RAFT end group (Figure-2.16). The molecular weight, characterized by both ^{1}H NMR and SEC, increases linearly with conversion, with reasonably low molecular weight dispersity indicating the controlled nature of the copolymerization. The change in the molecular weight distribution of the copolymers with conversion is plotted in Figure-2.15 (b), which shows the distribution plots shift towards higher molecular weight as the copolymer conversion increases.

Table-2.6: Conversion data for the synthesis of St-AN80 copolymers in bulk at 80 °C characterized by ^{1}H NMR.

Reaction time	[H] from St	St conversion (%)	[H] from AN	AN conversion (%)	Overall copolymer conversion (%)
0 min	87.28	-	20.85	-	-
20 mins	83.38	4.47	18.42	11.65	5.91
1 hour	71.87	17.66	14.64	29.78	20.08
2 hours	67.96	22.14	11.24	46.09	26.93
5 hours	45.66	47.69	7.02	66.33	51.41
10 hours	36.81	57.83	6.12	70.65	60.39
20 hours	34.16	60.86	4.41	78.85	64.46

Table-2.7: The molecular weight and molecular weight dispersity data for St-AN80 copolymers characterized by ^{1}H NMR and SEC.

Reaction time	Copolymer conversion (%)	M_n (^{1}H NMR)	M_n (SEC)	$Đ_M$ (SEC)
20 mins	5.91	1700	1500	1.23
1 hour	20.08	5000	5000	1.12
2 hours	26.93	8800	7400	1.16
5 hours	51.41	13100	11200	1.24
10 hours	60.39	16000	13100	1.23
20 hours	64.46	20800	14200	1.24

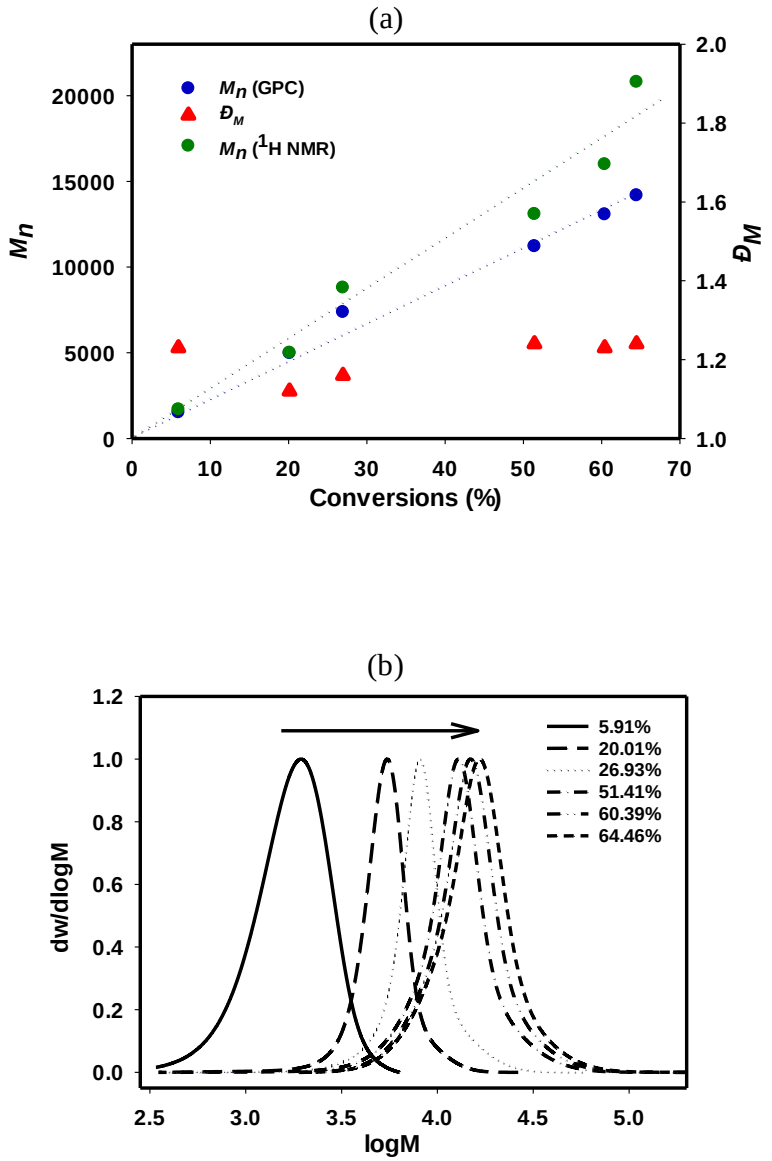

Figure-2.15: (a) Changes in the molecular weight and molecular weight dispersity and, (b) molecular weight distribution of St-AN80 copolymers with conversion characterized by SEC. The arrow in the distribution plot indicates increasing molecular weight with conversion.

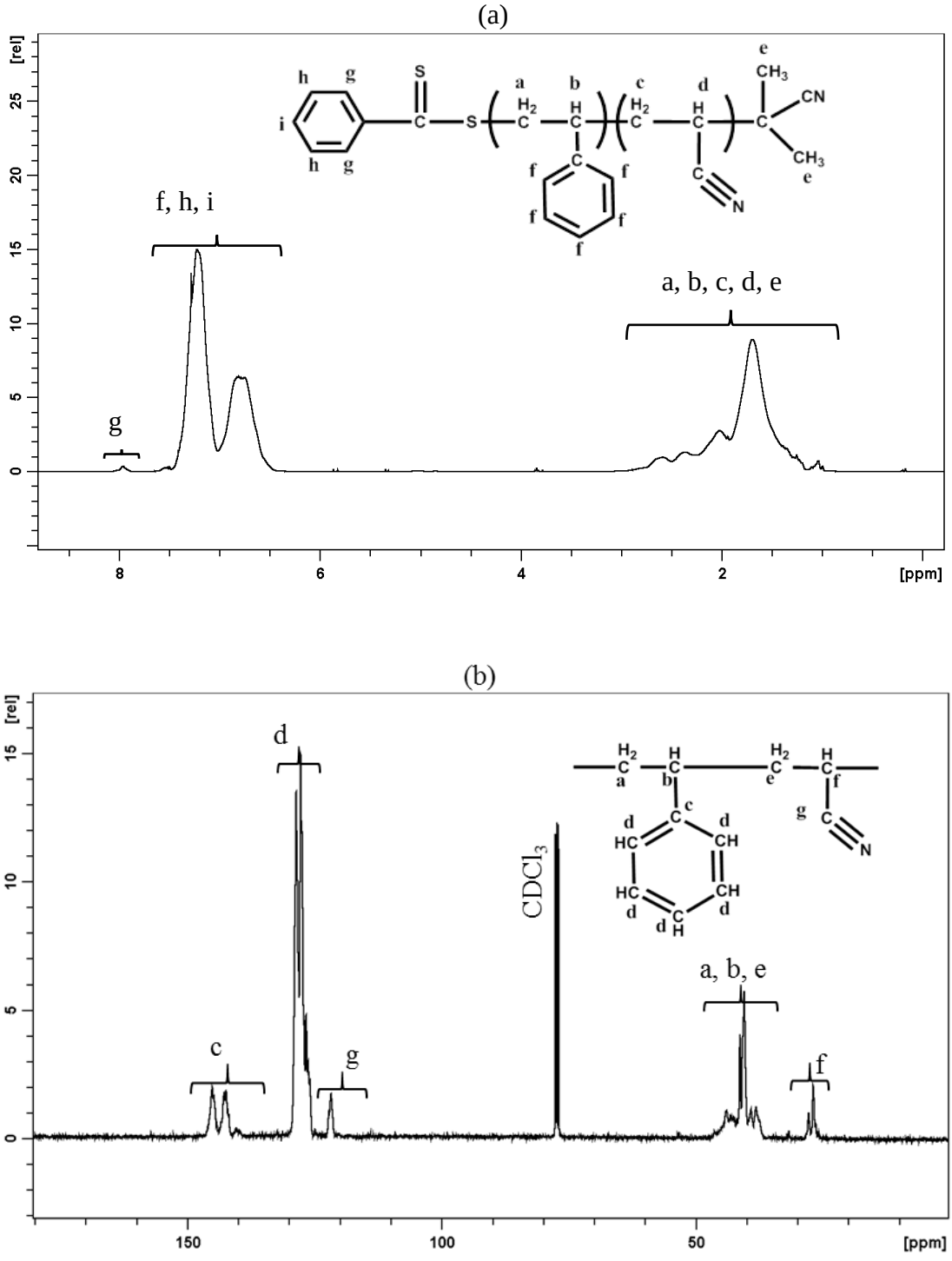

Figure-2.16: (a) ^{1}H NMR and (b) quantitative ^{13}C NMR for St-AN80 copolymer at 64.46% conversion with corresponding proton and carbon peaks.

The composition of the St-AN80 copolymer at each conversion was characterized using ^{1}H and ^{13}C NMR as shown in Figure-2.16. The compositions from the ^{1}H NMR was calculated by comparing the aromatic proton peaks from St, to that of the backbone protons from AN. In quantitative ^{13}C NMR, the aromatic carbon peak was compared to the carbon bonded to nitrogen in AN to determine the copolymer compositions. The experimental compositions are plotted against the copolymer conversion to compare with the theoretical *instantaneous* composition predicted using REACT computer program which shows excellent agreement with the theoretical predictions for St-AN80 copolymers as shown in Figure-2.17.

The St centred and AN centred triad fractions were determined by quantifying the triad peaks in quantitative ^{13}C NMR, shown in Table-2.8 and Figure-2.18. The change in experimental triad fractions with conversion for both St centred and AN centred triads mostly follow the predicted trend, though the change in the St centred triad fractions is somewhat larger than predicted. The error bars for the experimental data are estimated with 95% confidence limits in a single value calculated from three measurements.

Table-2.8: The compositions and triad fractions of St-AN80 copolymers calculated from ^{1}H and ^{13}C NMR spectra.

Conv. (%)	F_{St}		**St-centred triad fractions**			**AN-centred triad fractions**		
	^{1}H NMR	**^{13}C NMR**	***F(SSS)***	***F(SSA)***	***F(ASA)***	***F(SAS)***	***F(SAA)***	***F(AAA)***
5.91	0.728	0.735	0.354	0.507	0.138	0.906	0.084	0.010
20.08	0.719	0.730	0.392	0.498	0.111	0.942	0.053	0.005
26.93	0.746	0.752	0.451	0.469	0.080	0.955	0.044	0.001
51.41	0.756	0.763	0.456	0.470	0.074	0.961	0.034	0.005
60.39	0.763	0.775	0.476	0.464	0.059	0.970	0.028	0.002
64.46	0.767	0.781	0.493	0.445	0.062	0.968	0.032	0.000

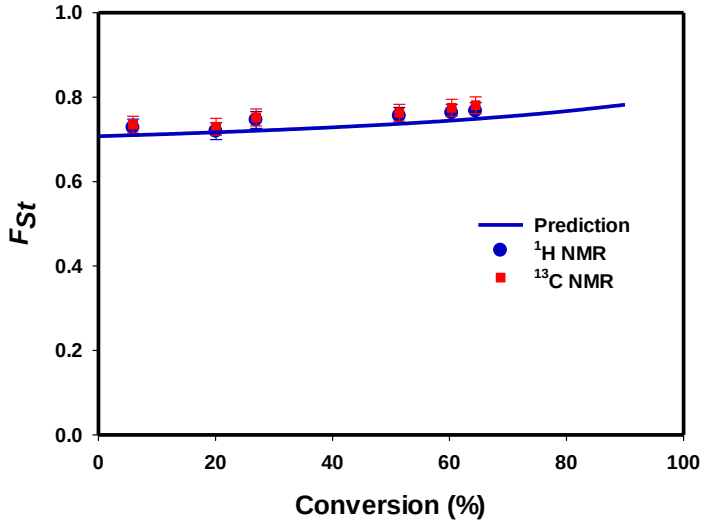

Figure-2.17: The change in the composition of styrene with conversion in St-AN80 copolymers characterized by ^{1}H NMR (●) and ^{13}C NMR (■) for 80% St feed composition compared to the predicted composition (solid line).

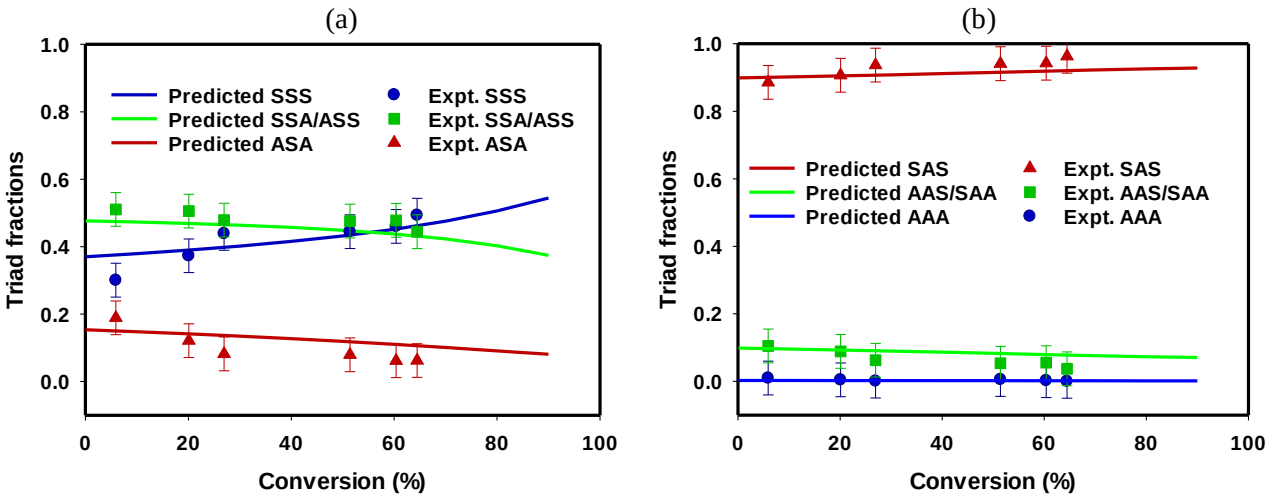

Figure-2.18: The change in the (a) St-centred and (b) AN-centred triad distribution with conversion in St-AN80 copolymers characterized by ^{13}C NMR for 80% St feed composition compared to the predicted composition.

2.5.3.2 St-AN60

Similar to the St-AN80 copolymers, the individual monomer and overall copolymer conversion from ^{1}H NMR was also determined for St-AN60 copolymers as listed in Table-2.9. The overall conversion increases with polymerization time, and reaches to as high as approximately 94% in 15 hours. As this composition is the azeotrope feed composition, the individual conversion of both St and AN monomer increases in a similar manner. The molecular weight determined by both ^{1}H NMR and SEC of the copolymer increases with the conversion, with low molecular weight dispersity (Table-2.10).

The molecular weights of St-AN60 copolymers have been plotted against the copolymer conversion and shows a linear increase (Figure-2.19). The increase in molecular weight is also supported by the molecular weight distribution plot, where the molecular weight distribution shifts from lower to higher molecular weight region as the copolymer conversion increases.

Table-2.9: Conversion data for the synthesis of St-AN60 copolymers in bulk at 80 °C characterized by ^{1}H NMR.

Reaction time	[H] from St	St conversion (%)	[H] from AN	AN conversion (%)	Overall copolymer conversion (%)
0 min	76.10	-	47.07	-	-
15 mins	72.51	4.72	43.72	7.12	5.68
20 mins	68.27	10.29	40.16	14.68	12.05
1 hour	58.25	23.46	33.65	28.51	25.48
2 hours	42.47	44.19	24.15	48.69	45.99
3 hours	34.20	55.06	16.99	63.90	58.60
4.5 hours	25.99	65.85	14.91	68.32	66.84
15 hours	5.60	92.64	1.82	96.13	94.04

Table-2.10: The molecular weight and molecular weight dispersity data for St-AN60 copolymers characterized by ^{1}H NMR.

Reaction time	Conversion (%)	M_n (^{1}H NMR)	M_n (SEC)	$Đ_M$ (SEC)
15 mins	5.68	1300	1100	1.26
20 mins	12.05	2300	3200	1.12
1 hour	25.48	5500	6400	1.13
2 hours	45.99	12200	10900	1.18
3 hours	58.60	16400	13500	1.23
4.5 hours	66.84	20100	15500	1.26
15 hours	94.04	23500	19600	1.31

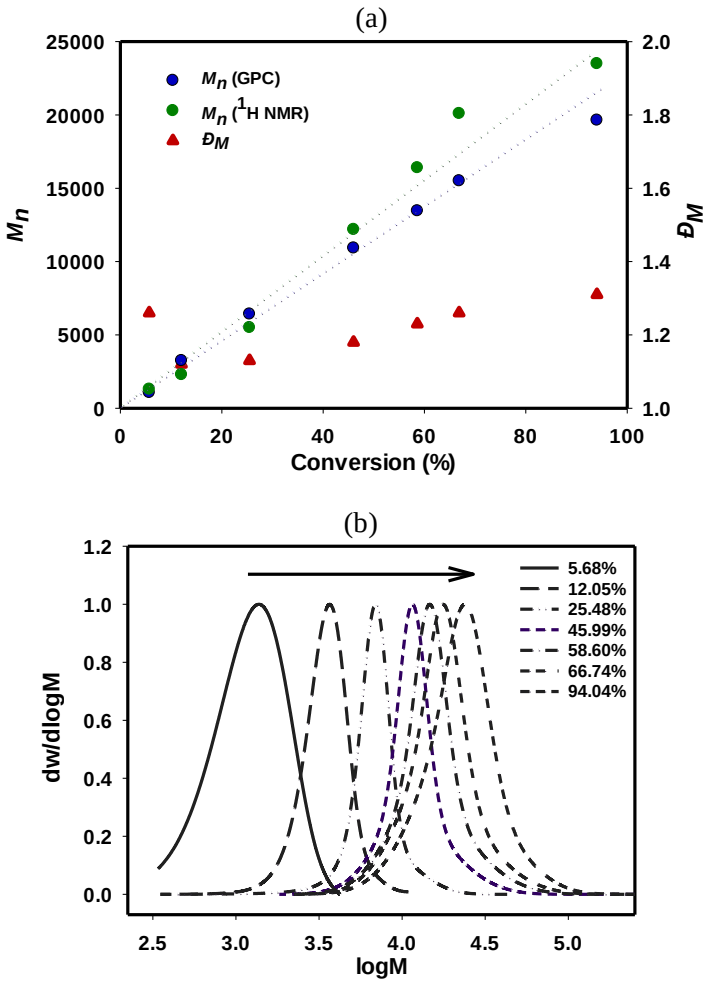

Figure-2.19: (a) Changes in the molecular weight and molecular weight dispersity characterized by SEC and ^{1}H NMR and, (b) molecular weight distribution of St-AN60 copolymers with conversion characterized by SEC. The arrow in distribution plot indicates increasing molecular weight with conversion.

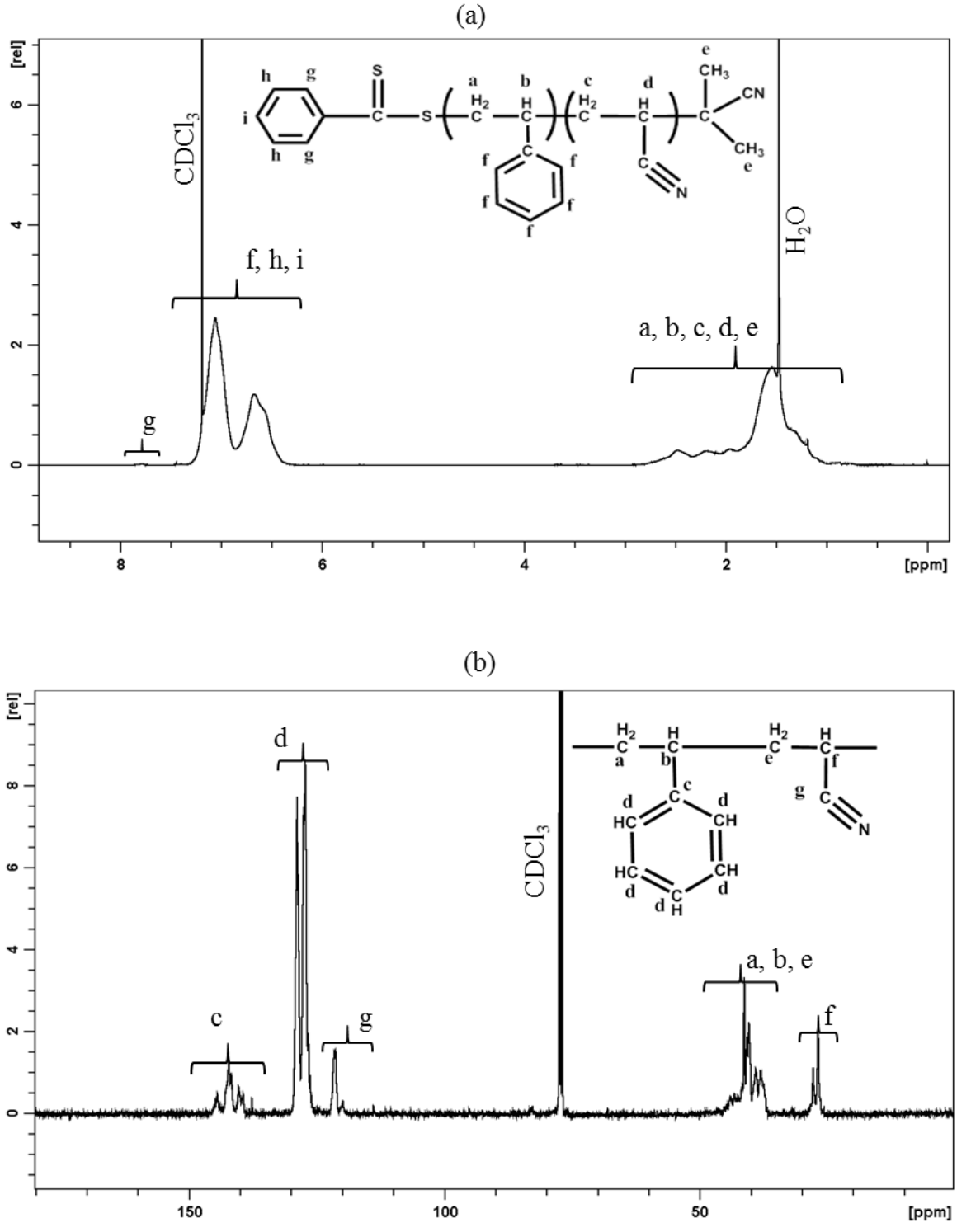

Figure-2.20: (a) ^{1}H NMR and (b) quantitative ^{13}C NMR for St-AN60 copolymer at 64.46% conversion with corresponding proton and carbon peaks.

The copolymer compositions for St-AN60 copolymers are plotted against conversion in Figure-2.21. St contents measured by both ^{1}H and ^{13}C NMR are in good agreement with the predicted compositions, and nearly constant with copolymer conversion. This indicates the formation of statistical copolymers with no drift along the copolymer chains. Beside the constant compositions, the statistical nature of the copolymer chains is also supported by the triad distributions plot (Figure-2.22). Both the St-centred triad fractions and AN-centred triad fractions are nearly constant with conversion.

Table-2.11: The compositions and sequence distributions of St-AN60 copolymers calculated from ^{1}H and ^{13}C NMR.

Conv. (%)	F_{St}		**St-centred triad fractions**			**AN-centred triad fractions**		
	^{1}H NMR	**^{13}C NMR**	***F(SSS)***	***F(SSA)***	***F(ASA)***	***F(SAS)***	***F(SAA)***	***F(AAA)***
5.68	0.647	0.654	0.189	0.486	0.324	0.819	0.179	0.002
12.05	0.596	0.641	0.176	0.502	0.322	0.848	0.150	0.002
25.48	0.602	0.633	0.166	0.529	0.305	0.858	0.141	0.000
45.99	0.600	0.637	0.181	0.526	0.293	0.858	0.141	0.000
58.60	0.594	0.649	0.216	0.508	0.276	0.864	0.136	0.000
66.84	0.604	0.641	0.189	0.542	0.269	0.872	0.128	0.001
94.04	0.605	0.649	0.221	0.530	0.249	0.879	0.120	0.001

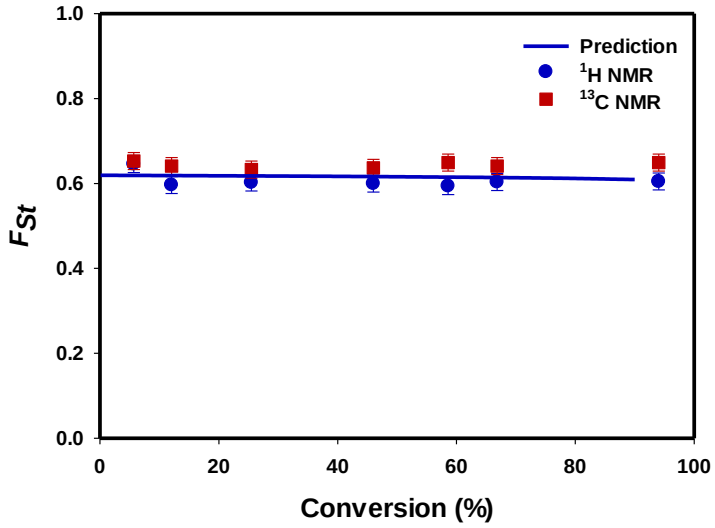

Figure-2.21: The change in the composition of styrene with conversion in St-AN60 copolymers characterized by ^{1}H NMR (●) and ^{13}C NMR (■) for 60% St feed compositions compared to the predicted compositions (solid line).

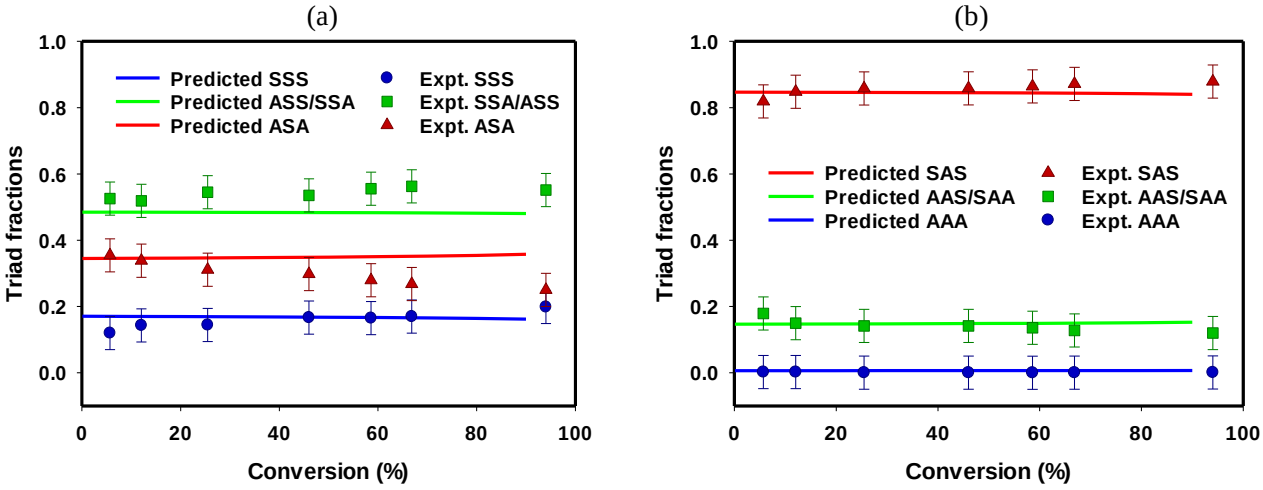

Figure-2.22: The change in the (a) St-centred and (b) AN-centred triad distribution with conversion in St-AN60 copolymers characterized by ^{13}C NMR for 60% St feed composition compared to the predicted composition.

2.5.3.3 Refractive index increment (*dn/dc* values) for St-AN copolymers in DMAc

The molecular weight and molecular weight dispersity data of the copolymers with high St content (St-AN80 and St-AN60) have been characterized by SEC using THF as eluent. However, unlike St-AN80 and St-AN60, the copolymers with high AN content (St-AN20 and St-AN10) are insoluble in THF. Therefore, to study the molecular weight data of St-AN20 and St-AN10 copolymers by SEC, *N, N*-dimethylacetamide (DMAc) has been used as the eluent.

In addition to the RI detector, the DMAc SEC was also equipped with a dual angle laser light scattering detector and a viscometer. Therefore, the absolute molecular weight of the St-AN copolymers with higher AN compositions was characterized using triple detector SEC. One of the important parameters for characterizing molecular weight and molecular weight dispersity with triple detection is the increment in the refractive index (*dn/dc)*.

The refractive index increment (*dn/dc*) is the rate of change of the refractive index with the concentration of a solution for a sample at a given temperature, wavelength and solvent. For analyzing the molecular weight and molecular weight dispersity of polymers with the light scattering data, *dn/dc* is an essential parameter. In this study, *dn/dc* values were determined for St and AN homopolymers and three different compositions of St-AN copolymers in DMAc solution.

One of the approaches to determine the *dn/dc* values of polymers is to measure the RI of the copolymers solutions at different concentrations. A pocket refractometer was used to measure the RI values which were plotted against the polymer solution concentrations (Figure-2.23). In each case, RI increases linearly as the concentration of polymer solution increases. Using the linear regression plot in Sigmaplot, the slope was determined for each plot, which is the *dn/dc* values for the polymers in DMAc.

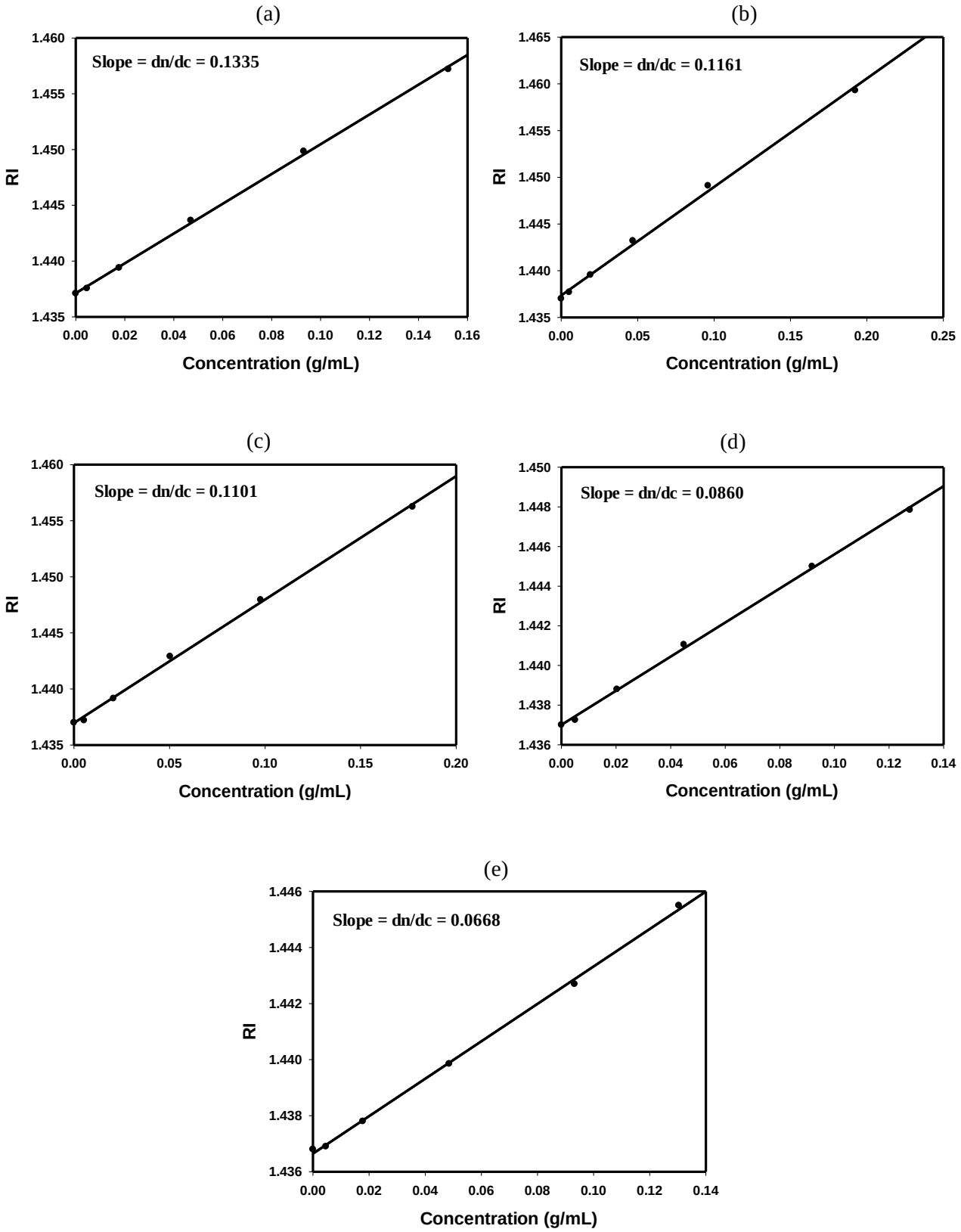

Figure-2.23: The change in the refractive index (RI) against the solution concentration of (a) PSt, (b) St-AN80, (c) St-AN60, (d) St-AN20 and (e) PAN in DMAc and their corresponding slope at room temperature.

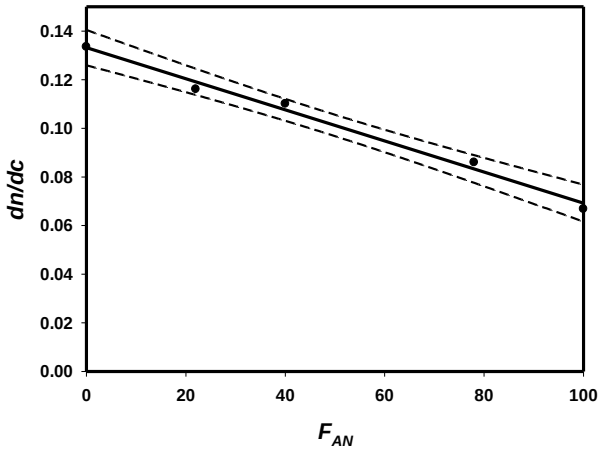

Figure-2.24: The dependence of *dn/dc* values on the St-AN copolymer composition in DMAc, with 95% confidence limit.

The dn/dc value found in this study for PSt in DMAc (0.1335 mL/g) is in close agreement with the value reported (0.148 mL/g) by Ono *et al* [284]. But there is no reported data on the dn/dc value of PAN in DMAc. However, Elbing *et al.* [285] and Kambe [286] reported the dn/dc for PAN in DMF is 0.082 mL/g and 0.085 mL/g respectively, which is close to the value found for PAN in DMAc in this study (0.0668 mL/g). The *dn/dc* values of the St, AN homopolymers, and three different copolymers, are then plotted against the AN compositions in the copolymer. As shown in Figure-2.24, the *dn/dc* value decreases with the increase in AN content in the St-AN copolymers, and possesses a linear relationship. This *dn/dc* vs AN compositions plot was used to determine the *dn/dc* values for other composition of St-AN copolymers, and applied to characterize their molecular weight data by triple detection in DMAc SEC.

2.5.3.4 St-AN20

Conversion of St monomer was found to be significantly faster than AN monomer, which agrees with the Mayo-Lewis plot (Figure-2.10), where the predicted St composition is much higher than the ideal copolymer plot at 20% St feed composition. After 4 hours of polymerization, nearly 98% of St was converted to polymer, while the conversion of AN monomer was only about 44%. Within 10 hours, almost 100% St monomer was converted to polymer, and an overall conversion of approximately 84% were achieved. The ^{1}H NMR data for St-AN20 copolymers was collected using DMSO-d6 as solvent, since St-AN copolymers with high AN content are insoluble in $CDCl_3$.

Table-2.12: Conversion data for the synthesis of St-AN20 copolymers in bulk at 80 °C characterized by ^{1}H NMR.

Reaction time	[H] from St	St conversion (%)	[H] from AN	AN conversion (%)	Overall copolymer conversion (%)
0 min	131.72	-	434.09	-	-
15 mins	109.30	17.02	414.04	4.62	7.10
1 hour	60.84	53.81	360.46	16.96	24.33
2.5 hours	15.25	88.42	281.78	35.09	45.75
4 hours	2.75	97.91	244.30	43.72	54.56
5 hours	0.40	99.70	163.75	62.28	69.76
6 hours	0.08	99.94	117.95	72.83	78.25
10 hours	0.19	99.86	84.29	80.58	84.44

Table-2.13: The molecular weight and molecular weight dispersity data for St-AN20 copolymers characterized by ^{1}H NMR and SEC.

Reaction time	Conversion (%)	*Mn* (^{1}H NMR)	*Mn* (SEC)		$Đ_M$ (SEC)	
			RI detector	Triple detector	RI detector	Triple detector
1 hour	24.33	6700	10901	10400	1.28	1.06
2.5 hours	45.75	11200	20557	19200	1.39	1.09
4 hours	54.56	13100	26287	22000	1.35	1.10
5 hours	69.76	15300	32781	29500	1.44	1.15
6 hours	78.25	18000	35640	30600	1.52	1.11
10 hours	84.44	21500	39052	32400	1.59	1.15

The molecular weight of St-AN20 copolymers, determined from the ^{1}H NMR data by comparing the copolymer peaks to the RAFT end group peak, shows a gradual increase in the molecular weight with conversion. Similar increase in molecular weight as well as in the molecular weight dispersity have also been observed from the data collected by SEC for both RI and triple detector. Both RI and triple detector provides reasonably similar molecular weights for St-AN20 at early conversion, however the molecular weight determined by these two detectors was significantly

different at higher conversion. The molecular weight dispersity determined by the RI detector was found to be unusually high, while it was unusually low for the triple detector. These low dispersity values could be due to poor separation of the SEC rather than a narrow molecular weight distribution which might be due to poor solubility of St in DMAc.

Furthermore, the molecular weight of the St-AN80 and St-AN60 copolymers determined by ^{1}H NMR and SEC were in good agreement with each other. However, for St-AN20, the molecular weights determined by ^{1}H NMR and SEC were significantly different from each other. This could be due to the differences in the hydrodynamic volume of the St-AN copolymer in THF and DMAc.

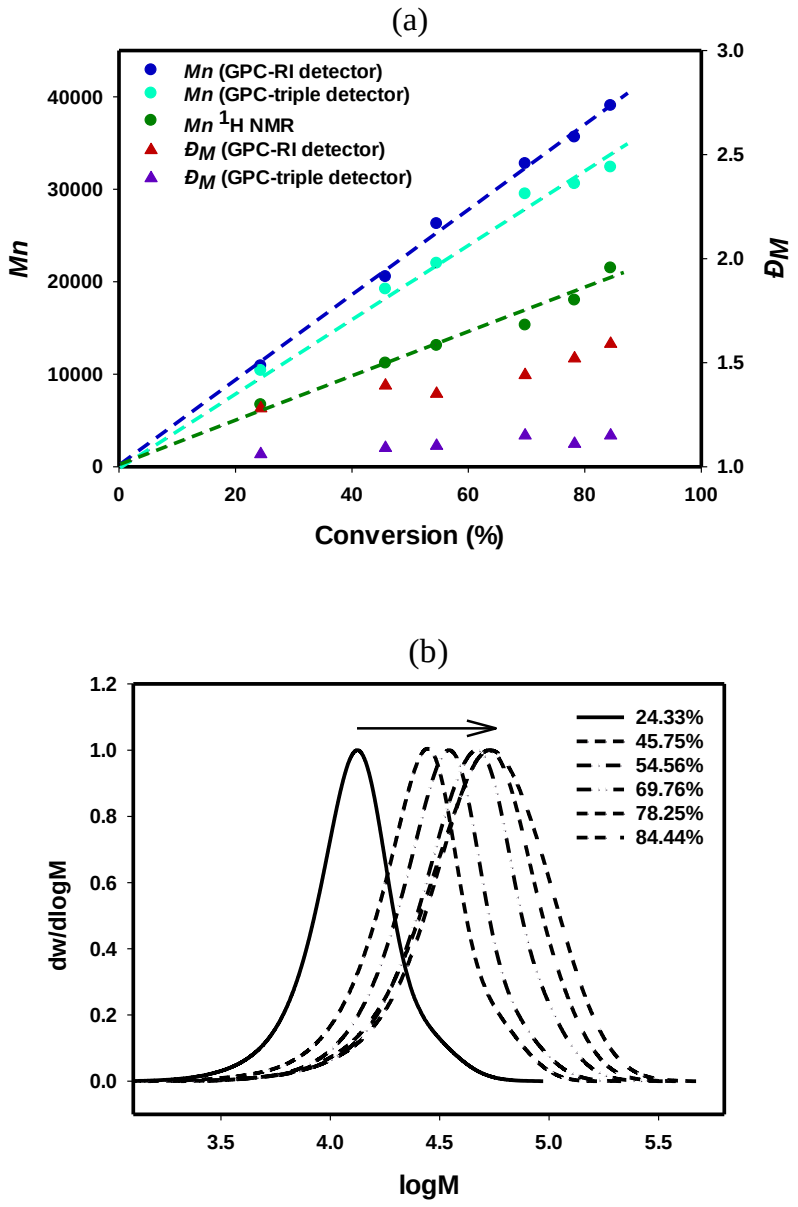

Figure-2.25: (a) Changes in the molecular weight and molecular weight dispersity and, (b) molecular weight distribution of St-AN20 copolymers with conversion characterized by SEC. The arrow in the distribution plot indicates increasing molecular weight with conversion.

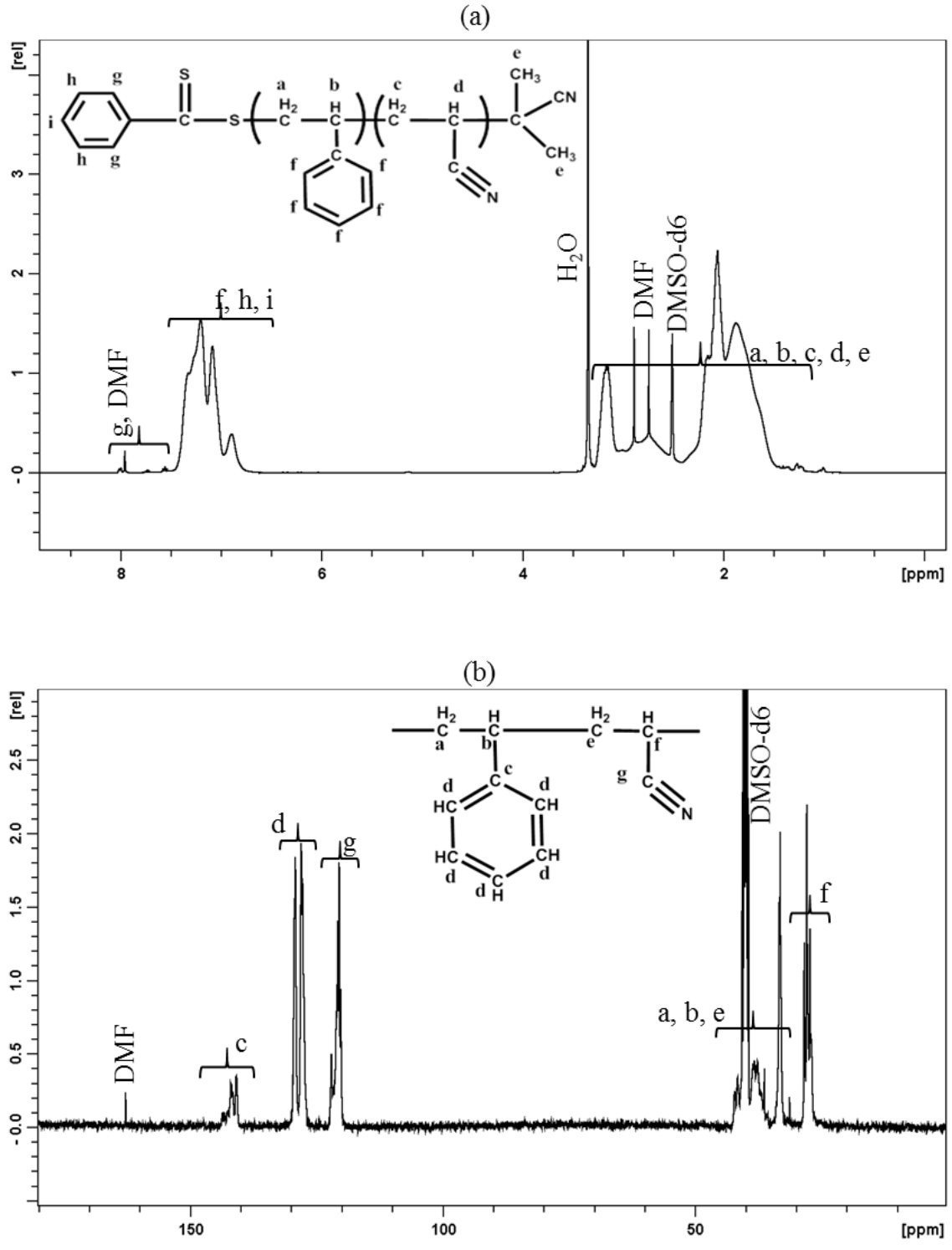

Figure-2.26: (a) ^{1}H NMR and (b) quantitative ^{13}C NMR, for St-AN20 copolymer at 64.46% conversion with corresponding proton and carbon peaks.

The compositions of St-AN20 copolymers at different conversion, measured by ^{1}H and ^{13}C NMR are in very good agreement with the *instantaneous* copolymer compositions predicted by the computer program REACT (Figure-2.27). The St compositions of the copolymers are found to be decreasing as the copolymer conversion increases, indicating significant drift in St content along the copolymer chains. Therefore, a spontaneous gradient in the copolymer chains of St-AN20 was achieved as a result of the differences in the reactivity ratios of St and AN monomer at 20% St feed composition.

Table-2.14: The compositions and sequence distributions of St-AN20 copolymers calculated from ^{1}H and ^{13}C NMR spectra.

Conv. (%)	F_{St}		**St-centred triad fractions**			**AN-centred triad fractions**		
	^{1}H NMR	**^{13}C NMR**	***F(SSS)***	***F(SSA)***	***F(ASA)***	***F(SAS)***	***F(SAA)***	***F(AAA)***
24.33	0.434	0.441	0.019	0.252	0.729	0.493	0.436	0.071
45.75	0.398	0.408	0.017	0.207	0.776	0.349	0.469	0.182
54.56	0.355	0.358	0.009	0.191	0.800	0.287	0.461	0.252
69.76	0.285	0.289	0.014	0.191	0.795	0.208	0.388	0.404
78.25	0.252	0.260	0.010	0.185	0.805	0.181	0.253	0.567
84.44	0.239	0.244	0.020	0.187	0.793	0.166	0.236	0.598

The successful synthesis of a spontaneous gradient in the structure of St-AN20 copolymer chains is also supported by the change in the St and AN centred triad distributions in the copolymer chains with copolymer conversion. The predicted and the experimental triad fractions are compared in Figure-2.28, and are in a good agreement. It is clear from the comparative plot of the triad distributions that both the St and AN centered triad fractions change as the copolymer conversion increases. The change in the AN centred triad fractions is more pronounced than the St centred triads. However, it is to be noted that, unlike the triad peaks of St-AN80 and St-AN60 in $CDCl_3$, the triad peaks of St-AN20 are not that well resolved in DMSO-d6. Therefore, the error associated with the triad fraction calculations from the ^{13}C NMR using DMSO-d6 as solvents are likely to be more significant than those in $CDCl_3$.

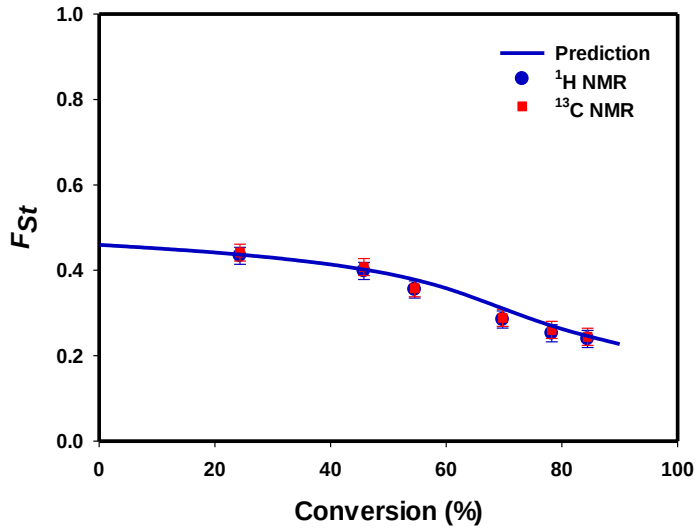

Figure-2.27: The change in the composition of styrene with conversion in St-AN20 copolymers characterized by ^{1}H NMR (●) and ^{13}C NMR (■) for 20% St feed compositions compared to the predicted compositions (solid line).

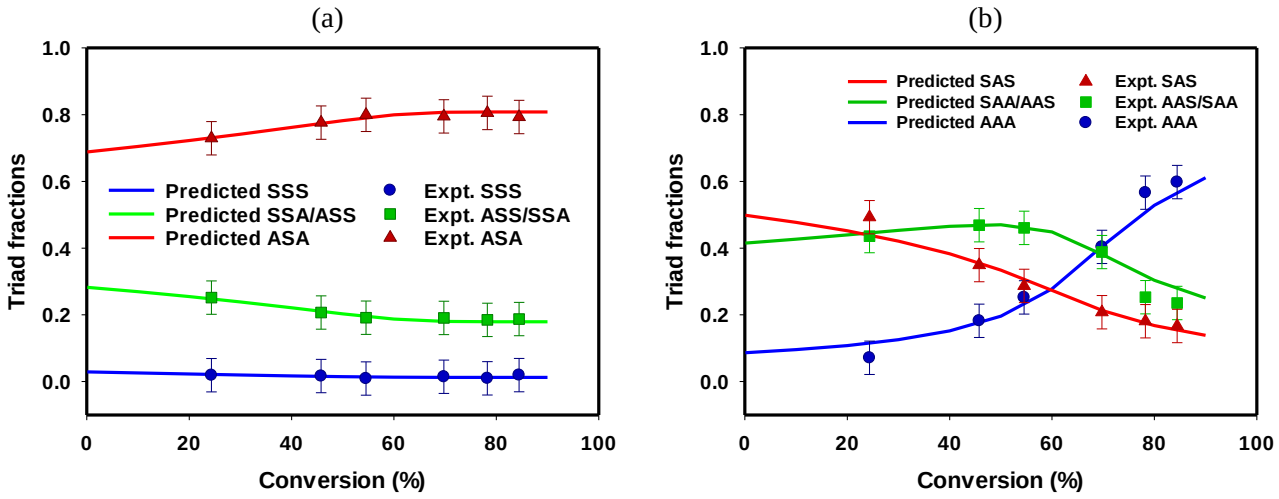

Figure-2.28: The change in the (a) St-centred and (b) AN-centred triad distribution with conversion in St-AN20 copolymers characterized by ^{13}C NMR for 20% St feed composition compared to the predicted composition.

2.5.3.5 St-AN10

Similar to the St-AN20 copolymer system, St-AN10 copolymer also shows significantly higher St copolymer composition than the ideal composition in the Mayo-Lewis plot. Therefore, the conversion of St monomer is faster than that of the AN monomer. Conversion of St reaches to more than 99% in just three hours, while it was about 56% for AN. Approximately 93% overall conversion was achieved in 11 hours for St-AN10 copolymer as determined by ^{1}H NMR.

Table-2.15: Conversion data for the synthesis of St-AN80 copolymers in bulk at 80 °C characterized by ^{1}H NMR.

Reaction time	**[H] from St**	**St conversion (%)**	**[H] from AN**	**AN conversion (%)**	**Overall copolymer conversion (%)**
0 min	431.81	-	3582.28	-	-
1hour	192.49	55.42	3113.92	13.07	17.31
2 hours	63.14	85.38	2376.90	33.65	38.82
3 hours	2.30	99.47	1576.44	55.99	60.34
4 hours	2.76	99.36	989.26	72.38	75.08
6 hours	0.27	99.94	590.99	83.50	85.15
11 hours	0.00	100.00	263.24	92.65	93.39

Table-2.16: The molecular weight and molecular weight dispersity data for St-AN10 copolymers characterized by ^{1}H NMR, and SEC.

Reaction time	**Conversion (%)**	***Mn* (^{1}H NMR)**	***Mn* (SEC)**		***Đ*$_M$ (SEC)**	
			RI detector	**Triple detector**	**RI detector**	**Triple detector**
1hour	17.31	4300	9021	7600	1.26	1.05
2 hours	38.82	8200	14693	11900	1.32	1.08
3 hours	60.34	10800	23964	17500	1.37	1.08
4 hours	75.08	16200	36463	26100	1.61	1.22
6 hours	85.15	19900	39822	26100	1.81	1.18
11 hours	93.39	21300	47045	35700	1.95	1.35

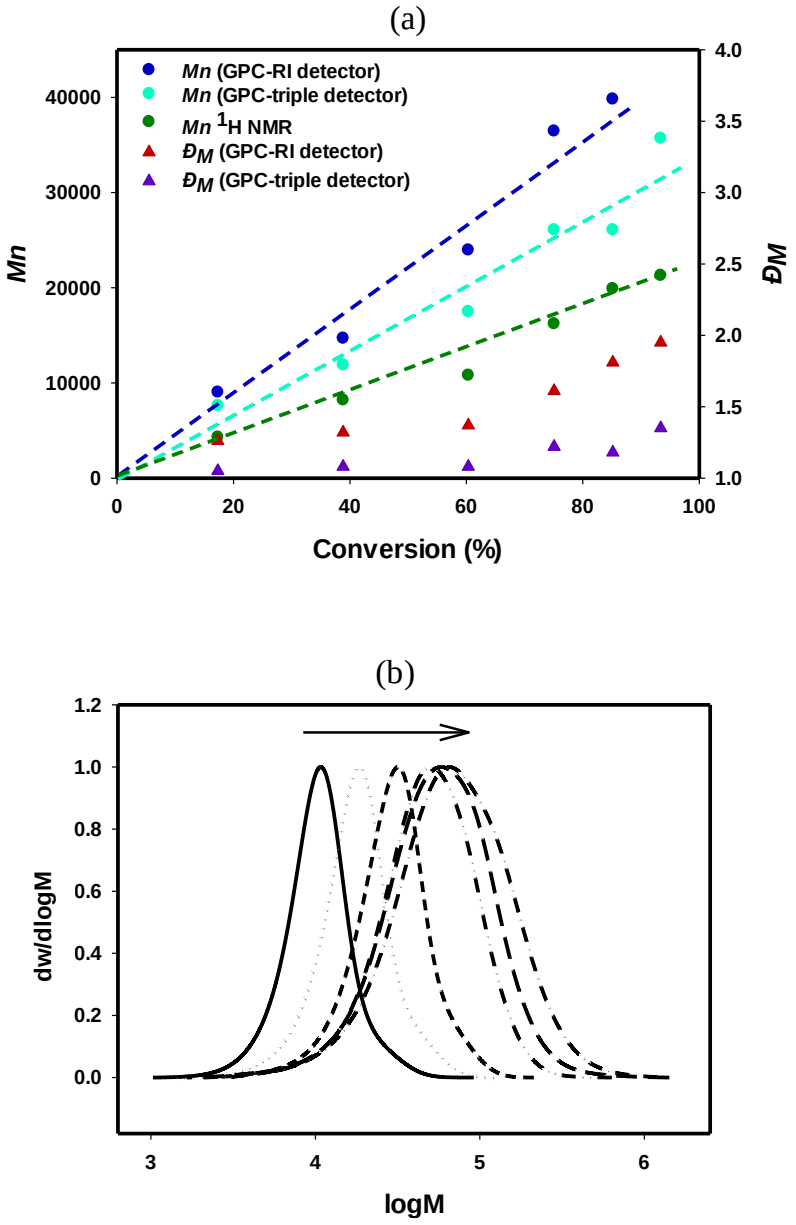

Figure-2.29: (a) Changes in the molecular weight (M_n) and molecular weight dispersity and, (b) molecular weight distribution of St-AN10 copolymers with conversion characterized by SEC. The arrow in the distribution plot indicates increasing molecular weight with conversion.

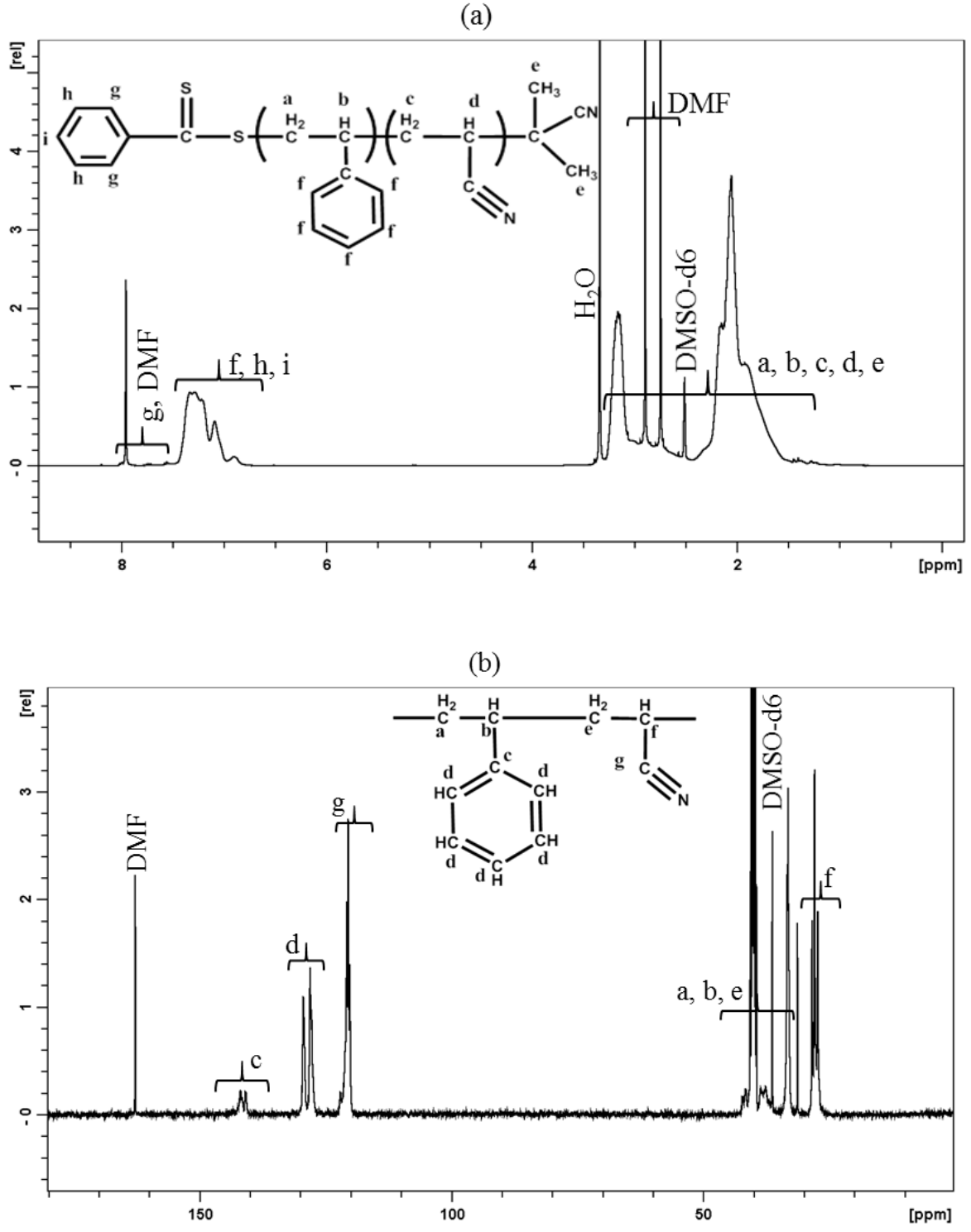

Figure-2.30: (a) ^{1}H NMR and (b) quantitative ^{13}C NMR, for St-AN10 copolymer at 64.46% conversion with corresponding proton and carbon peaks.

The molecular weight and molecular weight dispersity data for St-AN10 copolymers studied by SEC and ^{1}H NMR are listed in Table-2.16 and also plotted in Figure-2.29. The trend in molecular weight looks somewhat similar to that for St-AN20. The molecular weight found from SEC using both RI and triple detector, and also calculated from ^{1}H NMR increases gradually with conversion. However, the copolymer molecular weights calculated from ^{1}H NMR were nearly half of that of the molecular weight found from SEC. The molecular weight of the copolymers determined by the SEC are significantly higher than those determined by ^{1}H NMR, which might be due to error in baseline correction in SEC.

Table-2.17: The compositions and sequence distributions of St-AN10 copolymers calculated from ^{1}H and ^{13}C NMR spectra.

Conv (%)	F_{St}		**St-centred triads**			**AN-centred triads**		
	^{1}H NMR	**^{13}C NMR**	***F(SSS)***	***F(SSA)***	***F(ASA)***	***F(SAS)***	***F(SAA)***	***F(AAA)***
17.31	0.331	0.355	0.012	0.141	0.847	0.240	0.493	0.266
38.82	0.303	0.320	0.005	0.110	0.885	0.145	0.401	0.455
60.34	0.224	0.236	0.010	0.080	0.909	0.075	0.287	0.638
75.08	0.142	0.147	0.006	0.100	0.894	0.051	0.165	0.784
85.15	0.123	0.131	0.006	0.096	0.898	0.043	0.140	0.817
93.39	0.125	0.135	0.002	0.159	0.838	0.037	0.150	0.814

The composition of St in the St-AN10 copolymer decreases as the copolymer conversion increase as found from both the ^{1}H and ^{13}C NMR data listed in Table-2.17. The St compositions in the copolymer have also been plotted against the copolymer conversion to compare with the values predicted by the REACT program. The experimental St compositions determined from ^{1}H and quantitative ^{13}C NMR are in excellent agreement with the predicted data (Figure-2.30). As predicted, the St-AN10 copolymer shows a significant drift in St composition in the copolymer, indicating the formation of a spontaneous gradient structure in the copolymer chains.

In addition to the change in the copolymer composition, the formation of a spontaneous gradient copolymer for 10% styrene feed is also strongly supported by the changes in the triad fractions with copolymer conversion (Figure-2.31 and Figure 2.32). Both the St and AN centred triad fractions were determined from quantitative ^{13}C NMR, and plotted against the conversion to compare with the predicted triad fractions. However, the changes in the AN centred triads are more significant than those of the St centred triads.

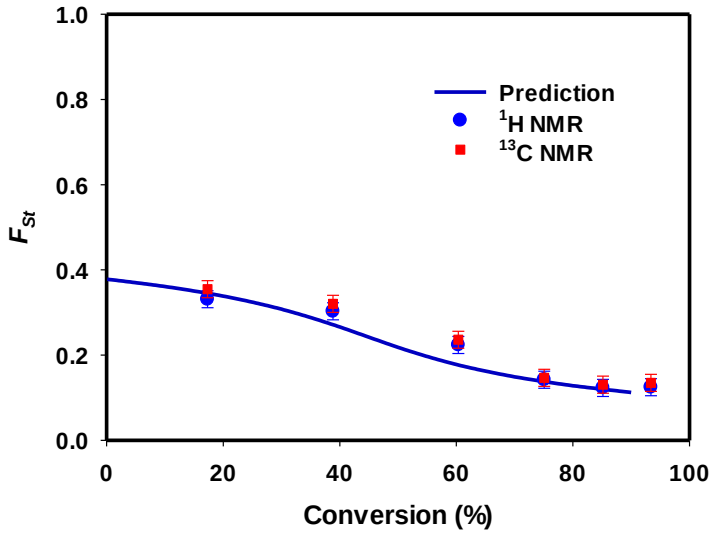

Figure-2.31: The change in the composition of styrene with conversion in St-AN10 copolymers characterized by ^{1}H NMR (●) and ^{13}C NMR (■) for 10% St feed compositions compared to the predicted compositions (solid line).

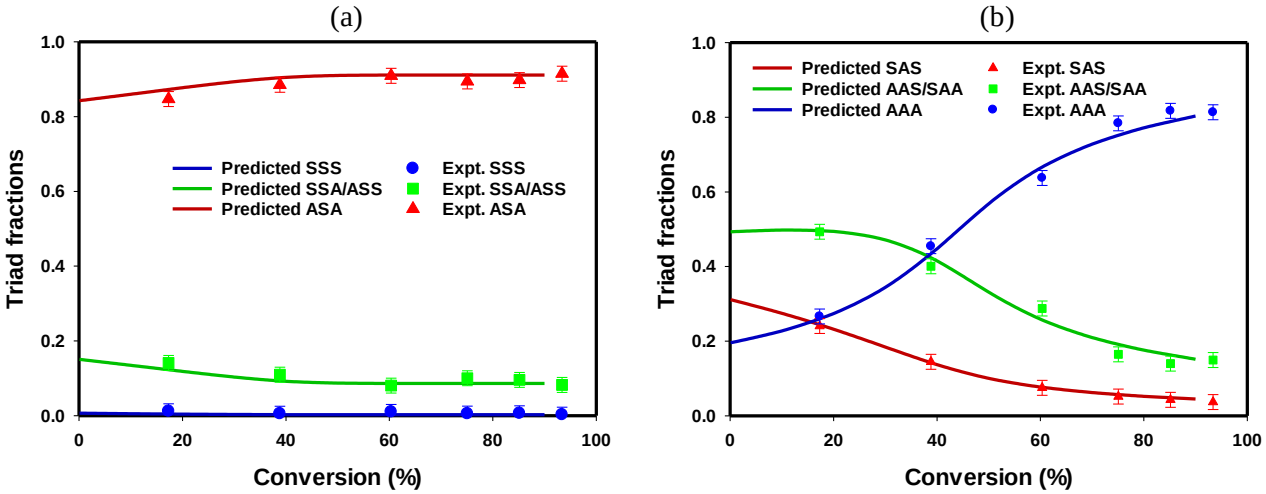

Figure-2.32: The change in the (a) St-centred and (b) AN-centred triad distribution with conversion in St-AN10 copolymers characterized by ^{13}C NMR for 10% St feed composition compared to the predicted composition.

2.6 Synthesis of styrene-acrylonitrile forced gradient (St-grad-AN) copolymers

As discussed in the previous sections, owing to the significant difference in their reactivity ratios, styrene and acrylonitrile monomer pairs produce natural gradients in compositions in their structure at certain feed compositions (80%, 20% and 10% St), while for the azeotrope composition (60% St), constant compositions have been found. Beside the natural gradient in the St-AN copolymer chains produced for batch polymerization of 80%, 20% and 10% St feed composition, a semi-batch continuous feeding method was also applied to produce composition drift in the copolymer chains to prepare forced gradient St-grad-AN60 copolymers, for azeotrope (60% St) composition.

2.6.1 Experimental procedure

In a 20 mL vial, 0.120 g (0.504×10^{-3} mole) of PABTC RAFT agent, 0.059 g (0.360×10^{-3} mole) of AIBN and 4.604 g (0.063 mole) of DMF was added to 3.185 g (0.060 mole) of acrylonitrile monomer. In another vial, 0.060 g (0.366×10^{-3} mole) of AIBN and 1.173 g (0.013 mole) of dioxane was added to 9.335 g (0.090 mole) of styrene. DMF was used as reference solvent to monitor the change in the conversion of acrylonitrile while dioxane was used for styrene. Both of the vials were sealed with rubber septa and degassed with N_2 gas for 30 minutes. The styrene monomer along with the solution was transferred to an air tight syringe. The vial with the acrylonitrile monomer was put into an oil bath at 70 °C for polymerization, and at the same time, the syringe containing the styrene monomer solution was connected to the vial to add the styrene continuously to the reaction system. Styrene solution was added at a rate of 1.1 mL/hour for 10 hours. Samples were collected from the reaction system at regular interval to monitor the progress of reaction.

2.6.2 Results and discussion

The crude reaction mixture collected during polymerization was characterized by ^{1}H NMR. The conversion of styrene and acrylonitrile was calculated by comparing the spectra to the initial spectrum, and the overall conversion were calculated using the ratio of monomer feed compositions. The percentage conversion of AN was calculated by comparison with the initial amount of AN. However, in case of St, the conversion was calculated based on the amount of St added up to that time point, and the overall percentage of St conversion was determined based on the total amount of St to be added. Table-2.18 shows the ^{1}H NMR data for the individual monomer conversion as well as the overall copolymer conversion.

Table-2.18: Conversion data for the synthesis of St-grad-AN60 copolymers in bulk at 80 °C characterized by ^{1}H NMR.

Reaction time	[H] from St	Conv. of added St (%)	Overall conv. of St (%)	[H] from AN	Conv. of AN (%)	Overall copolymer conv. (%)
0 hour	81	-	-	91	-	-
1.5 hours	42	48.52	7.01	68	25.27	14.32
4 hours	28	65.93	25.41	35	61.54	39.86
6 hours	27	66.67	38.54	15	83.52	56.53
8 hours	31	62.17	47.92	5	94.35	66.49
11 hours	21	74.07	74.07	3	96.59	83.08

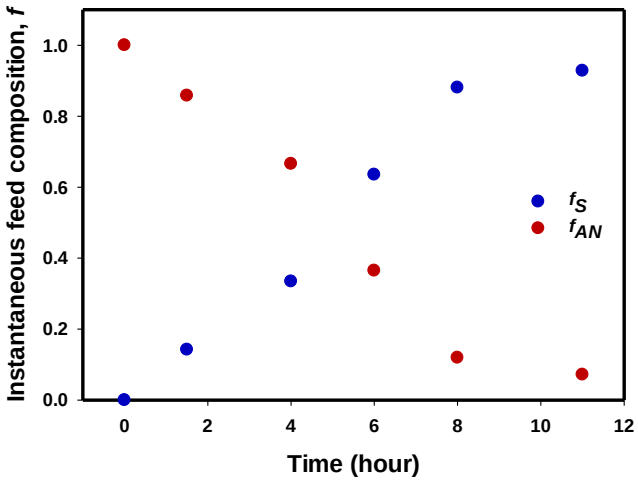

Figure-2.33: The change in the instantaneous monomer compositions with polymerization time for St-grad-AN60 copolymer synthesis characterized by ^{1}H NMR.

The polymerization reaction was started with all of the acrylonitrile monomer in the reaction mixture, and styrene was gradually added to the reaction system. At the very beginning of the reaction, there was only acrylonitrile monomer in the system. As the reaction time progressed, with the addition of St, the instantaneous acrylonitrile feed composition decreased while styrene feed composition increased. This allows the copolymer chain to start with acrylonitrile monomer units, and gradually incorporating styrene units, and in the end when most of the AN monomer is converted to polymer, the copolymer chains will be styrene dominant. The changes in the instantaneous St and AN monomer fractions in the reaction system are plotted against the

polymerization time in Figure-2.33, and shows a gradual increase in St composition with time as additional St monomer was added to the system, while the instantaneous composition of AN decreases.

The collected copolymer samples from the reaction system were diluted by adding a small amount of THF and the copolymers were precipitated in a methanol-water mixture. The filtered and purified copolymers were then dried in a vacuum oven at room temperature to a constant weight. The molecular weight and molecular weight dispersity of the copolymers were characterized by SEC, and ^{1}H and ^{13}C NMR were used to determine the compositions of the copolymers as well as their triad fractions. Molecular weight of the copolymers were also determined from ^{1}H NMR by comparing the copolymer peaks to those of the RAFT end group peaks.

Table-2.19: The molecular weight and molecular weight dispersity data for St-grad-AN60 copolymers characterized by ^{1}H NMR.

Reaction time	Conversion (%)	M_n (^{1}H NMR)	M_n (SEC)	$Đ_M$ (SEC)
1.5 hours	14.32	1818	4700	1.25
4 hours	39.86	5410	9100	1.19
6 hours	56.53	6511	12900	1.20
8 hours	66.49	10376	14200	1.31
11 hours	83.08	11025	17700	1.49

The molecular weight determined by both SEC and ^{1}H NMR techniques are plotted against the copolymer compositions (Figure-2.34 (a)). The molecular weights determined from these two methods are little different from each other, but in both cases, copolymer molecular weight increases linearly with the conversion for St-grad-AN60 copolymers with reasonable molecular weight dispersity characterized by SEC. The increase in the molecular weight with conversion is also clear from the molecular weight distribution plot for the copolymers with conversion, which shows the gradual shifting from lower molecular weights to higher molecular weights as the conversion increases.

The conversion of the St-grad-AN60 increases linearly with time as shown in Figure-2.35. The St composition in the St-grad-AN60 copolymer gradually increases when plotted against the copolymer conversion as well as against St feed composition. The gradual change in the St

composition with conversion of copolymer proves the successful synthesis of forced gradient copolymers using the continuous feeding approach.

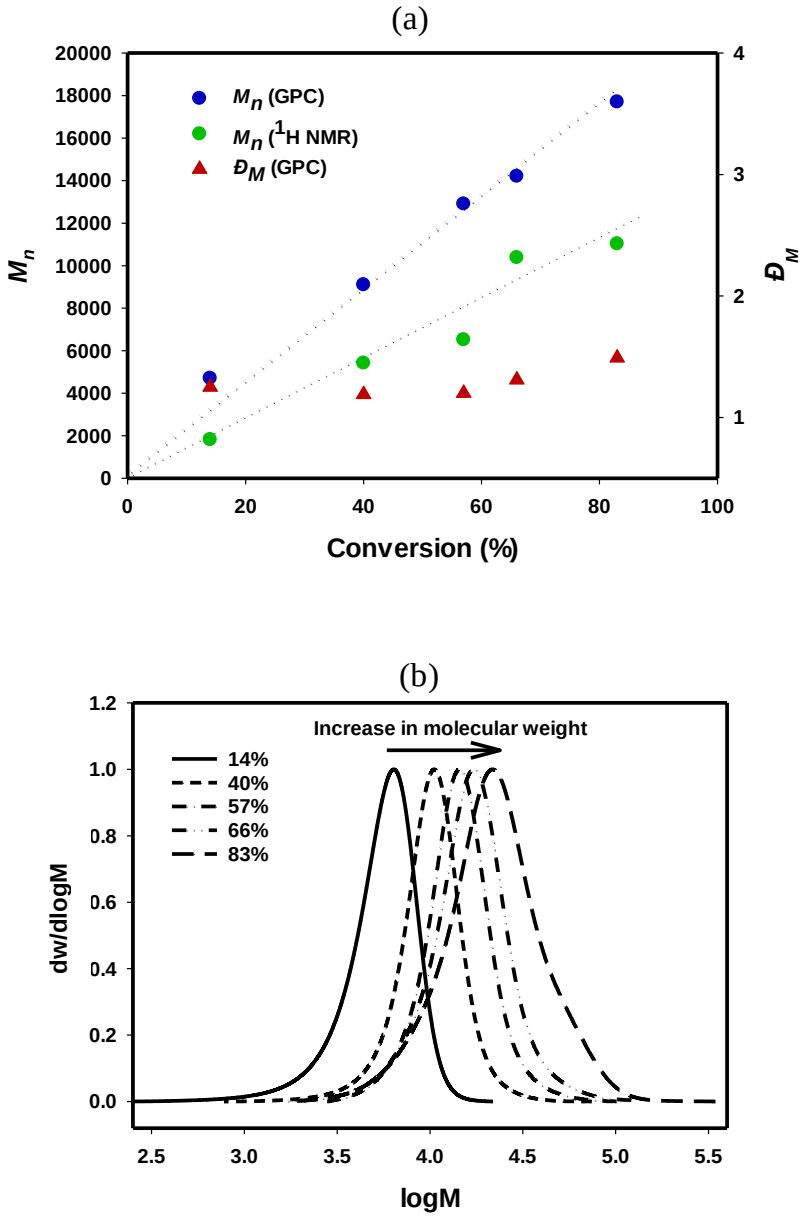

Figure-2.34: (a) Change in the molecular weight and molecular weight dispersity characterized by SEC, and the molecular weight characterized by ^{1}H NMR, plotted against the overall conversion of St-grad-AN60 copolymer. Figure (b) shows the changes in the molecular weight distribution with increasing copolymer conversion.

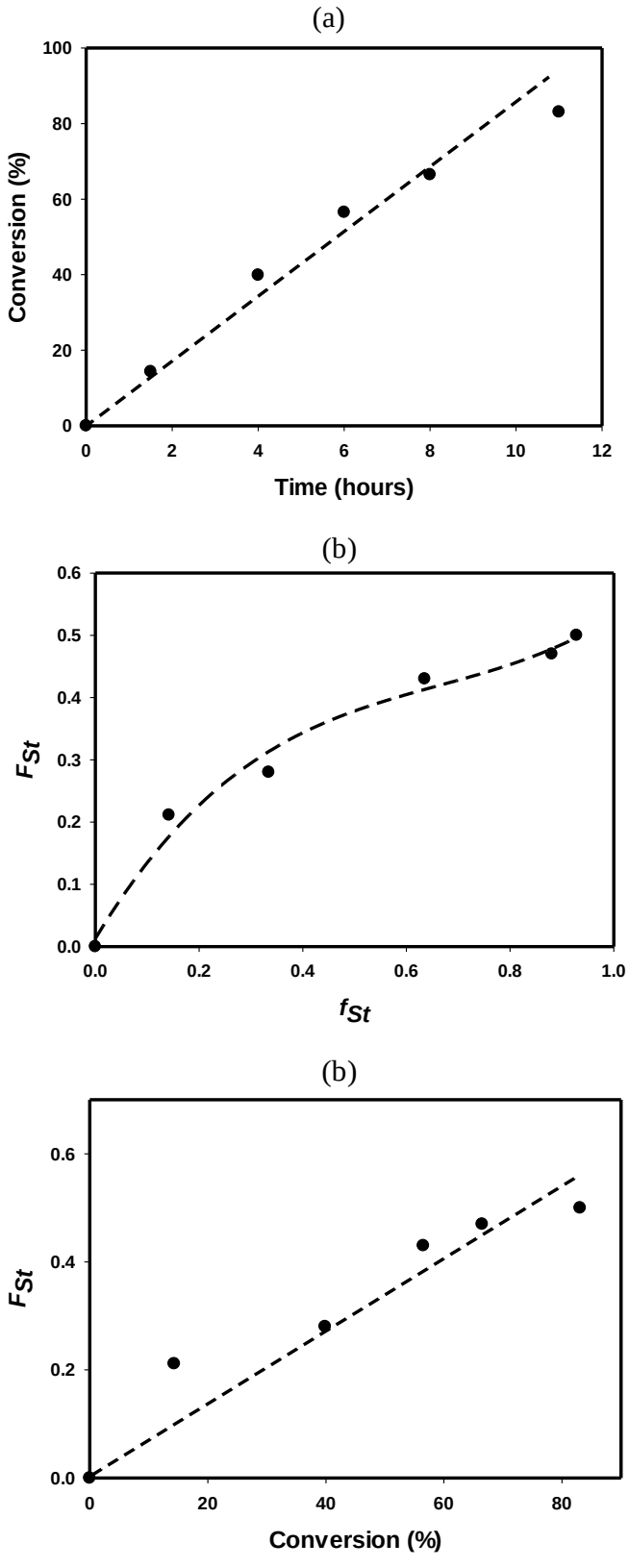

Figure-2.35: (a) Change of conversion of St-grad-AN60 copolymer with time, (b) change in the St composition in the copolymer with St feed composition, and (c) change in the St composition in the copolymer with copolymer conversion, characterized by ^{1}H NMR.

Table-2.20: The composition and triad fractions for the St-grad-AN60 copolymers characterized by ^{1}H and quantitative ^{13}C NMR.

Conv. (%)	F_{St} (^{1}H NMR)	F_{St} (^{13}C NMR)	St-centred triad fractions			AN-centred triad fractions		
			F(SSS)	*F(SSA/ASS)*	*F(ASA)*	*F(SAS)*	*F(SAA/AAS)*	*F(AAA)*
14.32	0.26	-	-	-	-	-	-	-
39.86	0.34	-	-	-	-	-	-	-
56.53	0.43	0.45	0.026	0.261	0.712	0.442	0.458	0.099
66.49	0.47	0.49	0.066	0.363	0.572	0.519	0.408	0.073
83.08	0.50	0.55	0.187	0.379	0.434	0.547	0.382	0.071

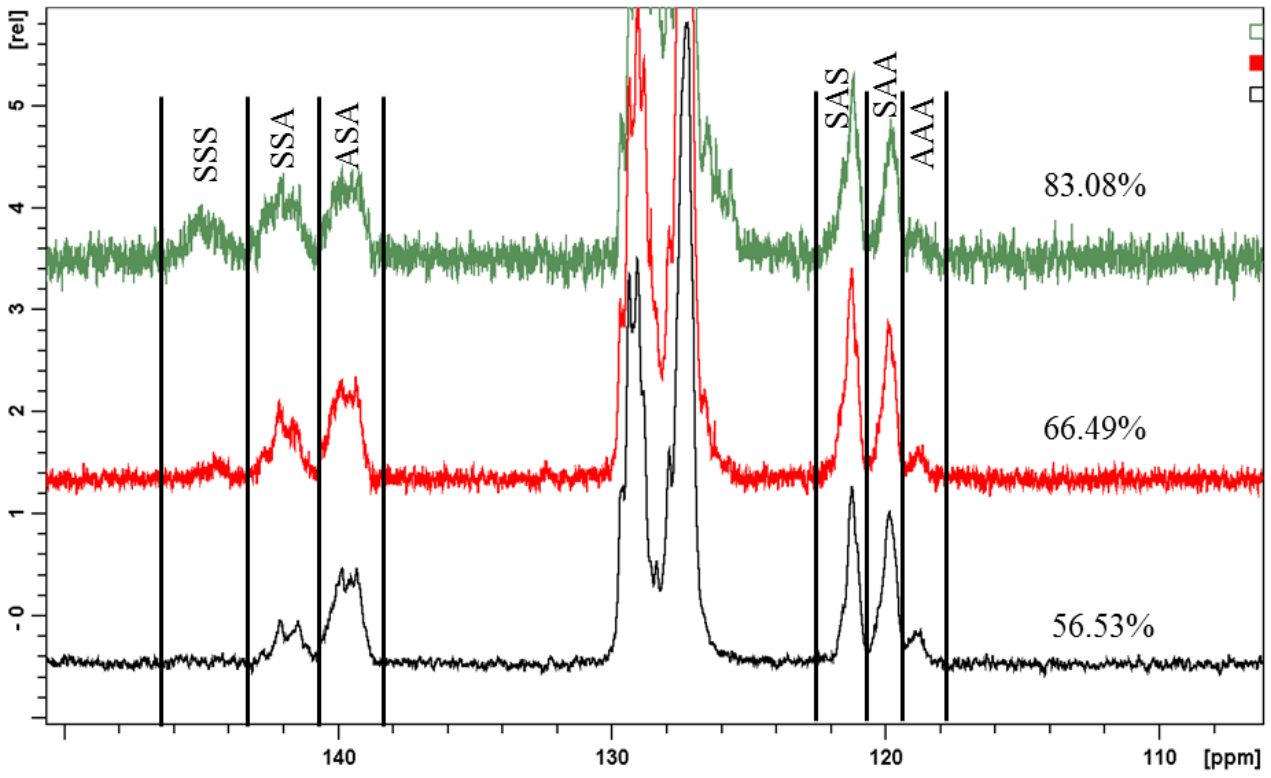

Figure-2.36: The change in the St and AN centred triads, as the copolymer conversion increases with continuous addition of St to the reaction system.

The triad fractions of the St-grad-AN60 copolymers were characterized by quantitative ^{13}C NMR. The formation of a gradient is also strongly supported by the change in the triad fractions of the copolymers as the copolymer conversion increases. Figure-2.37 shows the bar plot for the St and AN centred triad fractions at different copolymer conversion. With gradual addition of St monomer into the reaction system, the fraction of triads containing two or three St units increases, while the opposite happens for the triad fractions with two or three AN units.

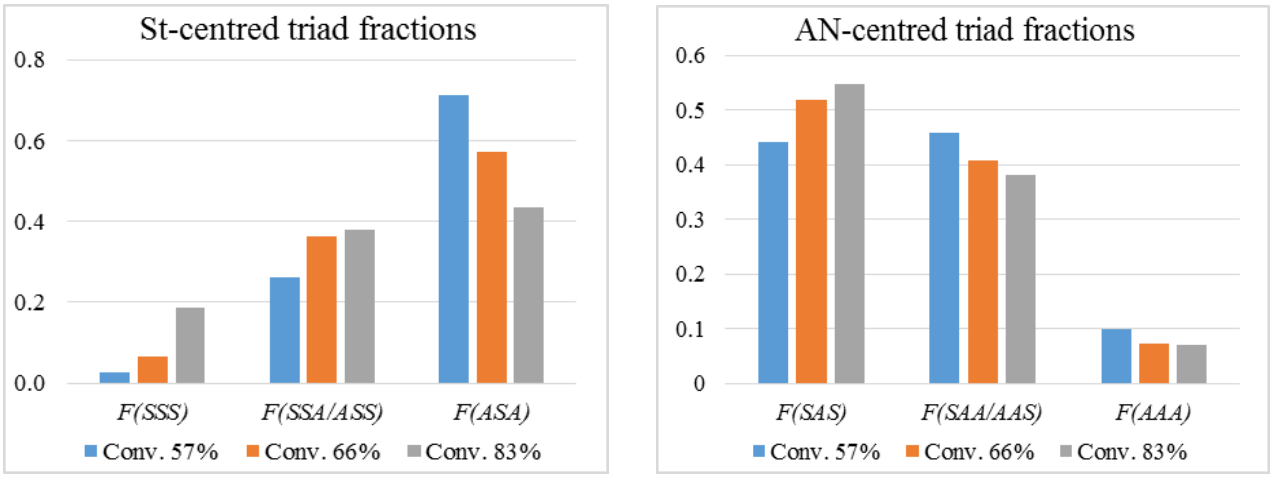

Figure-2.37: Bar plots for the St and AN centred triad fractions against the conversion of St-grad-AN60 copolymers, characterized by quantitative ^{13}C NMR.

2.7 Synthesis of St and AN homopolymers and St-AN block copolymers

2.7.1 Synthesis of St and AN homopolymers

Styrene and Acrylonitrile homopolymers have been synthesized by RAFT polymerization using PABTC as the RAFT agent. The homopolymers were prepared to study their properties in comparison with the properties of the copolymers. Also the homopolymers have been used as the macro-RAFT agents for the synthesis of block copolymers by the chain extension method.

Styrene homopolymer with different molecular weights have been synthesized by varying the ratio of monomer to RAFT agent. Since the polymerization rate of St homo-polymerization is quite slow at low temperatures, 1,1′-azobis(cyclohexanecarbonitrile) with a half-life of 10 hours at 88 °C temperature, was used as the initiator specifically for polystyrene synthesis. The ratio of RAFT agent to initiator was 10:1 to achieve a St homopolymer with low molecular weight dispersity at 90 °C temperature in bulk. A small amount of dioxane was added to the reaction system to use as a reference for calculating the conversion, and the conversion was kept under 50%. The resultant polymers were precipitated in methanol, and dried in the vacuum oven. The molecular weight and molecular weight dispersity of the PSt was characterized by ^{1}H NMR, and also by SEC using THF as the eluent.

Homopolymers of acrylonitrile were synthesized at 70 °C using AIBN as initiator and DMF as solvent. Due to the insolubility of polyacrylonitrile (PAN) in THF, the molecular weight and molecular weight dispersity was characterized by ^{1}H NMR and SEC.

2.7.2 Synthesis of St-AN block copolymers

Block copolymers of styrene and acrylonitrile with molecular weights similar to those of the St-AN statistical copolymers have been synthesized by the chain extension method. PSt homopolymers with different molecular weights were used as the macro-RAFT agent to produce polystyrene-block-polyacrylonitrile (PSt-b-PAN) with different copolymer compositions.

The chain extension process was carried out at 70 °C temperature using AIBN as the initiator, and DMF was used as the solvent. The ratio of the AN monomer and PSt macro-RAFT agent was set to achieve the target copolymer compositions. The resultant copolymer was characterized by SEC, and also by ^{1}H NMR, to determine the copolymer compositions. Table-2.21 shows the molecular weight and composition data for the PSt-b-PAN copolymers.

Table-2.21: Molecular weight, molecular weight dispersity characterized by SEC, and the composition of copolymer characterized by ^{1}H NMR. The number at the end of the block copolymer indicates the St composition in the copolymers.

Designation	***Mn*** **(PSt)**	$Đ_M$ **(PSt)**	***Mn*** **(PSt-b-PAN)**		$Đ_M$ **(PSt-b-PAN)**		**Copolymer compositions (St:AN) by ^{1}H NMR**
			RI detector	**Triple detector**	**RI detector**	**Triple detector**	
PSt-b-PAN27	3100	1.10	11400	11500	1.59	1.03	27:73
PSt-b-PAN36	5100	1.09	14400	14600	1.45	1.06	36:64
PSt-b-PAN68	11300	1.11	15900	-	1.40	-	68:32
PSt-b-PAN83	10300	1.06	12100	11816	1.44	1.04	83:17

PSt-b-PAN copolymers with four different copolymer compositions have been synthesized. As Table-2.21 shows, the PSt chains have successfully been extended to produce the block copolymers. The molecular weight distribution of the PSt homopolymers are compared to those of the resultant PSt-b-PAN. In each case, the molecular weight distribution plot of the copolymer moved to the higher molecular weight region. For the copolymers with low St composition, the copolymer molecular weight distribution plot shows a small amount of tailing in the low molecular weight region. This could be due to a fraction of the PSt dead chains.

In comparison, for the block copolymers with high St compositions, the copolymer molecular weight distribution plots show a slight shifting of the plot towards the higher molecular weight region. However, the copolymers show slight tailing at molecular weight lower than the homopolymers. It is to be noted that THF has been used as the eluent to characterize the homopolymers while DMAc was used for the copolymers. Therefore, this could be due to the differences in the hydrodynamic volume of the homo and copolymers in the THF and DMAc respectively.

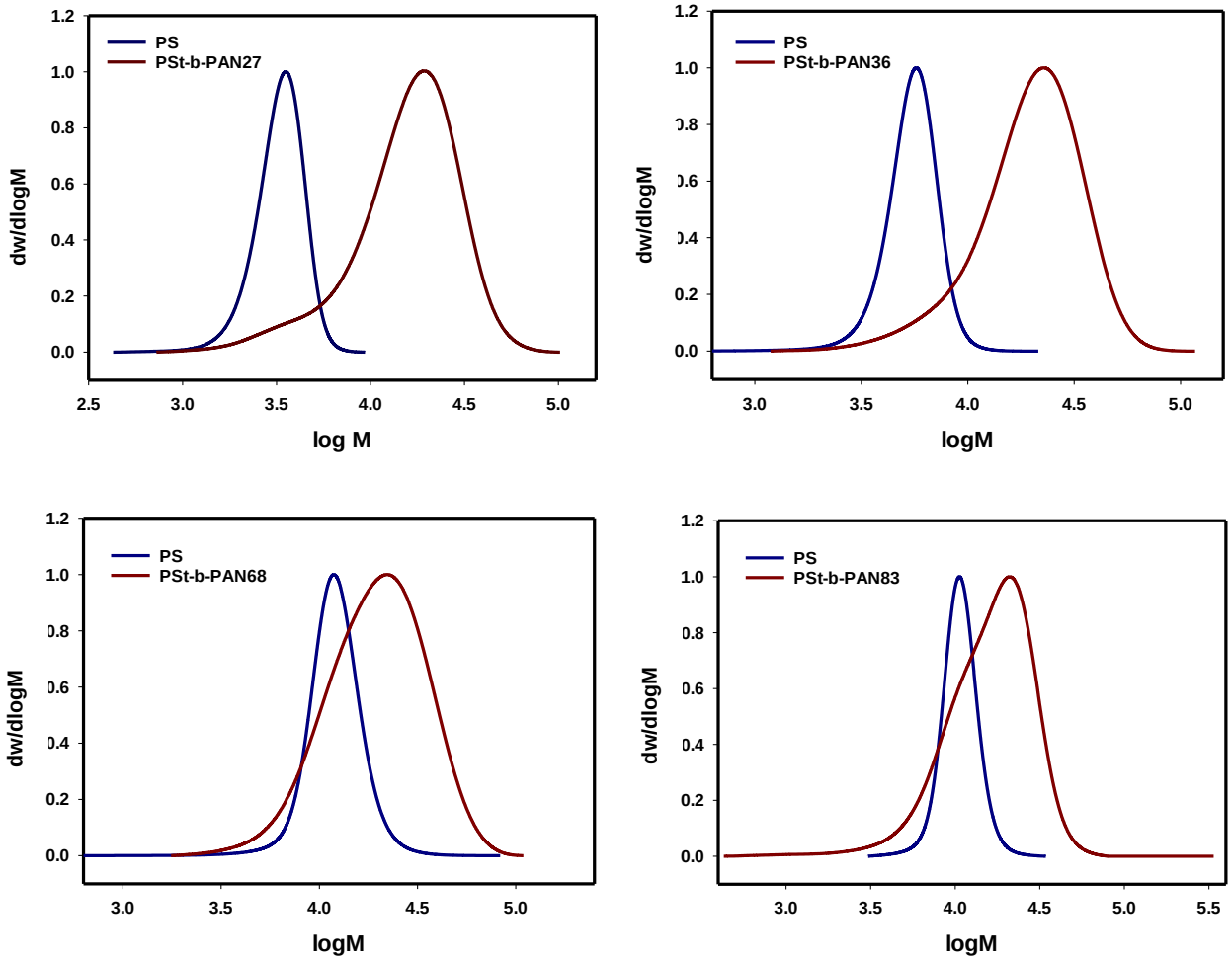

Figure-2.38: Comparison of molecular weight distribution plots of PSt homopolymers with the corresponding PSt-b-PAN copolymers.

The ^{1}H NMR spectra of the PSt homopolymer and the PSt-b-PAN27 copolymer are shown in Figure-2.39. The spectrum of the PSt shows a broad peak for the aromatic protons at around 6.2-7.2 ppm, and a broad peak for the backbone protons at around 1.0-2.2 ppm. After successful chain extension with AN monomer, the peak for the AN protons can be seen in Figure-2.39 (b) at chemical shifts around 2.1 and 3.1 ppm. The copolymer compositions have been determined by comparing the aromatic proton peak from PSt to the peak at around 3.1 from PAN.

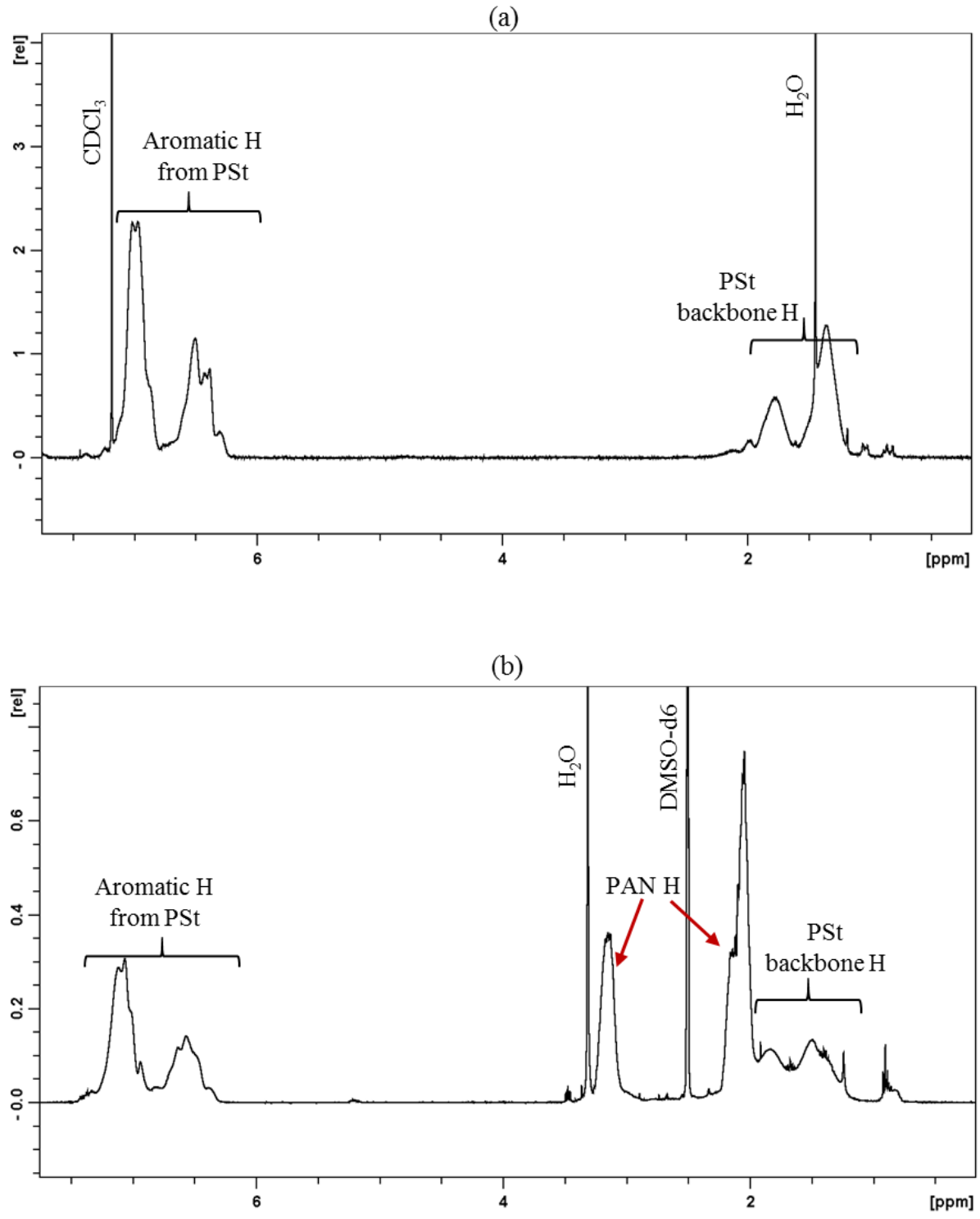

Figure-2.39: (a) ^{1}H NMR of PSt homopolymer, and (b) ^{1}H NMR of PSt-b-PAN36.

2.8 St-AN statistical copolymers prepared by CvRP method

In addition to the St-AN copolymers synthesized by the RAFT method, St-AN statistical copolymers have been synthesized using CvRP. For specific monomer feed compositions (80%, 20% and 10%), the copolymers synthesized by RAFT possess gradients along the individual copolymer chains, while in the CvRP technique, new chains are being created at every instant and the composition of the chains created at a particular instant depends on the instantaneous monomer composition in the system. Therefore, the composition gradients produced by CvRP could be termed as inter-chain gradient, while it is intra-chain for RAFT polymerization.

2.8.1 Experimental procedure

For comparison purposes, St-AN copolymers with similar molecular weights to the RAFT St-AN copolymers were prepared by CvRP for the same four St feed compositions. The molecular weight of the copolymers were controlled by optimizing the ratio of monomer to initiator. The reaction mixtures, as per as Table-2.22 for each feed composition, were added into a 20 mL vial, and purged with N_2 gas for 60 minutes. After purging, the reaction mixture was divided into several vials inside a N_2 glove box, and the vials were sealed with rubber septa. All the vials were placed together in an oil bath for polymerization at 80 °C, and after certain a polymerization time, the vials were collected from the oil bath to quench the polymerization reaction in an ice bath. The copolymers were precipitated and dried in the vacuum oven to constant weight.

Table-2.22: Reaction conditions for the synthesis of St-AN copolymers by CvRP process for 80%, 60%, 20% and 10% St feed composition at 80 °C temperature.

Copolymer	St	AN	AIBN	Solvent
St-AN80	3.998 g 0.038 mole	0.515 g 0.010 mole	0.315 g 1.921 mmole	DMF 0.515 g (7.055 mmole)
St-AN60	4.998 g 0.048 mole	1.737 g 0.024 mole	0.189 g 1.152 mmole	DMF 0.372 g (5.096 mmole)
St-AN20	1.805 g 0.017 mole	3.875 g 0.073 mole	0.354 g 2.159 mmole	DMF 12.648 g (0.173 mole)
St-AN10	1.080 g 0.010 mole	4.500 g 0.085 mole	0.520 g 3.171 mmole	DMF 14.032 g (0.192 mole)

2.8.2 Results and discussion

The molecular weight data, copolymer composition and the triad distribution of the St-AN copolymers synthesized by CvRP were characterized using SEC, ^{1}H and ^{13}C NMR. Similar to those of the RAFT copolymers, for St-AN copolymers with high St composition, THF was used as the eluent for SEC study, while the eluent was DMAc for the copolymers with high AN content. The experimental copolymer compositions and triad distributions of the St-AN copolymers for all four feed compositions were then compared with the data predicted by REACT.

The individual monomer and copolymer conversion characterized by ^{1}H NMR for the St-AN copolymers synthesized by CvRP followed a similar trend as seen for the RAFT method. As assumed from Mayo-Lewis plot, the individual St conversion for St-AN80 was slower than AN, while both of the monomer conversion increased approximately in a similar rate for the azeotrope composition in St-AN60. On the other hand, conversion of St was significantly faster than AN for both St-AN20 and St-AN10, owing to the significant deviation of the St composition in the Mayo-Lewis plot from the ideal copolymer composition. The data for the conversion, molecular weights, compositions and triad distributions for the St-AN copolymers synthesized by CvRP technique are given in Table-2.23 to Table-2.34, and Figure-2.40 to Figure-2.47.

The molecular weight data for all for St-AN copolymer shows molecular weights comparable to those of the RAFT copolymers with reasonable molecular weight dispersity. However, the molecular weight and molecular weight dispersity for St-AN20 and St-AN10, from the RI and triple detectors were significantly different, as was found for these particular copolymers synthesized by RAFT. The experimental compositions and triad distributions characterized by ^{1}H and ^{13}C NMR showed excellent agreement with the data predicted by REACT. The composition and triad distributions showed a slight drift with conversion for St-AN80 copolymers, while the drift was significantly stronger for St-AN20 and St-AN10 copolymers. For St-AN60 with azeotrope composition, the composition and triad distributions were nearly constant with conversion.

2.8.2.1 St-AN80

Table-2.23: Conversion data for the synthesis of St-AN80 copolymers in bulk at 80 °C characterized by ^{1}H NMR.

Reaction time	[H] from St	St conversion (%)	[H] from AN	AN conversion (%)	Overall copolymer conversion (%)
0 min	528	-	113	-	-
20 mins	309	41.52	78	30.47	39.31
40 mins	220	58.33	22	80.12	62.68
1 hour	109	79.35	8	92.50	81.98

Table-2.24: The molecular weight and molecular weight dispersity data for the St-AN80 copolymers for different copolymer conversion characterized by SEC.

Reaction time	Conversion (%)	M_n (SEC)	$Đ_M$ (SEC)
20 mins	39.31	13700	1.59
40 mins	62.68	12000	1.70
1 hour	81.98	13100	1.99

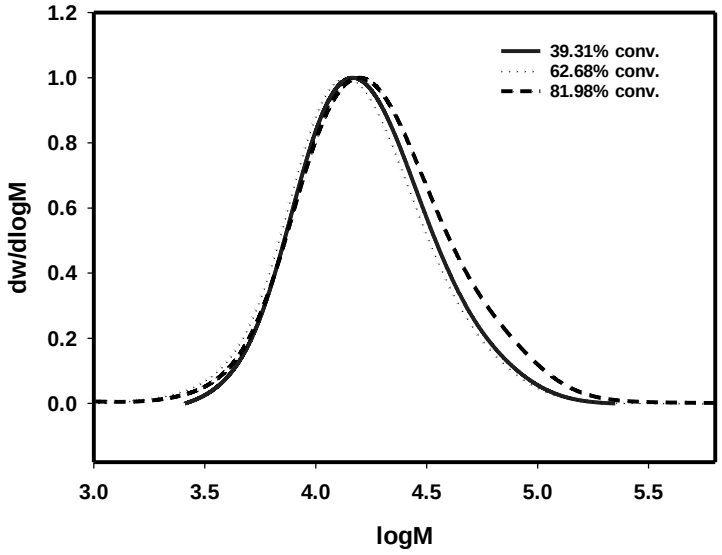

Figure-2.40: Molecular weight distribution plots for St-AN80 CvRP copolymers for 39.31%, 62.68% and 81.98% copolymer conversion characterized by SEC using.

Table-2.25: The copolymer compositions and sequence distributions of St-AN80 copolymers calculated from ^{1}H and ^{13}C NMR spectra.

Conv. (%)	F_{St} **^{1}H NMR**	F_{St} **^{13}C NMR**	**St-centred triad fractions**			**AN-centred triad fractions**		
			F(SSS)	***F(SSA)***	***F(ASA)***	***F(SAS)***	***F(SAA)***	***F(AAA)***
39.31	0.73	0.75	0.380	0.508	0.111	0.943	0.055	0.002
62.68	0.74	0.76	0.447	0.479	0.074	0.926	0.072	0.002
81.98	0.76	0.79	0.491	0.440	0.069	0.954	0.044	0.002

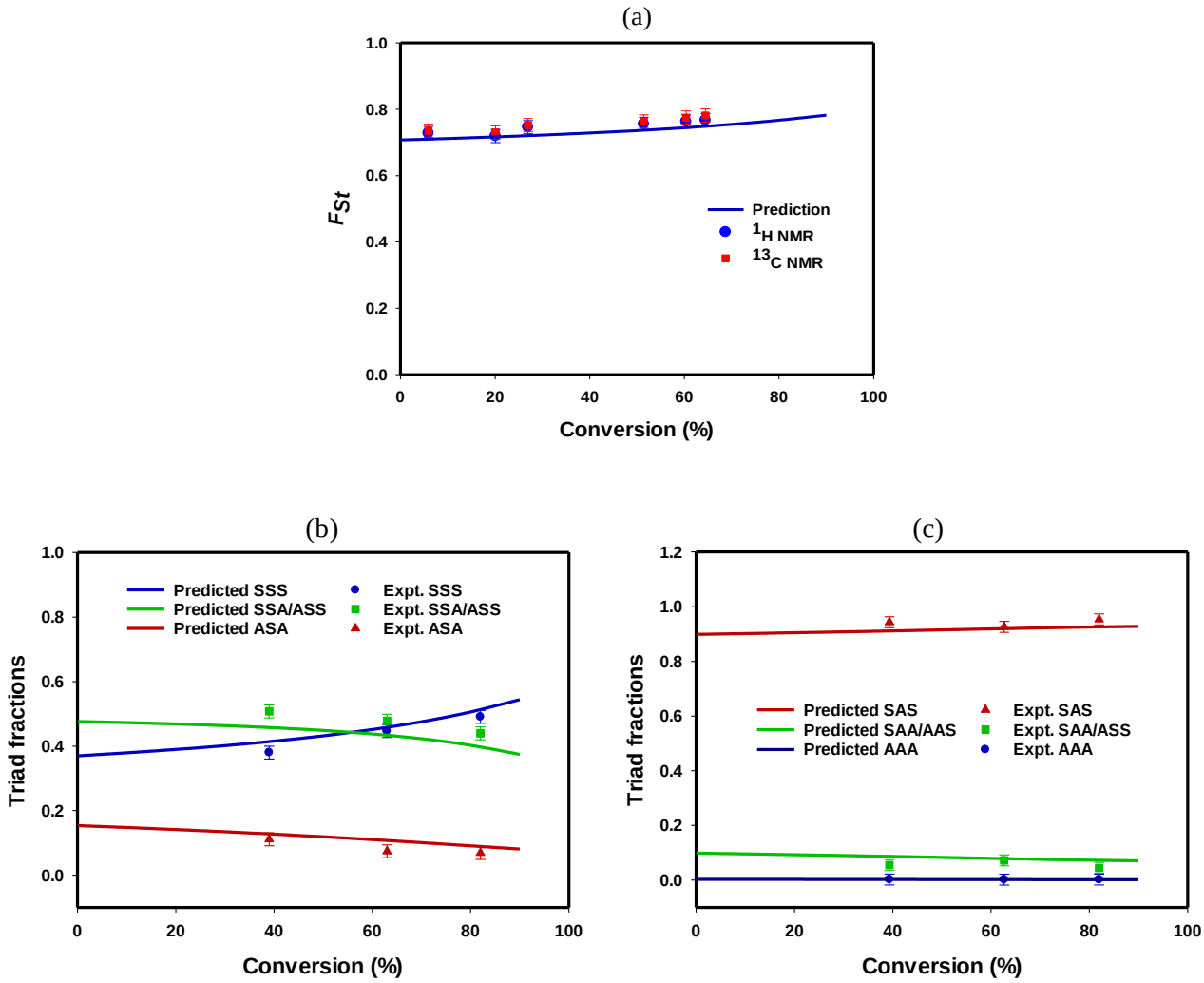

Figure-2.41. The change in the (a) composition of St in the copolymers characterized by ^{1}H NMR and ^{13}C NMR; (b) St-centred triad fractions and (c) AN-centred triad fractions characterized by quantitative ^{13}C NMR, with conversion for St-AN80.

2.8.2.2 St-AN60

Table-2.26: Conversion data for the synthesis of St-AN60 copolymers in bulk at 80 °C characterized by ^{1}H NMR.

Reaction time	[H] from St	St conversion (%)	[H] from AN	AN conversion (%)	Overall copolymer conversion (%)
0 min	1021	-	617	-	-
15 mins	680	33.33	410	33.58	33.56
30 mins	651	36.17	380	38.31	38.10
1 hour	520	49.07	287	53.39	52.96
1.5 hours	311	69.54	174	71.77	71.55

Table-2.27: The change in the molecular weight and molecular weight dispersity of the St-AN60 copolymers with conversion.

Reaction time	Conversion (%)	M_n (SEC)	$Đ_M$ (SEC)
15 mins	33.56	15200	1.81
30 mins	38.10	14100	1.79
1 hour	52.96	14000	1.73
1.5 hours	71.55	13100	1.80

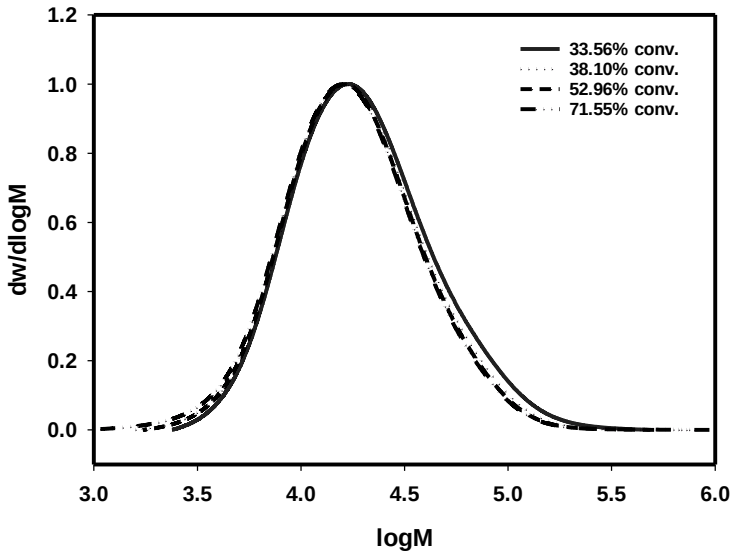

Figure-2.42: Molecular weight distribution plot for St-AN60 CvRP copolymers for 33.56%, 38.10%, 52.96% and 71.55% copolymer conversion characterized by SEC.

Table-2.28: The copolymer compositions and sequence distributions of St-AN60 copolymers calculated from ^{1}H and ^{13}C NMR spectra.

Conv. (%)	F_{St} **^{1}H NMR**	F_{St} **^{13}C NMR**	**St-centred triad fractions**			**AN-centred triad fractions**		
			F(SSS)	***F(SSA)***	***F(ASA)***	***F(SAS)***	***F(SAA)***	***F(AAA)***
33.56	0.60	0.62	0.139	0.571	0.290	0.858	0.132	0.010
38.10	0.64	0.63	0.143	0.566	0.291	0.865	0.120	0.014
52.96	0.67	0.66	0.197	0.577	0.226	0.896	0.093	0.010
71.55	0.63	0.64	0.165	0.583	0.252	0.857	0.138	0.004

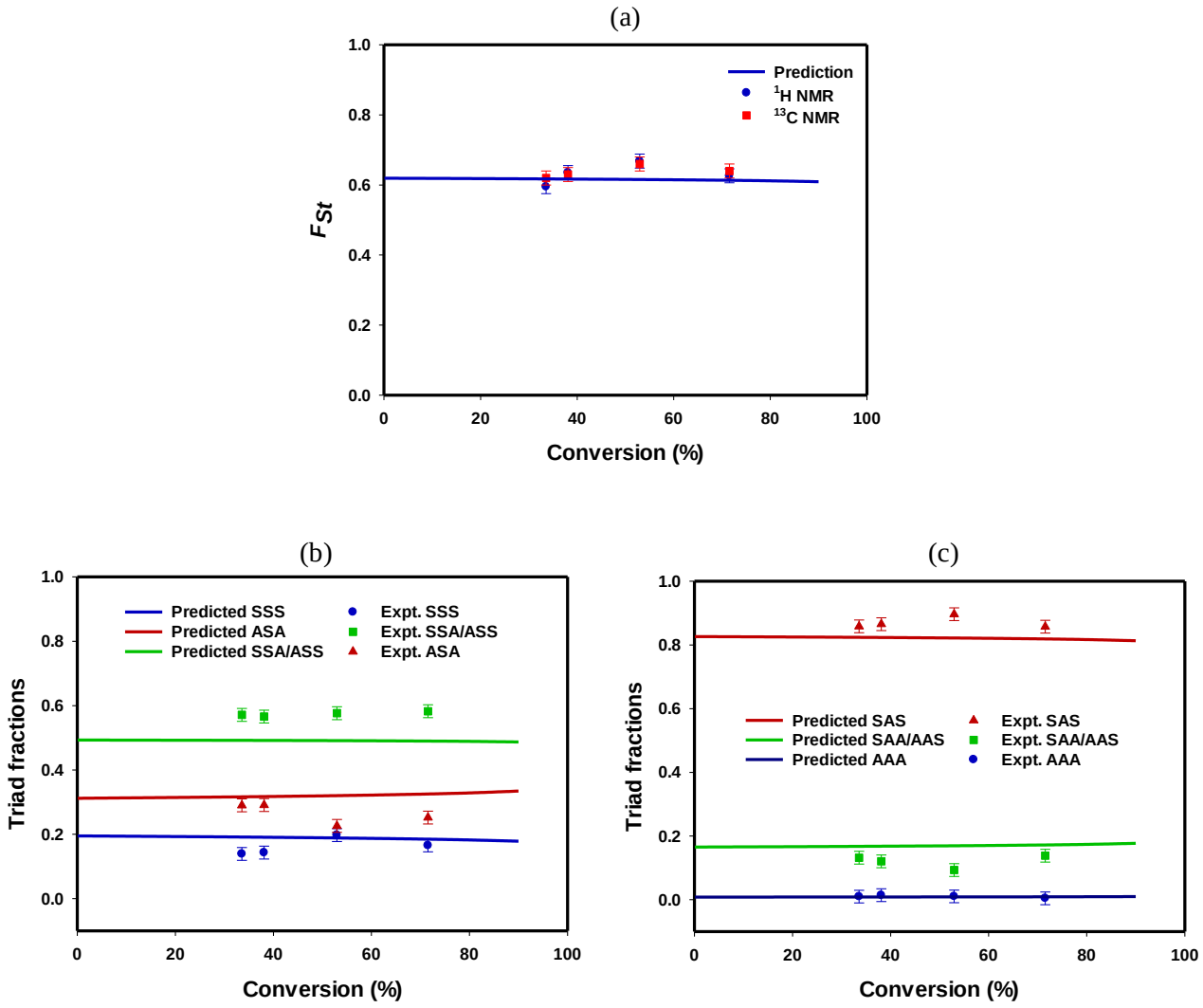

Figure-2.43. The change in the (a) composition of St in the copolymers characterized by ^{1}H NMR and ^{13}C NMR; (b) St-centred triad fractions and (c) AN-centred triad fractions characterized by quantitative ^{13}C NMR, with conversion for St-AN60.

2.8.2.3 St-AN20

Table-2.29: Conversion data for the synthesis of St-AN20 copolymers in bulk at 80 °C characterized by ^{1}H NMR.

Reaction time	[H] from St	St conversion (%)	[H] from AN	AN conversion (%)	Overall copolymer conversion (%)
0 min	9.70		39.79		
10 mins	4.86	49.90	31.54	20.73	26.57
20 mins	0.18	98.14	19.11	51.97	61.21
40 mins	0.00	100.00	13.08	67.13	73.70
1 hour	0.00	100.00	11.50	71.10	76.88

Table-2.30: The molecular weight and molecular weight dispersity data for St-AN20 copolymers characterized by SEC.

Reaction time	Conversion (%)	M_n (SEC)		$Đ_M$ (SEC)	
		RI detector	Triple detector	RI detector	Triple detector
10 mins	26.57	18000	27200	2.14	1.28
20 mins	61.21	14100	12500	1.92	1.22
40 mins	73.70	15200	10300	1.88	1.50
1 hour	76.88	15500	10000	1.84	1.52

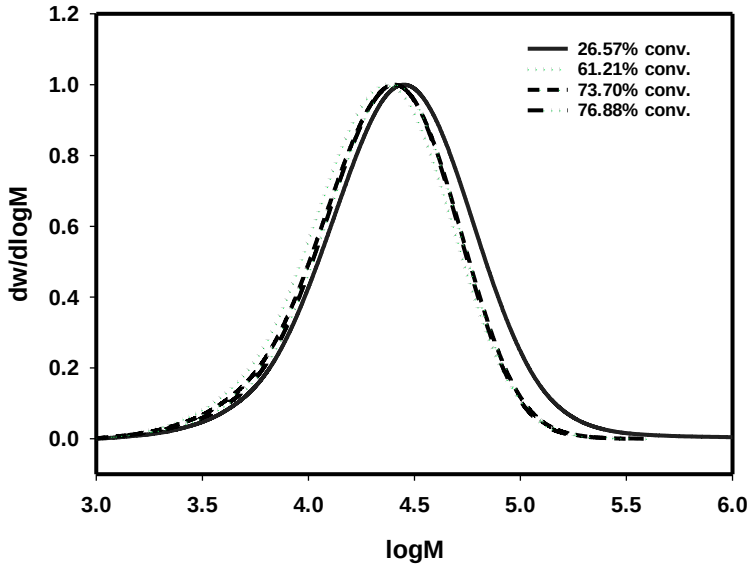

Figure-2.44: Molecular weight distribution plot for St-AN20 CvRP copolymers for 26.57%, 61.21%, 73.70%, and 76.88% copolymer conversion characterized by SEC.

Table-2.31: The copolymer compositions and sequence distributions of St-AN20 copolymers calculated from ^{1}H spectra and quantitative ^{13}C NMR.

Conv. (%)	F_{St} **^{1}H NMR**	F_{St} **^{13}C NMR**	**St-centred triad fractions**			**AN-centred triad fractions**		
			F(SSS)	***F(SSA)***	***F(ASA)***	***F(SAS)***	***F(SAA)***	***F(AAA)***
26.57	0.40	0.40	0.022	0.191	0.787	0.406	0.524	0.070
61.21	0.32	0.33	0.014	0.181	0.805	0.232	0.485	0.283
73.70	0.26	0.27	0.008	0.173	0.820	0.184	0.438	0.378
76.88	0.21	0.22	0.019	0.194	0.787	0.157	0.412	0.430

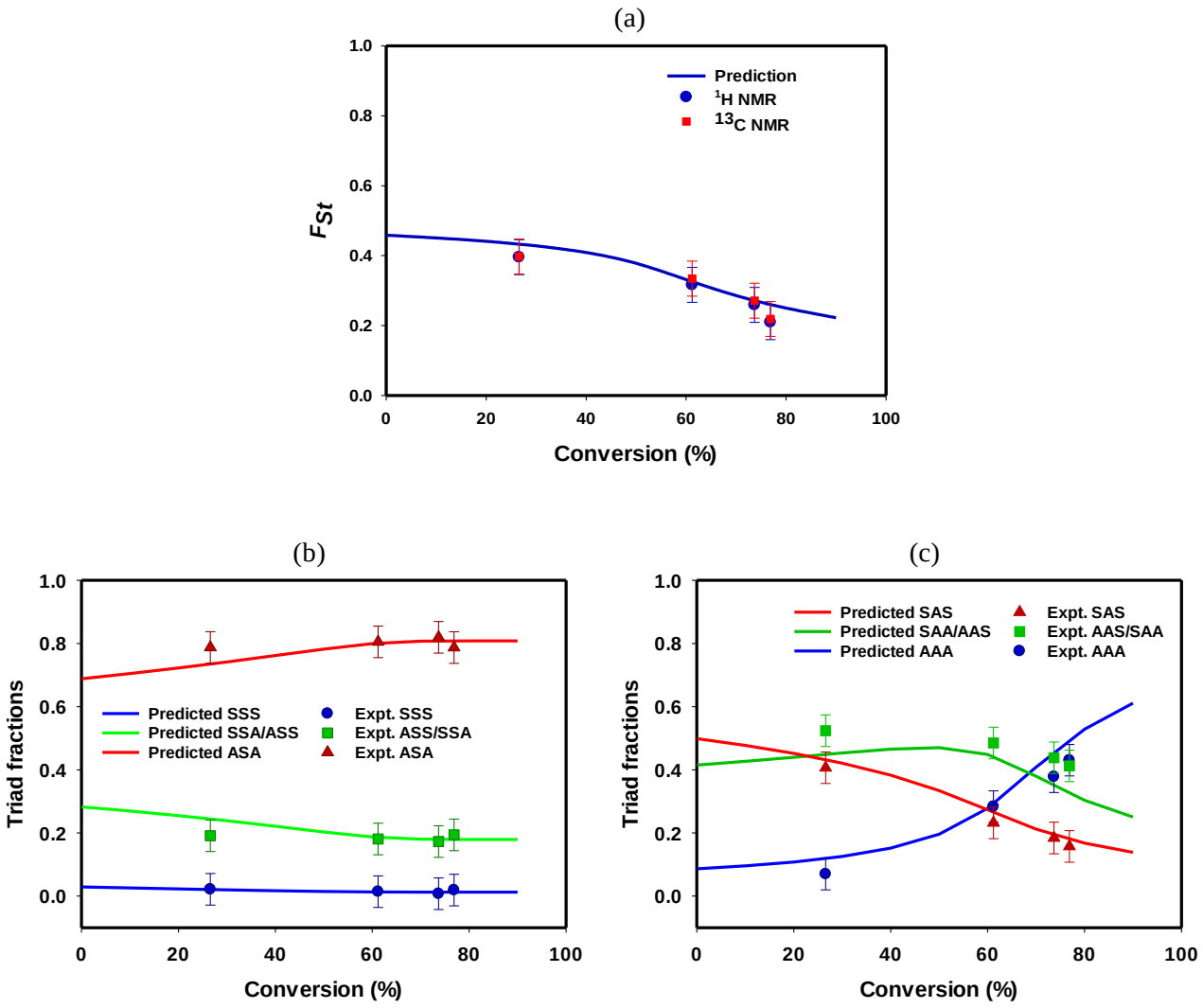

Figure-2.45. The change in the (a) composition of St in the copolymers characterized by ^{1}H NMR and ^{13}C NMR; (b) St-centred triad fractions and (c) AN-centred triad fractions characterized by quantitative ^{13}C NMR, with conversion for St-AN20.

2.8.2.4 St-AN10

Table-2.32: Conversion data for the synthesis of St-AN10 copolymers in bulk at 80 °C characterized by ^{1}H NMR.

Reaction time	[H] from St	St conversion (%)	[H] from AN	AN conversion (%)	Overall copolymer conversion (%)
0 min	5.04		38.57		
10 mins	3.22	0.36	37.03	0.04	7.20
20 mins	0.15	0.97	28.65	0.26	32.85
30 mins	0.00	1.00	19.92	0.48	53.52
40 mins	0.00	1.00	15.92	0.59	62.85
50 mins	0.00	1.00	12.49	0.68	70.86

Table-2.33: The change in the molecular weight and molecular weight dispersity of the St-AN10 copolymers with conversion characterized by SEC.

Reaction time	Conversion (%)	M_n (SEC)		$Đ_M$ (SEC)	
		RI detector	Triple detector	RI detector	Triple detector
10 mins	7.20	20600	20300	1.87	1.19
20 mins	32.85	15700	11500	1.90	1.37
30 mins	53.52	14000	9100	1.93	1.38
45 mins	62.85	17200	8600	1.76	1.49
1 hour	70.86	15300	11100	1.94	1.28

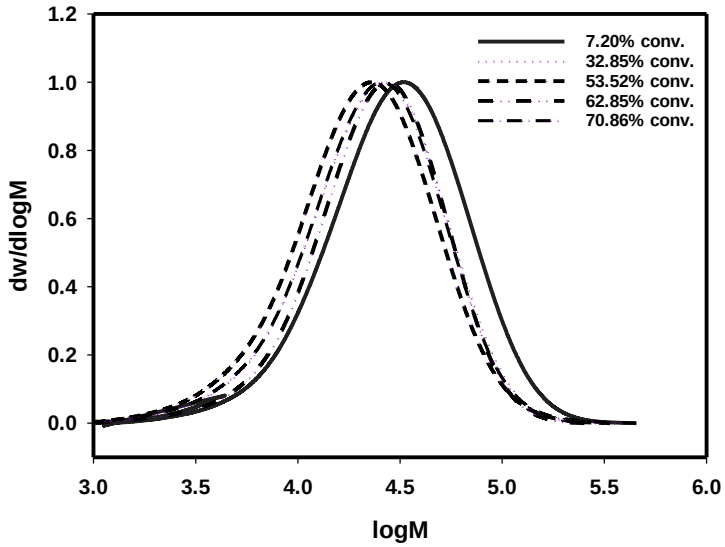

Figure-2.46: Molecular weight distribution plot for St-AN10 CvRP copolymers for 7.20%, 32.85%, 53.52%, 62.85%, and 70.86% copolymer conversion characterized by SEC.

Table-2.34: The copolymer compositions and sequence distributions of St-AN10 copolymers calculated from ^{1}H spectra and quantitative ^{13}C NMR.

Conv.	F_{St}	F_{St}	**St-centred triad fractions**			**AN-centred triad fractions**		
(%)	**^{1}H NMR**	**^{13}C NMR**	***F(SSS)***	***F(SSA)***	***F(ASA)***	***F(SAS)***	***F(SAA)***	***F(AAA)***
7.20	0.32	0.33	0.013	0.120	0.867	0.257	0.517	0.226
32.85	0.26	0.27	0.005	0.118	0.877	0.154	0.479	0.367
53.52	0.17	0.18	0.005	0.112	0.883	0.119	0.317	0.564
62.85	0.14	-	-	-	-	-	-	-
70.86	0.14	0.15	0.000	0.093	0.907	0.100	0.281	0.619

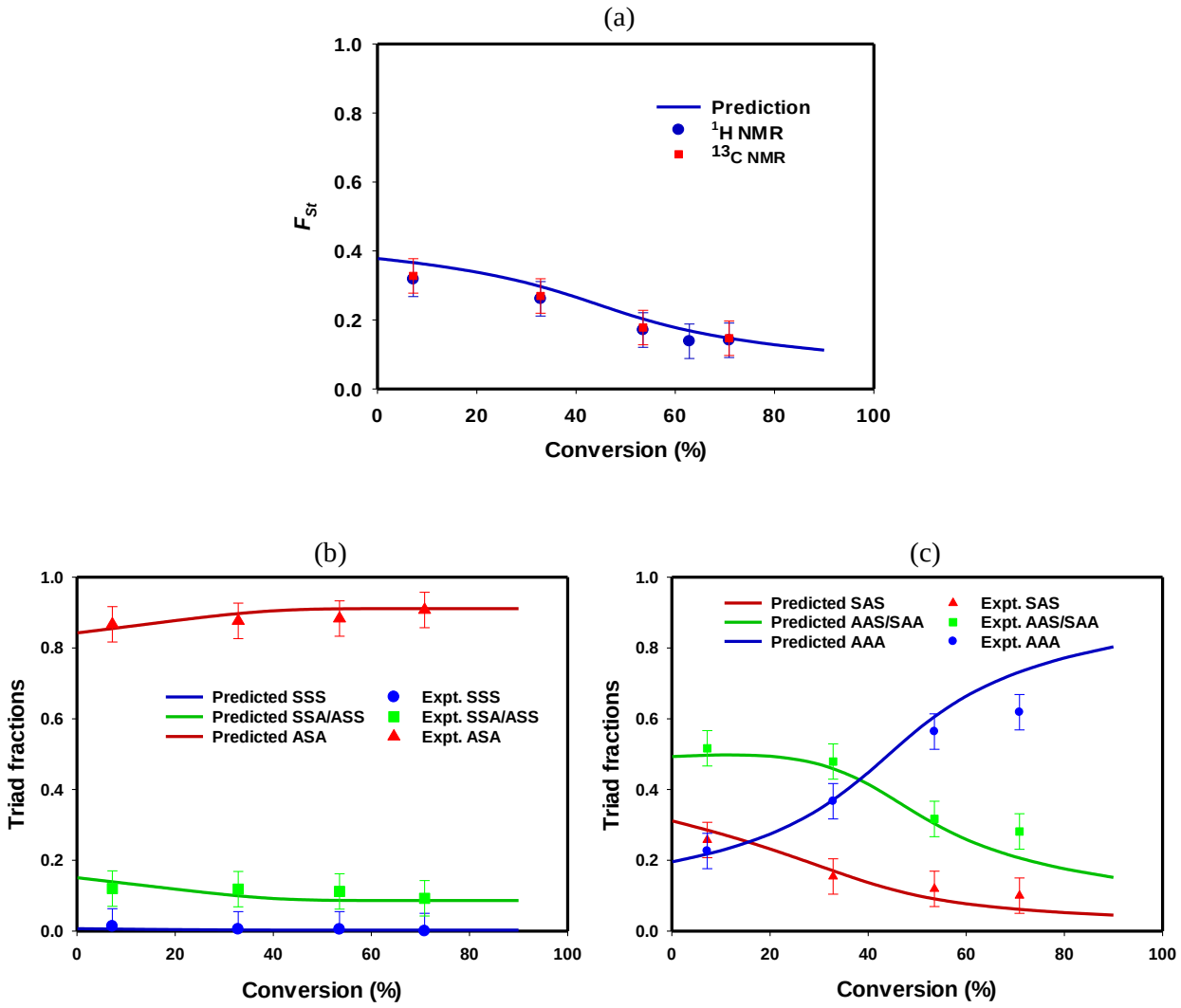

Figure-2.47. The change in the (a) composition of St in the copolymers characterized by ^{1}H NMR and ^{13}C NMR; (b) St-centred triad fractions and (c) AN-centred triad fractions characterized by quantitative ^{13}C NMR, with conversion for St-AN10.

2.9 Conclusions

The styrene-acrylonitrile copolymer system have been chosen in this project so as to exploit the ability of this monomer pair to produce a natural gradient in the copolymer chains due to the difference in the reactivity ratios of styrene and acrylonitrile. The reactivity ratios for nine different monomer feed compositions were determined at 80 °C in bulk RAFT polymerization from the triad fractions of the copolymers at low conversion (less than 10%). The effect of feed composition on the reactivity ratios was evident, and was explained based on the bootstrap model.

The Mayo-Lewis plot was used to select four different monomer feed compositions for high-conversion kinetics studies, and a computer program REACT was used to predict the *instantaneous* composition and triad distribution data. The experimental compositions and triad distributions were found to be in close agreement with the predicted data for all four different feed compositions. St-AN80, St-AN20 and St-AN10 resulted in a gradual change in their compositions and triad distributions, while for the azeotrope feed composition (St-AN60), the composition and triad distributions were nearly constant throughout the whole conversion. Similar agreement in experimental compositions and triad distributions with the predicted data have also been observed for the St-AN copolymers with the same four feed compositions synthesized by CvRP. However, it is to be noted that there is a fundamental difference between the type of gradient in the RAFT copolymers and the CvRP copolymers. The gradient in the RAFT copolymers are intra-chain, while it is inter-chain in the CvRP copolymers.

In addition to the natural gradient produced in the structures of St-AN batch copolymers synthesized by the RAFT process, the continuous feeding approach was employed to synthesize forced gradient copolymers for the azeotrope feed composition. In this process, the polymerization reaction was started with 100% AN monomer, and St was gradually added to the polymerization mixture. The composition and triad distribution plots proved the successful incorporation of St monomer in to the copolymer chains. Using PSt homopolymers as the macro-RAFT agent, block copolymers of St and AN of four different compositions were synthesized by the chain extension method.

2.10 References

[238] Ziemba GP. Acrylonitrile polymers; acrylonitrile-styrene copolymers. Encycl Polym Sci Technol. 1964;1:425-35.

[239] McKee GE, Kistenmacher A, Goerrissen H, Breulmann M. Synthesis, Properties and Applications of Acrylonitrile–Styrene–Acrylate Polymers. Modern Styrenic Polymers: Polystyrenes and Styrenic Copolymers. Chichester, UK. : John Wiley & Sons, Ltd; 2003. p. 341-62.

[240] Lewis FM, Mayo FR, Hulse WF. Copolymerization. II. The copolymerization of acrylonitrile, methyl methacrylate, styrene, and vinylidene chloride. J Am Chem Soc. 1945;67:1701-5.

[241] Fordyce RG, Chapin EC. Copolymerization. I. The mechanism of emulsion copolymerization of styrene and acrylonitrile. J Am Chem Soc. 1947;69:581-3.

[242] Ehrlich P, De Lollis NJ. Dielectric relaxation in a styrene-acrylonitrile copolymer during and after its polymerization. J Res Natl Bur Stand (U S). 1953;51:145-54.

[243] Hill DJT, Lang AP, Munro PD, O'Donnell JH. The effect of solvent on the styrene-acrylonitrile copolymerization. Eur Polym J. 1992;28:391-8.

[244] Blanks RF, Shah BN. Kinetics of bulk polymerization of styrene-acrylonitrile copolymers. J Polym Sci, Polym Chem Ed. 1976;14:2589-93.

[245] Kaim A. Terminal and penultimate reactivity ratios in the styrene-acrylonitrile free-radical copolymerization system in bulk. J Macromol Sci, Pure Appl Chem. 1998;A35:577-88.

[246] Hill DJT, O'Donnell JH, O'Sullivan PW. Analysis of the mechanism of copolymerization of styrene and acrylonitrile. Macromolecules. 1982;15:960-6.

[247] Sandner B, Loth E. Effect of the interaction of molecules on radical copolymerization. II. Effect of solvents on the radical-initiated copolymerization of acrylonitrile with styrene. Faserforsch Textiltech. 1976;27:633-7.

[248] Guyot A, Guillot J. Acrylonitrile copolymerizations. I. Penultimate effects. J Macromol Sci, Chem. 1968;2:887-901.

[249] Asakura J, Yoshihara M, Matsubara Y, Maeshima T. Effect of solvent on the radical copolymerizability of styrene with acrylonitrile. J Macromol Sci, Chem. 1981;A15:1473-8.

[250] Sandner B, Loth E. Effect of the interaction of molecules on the free radical copolymerization. I. Application of antepenultimate and complex association models to the radical initated bulk copolymerization of acrylonitrile with styrene. Faserforsch Textiltech. 1976;27:571-7.

[251] Djekhaba S, Graillat C, Guillot J. Copolymerization of acrylonitrile with styrene. Contribution to the study of azeotropes in emulsion. Eur Polym J. 1986;22:729-34.

[252] Lee KC, Gan LM, Chew CH, Ng SC. Copolymerization of styrene and acrylonitrile in ternary oil-in-water microemulsions. Polymer. 1995;36:3719-25.

[253] Sanghvi PG, Patel AC, Gopalkrishnan KS, Devi S. Reactivity ratios and sequence distribution of styrene-acrylonitrile copolymers synthesized in microemulsion medium. Eur Polym J. 2000;36:2275-83.

[254] Riess G, Desvalois M. Dispersion copolymerization of styrene and acrylonitrile in organic media. J Polym Sci, Polym Lett Ed. 1977;15:49-54.
[255] Plochocka K, Harwood HJ. Solvent effect in radical copolymerization and sequence distribution of monomers in copolymers of styrene with methacrylic acid. Polym Prepr, Am Chem Soc, Div Polym Chem. 1978;19:240-4.
[256] Harwood HJ. Structures and compositions of copolymers. Makromol Chem, Macromol Symp. 1987;10-11:331-54.
[257] Klumperman B, Kraeger IR. Effect of Solvent on the Copolymerization of Styrene and Acrylonitrile. Application of the Bootstrap Effect to the Penultimate Unit Model. Macromolecules. 1994;27:1529-34.
[258] Kaim A. "Bootstrap model" for the copolymerization of the methyl methacrylate-styrene system in the presence of methyl cyanoacetate. J Macromol Sci, Pure Appl Chem. 1996;A33:1711-22.
[259] Fernandez-Garcia M, Fernandez-Sanz M, Madruga EL, Cuervo-Rodriguez R, Hernandez-Gordo V, Fernandez-Monreal MC. Solvent effects on the free-radical copolymerization of styrene with butyl acrylate. I. Monomer reactivity ratios. J Polym Sci, Part A: Polym Chem. 2000;38:60-7.
[260] An Q, Qian J, Yu L, Luo Y, Liu X. Study on kinetics of controlled/living radical polymerization of acrylonitrile by RAFT technique. J Polym Sci, Part A: Polym Chem. 2005;43:1973-7.
[261] Liu X-H, Li Y-G, Lin Y, Li Y-S. 2-Cyanoprop-2-yl dithiobenzoate mediated reversible addition-fragmentation chain transfer polymerization of acrylonitrile targeting a polymer with a higher molecular weight. J Polym Sci, Part A: Polym Chem. 2007;45:1272-81.
[262] Moskowitz JD, Abel BA, McCormick CL, Wiggins JS. High molecular weight and low dispersity polyacrylonitrile by low temperature RAFT polymerization. J Polym Sci, Part A: Polym Chem. 2016;54:553-62.
[263] Laus M, Papa R, Sparnacci K, Alberti A, Benaglia M, Macciantelli D. Controlled Radical Polymerization of Styrene with Phosphoryl- and (Thiophosphoryl)dithioformates as RAFT Agents. Macromolecules. 2001;34:7269-75.
[264] McLeary JB, Calitz FM, McKenzie JM, Tonge MP, Sanderson RD, Klumperman B. Beyond Inhibition: A 1H NMR Investigation of the Early Kinetics of RAFT-Mediated Polymerization with the Same Initiating and Leaving Groups. Macromolecules. 2004;37:2383-94.
[265] Hong J, Wang Q, Lin Y, Fan Z. Styrene Polymerization in the Presence of Cyclic Trithiocarbonate. Macromolecules. 2005;38:2691-5.
[266] Chernikova EV, Poteryaeva ZA, Plutalova AV. Controlled copolymerization of acrylonitrile in bulk via the reversible addition-fragmentation chain-transfer mechanism. Polym Sci, Ser B. 2014;56:109-17.
[267] Huang J, Zhao S, Gao X, Luo Y, Li B. Ab Initio RAFT Emulsion Copolymerization of Styrene and Acrylonitrile. Ind Eng Chem Res. 2014;53:7688-95.

[268] Fan D, He J, Xu J, Tang W, Liu Y, Yang Y. Synthesis of SAN-containing block copolymers using RAFT polymerization. J Polym Sci, Part A: Polym Chem. 2006;44:2260-9.
[269] Wang G-x, Liu Y-b. Synthesis of styrene-acrylonitrile copolymer by AGET-ATRP polymerization. Gaoxiao Huaxue Gongcheng Xuebao. 2014;28:365-9.
[270] Tsarevsky NV, Sarbu T, Goebelt B, Matyjaszewski K. Synthesis of Styrene-Acrylonitrile Copolymers and Related Block Copolymers by Atom Transfer Radical Polymerization. Macromolecules. 2002;35:6142-8.
[271] Larnaudie SC, Brendel JC, Jolliffe KA, Perrier S. Cyclic peptide-polymer conjugates: Grafting-to vs grafting-from. J Polym Sci, Part A: Polym Chem. 2016;54:1003-11.
[272] Goldfinger G, Steidlitz M. Temperature dependence of copolymerization. J Polym Sci. 1948;3:786-9.
[273] Netopilik M, Kratochvil P. Polystyrene-equivalent molecular weight versus true molecular weight in size-exclusion chromatography. Polymer. 2003;44:3431-6.
[274] Guillaneuf Y, Castignolles P. Using apparent molecular weight from SEC in controlled/living polymerization and kinetics of polymerization. J Polym Sci, Part A: Polym Chem. 2008;46:897-911.
[275] Arita K, Ohtomo T, Tsurumi Y. Analysis of the monomer sequence distribution in alternating acrylonitrilestyrene copolymers by 13C-NMR. Journal of Polymer Science: Polymer Letters Edition. 1981;19:211-6.
[276] Pichot C, Pham Q-t. Acrylonitrile copolymerization. Sequence distribution in acrylonitrile-styrene copolymers by 13C NMR: Conversion and solvent effects. Die Makromolekulare Chemie. 1979;180:2359-70.
[277] Stejskal EO, Schaefer J. Carbon-13 Nuclear Magnetic Resonance Characterization of Heterogeneous Sequence Distributions in Styrene-Acrylonitrile Copolymers. Macromolecules. 1974;7:14-7.
[278] Brar AS, Charan S. Reactivity ratios and microstructure determination of vinyl acetate-ethyl methacrylate copolymers. Polymer. 1996;37:2451-7.
[279] Hill DJT, Lang AP, O'Donnell JH. The study of the copolymerization of styrene and acrylonitrile to high conversion. Application of low-conversion reactivity ratios. Eur Polym J. 1991;27:765-72.
[280] Klumperman B, O'Driscoll KF. Interpreting the copolymerization of styrene with maleic anhydride and with methyl methacrylate in terms of the bootstrap model. Polymer. 1993;34:1032-7.
[281] Cais RE, Farmer RG, Hill DJT, O'Donnell JH. An analysis of the complex participation model for free-radical copolymerization. Macromolecules. 1979;12:835-9.
[282] Hill DJT, O'Donnell JH, O'Sullivan PW. Methyl methacrylate-chloroprene copolymerization: an evaluation of copolymerization models. Polymer. 1984;25:569-73.
[283] Hill DJT, O'Donnell JH. Evaluation of alternative models for the mechanism of chain-growth copolymerization. Makromol Chem, Macromol Symp. 1987;10-11:375-94.

[284] Ono Y, Ishida T, Soeta H, Saito T, Isogai A. Reliable dn/dc Values of Cellulose, Chitin, and Cellulose Triacetate Dissolved in LiCl/N,N-Dimethylacetamide for Molecular Mass Analysis. Biomacromolecules. 2016;17:192-9.
[285] Elbing E, Parts AG. Interference refractometry of polymer solutions. Makromol Chem. 1965;82:270-6.
[286] Kambe Y. Experimental difficulties of light scattering from copolymer solutions. Angew Makromol Chem. 1976;54:71-6.

Chapter 3: Properties of Styrene-Acrylonitrile Copolymers

3.1 Introduction

A number of studies have already reported through both theoretical and practical investigations that the properties of copolymers are strongly dependent on the structures of the copolymer chains [48, 51, 64, 75, 81]. Gradient copolymers of similar copolymer composition as the block and statistical copolymers, are unique in terms of their copolymer chain structures. Studies suggest that the thermal properties, interfacial properties as well as the solution properties of the gradient copolymers are very different from those of the block and statistical copolymers [49, 56, 77, 81]. The thermal properties of St-AN copolymers and also their properties as thin films are investigated in this study. The aim is to compare the effect of statistical, block and gradient structures of the St-AN copolymers on their properties. Furthermore, the properties of the copolymers synthesized by the RAFT and CvRP methods were compared to study the effect of inter-chain and intra-chain gradients in the copolymer structures.

3.2 Characterization Techniques

3.2.1 Thermogravimetric analysis (TGA) and Dynamic Scanning Calorimetry (DSC)

The thermal properties of the synthesized copolymers were characterized using TGA and DSC, using a Mettler Toledo instrument. The samples were heated in Mettler Toledo aluminium pans at 10 °C/minute starting from 25 °C to 500 °C to collect the TGA data. For DSC results, the samples were heated from -25 °C to 200 °C at 10 °C/minute, and held at 200 °C for 5 minutes to erase the thermal history. The samples were then cooled to -25 °C, and reheated again to 200 °C at 10 °C/minute. The glass transition for the samples were determined from the second heat scan. Approximately 3-6 mg of polymer sample was used for each run of the DSC. Both TGA and DSC data were collected in N_2 environment.

3.2.2 X-ray Photoelectron Spectroscopy (XPS)

In this study, the XPS analyses were conducted using a Kratos AXIS Ultra X-ray Photoelectron Spectrometer with a monochromatic Al Kα x-ray source (1486.6 eV) at 225 W (15 kV, 15 mA). The survey (wide) scans were carried out over 1200 – 0 eV binding energy range with pass energy of 160 eV at 1.0 eV steps and 100 ms dwell time. For narrow (high-resolution) scans the pass

energy was lowered to 20 eV, with 0.05 eV steps and 250 ms dwell time. The base pressure in the analysis chamber was 1.0 x 10^{-9} Torr and during sample analysis it was 1.0 x 10^{-8} Torr. The number of sweeps were adjusted depending on the intensity of a particular peak. The angular dependent XPS data have been collected by changing the incident angle of the X-ray radiation from 0° to 60°, and the approximate penetration depth at these two incident angles are 10 nm and 5 nm respectively. The spectra were charge corrected using the adventitious C 1s signal at 284.8 eV. The data were analysed using CASA XPS software.

3.2.3 Contact Angle Measurement

The surface free energy of the polymer thin films was characterized by measuring the contact angles of different liquids on the thin films surface. An OCA20 contact angle system comprised of a combined stage and lens assembly fitted with a Kodak Digital Science camera linked to Kodak Digital Science Picture Postcard Software imaging program was used to measure the static contact angles at room temperature. The samples were placed on a Teflon stage and backlit, and a 50 µL glass syringe was used to apply the liquid droplet on to the thin films at room temperature. The size of the drops were 5-10 µL depending on the type of liquids, and the error of the contact angle data was calculated from six measurements for a single sample.

3.3 Thermal properties of St-AN copolymers

The thermal behaviour of copolymers are directly dependent on the composition and also on the distribution of monomer units in the copolymer chains. The effect of copolymer compositions and chain structures has been discussed in detail in Section 1.2.3.2. In several studies, it has been reported that gradient copolymers possess a broad T_g, while statistical copolymers gives a sharp transition and block copolymers gives two T_gs, one for each block (when there is a significant difference between the T_gs of each block) [52, 81, 117, 172].

Being two of the most popular monomers, the thermal behaviour of polymers of St and AN monomers are well studied. Especially for PSt, a number of studies reported the glass transition temperature (T_g) data, ranging from as low as 62 °C to 108 °C depending on the polymer molecular weight and characterization technique [287-291]. Both the TGA and DSC data have been collected for the PSt homopolymer synthesized by the RAFT method in this study with molecular weight 11300, as shown in Figure-3.1. The TGA curve shows that PSt starts degrading as the temperature reaches approximately 350 °C which is in close agreement with the literature report [287]. The

glass transition temperature found from the DSC heating curve and heating curve first derivative was found to be 100.5 ºC, which is also within the reported range of T_g values.

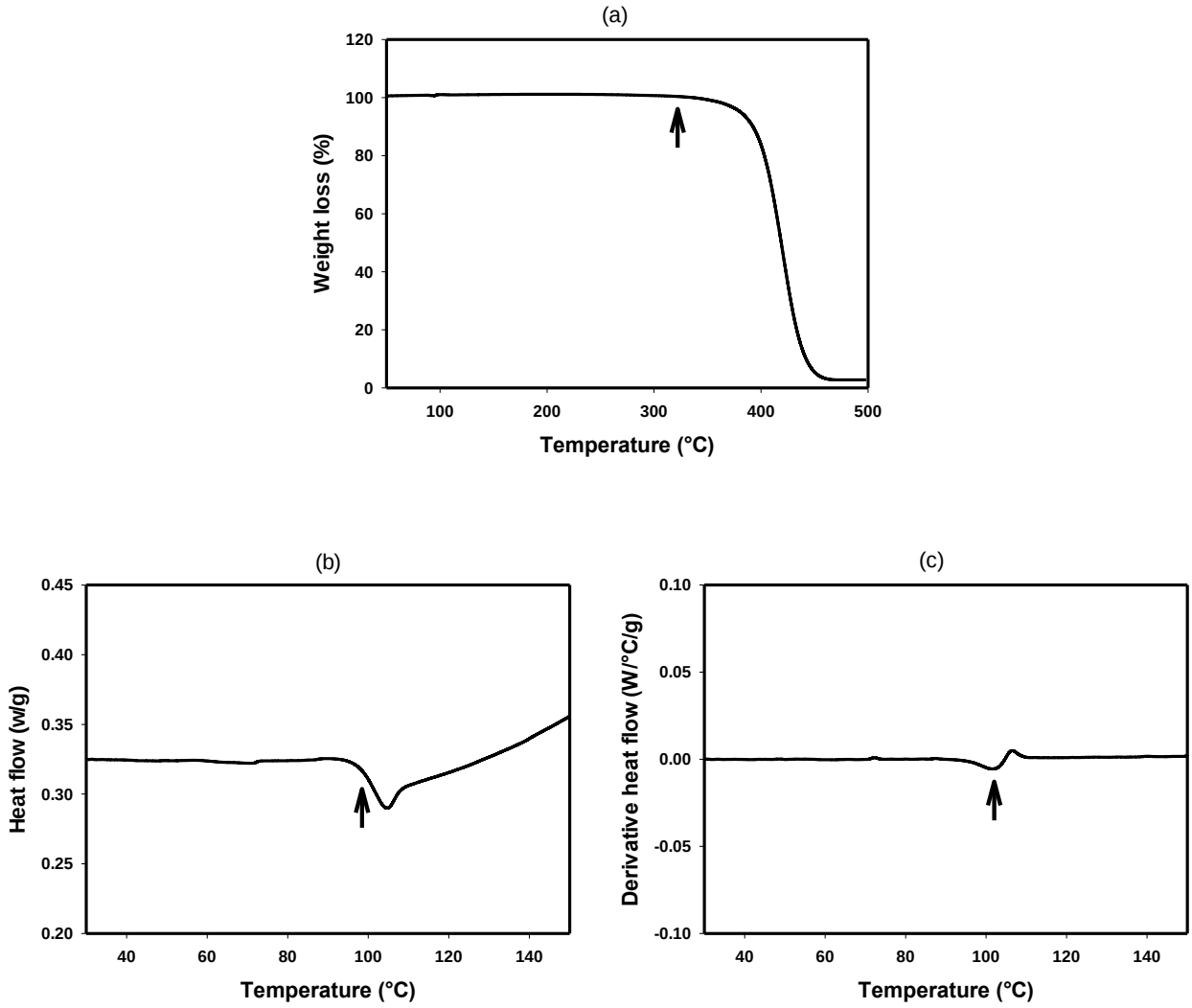

Figure-3.1: (a) TGA curve, (b) DSC heating curve, and (c) first derivative of DSC heating curve for PSt homopolymer.

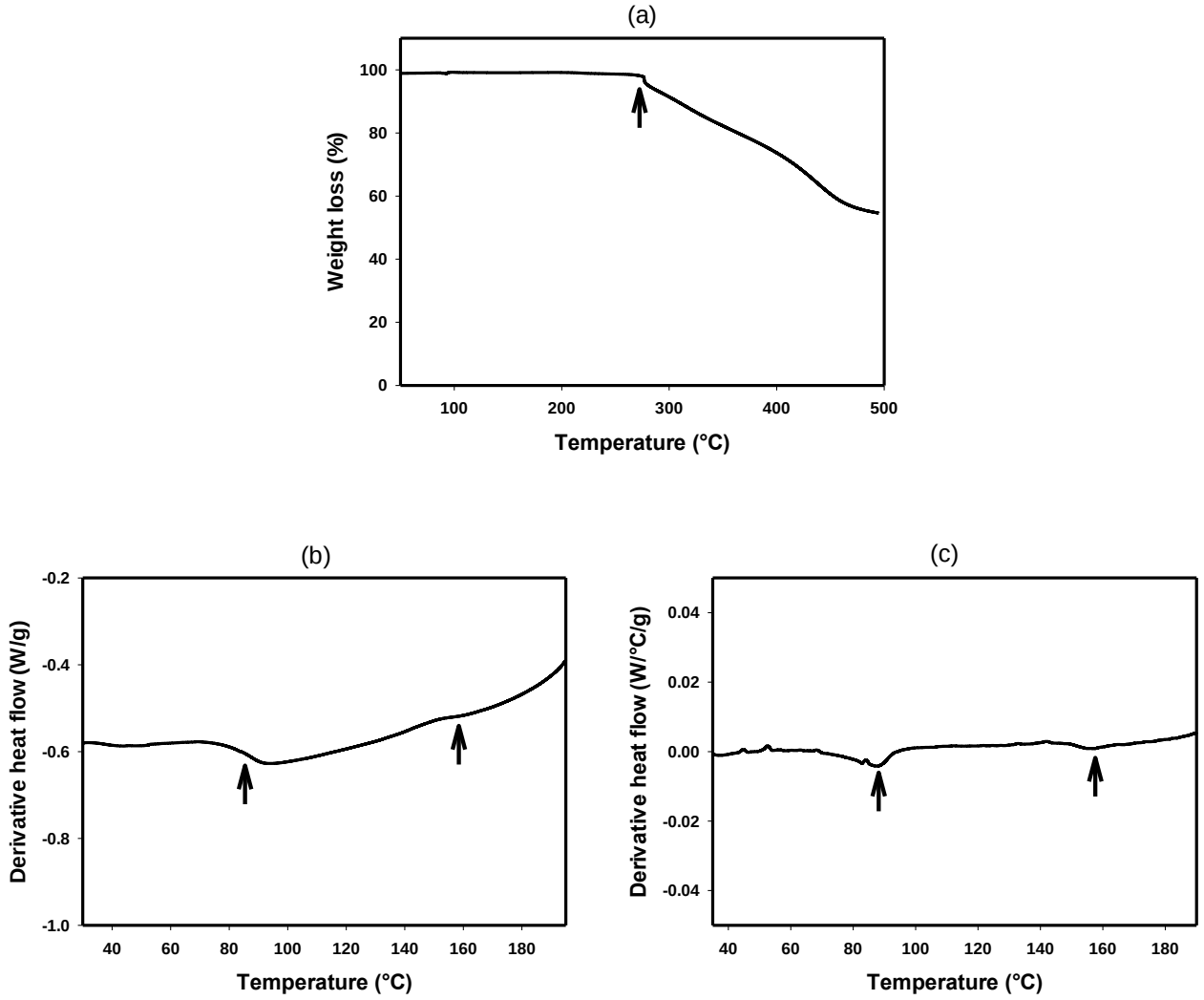

Figure-3.2: (a) TGA curve, (b) DSC heating curve, and (c) 1st derivative of DSC heating curve for PAN homopolymer.

In contrary, the thermal properties of PAN are not as well characterised [292]. The literature reports a very broad range for the T_g values of PAN from 39 °C to 180 °C [292-299]. Several studies mention two T_g values for PAN homopolymers using DMA and DSC studies, one in the range of ~90-110 °C and another at 140-170 °C [299-302], while some other studies reported a single T_g [303-307]. Bashir [299] did an extensive study on the 'unusual nature of the glass transition temperature of PAN and to justify the source of two T_g values, he proposed that un-oriented PAN exhibits a two-phase morphology consisting of laterally-ordered and amorphous domains, and this leads to two glass transitions. For oriented PAN, only one glass transition was reported [299].

The TGA plot (Figure-3.2) shows that PAN starts degrading at temperature close to 276 °C which is similar to the reported values [306, 308]. However, the DSC curve and the 1st derivative of the DSC curve show two transitions for PAN homopolymer, one at ~88 °C and another at ~157 °C. The second transition appears to be much weaker than the lower temperature transition. The difference between the first T_g for PAN (the stronger transition), and the T_g of PSt homopolymer is very small.

The DSC curves and the 1st derivative of the DSC curves for the St-AN copolymers synthesized by the RAFT and CvRP methods are shown in Figure-3.3 to Figure-3.7. Based on the literature, a broad T_g should be observed for St-AN80, St-AN20 and St-AN10 copolymers due to the gradient in their structure, while St-AN60 should provide a single sharp T_g due to its statistical nature. As the figures show (Figure-3.3, 3.5, 3.6), the St-AN copolymers synthesized by RAFT methods show broad T_gs in their DSC plots, and the transition is clearer in the 1st derivative of the heating curve. However, the same copolymers synthesized by the CvRP method show narrow T_gs, despite having gradients in their structures. The gradients along a single chain is producing a broad T_g for the RAFT copolymers, while it is not true for the gradients across the chains, as in the CvRP copolymers.

For the St-AN60 copolymers, at the azeotrope feed composition synthesized by both methods, a sharp single transition is obtained which agrees with the prediction for a statistical copolymer. However, instead of two T_gs predicted for the block copolymers, St-block-AN copolymer gives a single transition just above 100 °C. No transition was seen around 87 °C or 157 °C for the PAN block. However, a very broad transition ranging from ~80 to 115 °C is found for the forced gradient copolymer St-grad-AN60 proving the presence of a strong gradient in their structure.

For all the St-AN batch copolymers as well as the block copolymers, the transitions are at temperatures above 100 °C, and no trace of transition is seen below that temperature. This suggests the presence of the second transition at ~157 °C of PAN in the copolymer. However, the breath of T_g (~80 °C to 115 °C) for the forced gradient copolymer again proves the presence of the first transition (~88 °C) of PAN. The DSC results found for the St-AN copolymers therefore indicate that the complex thermal behaviour of PAN homopolymer is carried over to the copolymer chains, producing complex thermal data for the St-AN copolymers.

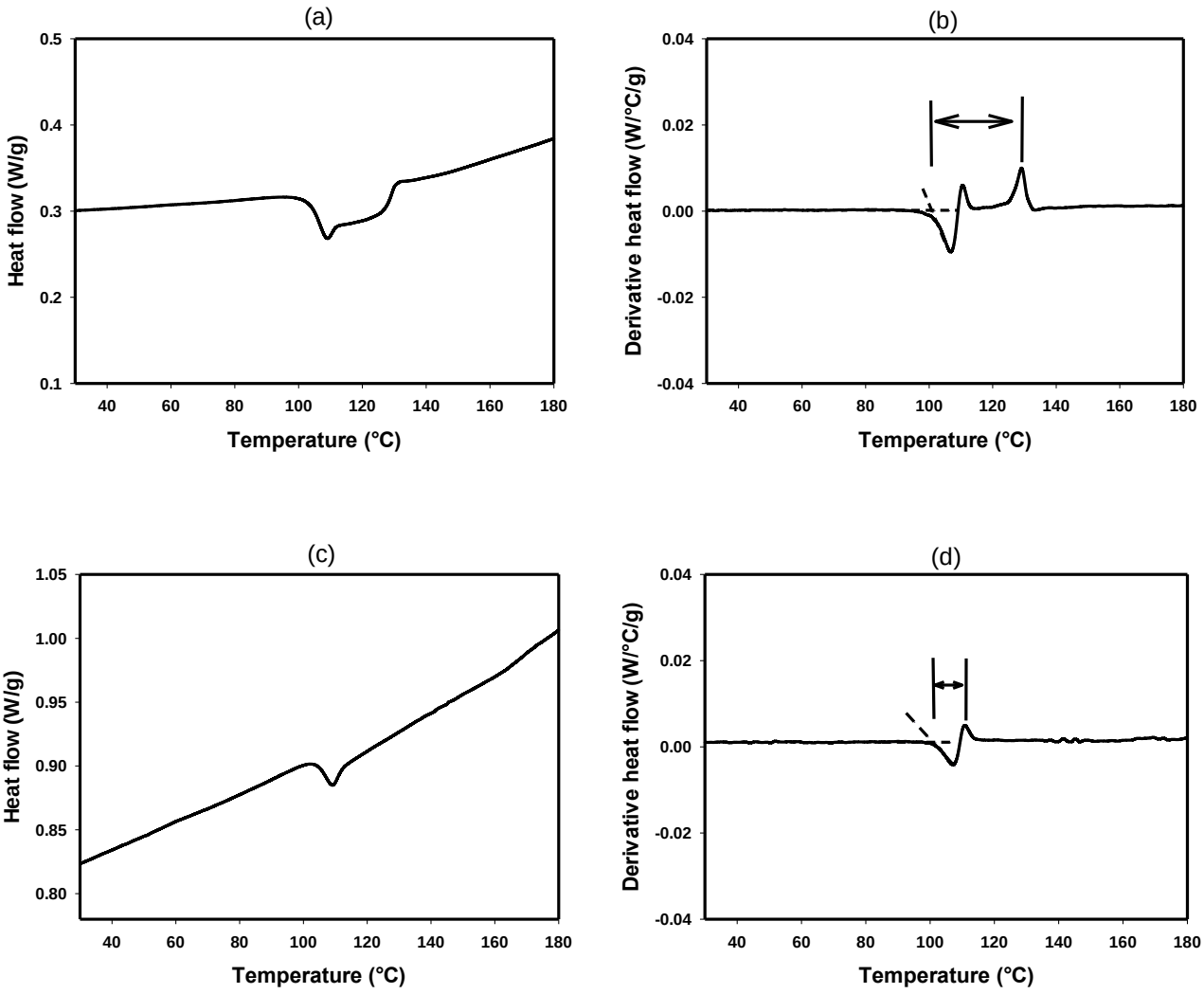

Figure-3.3: (a) DSC heating curve, (b) 1st derivative of DSC heating curve for St-AN80 copolymers synthesized by RAFT; (c) DSC heating curve, (d) 1st derivative of DSC heating curve for St-AN80 copolymers synthesized by the CvRP method.

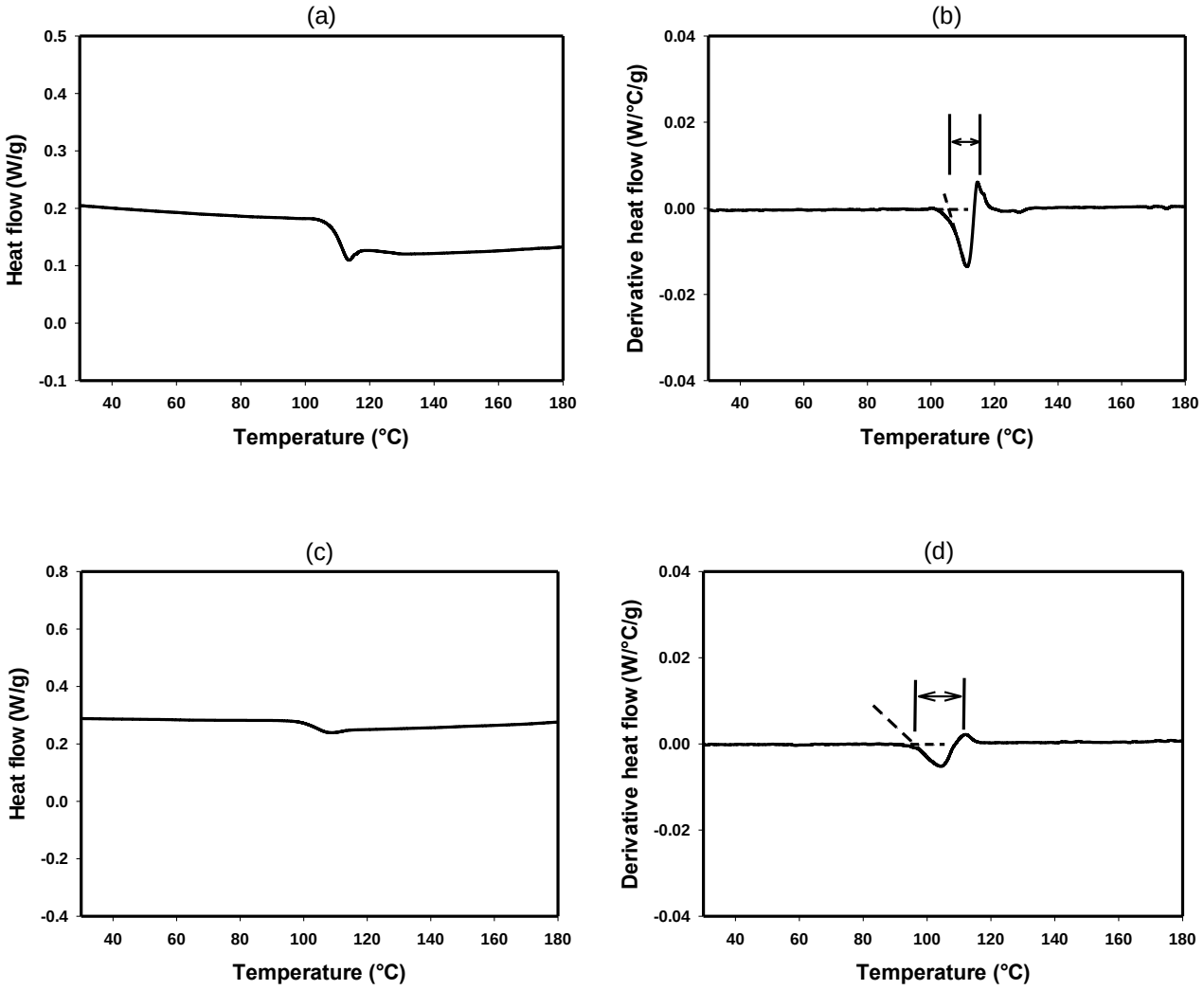

Figure-3.4: (a) DSC heating curve, (b) 1st derivative of DSC heating curve for St-AN60 copolymers synthesized by RAFT; (c) DSC heating curve, (d) 1st derivative of DSC heating curve for St-AN60 copolymers synthesized by the CvRP method.

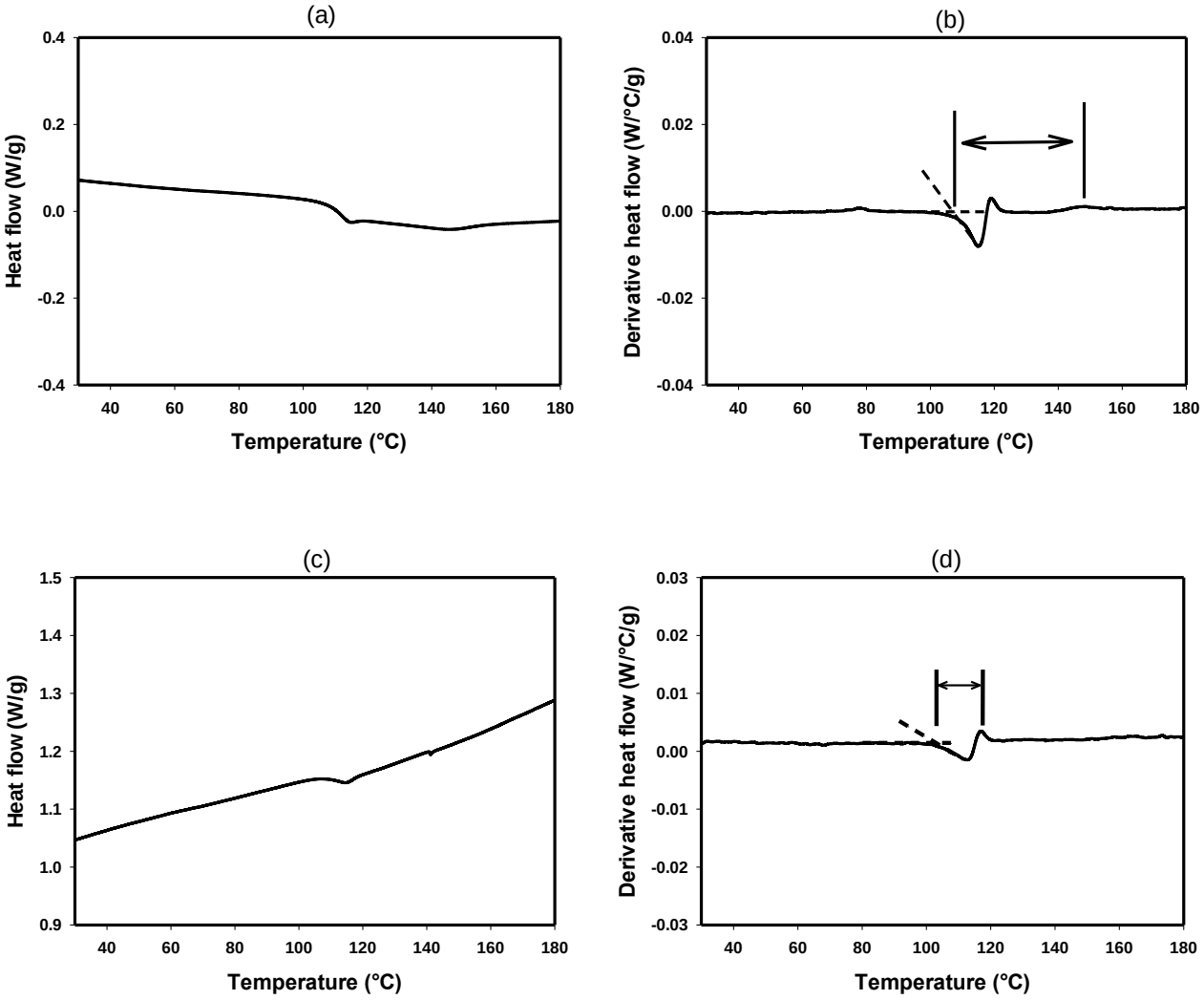

Figure-3.5: (a) DSC heating curve, (b) 1st derivative of DSC heating curve for St-AN20 copolymers synthesized by RAFT; (c) DSC heating curve, (d) 1st derivative of DSC heating curve for St-AN20 copolymers synthesized by the CvRP method.

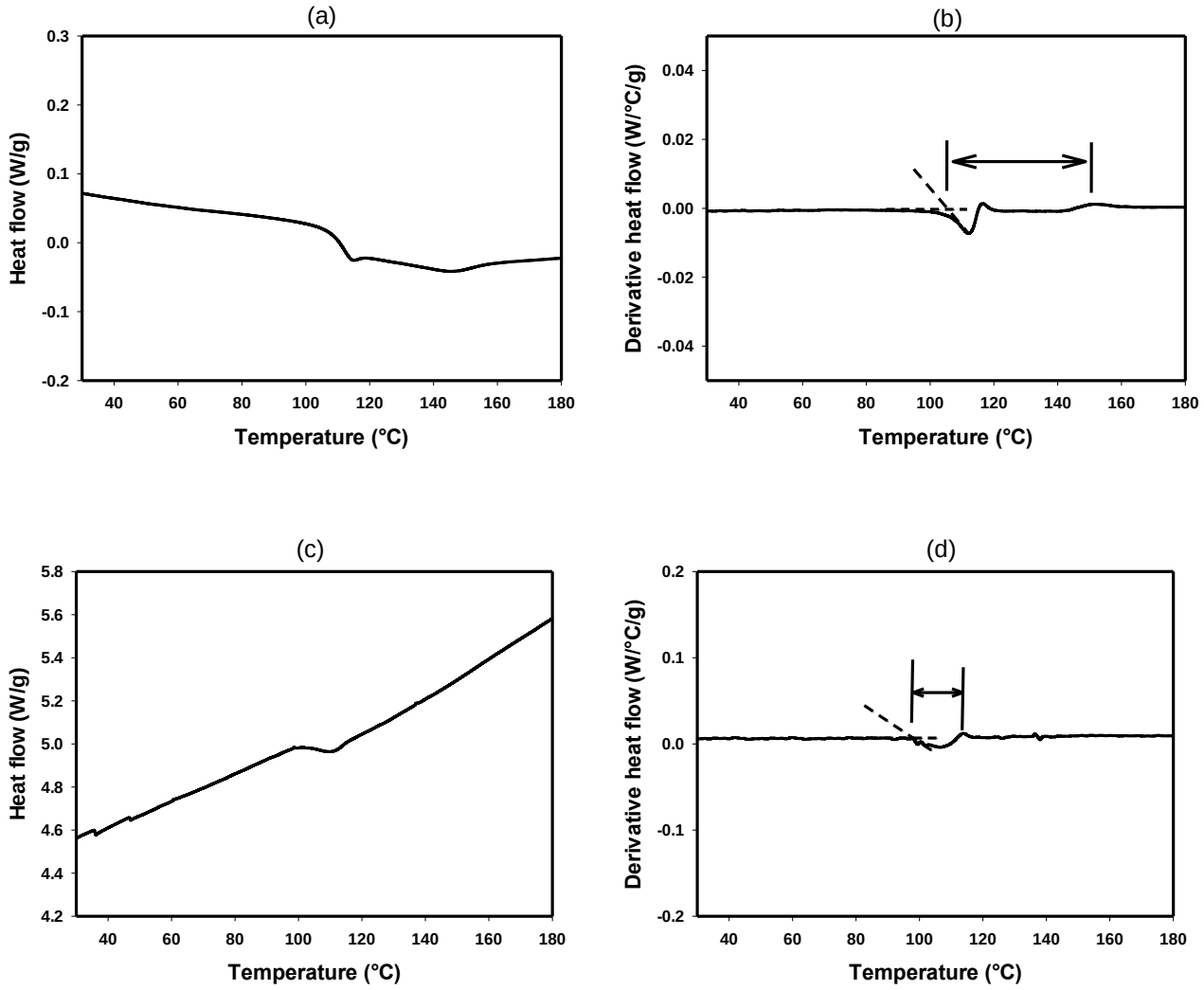

Figure-3.6: (a) DSC heating curve, (b) 1st derivative of DSC heating curve for St-AN10 copolymers synthesized by RAFT; (c) DSC heating curve, (d) 1st derivative of DSC heating curve for St-AN10 copolymers synthesized by the CvRP method.

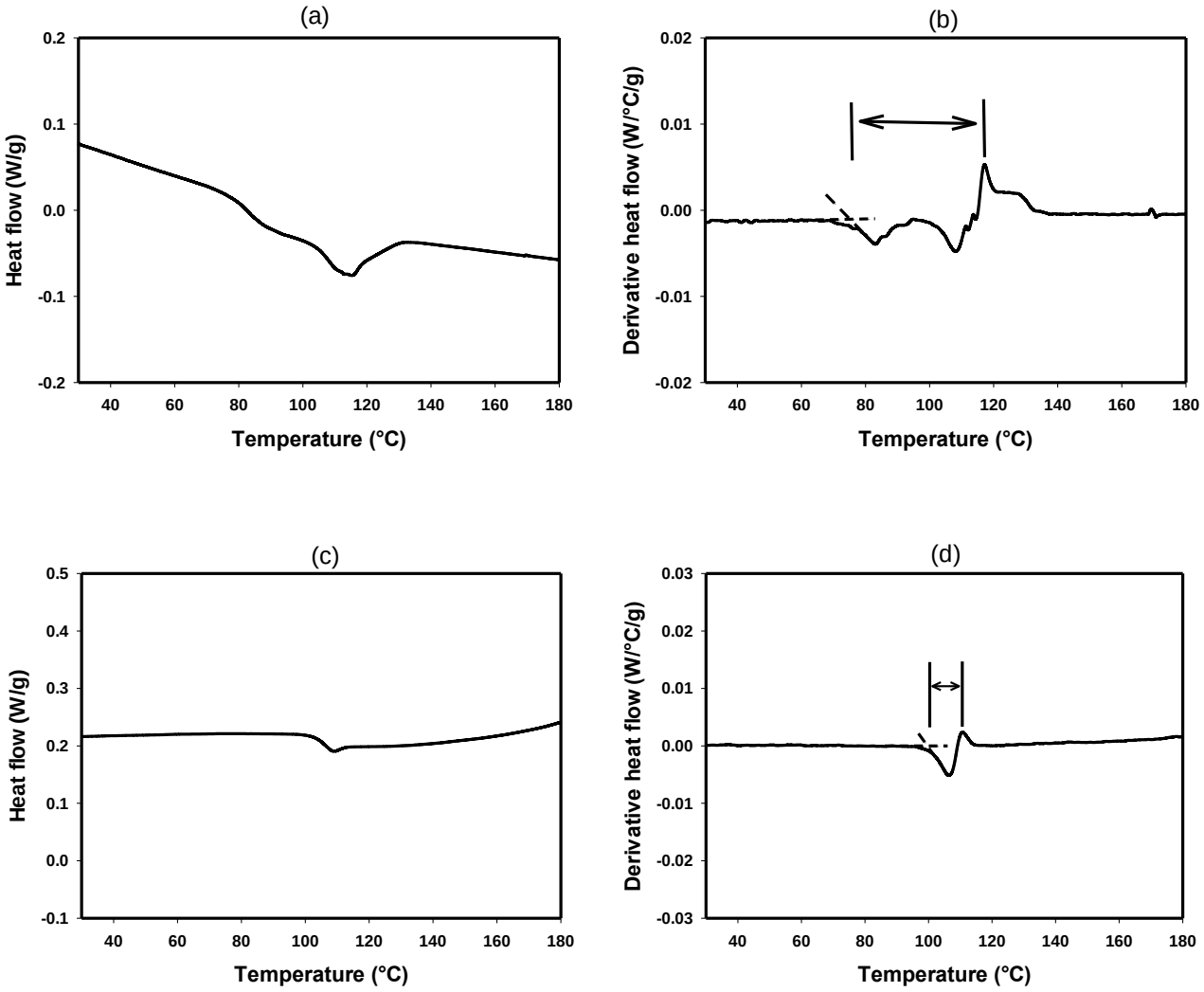

Figure-3.7: (a) DSC heating curve, (b) 1st derivative of DSC heating curve for St-grad-AN60 copolymers synthesized by RAFT; (c) DSC heating curve, (d) 1st derivative of DSC heating curve for St-block-AN68 copolymers synthesized by RAFT.

3.4 Preparation of thin films of St-AN copolymers

St and AN homopolymers and their copolymers were coated on to silicon wafer to prepare thin polymeric films either by spin coating or dip coating. A suitable coating method and a suitable solvent were selected to ensure uniform thin films in order to study the copolymer properties on the thin films. A range of solvents such as DMF [309-311], 1,2-dichloroethane [312, 313], acetone [314], methyl ethyl ketone [315], THF [316], dichloromethane[317] have been reported to be used to prepare thin films of St-AN copolymers either by spin coating or solvent casting.

Among the solvents reported to be used for preparing St-AN copolymer thin films, DMF is the most commonly-used, and hence was used in this study to prepare thin polymeric films. St-AN60 copolymer was suspended in DMF to prepare 3 wt% solution, and spin coated on to a silicon wafer. Prior to spin coating, the silicon wafer was cleaned by sonicating the wafers in methanol, isopropyl alcohol, and acetone consecutively, for 5 minutes in each. However, the films spin coated using DMF as solvent results in a rough and non-uniform surface (Figure-3.8). The thickness of the thin films were measured by a SCI Filmtek 2000M. For each sample, thickness of nine different spots were measured and size of each spot was 5 μm by 2 μm. The Filmtek data shows thin film thickness values ranging from nanometres to micrometres.

The concentration of polymer solutions were varied from 0.5 wt% to 10 wt% and also several different spin speeds were used in an attempt to achieve uniformity in the thin films, but unfortunately in every cases the film thicknesses were found to be varying from nanometres to micrometres as measured by Filmtek. Similar results were found for the PSt, PAN homopolymers and other compositions of St-AN copolymers, when DMF was used as the solvent for spin coating.

As an alternative, the dip coating process was applied to prepare thin films of St-AN60 copolymers using DMF as solvent for three different solution concentrations. A clean silicon wafer was slowly dipped into the polymer solution, removed after 30 seconds followed by drying in a vacuum oven for 72 hours. However, for each concentration, films with irregular thicknesses were found as shown in Figure-3.9. In addition to varying the concentration and spin speed, an alternative approach was applied to clean the silicon wafer surface. The wafer surface was treated with oxygen plasma etching for 30 s prior to spin coating of the polymer solution, which provided thin films with random microstructures and varying thickness as shown in Figure-3.10.

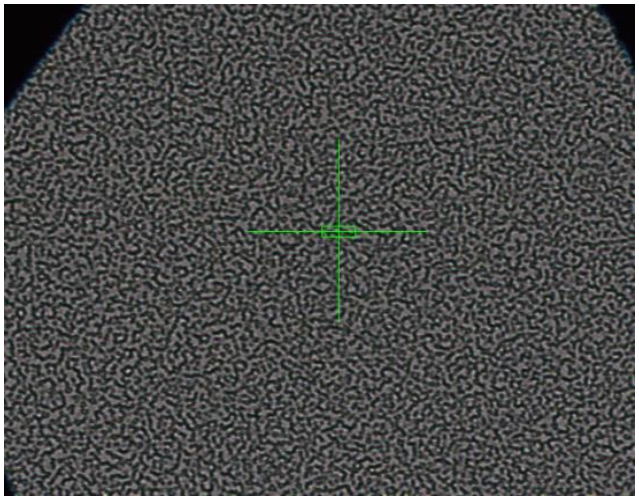

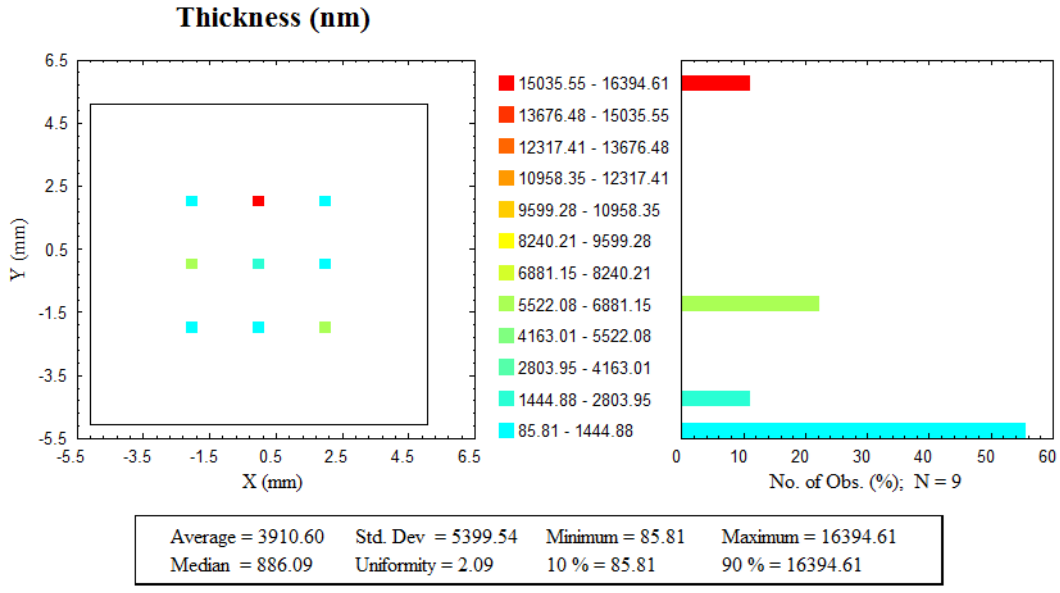

Figure-3.8: Microscopic image (top) and the thickness data by collecting film thickness for nine different points (bottom) for St-AN60 copolymer thin films spin coated on to silicon wafer using DMF as solvent. The size of each measurement spot as shown by the rectangle in the microscopic image is 5 µm by 2 µm.

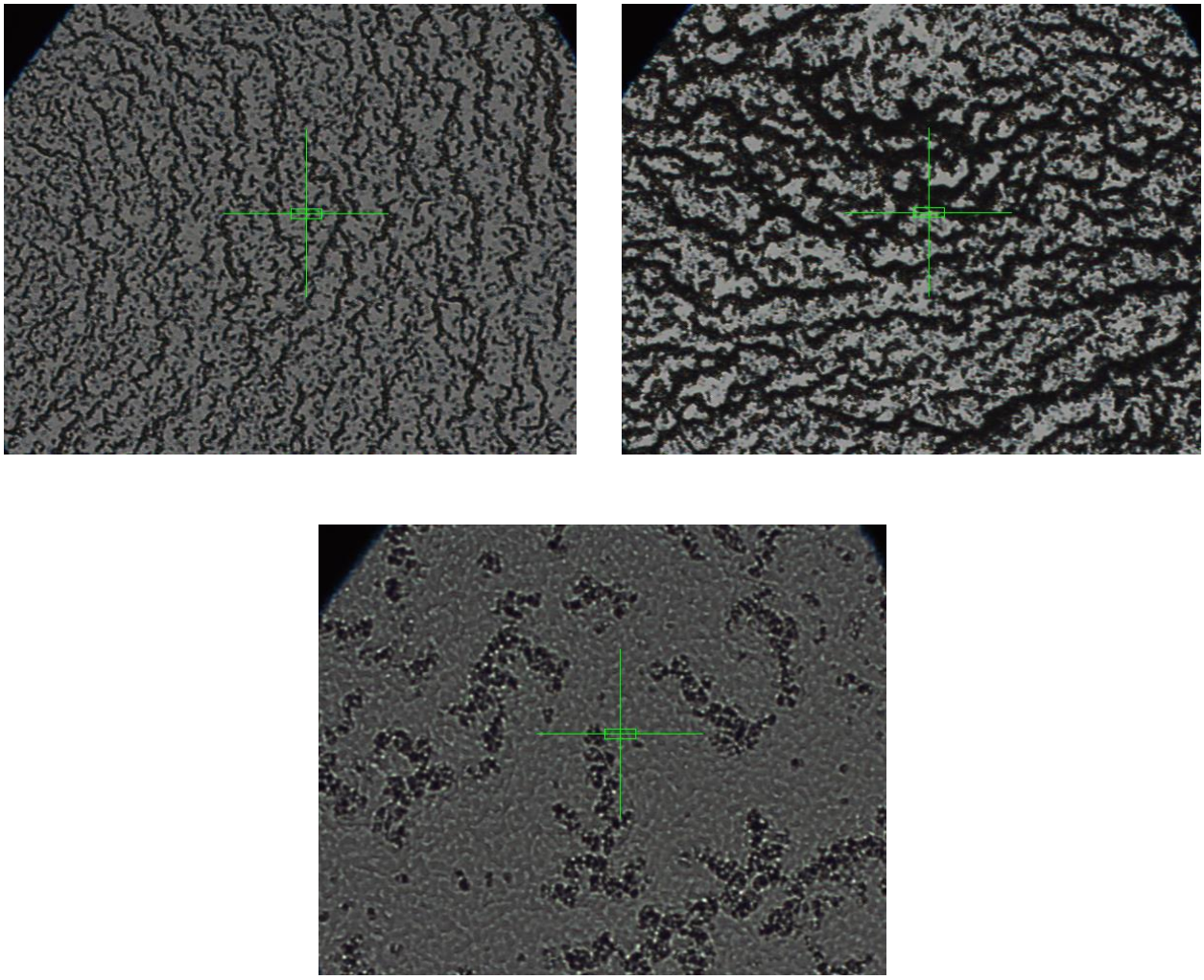

Figure-3.9: The microscopic image of St-AN60 copolymer thin films prepared by dip coating technique for 1 wt% (top left), 2 wt% (top right) and 4 wt% (bottom) copolymer solution in DMF.

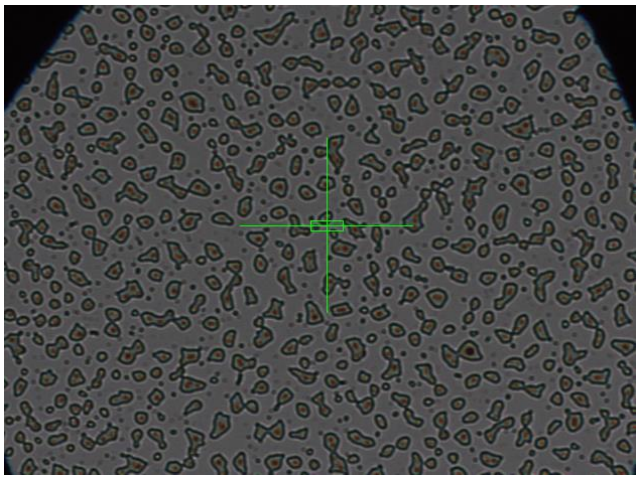

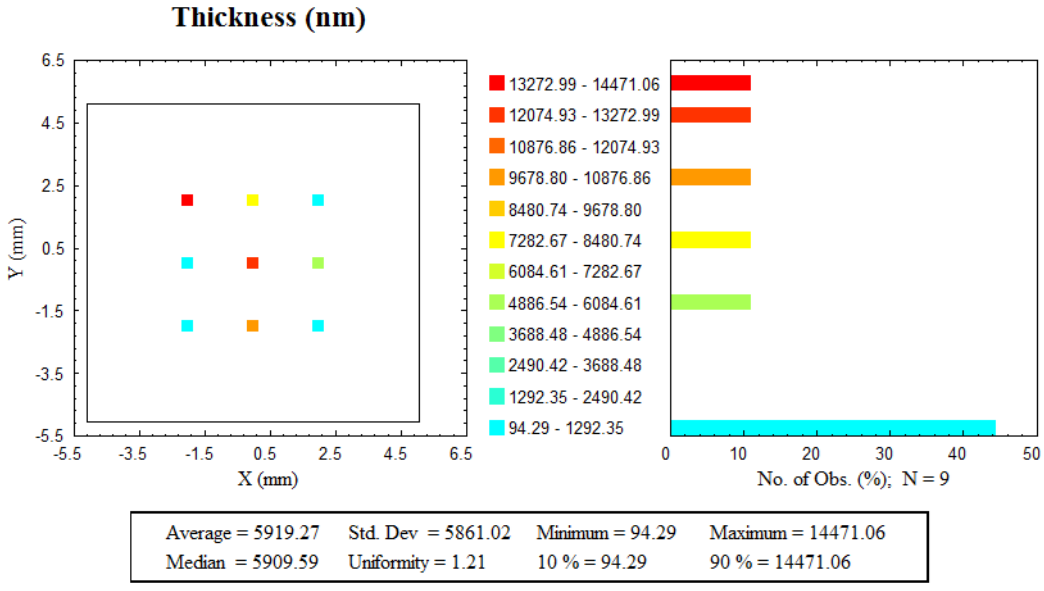

Figure-3.10: Microscopic image (top) and the thickness data by collecting film thickness for nine different points (bottom) for St-AN60 copolymer thin films spin coated on to silicon wafer cleaned with oxygen plasma etching, using DMF as solvent.

Methyl ketones have been reported to be used to prepare thin films of St-AN copolymers with high St compositions by spin coating [315, 318]. Therefore, as an alternative of DMF, methyl isobutyl ketone (MIK) was used to prepare 3 wt% solution of St-AN60 copolymers. After passing through a PTFE 0.45 micron 13 mm filter to remove the insoluble impurities including undissolved polymer, the solution was spin coated for 60 s at 4000 rpm, on to a clean silicon wafer. The microscopic image, as well as the thickness data (Figure-3.11) shows very uniform film thickness for St-AN60 copolymer thin films using MIK as solvent. The average film thickness was found to be 89.5 nm, with very low standard deviation (0.53 nm). Hence, MIK was used to prepare thin films of the St-AN80, St-AN60, St-grad-AN60 as well as the PSt homopolymers. In all cases, polymeric thin films with excellent uniformity was formed with average thickness ~90 nm.

Unlike PSt homopolymer and the St-AN copolymers with high St composition, the PAN homopolymer, PSt-block-PAN copolymers, St-AN20 and St-AN10 copolymers are insoluble in MIK. Since DMF is a good solvent for PAN homopolymer, as well as St-AN copolymers with high AN compositions, and MIK is found to provide uniform thin films for St-AN copolymers with high St compositions, a 50:50 mixture of DMF and MIK was used to prepare 3 wt% PAN solution and spin coated on to silicon wafer. The thin films formed in this process contained irregular cracks which were visible even to the naked eye (Figure-3.12).

Peng et al. [319] reported the use of 1,1,1,3,3,3-hexafluoro-2-propanol (HFIP) as solvent to prepare PAN polymer thin films with nano-scale roughness and controllable thickness by the dip coating process. HFIP is a highly volatile solvent with very low boiling point (59 °C), which is capable of dissolving PAN homopolymer as well as St-AN copolymers with high AN compositions. A 2 wt% solution of PAN was prepared using HFIP as solvent and the clean silicon wafer was slowly dipped in to the polymer solution. After 30s the wafer was slowly removed from the solution and left at ambient temperature to dry off the remaining solvent. The film thickness measured by Filmtek showed very uniform thin films with standard deviation as low as 1.87 nm for thickness data of nine different points (Figure-3.13). Therefore, HFIP was also used to prepare thin films of St-AN20, St-AN10 and St-block-AN copolymers, and in each case thin films with very uniform thickness were formed.

These uniform thin films of St-AN copolymers prepared by using MIK and HFIP as solvents were then used to characterize by XPS and contact angle measurements to study the copolymer properties.

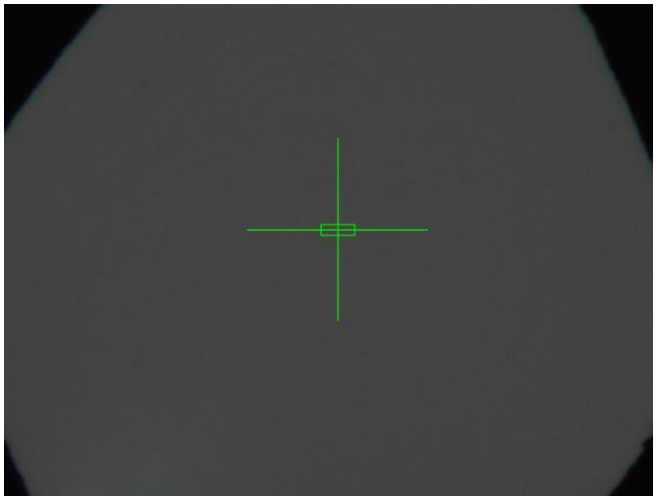

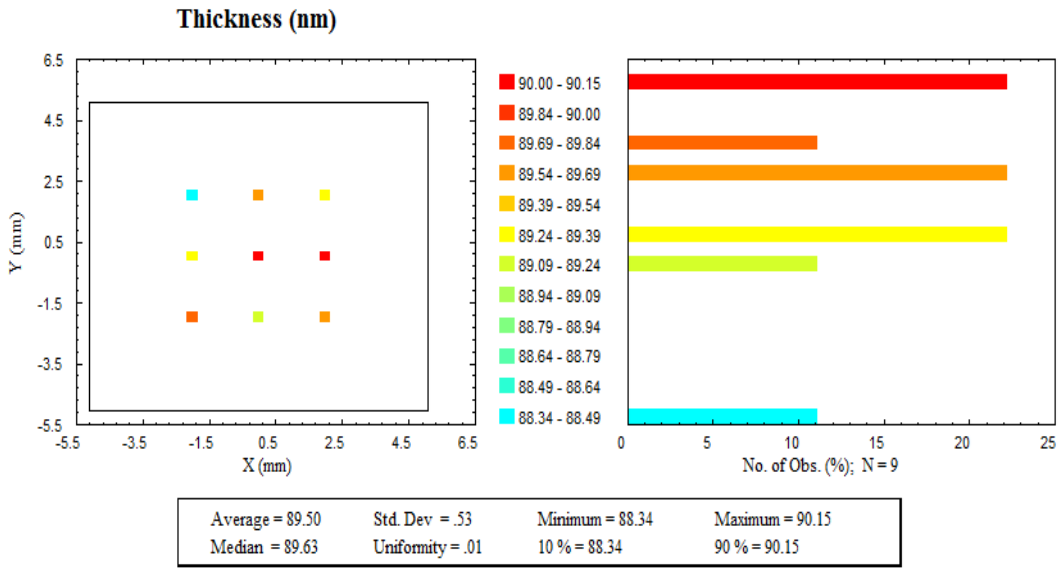

Figure-3.11: Microscopic image (top) and the thickness data by collecting film thickness for nine different points (bottom) for St-AN60 copolymer thin films spin coated on to silicon wafer using MIK as solvent.

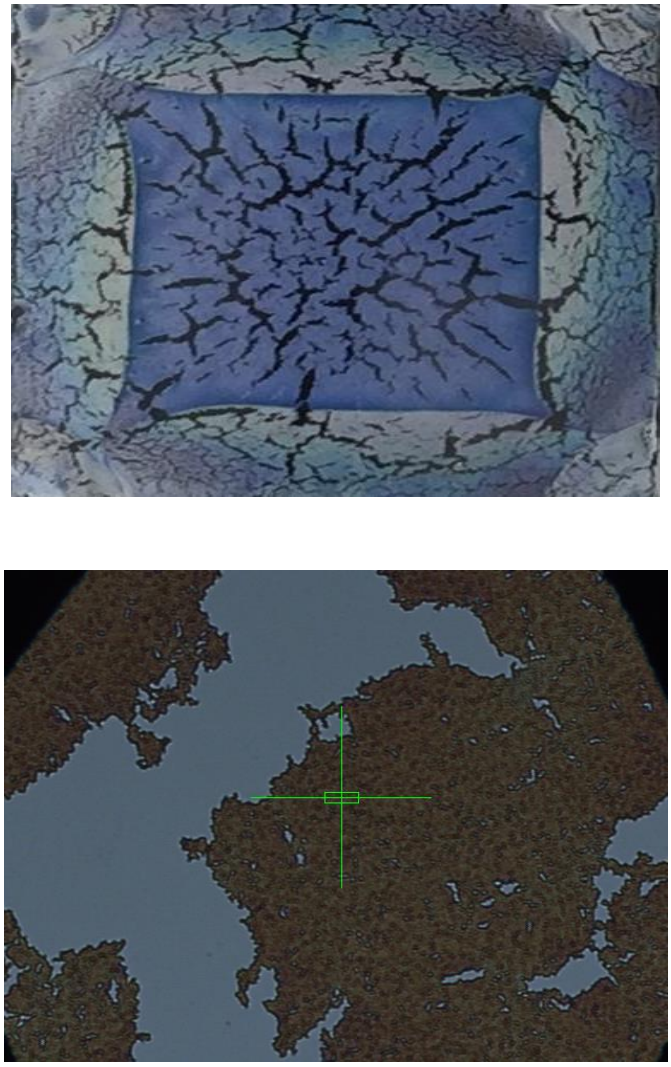

Figure-3.12: Normal image captured by mobile camera (top) and microscopic image (bottom) of the PAN thin films surface spin on to silicon wafer using 50:50 mixture of DMF and MIK as solvent.

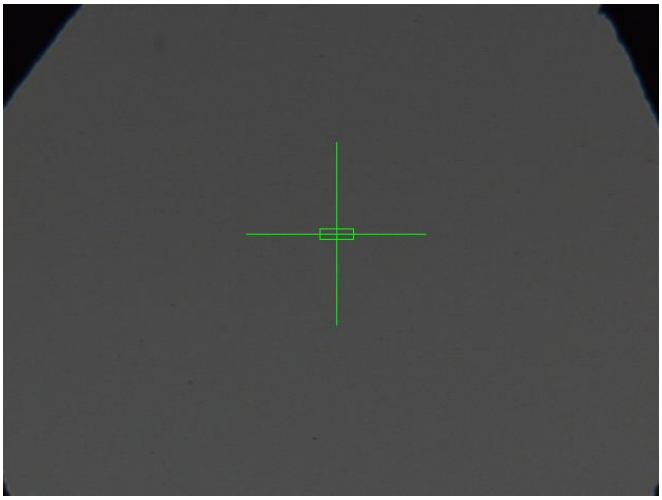

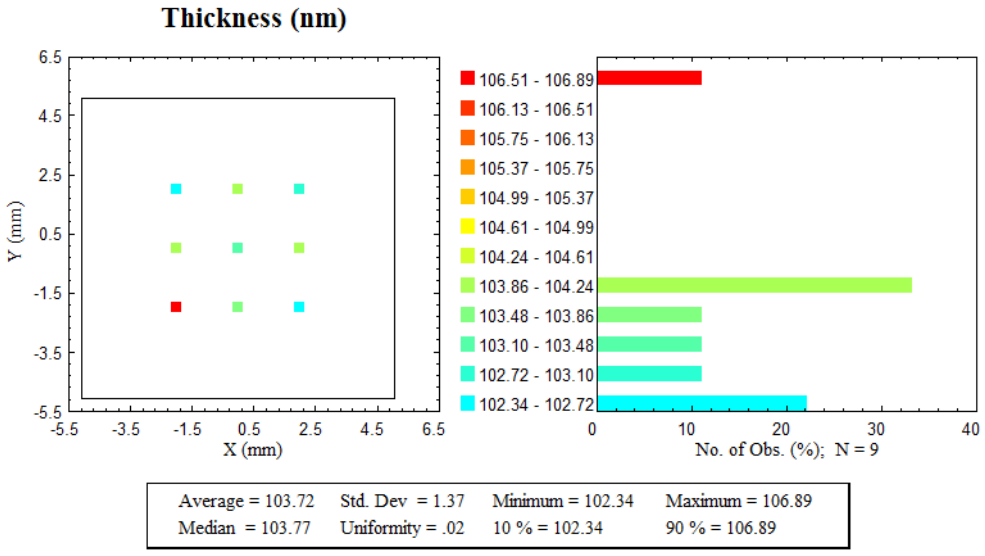

Figure-3.13: Microscopic image (top) and the thickness data (bottom) for PAN homopolymer thin films formed by dip coating, using HFIP as the solvent.

3.5 XPS study of St-AN copolymer thin films

X-ray photoelectron spectroscopy (XPS) is a useful technique that has been used extensively to study the surface composition of polymer and copolymer thin films [320-323]. It is reported to be a highly sensitive surface analysis technique which probes the top 10 nm of a polymeric film, and specifically useful for analysing the elemental composition and chemical-bonding state of the surface [324, 325]. A number of studies have reported the XPS studies of PSt and PAN homopolymers, and their copolymer thin films [325-332]. In this study, the surface composition of the PSt and PAN homopolymers, and different compositions of St-AN statistical, block and gradient copolymer thin films have been studied using a Kratos AXIS Ultra XPS. The survey data were collected with pass energy 160 eV at 1.0 eV step size, and for high resolution, the pass energy was 20 eV at 0.05 eV step size. The data have been collected at 0° and 60° incident angle, and the approximate penetration depths at these two incident angles are 10 nm and 5 nm respectively.

3.5.1 Effect of RAFT end group on XPS data

The PSt and PAN homopolymers, as well as their copolymers synthesized by the RAFT method contain the RAFT end groups at the end of their chains, which could influence the usual properties of the polymers on the thin film surface. PSt homopolymer and one of the St-AN copolymers (St-AN20) synthesized by the RAFT method has been chosen to remove the RAFT end group, and the effect of the end group was studied by comparing the XPS data before and after removing the end group.

The end group was cleaved by treating the polymer with AIBN initiator using dioxane as the solvent. The molar ratio of polymer and initiator was 1:100. After sealing with a rubber septum, the mixture was purged with Ar gas for 30 minutes and stirred in an oil bath at 80 °C temperature for six hours. The initial pink colour disappeared giving a colourless solution. The copolymer was precipitated in methanol and after several washing steps the polymer was dried in vacuum oven at room temperature. The copolymers before and after cleaving the RAFT end groups were characterized by UV and ^{1}H NMR spectroscopy to confirm the complete removal of the end group.

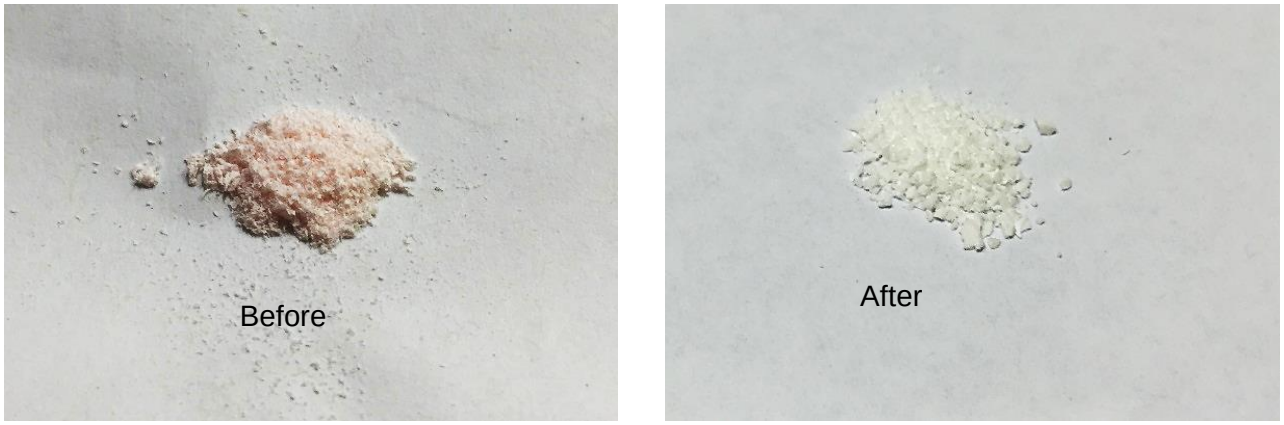

Figure-3.14: The change in colour after cleaving the RAFT end group. The pink colour due to the end group disappears once it is cleaved and gives white/colourless polymers.

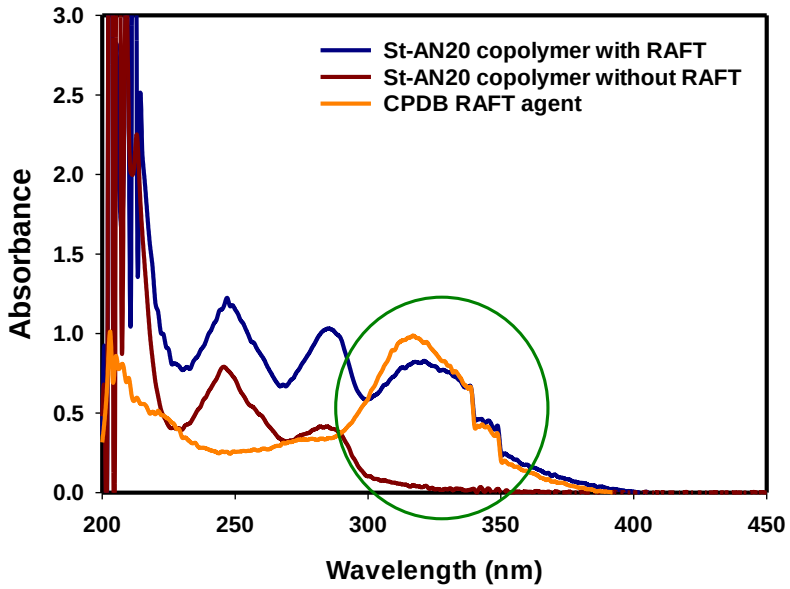

Figure-3.15: The change in the UV spectra after cleaving the RAFT end group. The peak at around 320 nm due to the RAFT end group disappears once the end group was cleaved.

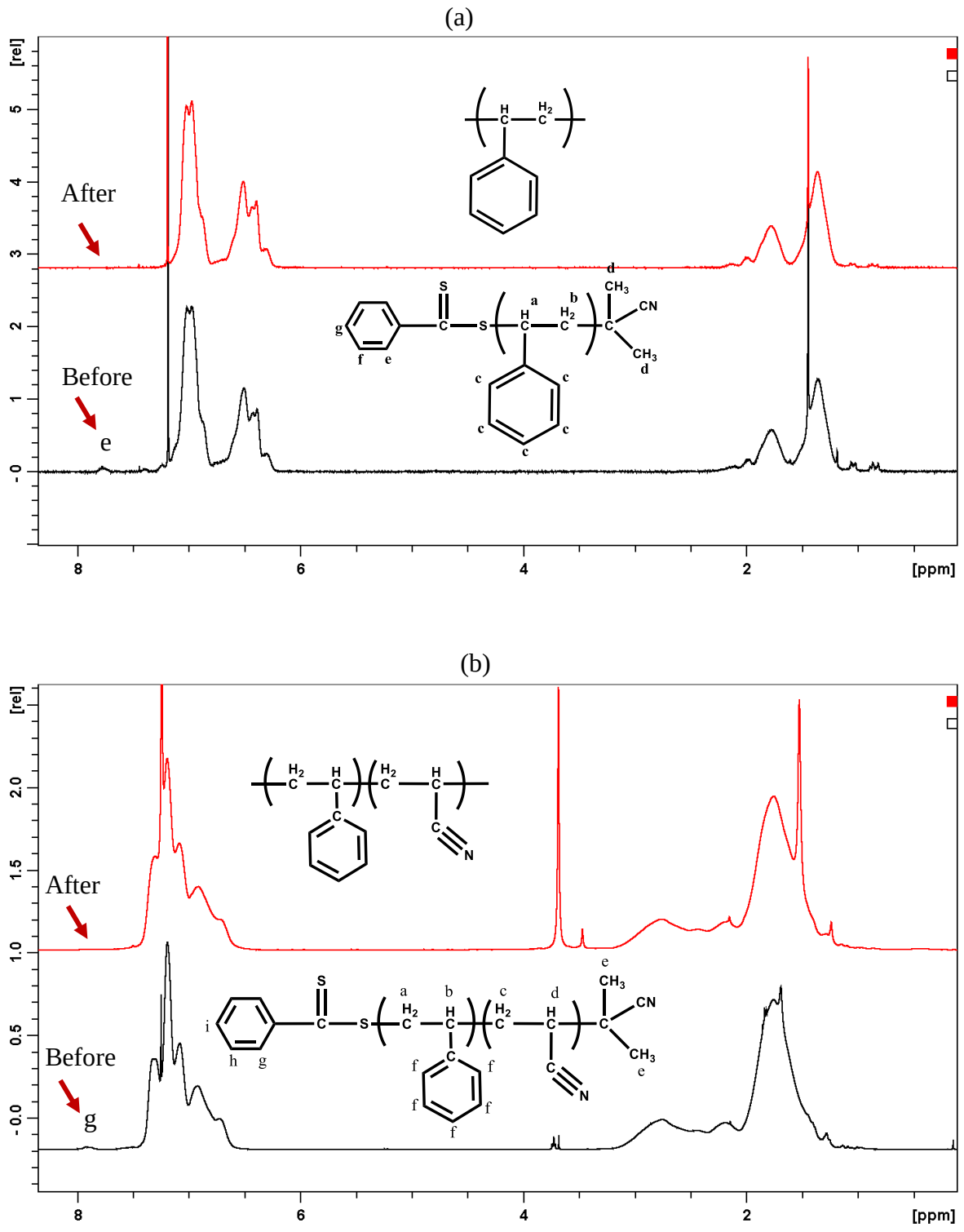

Figure-3.16: Comparative ^{1}H NMR spectra for (a) PSt homopolymer and (b) St-AN20 copolymer before and after cleaving the RAFT end group which shows the change in the peak at around 8 ppm.

The initial sign of the RAFT end group removal is the change in the colour of the copolymers. The presence of the RAFT end group in the copolymer chains gives the polymer powder a pink colour, which disappears upon the treatment with AIBN, and produces a white/colourless powder after cleaving RAFT end group. Figure-3.14 shows the copolymer St-AN20 copolymer powders before and after cleaving the RAFT end group.

The removal of the RAFT end group was confirmed by comparing the UV spectrum of the RAFT end group with the St-AN20 copolymers spectra before and after cleaving the end group. The peak at around 315 nm for the RAFT end group shown in Figure-3.15, can be seen for the St-AN20 copolymer before cleaving the RAFT end group. However, after cleaving the end group, the peak at around 315 nm disappeared, which indicates the complete removal of the RAFT end group.

The removal of the end group was further confirmed from the comparison of the ^{1}H NMR of the PSt homopolymer and St-AN20 copolymer before and after cleaving the end group. The aromatic proton from the CBDB RAFT agent gives a well resolved peak at around 8 ppm for both PSt homopolymer and St-AN20 copolymer. As shown in Figure-3.16, the peak for the end group disappears after cleaving the end group.

The XPS survey data have been collected for the homo and copolymer before and after cleaving the RAFT agent. XPS detects two small peaks for sulfur, one at binding energy at 229 eV for 2 s electron and another one at binding energy 165 eV for 2p electron (Figure-3.17). However, no such peak for sulfur has been seen for St-AN20 copolymer (Figure-3.18). This could be due to the low molecular weight of the homopolymer PSt (M_n = 4600) compared to that of the copolymer (M_n = 13100). The XPS data for the St-AN20 copolymer on the film also does not show a sulfur peak. This means, the end group in the copolymer does not preferentially concentrate at the surface and hence will not affect the XPS composition data of the St-AN copolymers. To verify this, the XPS survey data was collected for PSt homopolymer with higher molecular weight (M_n = 11300), and as expected, no trace of the sulfur peak was found. Based on this study, the XPS studies of the copolymers were continued without cleaving the RAFT end groups.

(a)

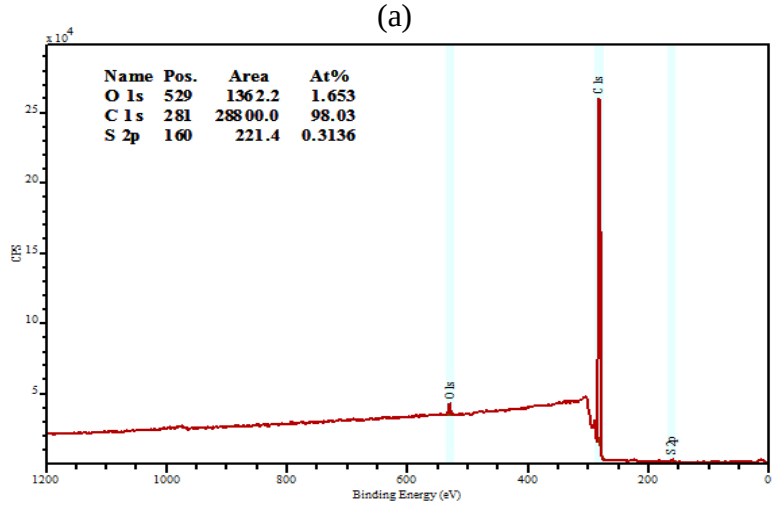

(b)

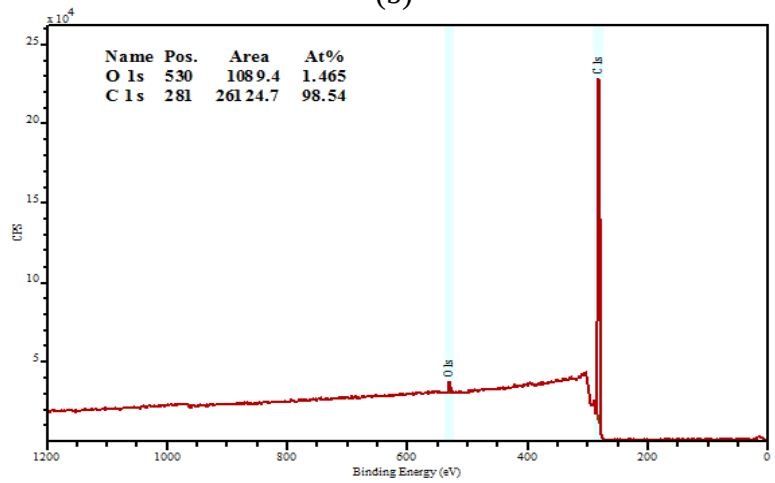

(c)

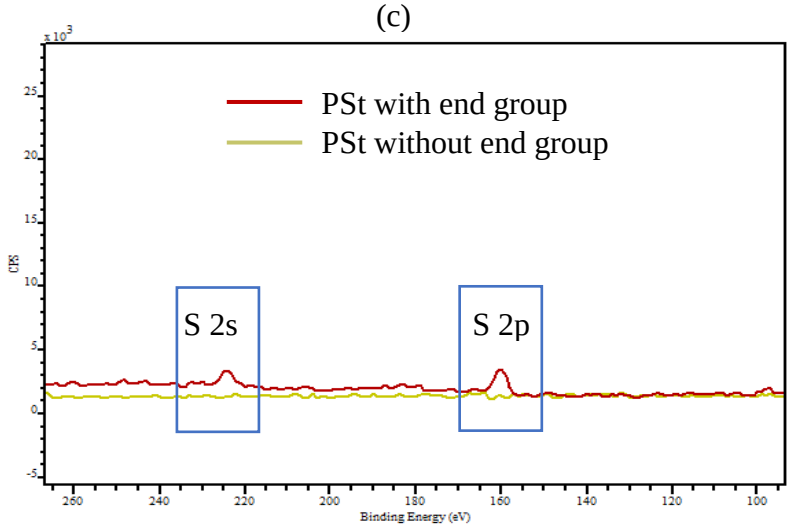

Figure-3.17: XPS survey scan data for PSt homopolymer (a) with RAFT end group, (b) without RAFT end group, and (c) comparison of their S peak region.

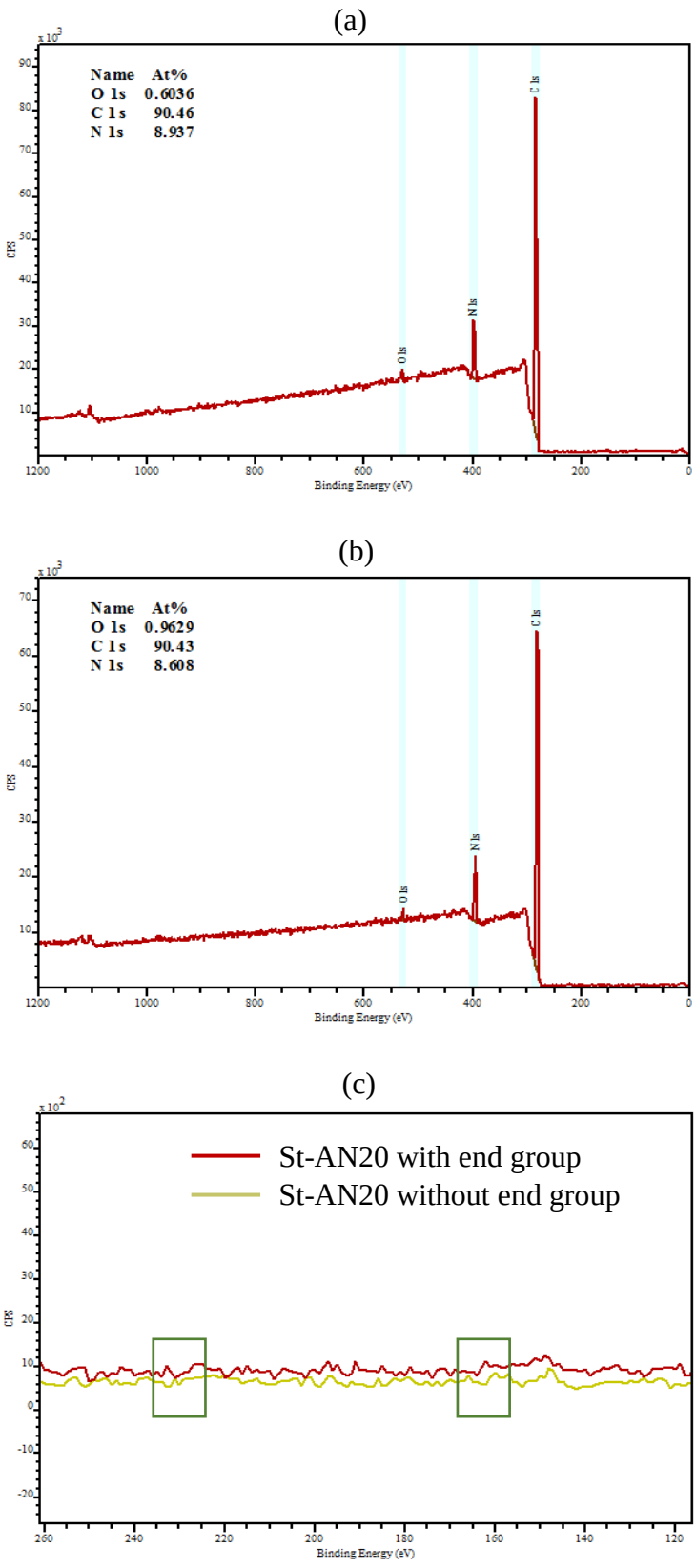

Figure-3.18: XPS survey scan data for (a) St-AN20 copolymer with RAFT end group, (b) without RAFT end group, and (c) comparison of their S peak region.

3.5.2 XPS studies of the homopolymer thin films

Survey and high resolution XPS data for PSt and PAN homopolymers are given in Figure-3.19 and Figure-3.20 respectively. Survey data for PSt shows the C peak at binding energy 285 eV, and S peak at 165 eV (close view is given in Figure-3.17). PAN shows C and N peaks at binding energies of 285 and 399 eV, respectively, but no peak for S was seen. This is again due to the difference in their molecular weight; PAN had significantly higher molecular weight (M_n = 21000) than that of PSt (M_n = 4600). Both of the homopolymers show small amounts of O in the survey data, which could be due to the oxygen trapped in the copolymer thin films.

High resolution spectra of the C 1s peak from PSt (Figure-3.19) shows both aliphatic and aromatic components at binding energy 284.8 eV and 285.0 eV, respectively. The ratio of aliphatic C (23.8%) and aromatic C (76.2%) from the high resolution was found to be in close agreement to the actual ratio 1:3. PAN gives three components in C 1s high resolution XPS for three different types of C (Figure-3.20) with a ratio of approximately 1:1:1, and a single component in the N 1s peak at 399.7 eV.

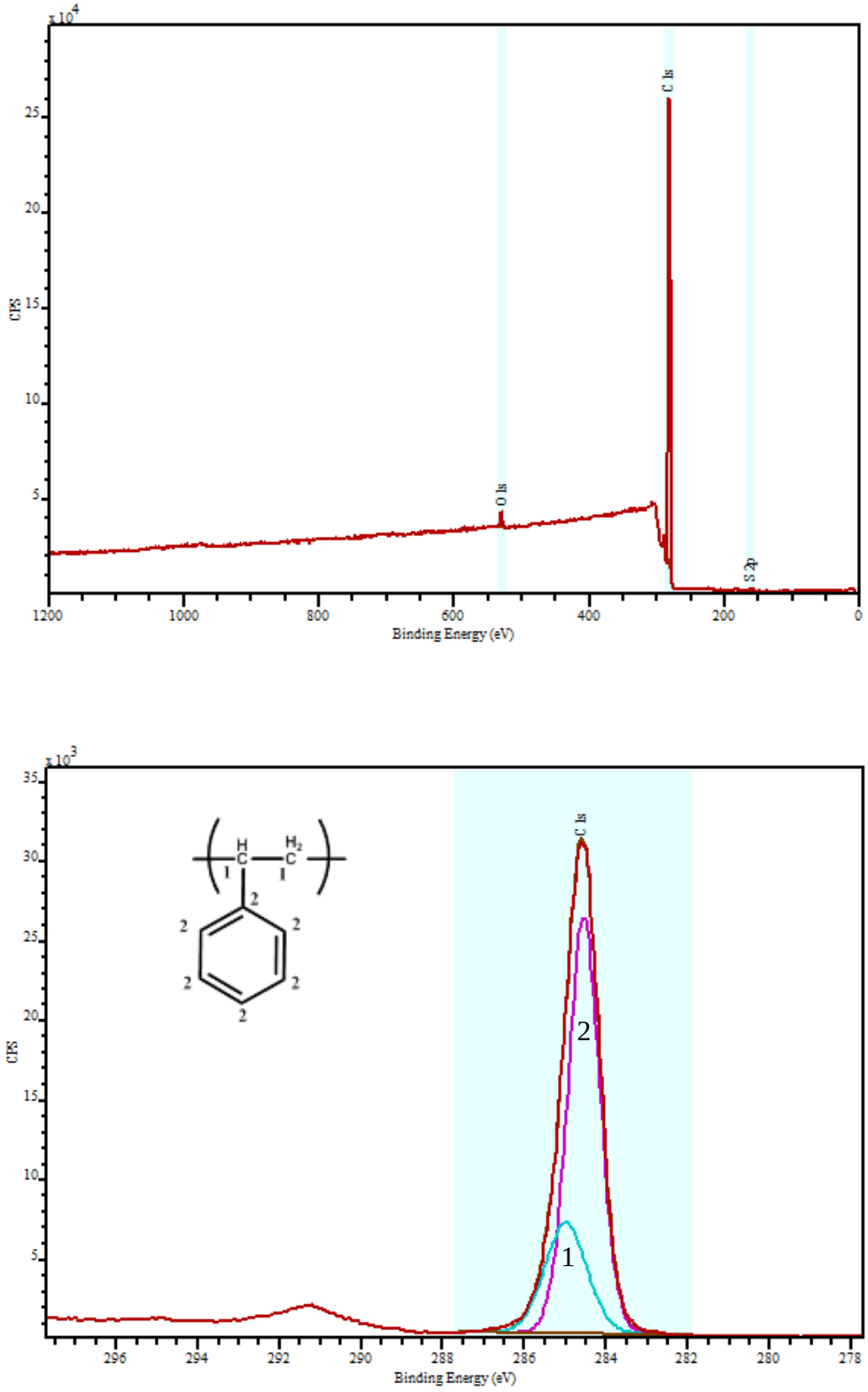

Figure-3.19: Survey (top) and high resolution (bottom) XPS data for PSt homopolymer thin film.

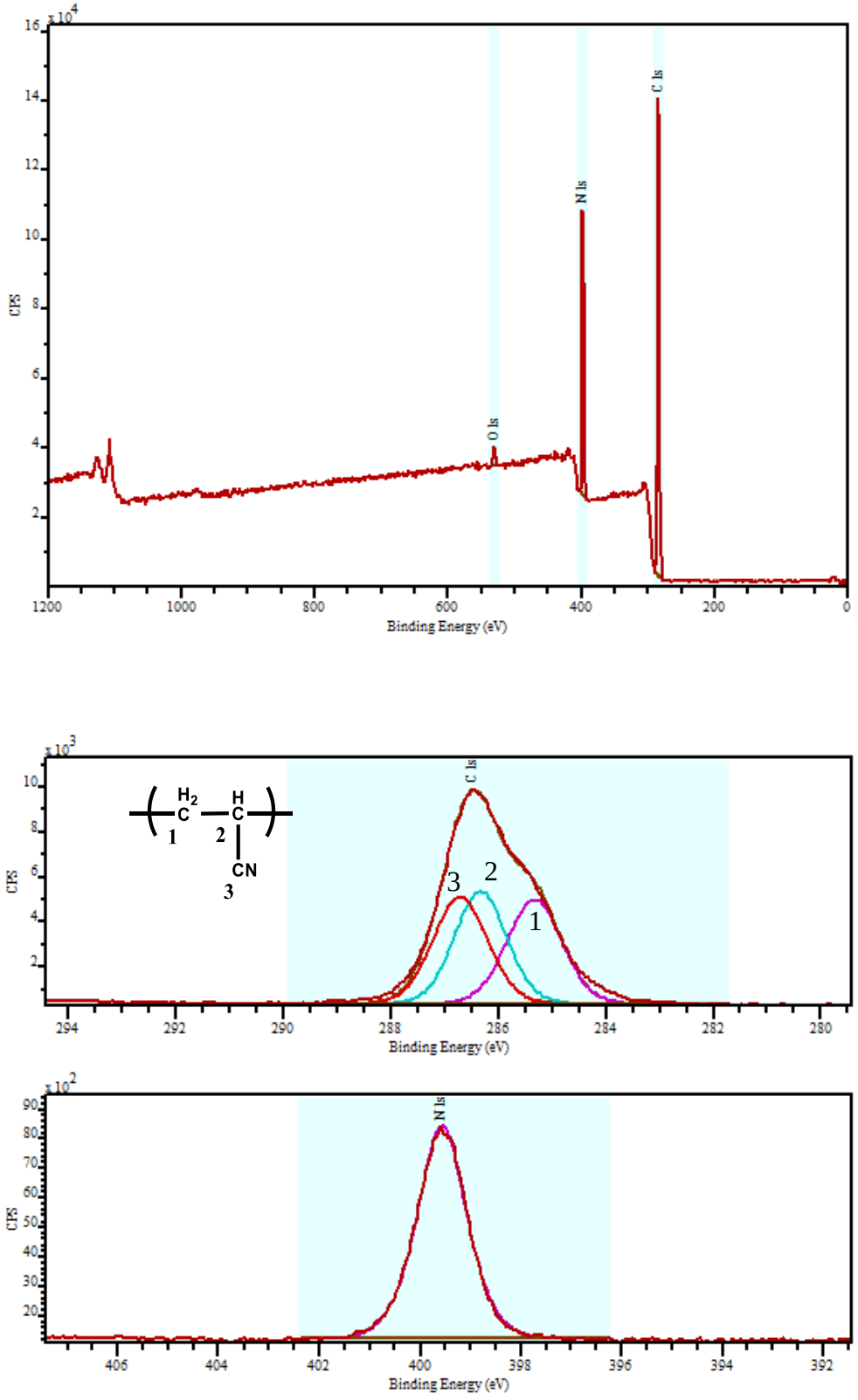

Figure-3.20: Survey (top) and high resolution (bottom) XPS data for PAN homopolymer thin film.

3.5.3 XPS studies of St-AN copolymer thin films

The surface composition of the thin films of statistical, block and gradient copolymers synthesized by RAFT and CvRP methods were studied by XPS data. Both survey and high resolution XPS data were collected at two different incident angles (at 0° and 60°, approximate penetration depth 10 nm and 5 nm respectively) to characterize the surface composition at two different depths. The copolymer compositions were also characterized after annealing the copolymer thin films for 10 hours under vacuum at 130 °C, to study the effect of annealing on surface composition on the copolymer thin films.

The fraction of St and AN was determined using the N content in the survey spectra of the thin films. As an example, Figure-3.21 shows a survey spectra for St-AN60 copolymer thin films, which shows the presence of 5.331% of N on the surface. Since the AN monomer unit contains 1 N atom and 3 carbons atoms,

Then total percentage of C from AN is = 5.331 x 3 = 16.0

Total percentage of C from St is = (94.67-15.993) = 78.7%

Therefore, composition of St is = $\frac{\left(\frac{78.677}{8}\right)}{\left(\frac{78.677}{8}\right)+\left(\frac{15.993}{3}\right)} = 0.65$

And composition of AN is = 1 - 0.65 = 0.35

The copolymer composition on the surface is St:AN = 0.65:0.35

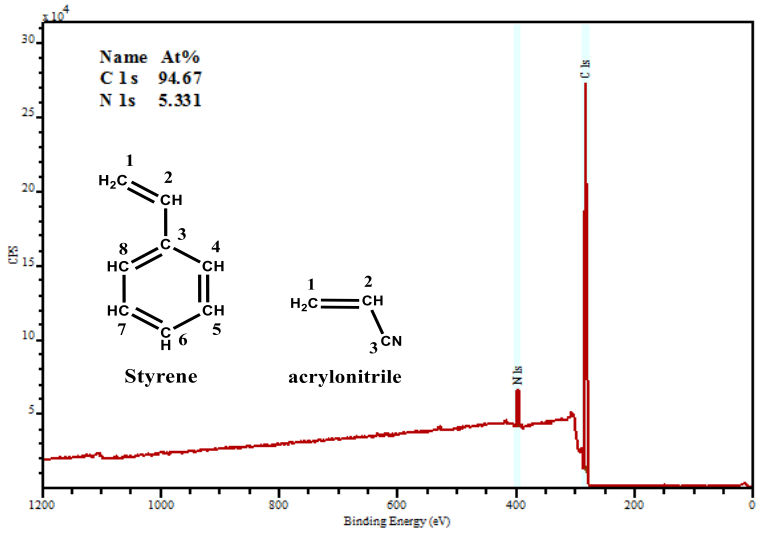

Figure-3.21: XPS survey spectrum for St-AN60 copolymer thin film, showing the atomic percentage of C and N on the surface.

The composition of the copolymer on the thin films surface for the statistical, block and gradient copolymers are listed in Table-3.1 to Table-3.10, and also the bar plots are given in Figure-3.23 to Figure-3.32. For the St-AN batch copolymers with different compositions synthesized by the RAFT and CvRP methods and for the forced gradient copolymers synthesized by the RAFT method, the XPS data have been collected for three different conversion. This gives an indication as to how the change in the copolymer composition and triad distribution of the copolymer chains affect the surface composition of the thin films. The errors in the bar plot were determined from six measurements for a single sample.

The copolymer composition and triad distribution for St-AN60 copolymers are constant with the copolymer conversion, whereas St-AN80 copolymers show a slight change in both composition and triad distribution. This is reflected on the XPS data of their copolymer thin films. The surface compositions characterized by XPS are slightly higher in St than the bulk composition determined from ^{13}C NMR, but there is no change in the surface composition at two different incident angles. The surface composition was unchanged even after annealing the thin film. The thin films of St-AN60 and St-AN80 copolymers synthesized by RAFT and CvRP method showed similar behaviour.

As described elsewhere, the fraction of St in St-AN20 and St-AN10 copolymers decrease with the copolymer conversion to produce a natural gradient in the copolymer chains. For these two copolymers, the St compositions in the thin films are significantly higher than the composition calculated from ^{13}C NMR. It should be noted that St is comparatively hydrophobic while AN is hydrophilic. Therefore, AN units have a tendency to move towards the substrate silicon wafer due to the presence of SiO_2, while St moves in the opposite direction. Hence, the styrene composition of St-AN20 and St-AN10 increases as the thin films are annealed above glass transition temperature of the copolymers. Through the annealing process, the St units move further to the thin film air interface while AN units move towards the substrate to achieve thermal equilibrium. The angle dependent XPS data show that the composition at 60° incident angle is much higher than that of at 0° incident angle. XPS data with 60° incident angle gives the composition of the top 5 nm of the thin film surface, while 0° gives the data of top 10 nm approximately. Therefore, the higher composition of St at 60° indicates the movement of St units towards the thin film and air interface.

The difference between the styrene composition determined from ^{13}C NMR and the XPS composition becomes more pronounced for the thin films prepared with higher conversion copolymers. This is reasonable considering the gradient structures of St-AN20 and St-AN10

copolymers. At the initial conversion, the copolymer produces chains with little or no change in the composition which causes little difference between the copolymer composition and thin film surface composition. However, the copolymer composition starts decreasing steeply after 55% and 40% conversion of St-AN20 and St-AN10 copolymer, respectively (Figure-3.26 and Figure-3.30), which is reflected in the difference of the copolymer composition and thin film surface compositions for these two copolymers at higher conversion. However, the difference in St composition is significantly higher for St-AN10 copolymers due to the stronger gradient produced in copolymer structures than that of St-AN20 copolymers. A similar effect of gradient in the copolymer structures on the thin film surface compositions have been found for St-AN20 and St-AN10 copolymer synthesized by CvRP method.

The forced gradient copolymer St-grad-AN60 copolymer thin films also follow the trend shown by the natural gradient copolymer thin films. The St compositions at the surface of the thin films are much higher than the bulk copolymer composition, and the difference between the composition in the copolymer and the surface composition increases for the thin films of copolymers with higher conversion. However, the biggest difference between the copolymer composition and the thin films surface composition is found for the block copolymers, especially for those with low St compositions. As spin coated thin films do not show much difference in the compositions, but after annealing, the composition of St on the surface increased significantly.

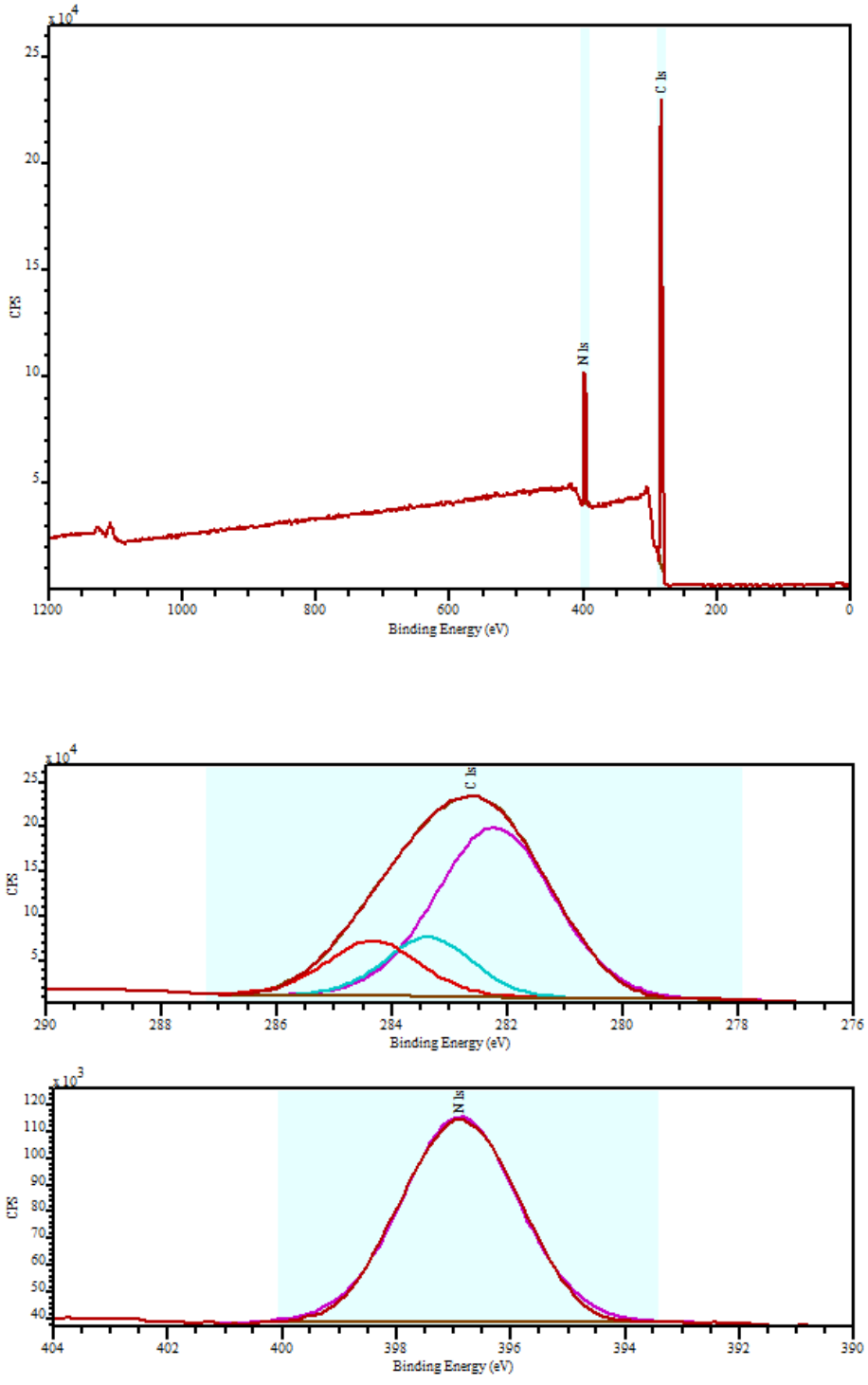

Figure-3.22: Survey (top) and high resolution (bottom) XPS data for St-AN20 copolymer thin film. The survey data shows the peak for C 1s and N 1s, and the high resolution data shows their components.

Table-3.1: Surface composition of RAFT St-AN80 copolymer thin films for different conversion, characterized by XPS at 0° and 60°, before and after annealing.

F(St)	Conv. 27%	Conv. 51%	Conv. 64%
^{13}C NMR	0.75	0.76	0.78
Un-annealed 0°	0.77	0.78	0.78
Un-annealed 60°	0.77	0.77	0.80
Annealed 0°	0.77	0.78	0.80
Annealed 60°	0.77	0.79	0.79

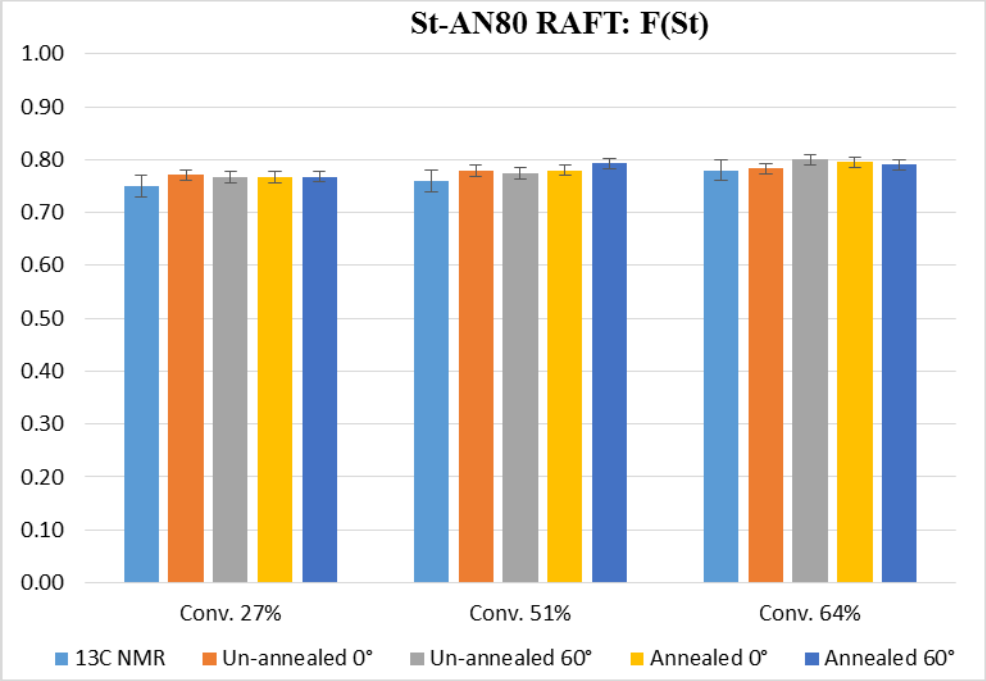

Figure-3.23: Comparison of the St compositions in RAFT St-AN80 copolymer characterized by ^{13}C NMR to those for the thin film surface compositions characterized by XPS at 0° and 60° incident angle, before and after annealing.

Table-3.2: Surface composition of RAFT St-AN60 copolymer thin films for different conversion, characterized by XPS at 0° and 60°, before and after annealing.

F(St)	conv. 46%	conv. 67%	conv. 94%
^{13}C NMR	0.64	0.64	0.65
Un-annealed 0°	0.65	0.67	0.67
Un-annealed 60°	0.67	0.67	0.68
Annealed 0°	0.66	0.67	0.67
Annealed 60°	0.67	0.68	0.69

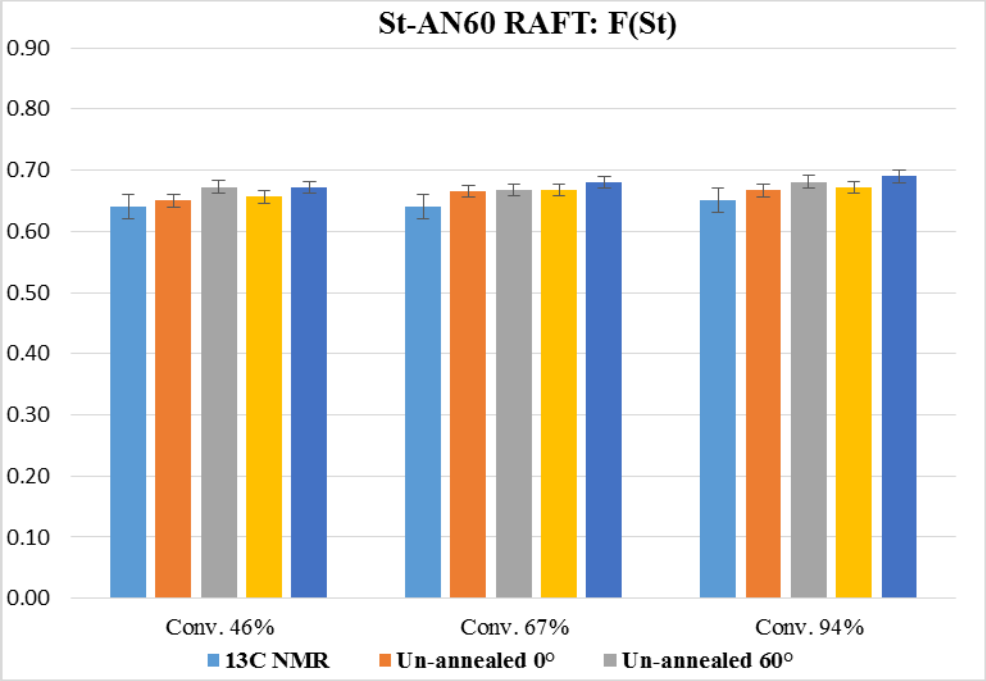

Figure-3.24: Comparison of the St compositions in RAFT St-AN60 copolymer characterized by ^{13}C NMR to those for the thin film surface compositions characterized by XPS at 0° and 60° incident angle, before and after annealing.

Table-3.3: Surface composition of RAFT St-AN20 copolymer thin films for different conversion, characterized by XPS at 0° and 60°, before and after annealing.

F(St)	Conv. 22%	Conv. 55%	Conv. 87%
^{13}C NMR	0.44	0.36	0.24
Un-annealed 0°	0.45	0.43	0.34
Un-annealed 60°	0.44	0.39	0.31
Annealed 0°	0.45	0.40	0.34
Annealed 60°	0.45	0.40	0.36

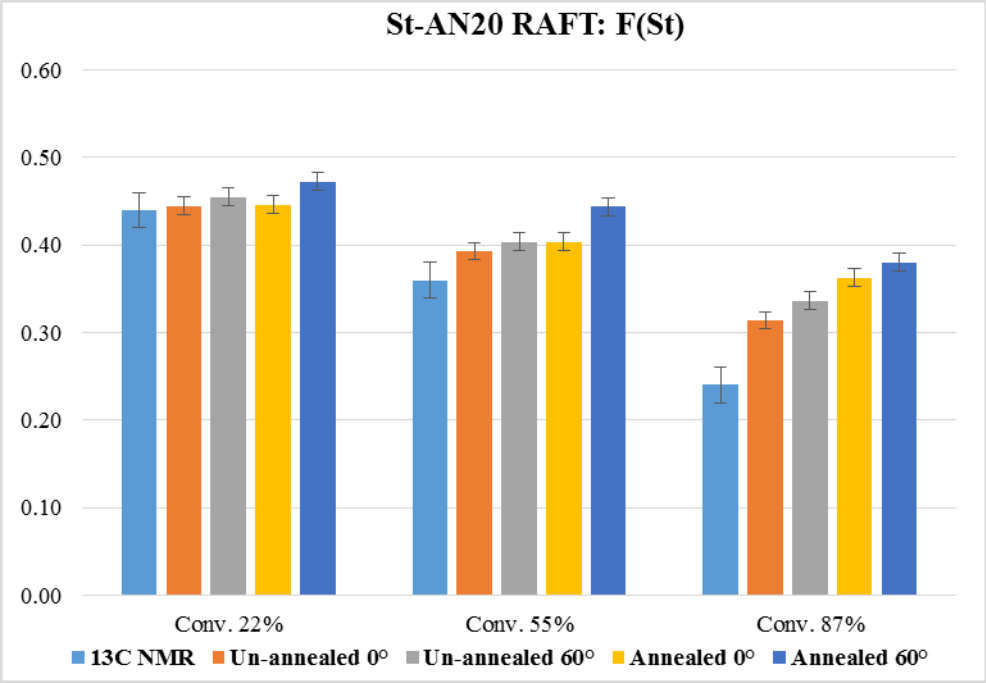

Figure-3.25: Comparison of the St compositions in RAFT St-AN20 copolymer characterized by ^{13}C NMR to those for the thin film surface compositions characterized by XPS at 0° and 60° incident angle, before and after annealing.

Table-3.4: Surface composition of RAFT St-AN10 copolymer thin films for different conversion, characterized by XPS at 0° and 60°, before and after annealing.

F(St)	Conv. 39%	Conv. 75%	Conv. 93%
^{13}C NMR	0.27	0.16	0.13
Un-annealed 0°	0.35	0.35	0.28
Un-annealed 60°	0.34	0.22	0.20
Annealed 0°	0.35	0.24	0.19
Annealed 60°	0.34	0.27	0.29

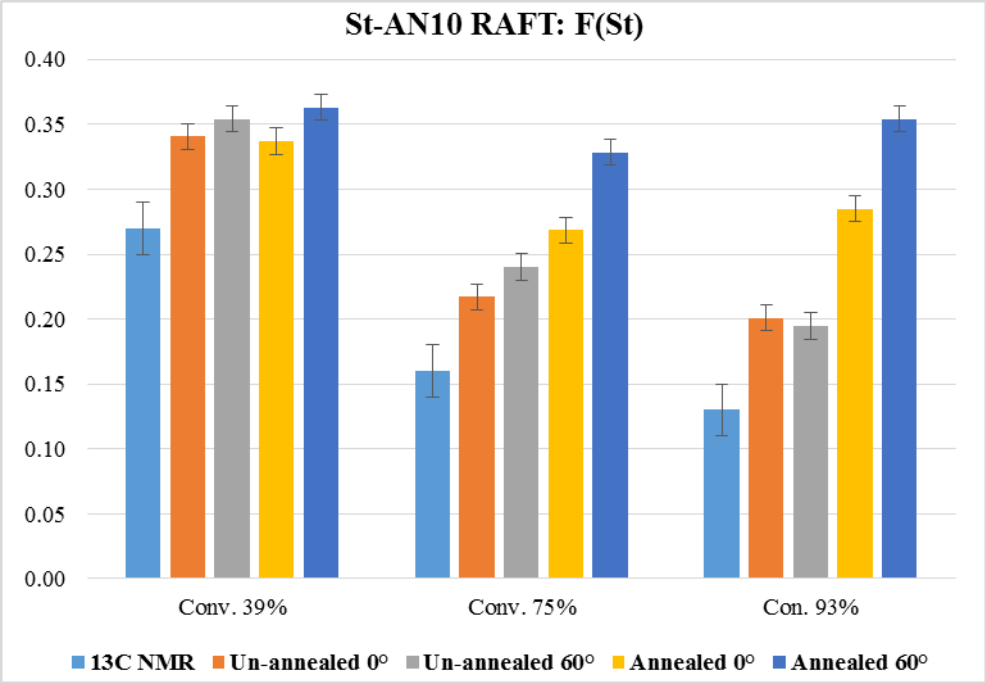

Figure-3.26: Comparison of the St compositions in RAFT St-AN10 copolymer characterized by ^{13}C NMR to those for the thin film surface compositions characterized by XPS at 0° and 60° incident angle, before and after annealing.

Table-3.5: Surface composition of RAFT St-grad-AN60 copolymer thin films for different conversion, characterized by XPS at 0° and 60°, before and after annealing.

F(St)	Conv. 57%	Conv. 63%	Conv. 83%
^{13}C NMR	0.45	0.49	0.55
Un-annealed 0°	0.48	0.53	0.62
Un-annealed 60°	0.50	0.55	0.68
Annealed 0°	0.51	0.58	0.71
Annealed 60°	0.54	0.63	0.78

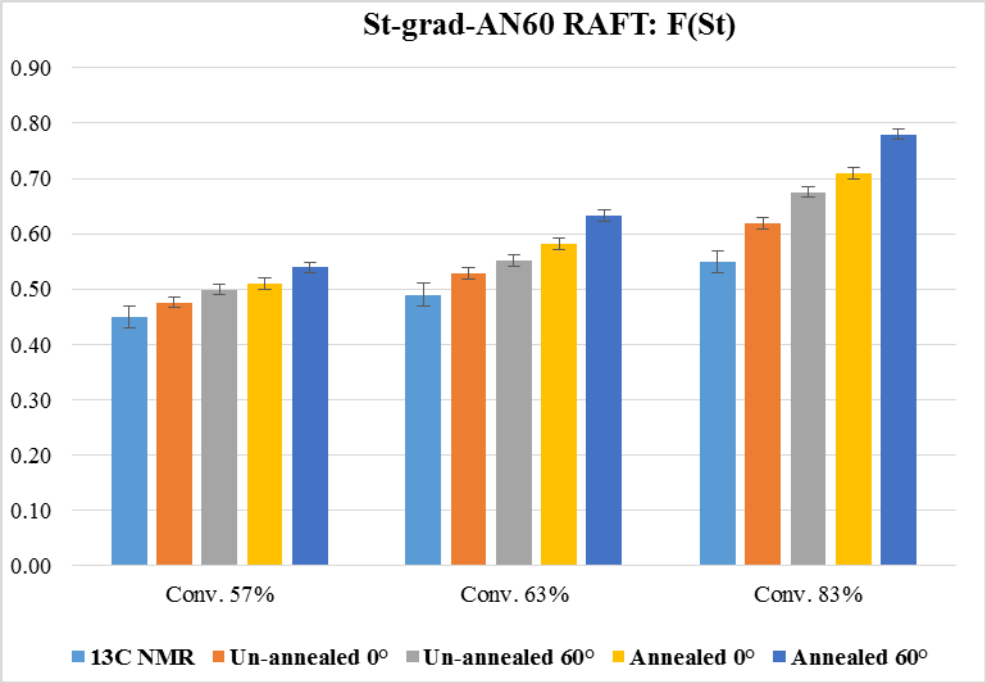

Figure-3.27: Comparison of the St compositions in RAFT St-grad-AN60 copolymer characterized by ^{13}C NMR to those for the thin film surface compositions characterized by XPS at 0° and 60° incident angle, before and after annealing.

Table-3.6: Surface composition of four different composition of RAFT PSt-b-PAN copolymer thin films, characterized by XPS at 0° and 60°, before and after annealing.

F(St)	PSt-b-PAN27	PSt-b-PAN36	PSt-b-PAN65	PSt-b-PAN83
^{13}C NMR	0.27	0.36	0.65	0.83
Un-annealed 0°	0.48	0.55	0.67	0.82
Un-annealed 60°	0.30	0.41	0.76	0.86
Annealed 0°	0.30	0.46	0.78	0.90
Annealed 60°	0.53	0.66	0.86	0.87

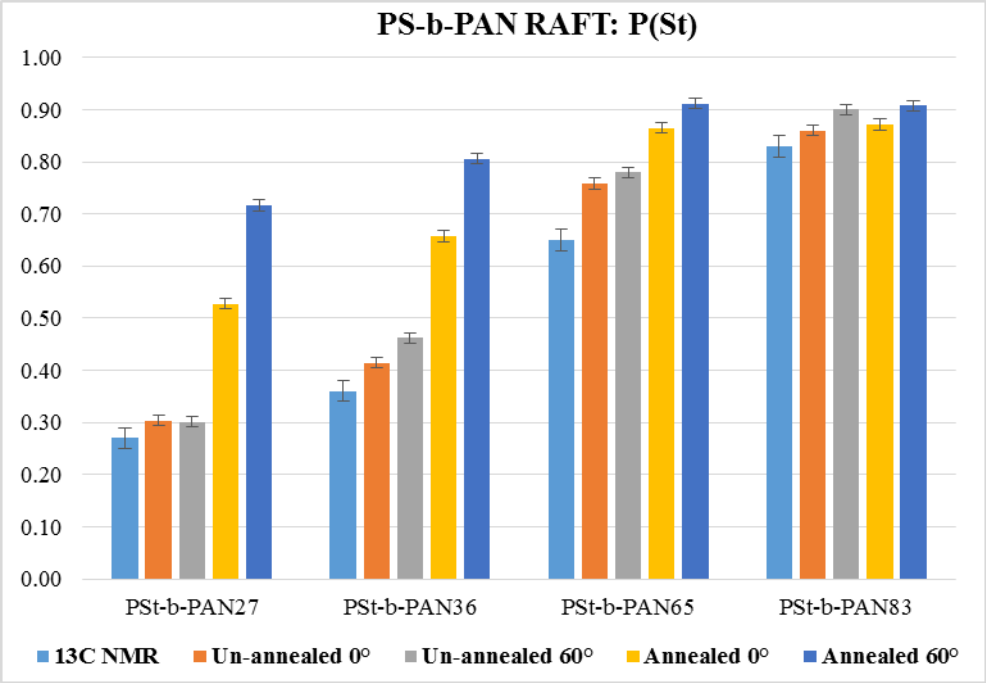

Figure-3.28: Comparison of the St compositions in RAFT PSt-b-PAN copolymers characterized by ^{13}C NMR to those for the thin film surface compositions characterized by XPS at 0° and 60° incident angle, before and after annealing.

Table-3.7: Surface composition of CvRP St-AN80 copolymer thin films for different conversion, characterized by XPS at 0° and 60°, before and after annealing.

F(St)	Conv. 39%	Conv. 63%	Conv. 82%
^{13}C NMR	0.73	0.74	0.76
Un-annealed 0°	0.73	0.75	0.79
Un-annealed 60°	0.74	0.76	0.80
Annealed 0°	0.74	0.76	0.84
Annealed 60°	0.75	0.78	0.85

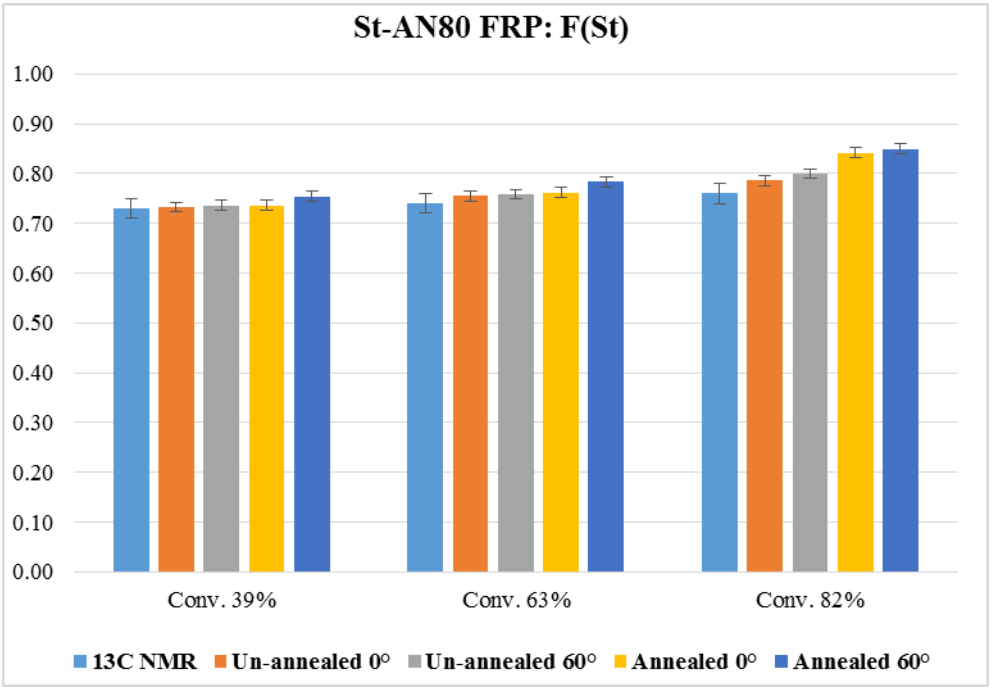

Figure-3.29: Comparison of the St compositions in CvRP St-AN80 copolymer characterized by ^{13}C NMR to those for the thin film surface compositions characterized by XPS at 0° and 60° incident angle, before and after annealing.

Table-3.8: Surface composition of CvRP St-AN60 copolymer thin films for different conversion, characterized by XPS at 0° and 60°, before and after annealing.

F(St)	Conv. 38%	Conv. 53%	Conv. 72%
^{13}C NMR	0.63	0.66	0.65
Un-annealed 0°	0.63	0.67	0.64
Un-annealed 60°	0.63	0.66	0.66
Annealed 0°	0.62	0.65	0.65
Annealed 60°	0.64	0.68	0.67

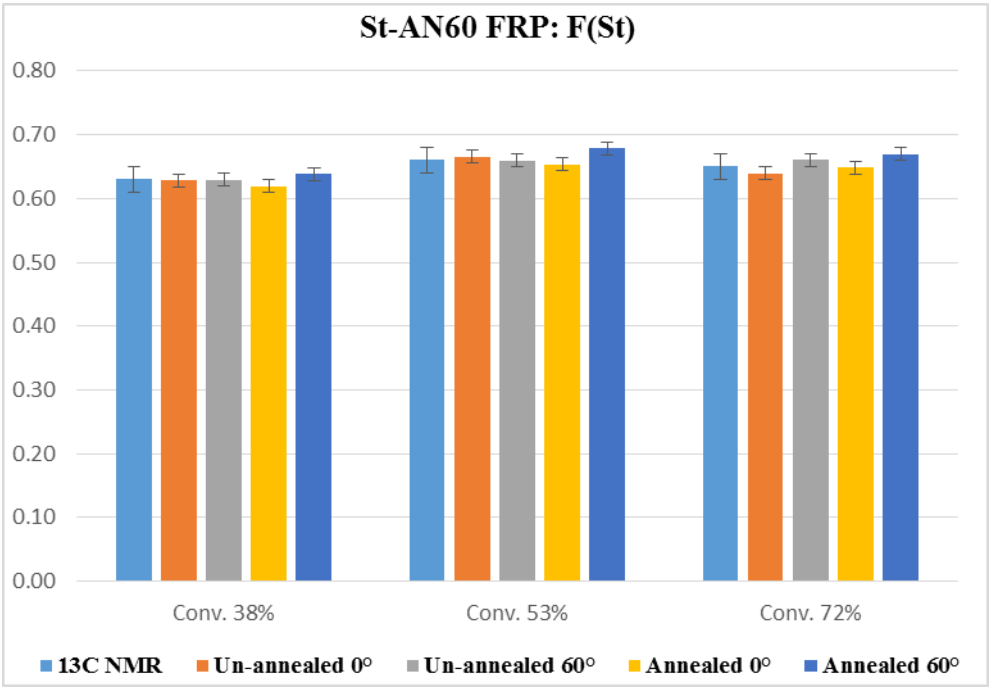

Figure-3.30: Comparison of the St compositions in CvRP St-AN60 copolymer characterized by ^{13}C NMR to those for the thin film surface compositions characterized by XPS at 0° and 60° incident angle, before and after annealing.

Table-3.9: Surface composition of CvRP St-AN20 copolymer thin films for different conversion, characterized by XPS at 0° and 60°, before and after annealing.

F(St)	Conv. 25%	Conv. 52%	Conv. 77%
^{13}C NMR	0.38	0.32	0.23
Un-annealed 0°	0.40	0.37	0.35
Un-annealed 60°	0.42	0.38	0.37
Annealed 0°	0.40	0.38	0.41
Annealed 60°	0.43	0.44	0.43

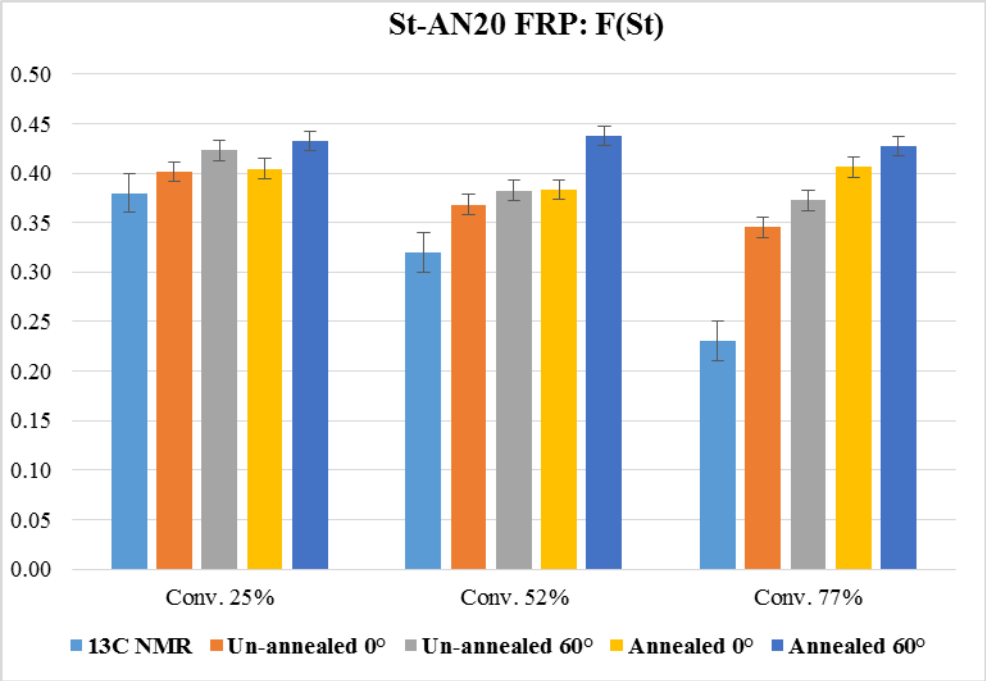

Figure-3.31: Comparison of the St compositions in CvRP St-AN20 copolymer characterized by ^{13}C NMR to those for the thin film surface compositions characterized by XPS at 0° and 60° incident angle, before and after annealing.

Table-3.10: Surface composition of CvRP St-AN10 copolymer thin films for different conversion, characterized by XPS at 0° and 60°, before and after annealing.

F(St)	Conv. 33%	Conv. 53%	Conv. 71%
^{13}C NMR	0.26	0.17	0.14
Un-annealed 0°	0.32	0.28	0.30
Un-annealed 60°	0.32	0.29	0.32
Annealed 0°	0.35	0.32	0.39
Annealed 60°	0.38	0.34	0.42

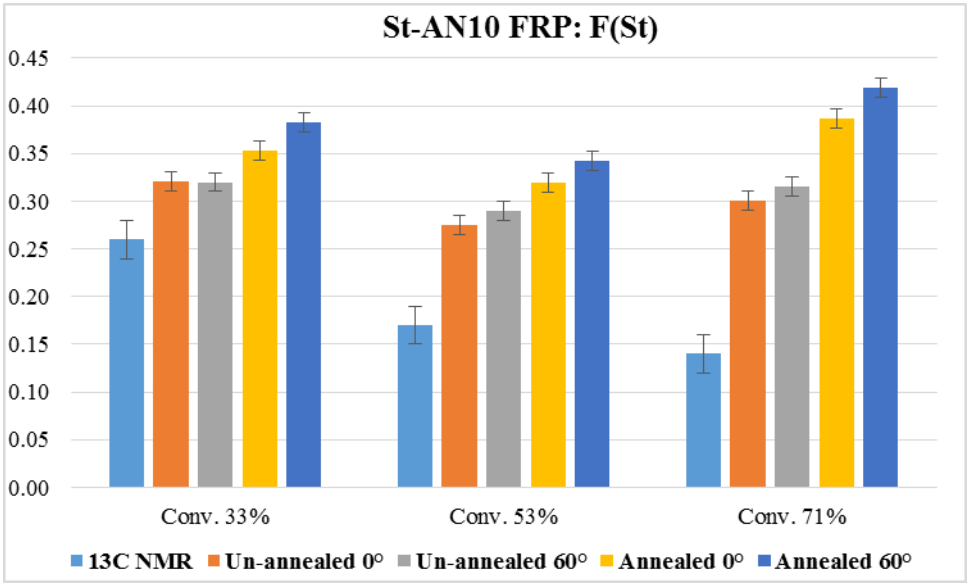

Figure-3.32: Comparison of the St compositions in CvRP St-AN10 copolymer characterized by ^{13}C NMR to those for the thin film surface compositions characterized by XPS at 0° and 60° incident angle, before and after annealing.

3.5.4 Comparison of XPS results

The comparative bar plots of the XPS data for thin films of the St-AN statistical, block and gradient copolymer synthesized by the RAFT method are shown in Figure-3.33 and Figure-3.34. The XPS results of the thin films of St-AN copolymers synthesized by the RAFT and CvRP methods are compared in Figure-3.35. St-AN60 is entirely statistical copolymer, while St-AN80 with very little composition drift is also nearly statistical. Therefore, the surface composition for the thin films of these two copolymer synthesized by both RAFT or CvRP method do not show much change in the St composition of the thin films even after annealing.

On the other hand, the composition of the thin film surface shows a large change after annealing, especially for the block copolymers with lower St composition in the copolymer. Though, the thin films of the block copolymers with high St composition do not show as much difference as the thin films with low St containing copolymer do. The surface composition of the thin films of the spontaneous gradients (St-AN20 and St-AN10) and the forced gradient copolymer (St-grad-AN60), are however in between of those of the statistical and block copolymers.

The XPS results of the thin films of statistical, block and gradient copolymers could be explained based on the effect of copolymer structure on phase their behaviour as discussed in section 1.2.3.1. The block copolymers go through complete phase segregation on the thin films by moving the St units towards the thin film-air interface and AN units towards the substrate, while no change occurs for the statistical copolymer. Gradient copolymers, on the other hand, due to the continuous gradient in composition of the copolymer chains, exhibits weak phase separation with a broad phase boundary.

Figure-3.35 shows the comparison of the surface composition determined by XPS for the thin films of copolymers synthesized by the RAFT and CvRP methods. For the weak gradient (St-AN80) and statistical (St-AN60) copolymer thin films, the copolymer composition does not change on the surface. However the gradient copolymers synthesized by the RAFT method, in which the copolymer composition changes along a single chain, behaves slightly different for the thin films than those of the gradient copolymers synthesized by the CvRP method, in which the composition changes across the copolymer chains. The effect of annealing is noticeably higher on the thin films of CvRP copolymers than those of the RAFT copolymers, due to the intra-chain and inter-chain gradient in the RAFT and CvRP copolymers respectively.

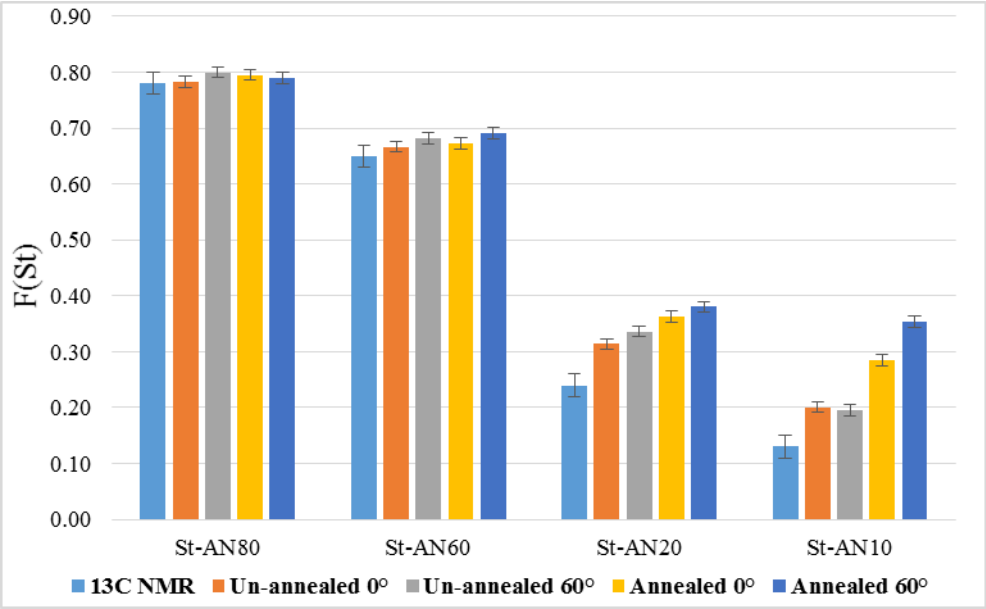

Figure-3.33: Comparison of the St compositions in the thin film surface for St-AN statistical and natural gradient copolymers synthesized by RAFT batch copolymerization method.

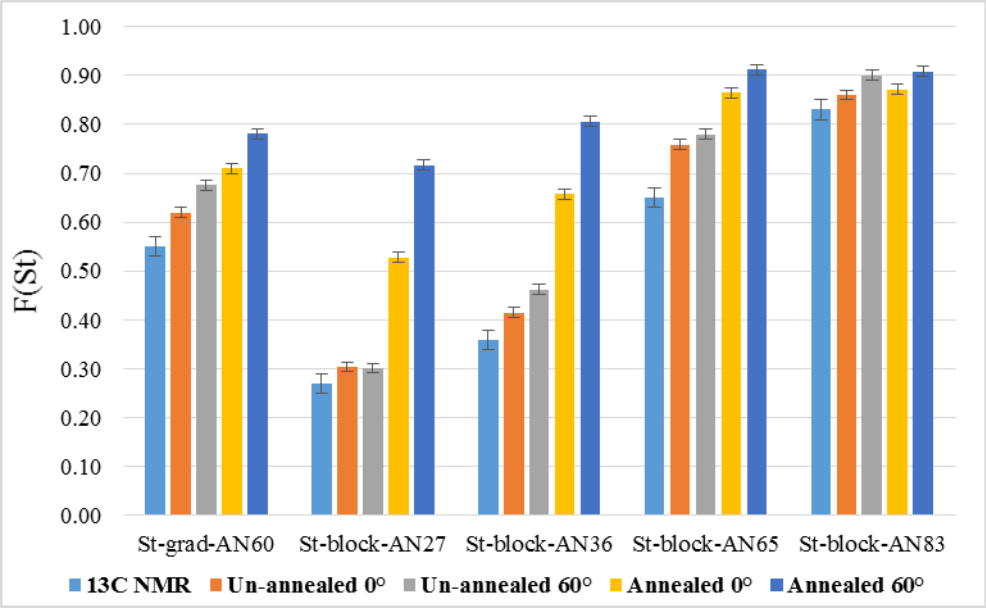

Figure-3.34: Comparison of the St compositions in the thin film surface for St-AN forced gradient and block copolymers synthesized by RAFT method.

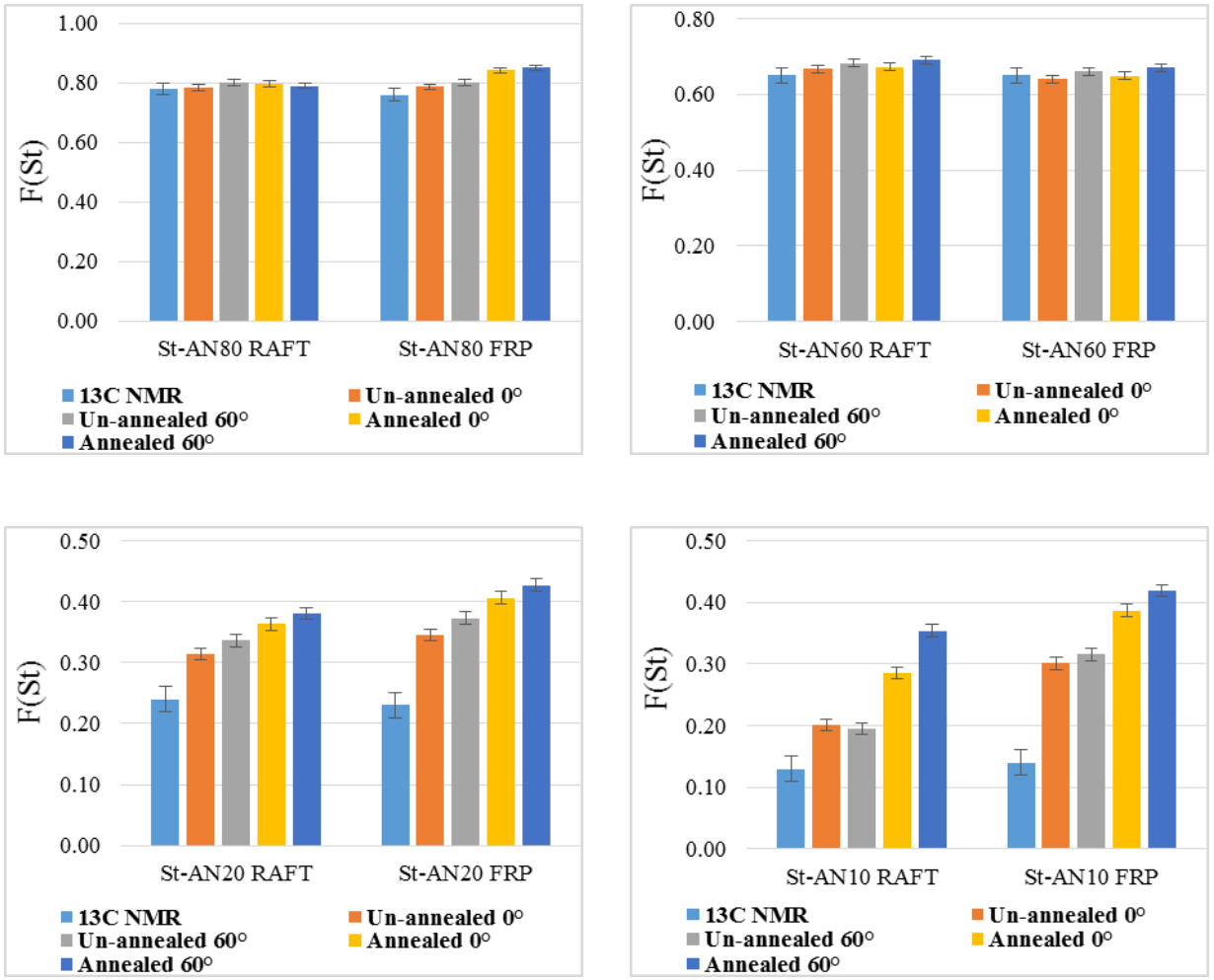

Figure-3.35: Comparison of XPS data for the thin films of RAFT and CvRP copolymer for four different compositions.

3.6 Contact angles and surface free energy studies of St-AN copolymer thin films

Surface free energy is one of the fundamental properties of copolymer thin films, and is strongly dependent on the surface and interfacial behaviour of the copolymers. Therefore, a study of the surface free energy (SFE) through contact angle measurements is one of the most common techniques to study the polymer and copolymer thin films. A number of literature studies have reported the contact angles and surface free energy of polymer and copolymer thin films [333-342], including the St-AN copolymer system [343-349]. Using the contact angles of liquids with different polarity, the SFE of a polymer or copolymer thin films could be measured either by the geometric mean (GM) method which is also known as Owens and Wendt method, the harmonic mean method, or the harmonic mean (HM) method, or the van Oss, Good, and Chaudhury (vOGC) method which is also known as the acid-base approach.

In this study, the static contact angles of PSt and PAN homopolymers, and their copolymer thin films were measured for water (H_2O) and thiodiglycol (TDG) using an OCA20 contact angle system at room temperature. SFE were measured for water-glycerine and water-thiodiglycol system by geometric mean method using the following equation.

$\gamma_L(1+\cos\theta) = 2.\sqrt{(\gamma_S^d.\gamma_L^d)} + 2.\sqrt{(\gamma_S^P.\gamma_L^P)}$……. [7]

Where, γ_L = surface free energy of the test liquid

γ_L^d = dispersive component of the surface free energy of the test liquid

γ_L^P = polar component of the surface free energy of the test liquid

γ_S = surface free energy of the solid

γ_S^d = dispersive component of the surface free energy of the solid

γ_S^P = polar component of the surface free energy of the solid

Table-3.11: The surface free energy components calculated by the geometric mean method for water and thiodiglycol [343].

Test liquid	Dispersive component, γ_L^d (mJ m^{-2})	Polar component, γ_L^p (mJ m^{-2})	Total surface free energy γ_L (mJ m^{-2})
Water	21.8	51.0	72.8
Thiodiglycol	38.4	15.6	54.0

The static contact angles of water and thiodiglycol measured at room temperature, for the thin films of St and AN homopolymers, and their copolymers synthesized by the RAFT method are given in Table-3.12. The contact angle values before and after the annealing process have also been plotted against AN composition in the copolymers in Figure-3.37 and Figure-3.38. The contact angle values for water and thiodiglycol on PSt and PAN homopolymer thin films found in this study are similar to the values reported in the literature [343]. As Figure-3.37 and Figure-3.38 show, before the annealing process, the contact angle of water and thiodiglycol decrease, as the composition of AN increases in the copolymer. However, the contact angles for the thin films of block copolymers with low AN compositions were significantly lower in comparison to those of the statistical copolymers for both water and thiodiglycol.

Both for water and thiodiglycol, the contact angle values increase as the films are annealed at 130 °C temperature for 10 hours, but the increase in the values are significantly different for copolymers with different structures. The block copolymers with high AN compositions go through the biggest changes in the contact angles after annealing for both water and thiodiglycol, while the change is very small for the statistical copolymer thin films. The change in the contact angle value for the spontaneous gradient copolymers are in between to those of the statistical and block copolymers. However, unlike the spontaneous gradient copolymer, the forced gradient copolymer does not show any change in the contact angle values after annealing.

The contact angle results are in close agreement with the results found in XPS studies. PSt units, being the hydrophobic part of the copolymers are likely to be moving towards the thin film-air interface, and the due to the comparative hydrophilic nature, AN units move towards the substrate. Therefore, after annealing, the surface composition of PSt in the thin film increases, which as a result increases the contact angle values. Due to phase segregation, the block copolymers show the biggest change in the surface composition, and hence in the contact angle values after annealing.

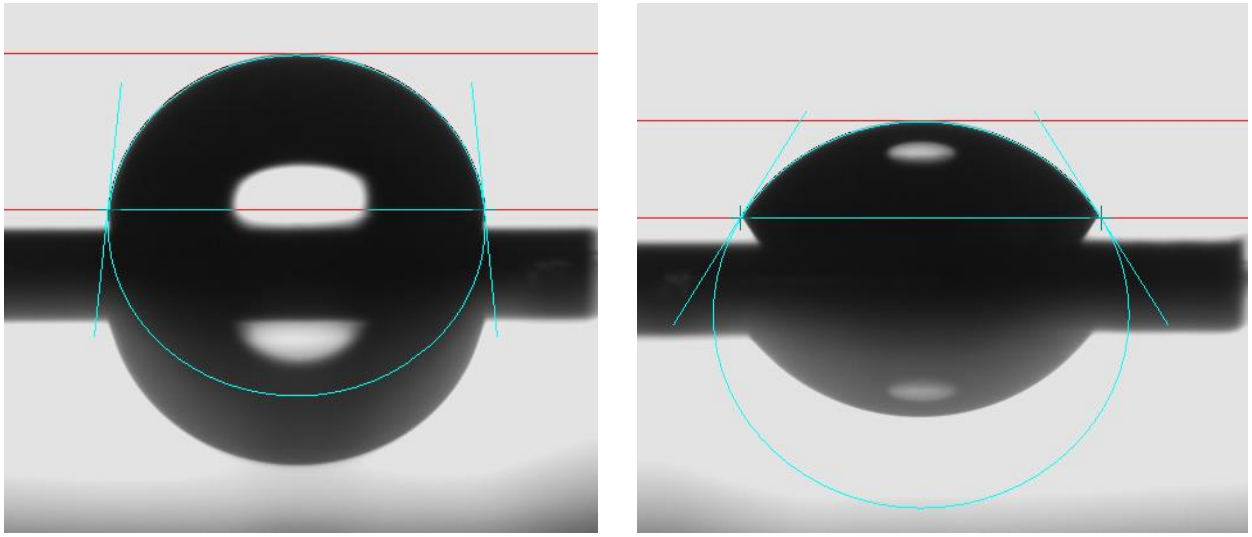

Figure-3.36: Static contact angle image of water (left) and thiodiglycol (right) on RAFT St-AN60 copolymer thin films before annealing.

Table-3.12: Contact angles of water and thiodiglycol on the thin films of statistical, block and gradient copolymers and homopolymers of St and AN synthesized by the RAFT method before and after annealing.

Designation	F_{AN} (**^{1}H NMR**)	**Water contact angle (°)**		**Thiodiglycol contact angle (°)**	
		Un-annealed	**Annealed**	**Un-annealed**	**Annealed**
PSt	0.00	88.3	92.2	60.6	61.1
St-AN80	0.22	87.1	86.5	57.1	58.5
St-AN60	0.35	81.6	83.8	53.7	55.0
St-AN20	0.76	74.7	78.7	47.0	49.9
St-AN10	0.87	65.0	74.7	43.6	49.5
PAN	1.00	55.6	65.2	19.7	35.7
St-grad-AN60	0.45	80.5	82.8	56.6	57.8
St-block-AN27	0.73	62.7	82.6	40.1	60.6
St-block-AN36	0.64	65.8	83.4	46.0	60.1
St-block-AN68	0.32	86.6	86.7	57.7	59.4
St-block-AN83	0.17	89.5	87.1	59.9	58.7

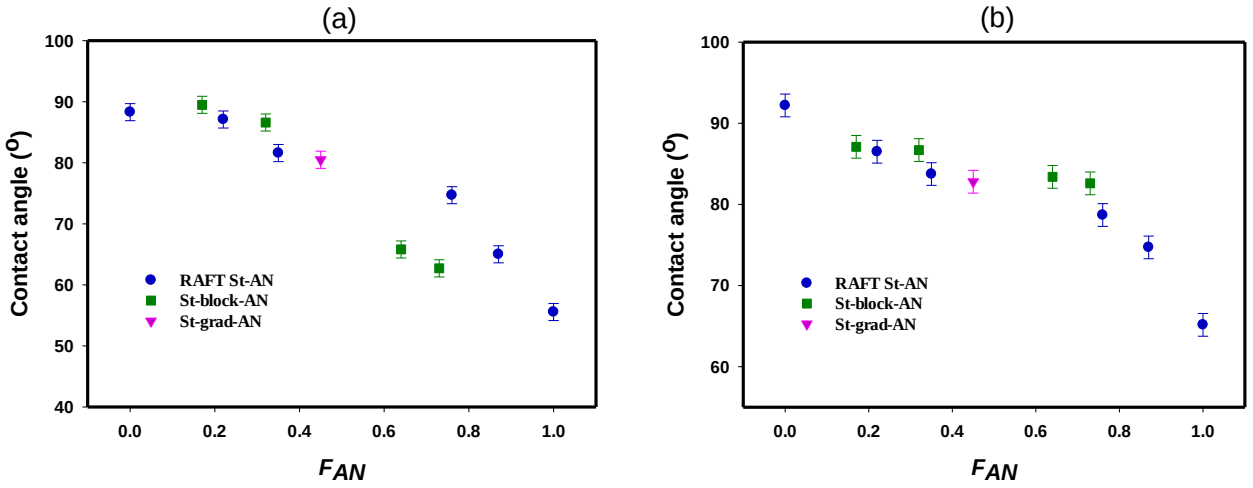

Figure-3.37: Contact angle of water on the thin films of St and AN homo and copolymers (a) before, and (b) after annealing at 130 °C for 10 hours.

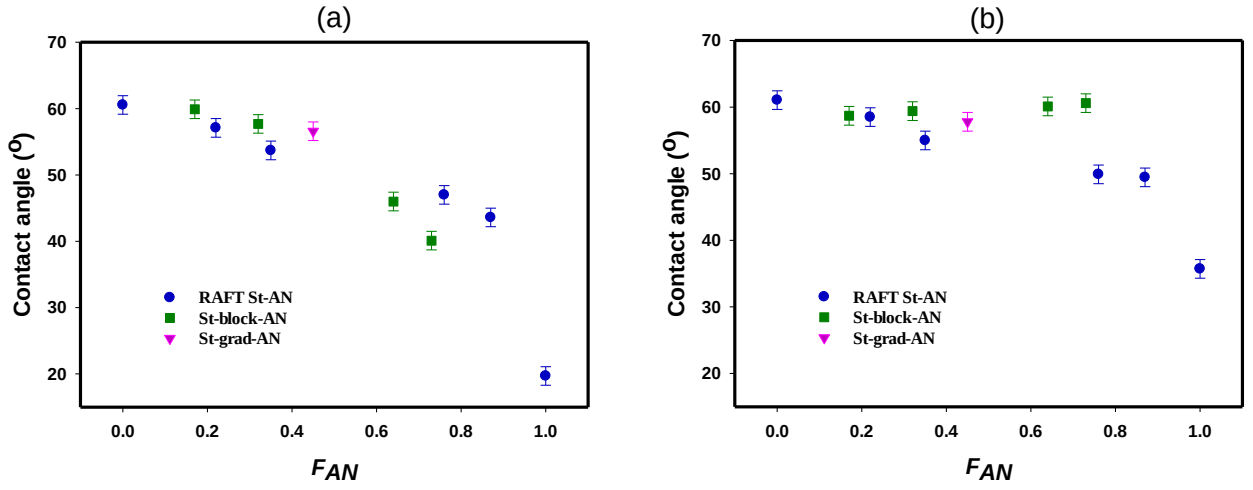

Figure-3.38: Contact angle of thiodiglycol on the thin films of St and AN homo and copolymers (a) before, and (b) after annealing at 130 °C for 10 hours.

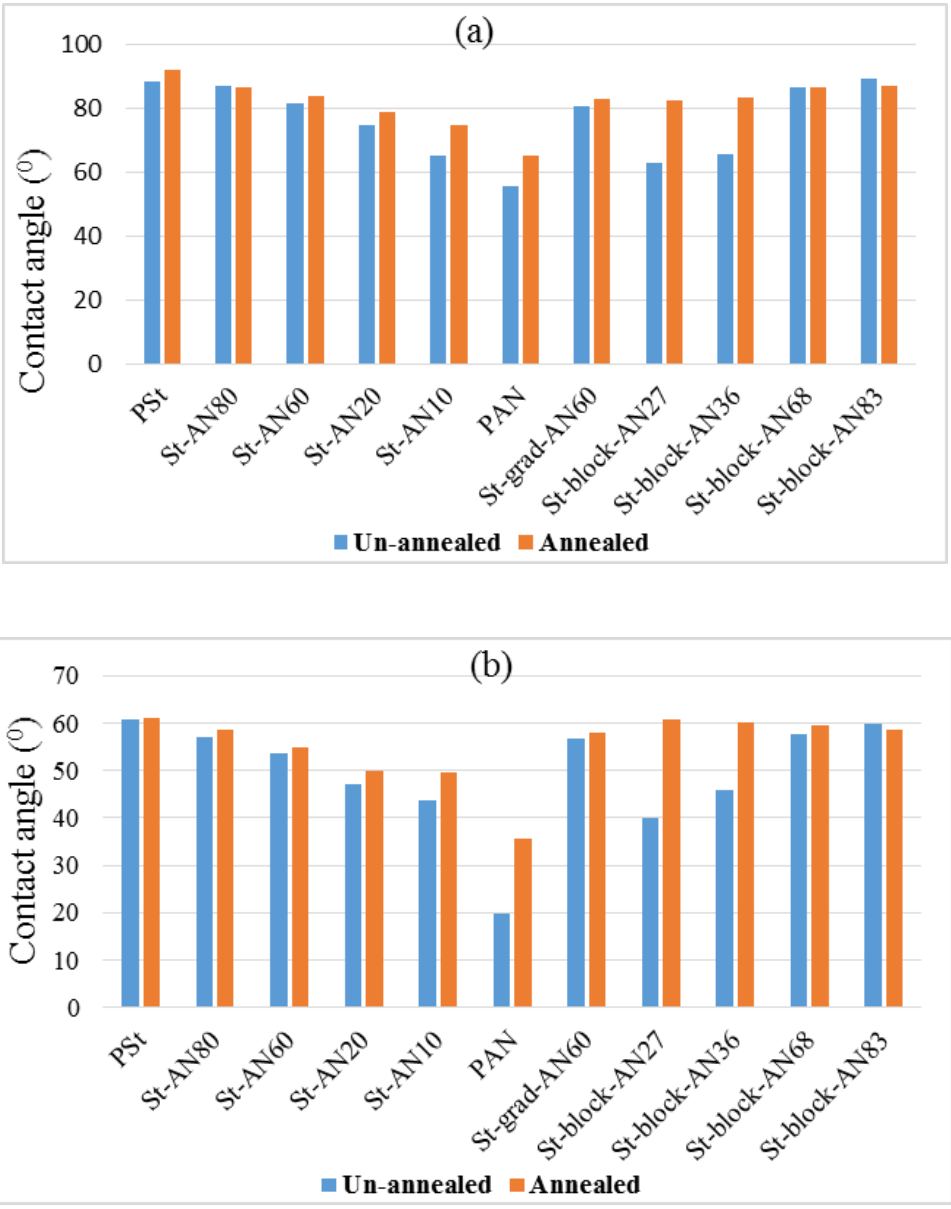

Figure-3.39: Comparison of contact angles of St and AN homopolymer, and their copolymer thin films for (a) water and (b) thiodiglycol.

The surface energies of the homopolymer and the copolymer thin films have been determined using the water and thiodiglycol contact angles by geometric mean method as given in Table-3.13. The surface energy of St-AN copolymers increase with the increase of AN composition in the copolymer, regardless of chain structure (Figure-3.40). However, the block copolymer thin films with high AN composition possess surface energy higher than the statistical copolymer with similar AN composition.

As a result of the annealing process, the increase in the PSt composition on the surface is also reflected in the surface energy data (Figure-3.41). Due to the lower surface energy value of PSt homopolymer, the annealing process causes an overall decrease in the surface energy values for St-AN copolymer thin films. However, similar to those of the XPS and contact angle data, the block copolymers with high AN compositions show the biggest decrease in the surface energy values after annealing. The thin films of the statistical copolymer do not show such change in the surface energy, while the change in the surface energy of the spontaneous gradient copolymers are in between to those of the block and statistical copolymer thin films. However, no noticeable difference in the contact angle and surface energy data have been observed for the thin films of the copolymers synthesized by the RAFT and CvRP process as shown in Figure-3.42.

Table-3.13: Surface free energy of the thin films of statistical, block and gradient copolymers and homopolymers of St and AN synthesized by the RAFT method before and after annealing.

Designation	F_{AN} (**^{1}H NMR**)	**Surface energy of un-annealed thin films**			**Surface energy of annealed thin films**		
		γ_S^d (mJ m^{-2})	γ_S^P (mJ m^{-2})	γ_S^{total} (mJ m^{-2})	γ_S^d (mJ m^{-2})	γ_S^P (mJ m^{-2})	γ_S^{total} (mJ m^{-2})
PSt	0.00	29.2	2.9	32.1	32.8	1.3	34.1
St-AN80	0.22	32.2	2.7	34.9	29.8	3.4	33.2
St-AN60	0.35	30.4	5.0	35.4	31.1	4.0	35.1
St-AN20	0.76	30.5	8.0	38.5	31.6	5.9	37.5
St-AN10	0.87	24.6	16.1	40.7	28.0	8.9	36.9
PAN	1.00	33.4	17.6	51.0	31.7	12.7	44.4
St-grad-AN60	0.45	25.9	6.8	32.7	26.9	5.5	32.4
St-block-AN27	0.73	28.4	13.7	42.1	23.5	6.7	30.2
St-block-AN36	0.64	20.6	20.0	40.6	24.8	5.9	30.7
St-block-AN68	0.32	28.3	3.7	32.0	29.0	3.5	32.5
St-block-AN83	0.17	34.1	1.7	35.8	30.2	3.1	33.3

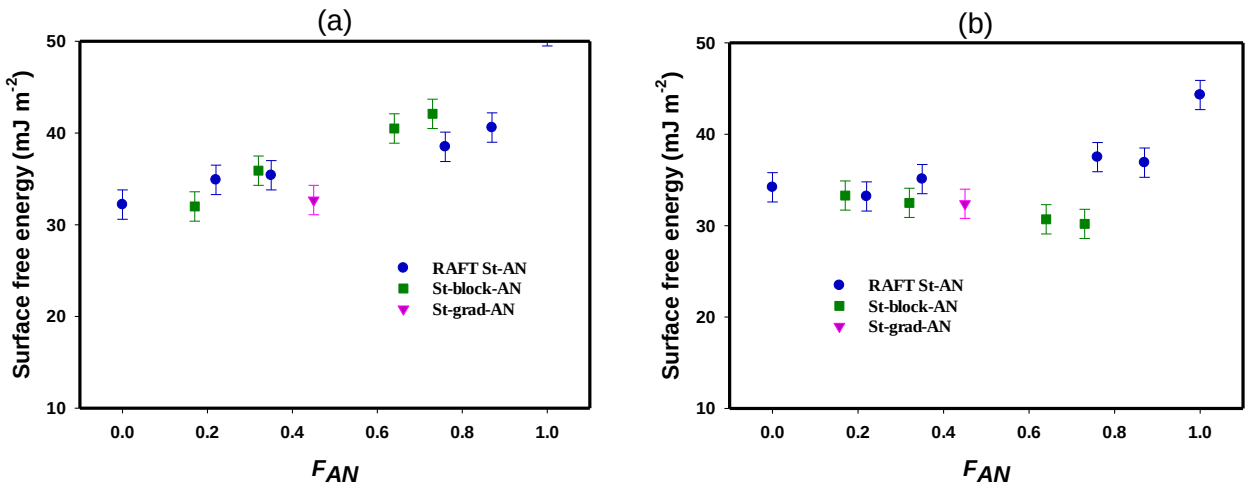

Figure-3.40: Surfac free energy of the thin films of St and AN homo and copolymers (a) before, and (b) after annealing at 130 °C for 10 hours.

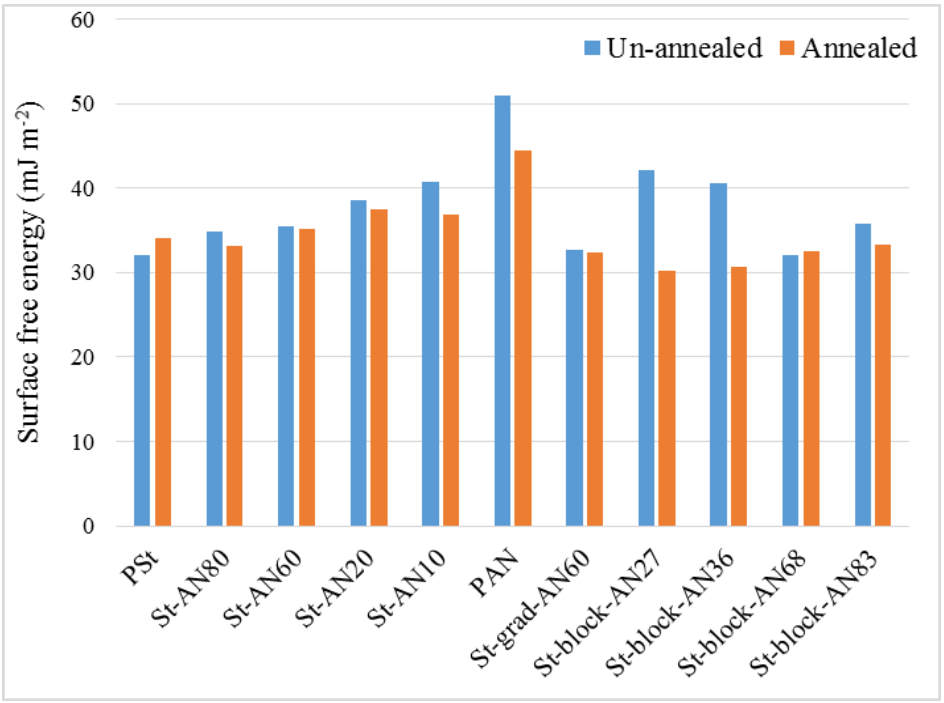

Figure-3.41: Comparison of surface energy of the thin films before and after annealing for St and AN homopolymer and copolymer thin films synthesized by the RAFT method.

Table-3.14: Contact angles of water and thiodiglycol on the thin films of St and AN copolymers synthesized by the CvRP batch method before and after annealing.

Designation	F_{AN} (^{1}H NMR)	Water contact angle (°)		Thiodiglycol contact angle (°)	
		Un-annealed	Annealed	Un-annealed	Annealed
St-AN80	0.24	87.2	89.2	57.8	59.3
St-AN60	0.37	81.1	83.0	53.5	53.7
St-AN20	0.78	73.7	78.2	49.8	48.7
St-AN10	0.85	76.6	78.0	44.8	49.8

Table-3.15: Surface free energy of the thin films of St and AN copolymers synthesized by the CvRP batch method before and after annealing.

Designation	F_{AN} (^{1}H NMR)	Surface energy of un-annealed thin films (mJ m^{-2})			Surface energy of annealed thin films (mJ m^{-2})		
		γ_s^d	γ_s^P	γ_s^{total}	γ_s^d	γ_s^P	γ_s^{total}
St-AN80	0.24	31.4	2.8	34.2	31.8	2.2	34.0
St-AN60	0.37	30.1	5.3	35.4	31.8	4.1	35.9
St-AN20	0.78	31.7	8.1	39.8	32.4	5.8	38.2
St-AN10	0.85	35.5	5.7	41.2	30.9	6.4	37.3

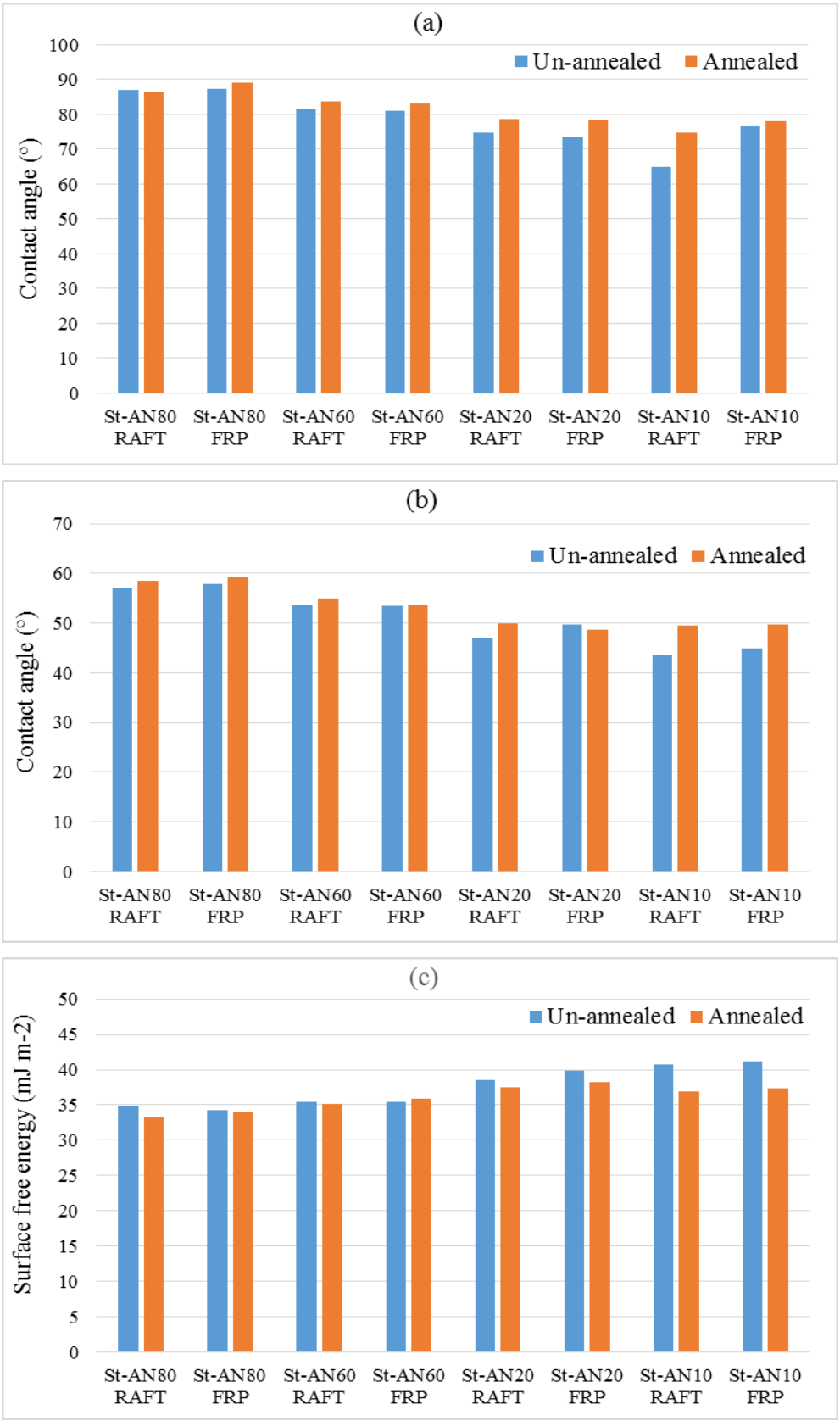

Figure-3.42: Comparative bar plot for (a) contact angle of water, (b) contact angle of thiodiglycol, and (c) surface free energy of the thin films of St-AN copolymers synthesized by RAFT and CvRP methods.

3.7 Conclusions

In this chapter, the thermal properties, and the properties of the thin films for St and AN homopolymers, and their statistical, block and gradient copolymers have been studied. The composition, as well as the sequence distribution of the St-AN copolymers showed significant effect on their thermal properties as well as surface properties. The thermal properties of the gradient copolymers, due to their unique chain structures, was found to be very different to those of the statistical and block copolymers. Because of small difference in the T_gs of the St and AN homopolymers, instead of two, the block copolymer shows one transition in the DSC heating curve, similar to those of the St-AN statistical copolymers. However, due to the composition gradient in their structures, broad transition in the DSC heating curves have been seen for the spontaneous (St-AN20, St-AN10) and forced gradient copolymers.

An XPS study was used to characterize the surface composition of the thin films of St and AN homopolymer, and their copolymers. The statistical, block and gradient copolymers of St and AN with similar copolymer composition showed different behaviours in the thin films due to the difference in their sequence distributions. XPS data showed that the composition of St in the thin film surface increases significantly after annealing for the block copolymers, while almost no change can be seen for the statistical copolymers. On the contrary, the gradient copolymer surface composition also showed noticeable change in the surface composition as a result of annealing, but not as significant as those of the block copolymers. The surface energy data determined from the contact angles of water and thiodiglycol on the thin films also follow the XPS results. These studies suggest, the block copolymers undergo phase segregation in the thin films surface by moving the St units towards the thin film-air interface and AN units towards the substrate, while no such phase segregation happens for the statistical copolymers. Rather than a complete phase segregation with clear boundary as in the block copolymers, gradient copolymers, due to their continuous composition drift, undergo a weak phase segregation with wide boundary. Therefore, with the unique chain structures, the properties of the gradient copolymers have been found to be very different to those of the block and statistical copolymers.

3.8 References

[48] Lefebvre MD, Olvera de la Cruz M, Shull KR. Phase Segregation in Gradient Copolymer Melts. Macromolecules. 2004;37:1118-23.

[49] Wang R, Li W, Luo Y, Li B-G, Shi A-C, Zhu S. Phase Behavior of Ternary Homopolymer/Gradient Copolymer Blends. Macromolecules (Washington, DC, U S). 2009;42:2275-85.

[51] Mok MM, Ellison CJ, Torkelson JM. Effect of Gradient Sequencing on Copolymer Order-Disorder Transitions: Phase Behavior of Styrene/n-Butyl Acrylate Block and Gradient Copolymers. Macromolecules (Washington, DC, U S). 2011;44:6220-6.

[52] Zhang G, Zhang Q, Wang Q, Zhan X, Chen F. Synthesis and properties of gradient copolymers of butyl methacrylate and fluorinated acrylate via RAFT miniemulsion copolymerizations. J Appl Polym Sci. 2016;133:n/a.

[56] Yu SM, Conticello VP, Zhang G, Kayser C, Fournier MJ, Mason TL, et al. Smectic ordering in solutions and films of a rod-like polymer owing to monodispersity of chain length. Nature (London). 1997;389:167-70.

[64] Sun X, Luo Y, Wang R, Li B-G, Zhu S. Semibatch RAFT polymerization for producing ST/BA copolymers with controlled gradient composition profiles. AIChE J. 2008;54:1073-87.

[75] Mok MM, Kim J, Torkelson JM. Gradient copolymers with broad glass transition temperature regions: Design of purely interphase compositions for damping applications. Journal of Polymer Science Part B: Polymer Physics. 2008;46:48-58.

[77] Jakubowski W, Juhari A, Best A, Koynov K, Pakula T, Matyjaszewski K. Comparison of thermomechanical properties of statistical, gradient and block copolymers of isobornyl acrylate and n-butyl acrylate with various acrylate homopolymers. Polymer. 2008;49:1567-78.

[81] Kim J, Mok MM, Sandoval RW, Woo DJ, Torkelson JM. Uniquely Broad Glass Transition Temperatures of Gradient Copolymers Relative to Random and Block Copolymers Containing Repulsive Comonomers. Macromolecules. 2006;39:6152-60.

[117] Guo Y, Zhang J, Xie P, Gao X, Luo Y. Tailor-made compositional gradient copolymer by a many-shot RAFT emulsion polymerization method. Polym Chem. 2014;5:3363-71.

[172] Guo Y, Gao X, Luo Y. Mechanical properties of gradient copolymers of styrene and n-butyl acrylate. J Polym Sci, Part B: Polym Phys. 2015;53:860-8.

[287] Nishizaki H, Yoshida K. Effect of molecular weight on various TGA methods in polystyrene degradation. J Appl Polym Sci. 1981;26:3503-4.

[288] Rieger J. The glass transition temperature of polystyrene. Results of a round robin test. J Therm Anal. 1996;46:965-72.

[289] Abushihada AM, Shunbo FE, Al-Hajjar F, Al-Sultan YY. Determination of the glass transition temperature of polystyrene, poly(vinyl chloride) and poly(methyl methacrylate) using gas chromatography. HRC CC, J High Resolut Chromatogr Chromatogr Commun. 1979;2:512-16.

[290] Blanchard LP, Hesse J, Malhotra SL. Effect of molecular weight on glass transition by differential scanning calorimetry. Can J Chem. 1974;52:3170-5.
[291] An L, He D, Jing J, Wang Z, Yu D, Jiang B, et al. Effects of molecular weight and interaction parameter on the glass transition temperature of polystyrene mixtures and its blends with polystyrene/poly (2,6-dimethyl-p-phenylene oxide). Eur Polym J. 1997;33:1523-8.
[292] Keavney JJ, Eberlin EC. The determination of glass transition temperatures by differential-thermal analysis. J Appl Polym Sci. 1960;3:47-53.
[293] Schatzki TF. Glass transitions in polymers. J Appl Polym Sci. 1961;5:S1-S2.
[294] Kolb HJ, Izard EF. Dilatometric studies of high polymers. I. Second-order transition temperature. J Appl Phys. 1949;20:564-71.
[295] Beevers RB. Dependence of the glass-transition temperature of polyacrylonitrile on molecular weight. J Polym Sci. 1964;2:5257-65.
[296] Wiley RH, Brauer GM. Refractometric determination of second-order transition temperatures in polymers. IV. Butadiene-acrylonitrile copolymers. J Polym Sci. 1948;3:704-7.
[297] Gerke RH. Second-order transition temperature of butadiene copolymers. J Polym Sci. 1954;13:295-300.
[298] Krigbaum WR, Tokita N. Melting-point-depression study of polyacrylonitrile. J Polym Sci. 1960;43:467-88.
[299] Bashir Z. Polyacrylonitrile, an unusual linear homopolymer with two glass transitions. Indian J Fibre Text Res. 1999;24:1-9.
[300] Andrews RD, Kimmel RM. Solid state structure and glass transition in polyacrylonitrile: the hetero-bonded solid state. J Polym Sci, Part B: Polym Lett. 1965;3:167-9.
[301] Illers KH. Calorimetric studies on polyacrylonitrile. Makromol Chem. 1969;124:278-81.
[302] Bajaj P, Padmanaban M. Thermal studies of copolymers of acrylonitrile with haloalkyl acrylates and methacrylates. Eur Polym J. 1984;20:513-16.
[303] Gupta DC, Agrawal JP, Sharma RC. Effect of comonomers on thermal degradation of polyacrylonitrile. J Appl Polym Sci. 1989;38:265-70.
[304] Hori T, Zhang HS, Shimizu T, Zollinger H. Change of water states in acrylic fibers and their glass transition temperatures by DSC measurements. Text Res J. 1988;58:227-32.
[305] Chawla S, Cai J, Naraghi M. Mechanical tests on individual carbon nanofibers reveals the strong effect of graphitic alignment achieved via precursor hot-drawing. Carbon. 2017;117:208-19.
[306] Ismar E, Sarac AS. Synthesis and characterization of poly (acrylonitrile-co-acrylic acid) as precursor of carbon nanofibers. Polym Adv Technol. 2016;27:1383-8.
[307] Sikkanthar S, Karthikeyan S, Selvasekarapandian S, Arunkumar D, Nithya H, Junichi K. Structural, electrical conductivity, and transport analysis of PAN-NH4Cl polymer electrolyte system. Ionics. 2016;22:1085-94.
[308] Lei S, Cao W, Fu Z, Xu L. The conjugated plane formed in polyacrylonitrile during thermal stabilization. J Appl Polym Sci. 2016;133:n/a.

[309] Guay D, Tourillon G, Viel P, Lecayon G. Spatially resolved electronic modifications of a thin poly(acrylonitrile) film induced by synchrotron radiation white beam. J Phys Chem. 1992;96:5917-21.
[310] Broglia MF, Acevedo DF, Langheinrich D, Perez-Hernandez HR, Barbero CA, Lasagni AF. Rapid fabrication of periodic patterns on poly(styrene-co-acrylonitrile) surfaces using direct laser interference patterning. Int J Polym Sci. 2015:721035pp.
[311] Leiston-Belanger JM, Penelle J, Russell TP. Synthesis and Microphase Separation of Poly(styrene-b-acrylonitrile) Prepared by Sequential Anionic and ATRP Techniques. Macromolecules. 2006;39:1766-70.
[312] You J, Shi T, Liao Y, Li X, Su Z, An L. Temperature dependence of surface composition and morphology in polymer blend film. Polymer. 2008;49:4456-61.
[313] Qian J, Xiao Z, Dong L, Tang D, Li M, Yang Q, et al. Morphology and crystallization behavior of PCL/SAN blends containing nanosilica with different surface properties. J Appl Polym Sci. 2016;133:n/a.
[314] Wen F, Xu Z, Xia W, Ye H, Wei X, Zhang Z. High-Energy-Density Poly(styrene-co-acrylonitrile) Thin Films. J Electron Mater. 2013;42:3489-93.
[315] Donald AM, Kramer EJ. The competition between shear deformation and crazing in glassy polymers. J Mater Sci. 1982;17:1871-9.
[316] Marwat ZK, Baloch MK. Investigating Miscibility of Polymers and Its Impact on the Morphology, Thermal, and Mechanical Properties of Polymer Blends. Int J Thermophys. 2015;36:2755-68.
[317] Algers J, Sperr P, Egger W, Kogel G, Maurer FHJ. Median implantation depth and implantation profile of 3-18 keV positrons in amorphous polymers. Phys Rev B: Condens Matter Mater Phys. 2003;67:125404/1-/7.
[318] Masson JL, Green PF. Pattern formation in a thin random copolymer film: Evolution of an intermediate morphology. J Chem Phys. 2000;112:349-55.
[319] Peng Y, Burtovyy R, Yang Y, Urban MW, Kennedy MS, Kornev KG, et al. Towards scalable fabrication of ultrasmooth and porous thin carbon films. Carbon. 2016;96:184-95.
[320] Liu S, Weng L-T, Chan C-M, Li L, Ho K-C, Jiang M. Surface characterization of poly(styrene-co-p-hexafluorohydroxyisopropyl-α-methyl styrene) copolymers by ToF-SIMS, XPS and contact angle measurements. Surf Interface Anal. 2000;29:500-7.
[321] Chan C-M. Polymer Surface Modification and Characterization: Hanser: New York; 1994.
[322] Briggs D, Fletcher IW, Reichlmaier S, Agulo-Sanchez JL, Short RD. SIMS applied to polymer surfaces. Part 18. Surface morphology of a PVC/PMMA blend studied by ToF-SIMS. Surf Interface Anal. 1996;24:419-21, 1 plate.
[323] Weng L-T, Ng K-M, Cheung ZL, Lei Y, Chan C-M. Quantitative analysis of styrene-pentafluorostyrene random copolymers by ToF-SIMS and XPS. Surf Interface Anal. 2006;38:32-43.

[324] Nobuta T, Ogawa T. Improvement of depth resolution in XPS analysis of fluorinated layer using C60 ion sputtering. Appl Surf Sci. 2009;256:1560-5.
[325] Chiang Y-C, Lee C-Y, Lee H-C. Surface chemistry of polyacrylonitrile- and rayon-based activated carbon fibers after post-heat treatment. Mater Chem Phys. 2007;101:199-210.
[326] Recek N, Primc G, Vesel A, Mozetic M, Avila J, Razado-Colambo I, et al. Degradation of albumin on plasma-treated polystyrene by soft X-ray exposure. Polymers (Basel, Switz). 2016;8:244/1-/17.
[327] Bebin P, Prud'Homme RE. x-ray photoelectron spectroscopy of miscible poly(methyl methacrylate)/poly(styrene-co-acrylonitrile) and immiscible poly(methyl methacrylate)/polyacrylonitrile polymer surfaces metallized by nickel. J Polym Sci, Part B: Polym Phys. 2004;42:1408-16.
[328] Lopez-Garcia J, Primc G, Junkar I, Lehocky M, Mozetic M. On the hydrophilicity and water resistance effect of styrene-acrylonitrile copolymer treated by CF4 and O2 plasmas. Plasma Processes Polym. 2015;12:1075-84.
[329] Liao Y, You J, Shi T, An L, Dutta PK. Phase Behavior and Dewetting for Polymer Blend Films Studied by In Situ AFM and XPS: From Thin to Ultrathin Films. Langmuir. 2007;23:11107-11.
[330] Wen G, Li X, Liao Y, An L. Surface phase separations of PMMA/SAN blends investigated by atomic force microscopy. Polymer. 2003;44:4035-45.
[331] Oultache AK, Prud'homme RE. XPS studies of nickel deposition on poly(methyl methacrylate) and poly(styrene-co-acrylonitrile). Polym Adv Technol. 2000;11:316-23.
[332] Wang PH, Pan CY. Preparation of styrene/acrylonitrile copolymer microspheres and their composites with metal particles. Colloid Polym Sci. 2000;278:245-9.
[333] Ucar IO, Doganci MD, Cansoy CE, Erbil HY, Avramova I, Suzer S. Combined XPS and contact angle studies of ethylene vinyl acetate and polyvinyl acetate blends. Appl Surf Sci. 2011;257:9587-94.
[334] Doganci MD, Cansoy CE, Ucar IO, Erbil HY, Mielczarski E, Mielczarski JA. Combined XPS and contact angle studies of flat and rough ethylene-vinyl acetate copolymer films. J Appl Polym Sci. 2012;124:2100-9.
[335] Grundke K, Poeschel K, Synytska A, Frenzel R, Drechsler A, Nitschke M, et al. Experimental studies of contact angle hysteresis phenomena on polymer surfaces - Toward the understanding and control of wettability for different applications. Adv Colloid Interface Sci. 2015;222:350-76.
[336] Suh HS, Kim DH, Moni P, Xiong S, Ocola LE, Zaluzec NJ, et al. Sub-10-nm patterning via directed self-assembly of block copolymer films with a vapor-phase deposited topcoat. Nat Nanotechnol. 2017;12:575-81.
[337] Song J, Ye Q, Lee WT, Wang X, He T, Shah KW, et al. Perfluoropolyether/poly(ethylene glycol) triblock copolymers with controllable self-assembly behaviour for highly efficient anti-bacterial materials. RSC Adv. 2015;5:64170-9.

[338] Chen A, Blakey I, Jack KS, Whittaker AK, Peng H. Control through monomer placement of surface properties and morphology of fluoromethacrylate copolymers. J Polym Sci, Part A: Polym Chem. 2015;53:2633-41.
[339] Cho Y-S, Ahn SH, Lee S-H. Fabrication and analysis of PMMA, ABS, PS, and PC superhydrophobic surfaces using the spray method. J Korean Phys Soc. 2013;63:218-24.
[340] Leiva A, Munoz N, Urzua M, Gargallo L, Radic D. Monolayers and thin films of dextran hydrophobically modified. J Braz Chem Soc. 2010;21:78-86.
[341] Youssef A, Pabon M, Severac R, Gilbert RG. The effect of copolymer composition on the surface properties of perfluoroalkylethyl acrylates. J Appl Polym Sci. 2009;114:4020-9.
[342] Epps TH, III, DeLongchamp DM, Fasolka MJ, Fischer DA, Jablonski EL. Substrate Surface Energy Dependent Morphology and Dewetting in an ABC Triblock Copolymer Film. Langmuir. 2007;23:3355-62.
[343] Adao MHVC, Saramago BJV, Fernandes AC. Estimation of the Surface Properties of Styrene-Acrylonitrile Random Copolymers from Contact Angle Measurements. J Colloid Interface Sci. 1999;217:94-106.
[344] Hameed N, Thomas SP, Abraham R, Thomas S. Morphology and contact angle studies of poly(styrene-co-acrylonitrile) modified epoxy resin blends and their glass fibre reinforced composites. eXPRESS Polym Lett. 2007;1:345-55.
[345] Kim G, Lee W-K, Kim W, Lee J-K, Ha C-S. Surface structure of polymethacrylate/SAN blend thin films: preliminary contact angle studies. Mol Cryst Liq Cryst Sci Technol, Sect A. 2002;377:341-4.
[346] Johansson B-L, Larsson A, Ocklind A, Ohrlund A. Characterization of air plasma-treated polymer surfaces by ESCA and contact angle measurements for optimization of surface stability and cell growth. J Appl Polym Sci. 2002;86:2618-25.
[347] Piglowski JM, Bryjak M. Surface studies of poly(methyl methacrylate)/poly(styrene-co-acrylonitrile) blends. Eur Polym J. 1998;34:1669-73.
[348] Lee W-K, Tanaka K, Takahara A, Kajiyama T, Ha C-S. Surface structure of blend films of styrene/acrylonitrile copolymer and poly(methyl methacrylate) (PMMA) or hydrolyzed PMMA. Bull Korean Chem Soc. 1997;18:958-61.
[349] Pticek Sirocic A, Hrnjak-Murgic Z, Jelencic J. The surface energy as an indicator of miscibility of SAN/EDPM polymer blends. J Adhes Sci Technol. 2013;27:2615-28.

Chapter 4: Synthesis of Hydroxystyrene – t-Butyl acrylate Copolymers

4.1 Introduction

Polymers containing phenolic group such as hydroxystyrene (HOST) homopolymer and the copolymers of HOST are of great importance due to their potential applications in the areas of photoresists, adhesives, metal treatment, plastic additives and compatibilizers in polymer blends [350-361]. Hydroxystyrene monomer however, is known to be unstable due to the acidic phenol proton [362-364], and therefore protected derivatives such as 4-acetoxystyrene (AOST) are utilized to synthesize homopolymer and copolymers of hydroxystyrene. Synthesis of AOST-tBA copolymers has been reported by CvRP as well as by the RAFT method [351, 365, 366]. Guo and co-workers [366] determined the reactivity ratios for AOST-tBA copolymer system for both CvRP (r_{AOST} = 1.082; r_{tBA} = 0.292) and RAFT (r_{AOST} = 0.896; r_{tBA} = 0.468) method, and found them to be close but different from each other. However, the reactivity ratios determined in their study for CvRP were similar to those reported by Ito *et al.*[351] for CvRP. This copolymer system has been chosen due to the similarity with the structure of one of the commercial photoresists TER60, and the aim was to study the structure – properties relationship.

In this study, AOST and t-butyl acrylate (tBA) statistical copolymers were synthesized using both the RAFT and CvRP batch copolymerization methods. In addition to the statistical copolymers, AOST-tBA block copolymers were synthesized by chain extension of AOST homopolymer, and AOST-tBA forced gradient copolymers synthesized by the continuous feed method. HOST-tBA copolymers with different chain structures were produced by de-acetylation of the AOST-tBA copolymers. However, unlike the St-AN system, neither AOST-tBA nor HOST-tBA give well resolved peaks for the triads in the ^{13}C NMR spectra. Therefore, a triad distribution study will not be possible to establish the formation of gradient structures in the AOST-tBA or HOST-tBA copolymer systems. Though few recent studies reported that it is possible to determine the distribution of chemical composition which involves complex methods [367-369].

4.2 Materials

The monomers 4-acetoxystyrene and t-butyl acrylate were purchased from Sigma Aldrich, and the inhibitor from the monomers were removed by passing through a basic alumina column prior to polymerization reactions. Azobisisobutyronitrile (AIBN) initiator was purchased from Sigma-

Aldrich, and purified by recrystallizing in methanol followed by drying in a vacuum oven at room temperature. Propanoicacidyl butyl trithiocarbonate (PABTC) RAFT agent was synthesized as described in the literature [370]. Solvent 1,4-dioxane was purchased from Ajax Finechem and N,N-dimethylformamide (DMF) was purchased from Merck Millipore.

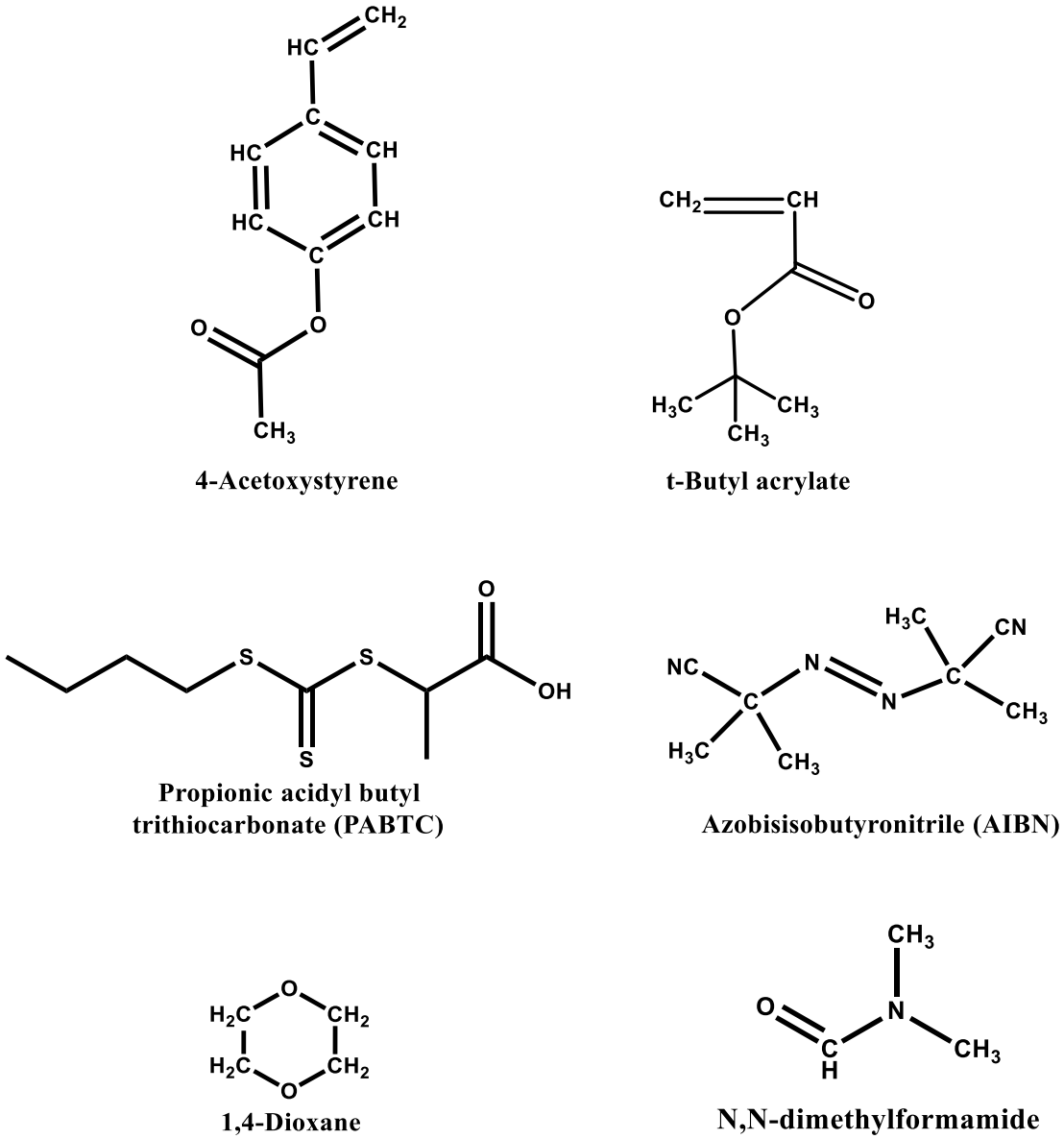

Figure-4.1: Materials used for the synthesis of St-AN copolymers.

4.3 Synthesis of AOST and tBA homopolymers by RAFT Polymerization

AOST and tBA homopolymers were synthesized by the RAFT method in bulk using PABTC as the RAFT agent, and AIBN as initiator. The monomer and the RAFT agent along with the initiator were placed in a 20 mL vial. After sealing the vial with a rubber septum, oxygen was removed from the reaction solution with N_2 gas, and allowed to react in an oil bath at 70 °C temperature. RAFT to initiator ratio was 10:1. The polymerization reaction was quenched in an ice bath after a certain time and the polymer solution was diluted by adding small amount of THF. The polymer solution was then added slowly into an excess amount of methanol to collect the polymer precipitate. The resulting pure polymer was then dried in a vacuum oven for 48 hours at room temperature to bring it to a constant weight.

4.4 Synthesis and Characterization of AOST-tBA Statistical Copolymers

AOST-tBA copolymers with three different feed compositions were synthesized by both the RAFT and CvRP methods. The reactant concentrations for the RAFT and CvRP synthesis of AOST-tBA copolymers are given in Table-4.1 and Table-4.2, respectively.

Table-4.1: Reaction concentration for the synthesis of AOST-tBA statistical copolymers by the RAFT method. The ratio at the end of the names of the copolymers indicates the mole ratio of AOST and tBA in the feed.

Designation	**AOST**	**tBA**	**RAFT agent (PABTC)**	**Initiator (AIBN)**	**Solvent (Dioxane)**
AOST-stat-tBA80:20	1.513 g (9.339 mmol)	0.296 g (2.312 mmol)	35.5 mg (0.149 mmol)	12.3 mg (0.075 mmol)	1.818 g (0.021 mol)
AOST-stat-tBA50:50	1.076 g (6.642mmol)	0.790 g (6.172mmol)	36.1 mg (0.152 mmol)	11.6 mg (0.071 mmol)	2.074 g (0.024 mol)
AOST-stat-tBA20:80	0.475 g (2.932mmol)	1.498 g (11.703mmol)	34.7 mg (0.146 mmol)	12.9 mg (0.079 mmol)	1.938 g (0.022 mol)

Table-4.2: Reaction concentration for the synthesis of AOST-tBA statistical copolymer by CvRP method. The ratio at the end of the names of the copolymers indicates the mole ratio of AOST and tBA in the feed.

Designation	**AOST**	**tBA**	**Initiator (AIBN)**	**Solvent (Dioxane)**
AOST-stat-tBA80	1.040 g (6.420 mmol)	0.211 g (1.648 mmol)	42.2 mg (0.257 mmol)	2.047 g (0.023 mol)
AOST-stat-tBA50	0.510 g (3.148 mmol)	0.408 g (3.188 mmol)	33.5 mg (0.204 mmol)	3.076 g (0.035 mol)
AOST-stat-tBA20	0.173 g (1.068 mmol)	0.525 g (4.102 mmol)	27.8 mg (0.170 mmol)	1.921 g (0.022 mol)

For both RAFT and CvRP, the polymerization reaction was carried out at 70 °C, and continued to a final conversion of more than 70%. At the end of polymerization, the reaction was quenched in an ice bath, and pure copolymers were collected by precipitating in excess methanol. The copolymers were then dried in a vacuum oven at room temperature to bring to constant weights.

The molecular weight and molecular weight dispersity of the AOST and tBA homopolymers, and their statistical copolymers were characterized by SEC using THF as eluent. ^{1}H and ^{13}C NMR were used to characterize the purity of the polymers and their compositions.

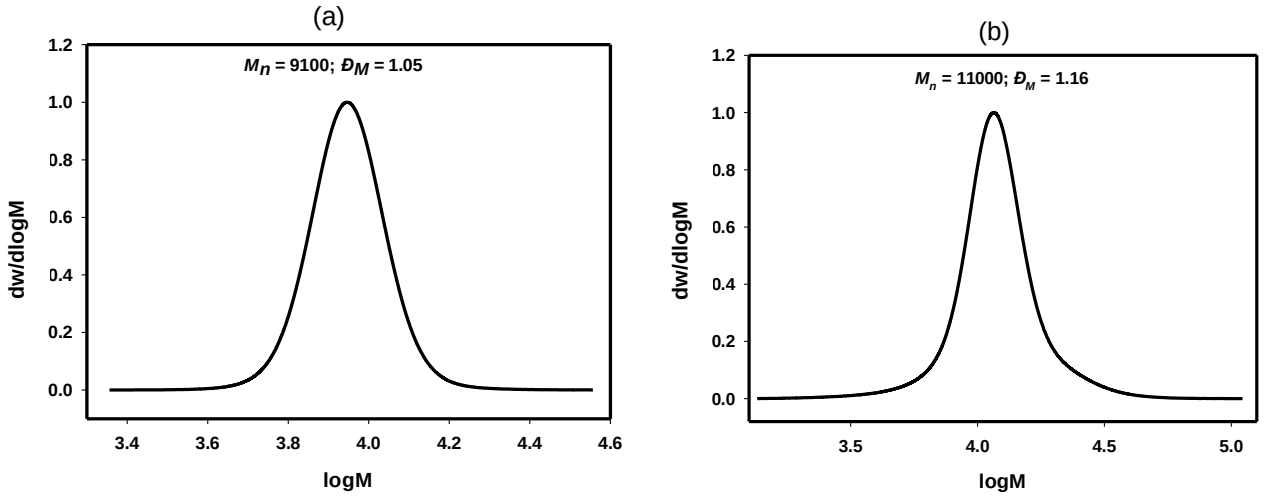

Figure-4.2: Molecular weight distribution plot for (a) AOST and (b) tBA homopolymers synthesized by RAFT method.

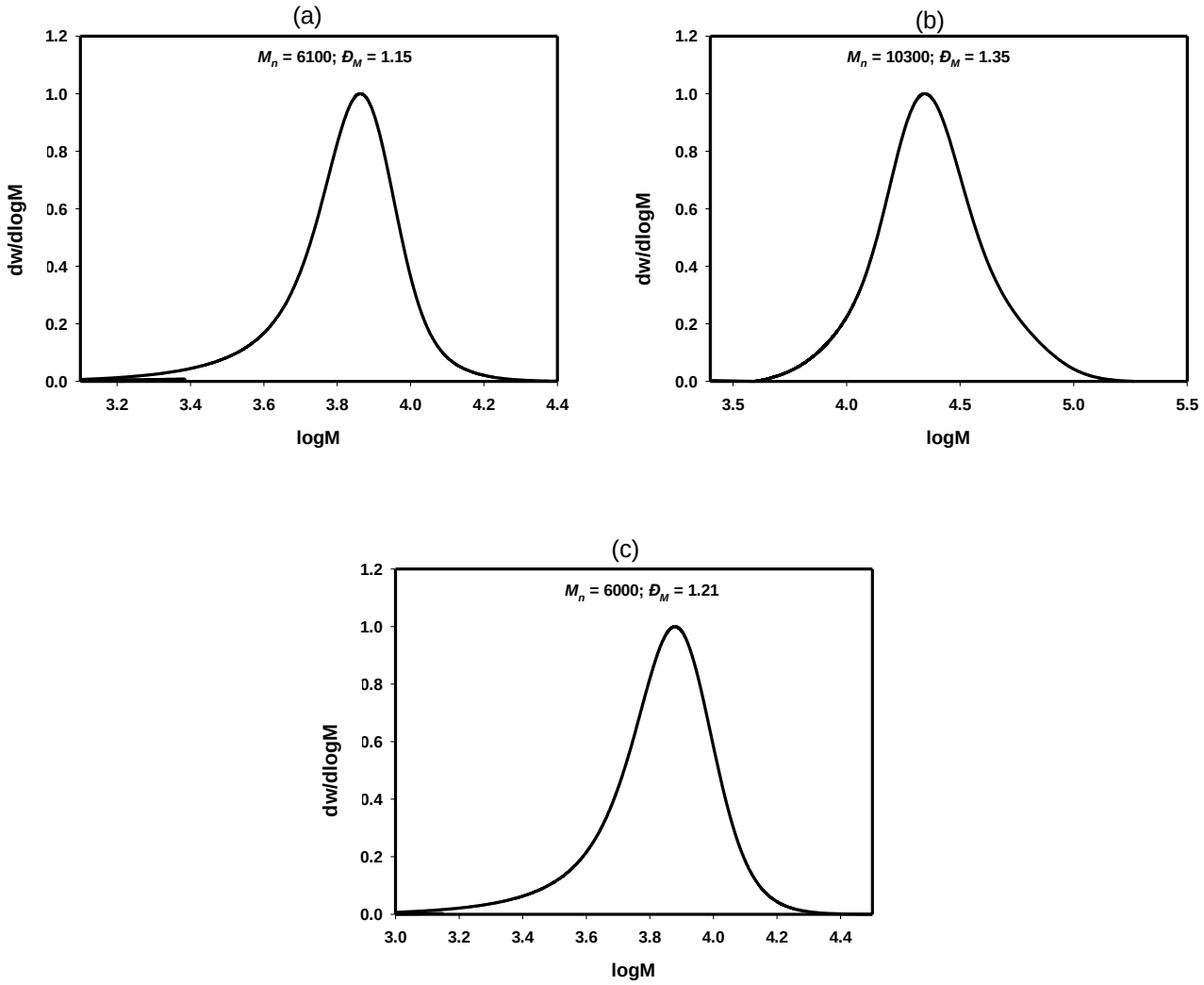

Figure-4.3: Molecular weight distribution of (a) AOST-stat-tBA80; (b) AOST-stat-tBA50 and (c) AOST-stat-tBA20 copolymers synthesized by RAFT method.

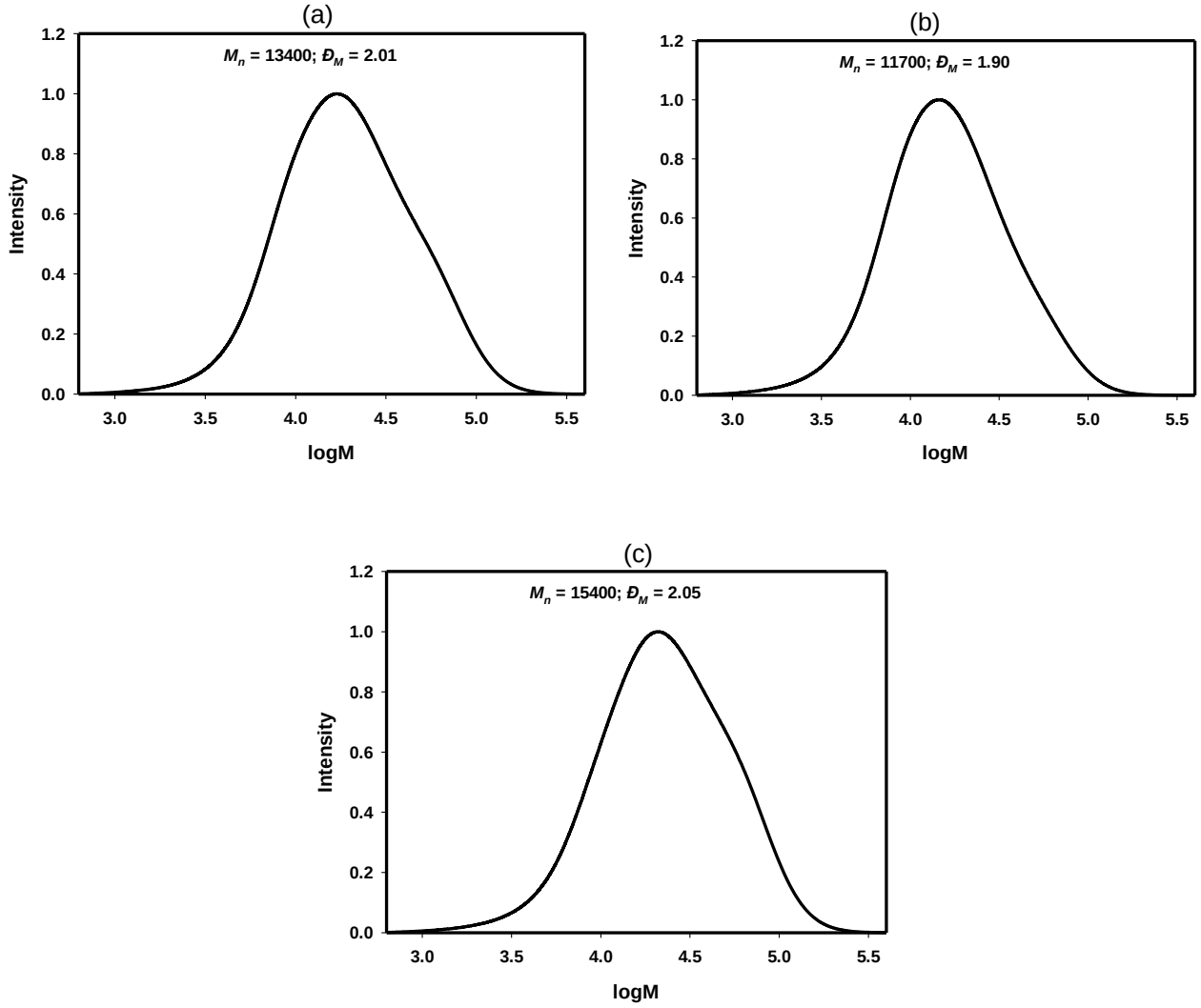

Figure-4.4: Molecular weight distribution of (a) AOST-stat-tBA80; (b) AOST-stat-tBA50 and (c) AOST-stat-tBA20 copolymers synthesized by CvRP method.

The molecular weight distribution plots are shown in Figure-4.2, 4.3 and 4.4 for the AOST and tBA copolymers synthesized by RAFT method, and their copolymers synthesized by RAFT and CvRP methods, respectively. The molecular weight and molecular weight dispersity characterized by SEC, and the copolymer composition characterized by ^{1}H NMR are given in Table-4.3 and Table-

4.4. RAFT polymerization method provides homopolymers and statistical copolymers of AOST and tBA with narrow molecular weight dispersity compared to the statistical copolymers synthesized by CvRP method.

The compositions of the AOST-stat-tBA copolymers were determined from the ^{1}H NMR of the purified copolymers. The intensities of the peaks due to the aromatic protons from AOST were compared to the tBA protons to calculate the copolymer compositions. The ^{1}H NMR spectra for the homopolymers or copolymers synthesized by RAFT method are shown in Figure-4.5 and Figure-4.6, using $CDCl_3$ as NMR solvent.

Table-4.3: Molecular weight, molecular weight dispersity and composition data for AOST and tBA homopolymers and their copolymers synthesized by RAFT method.

Designation	M_n **(SEC)**	$Đ_M$ **(SEC)**	**Copolymer compositions (AOST:tBA)**
PAOST	9100	1.05	-
PtBA	11000	1.16	-
AOST-stat-tBA80:20	6100	1.15	78:22
AOST-stat-tBA50:50	10300	1.35	48:52
AOST-stat-tBA20:80	6000	1.21	29:71

Table-4.4: Molecular weight, molecular weight dispersity and composition data for AOST and tBA homopolymers and their copolymers synthesized by CvRP method.

Designation	M_n **(SEC)**	$Đ_M$ **(SEC)**	**Copolymer compositions (AOST:tBA)**
AOST-stat-tBA80:20	13400	2.01	78:22
AOST-stat-tBA50:50	11700	1.90	56:44
AOST-stat-tBA20:80	15400	2.05	20:80

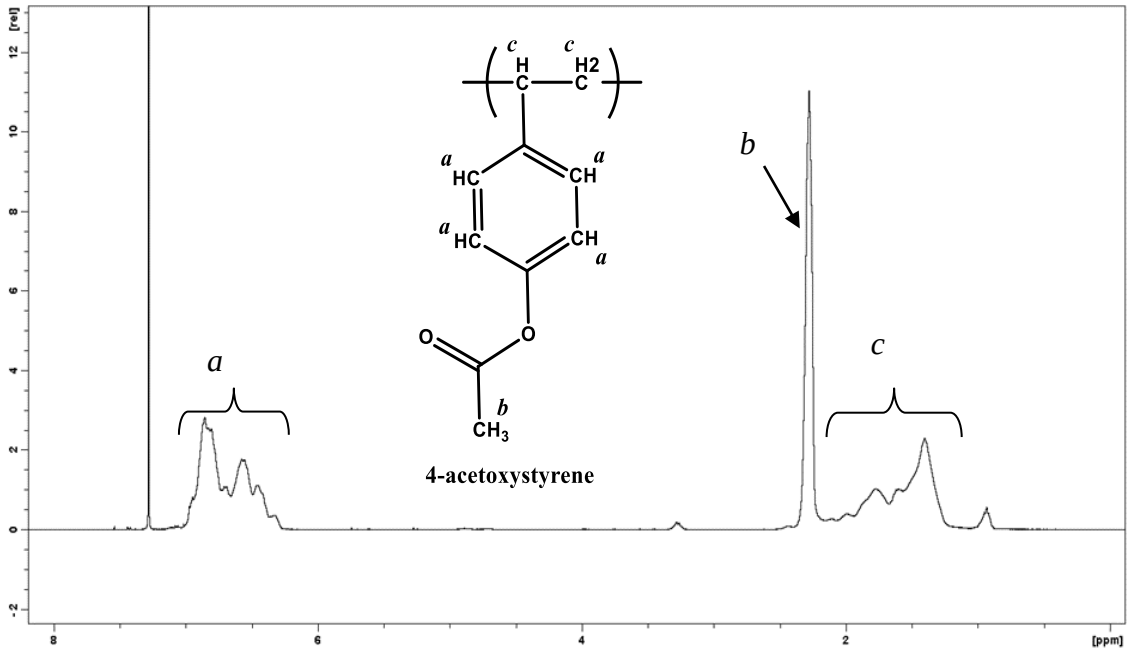

(b)

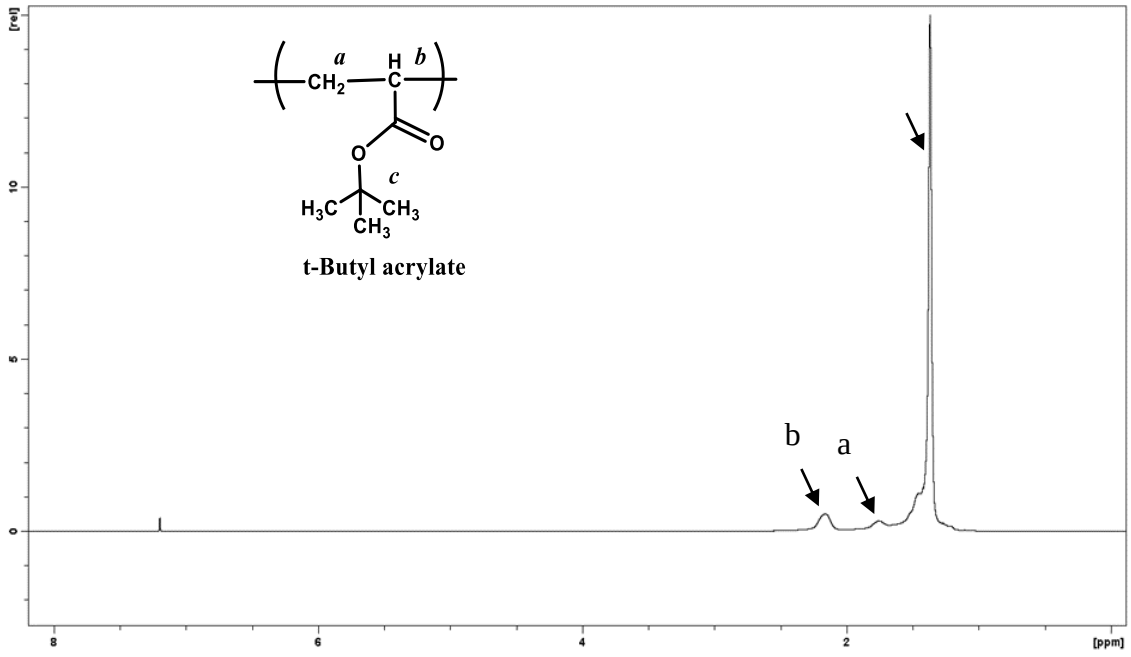

Figure-4.5: ^{1}H NMR of purified (a) PAOST and (b) PtBA homopolymers using $CDCl_3$ as solvent.

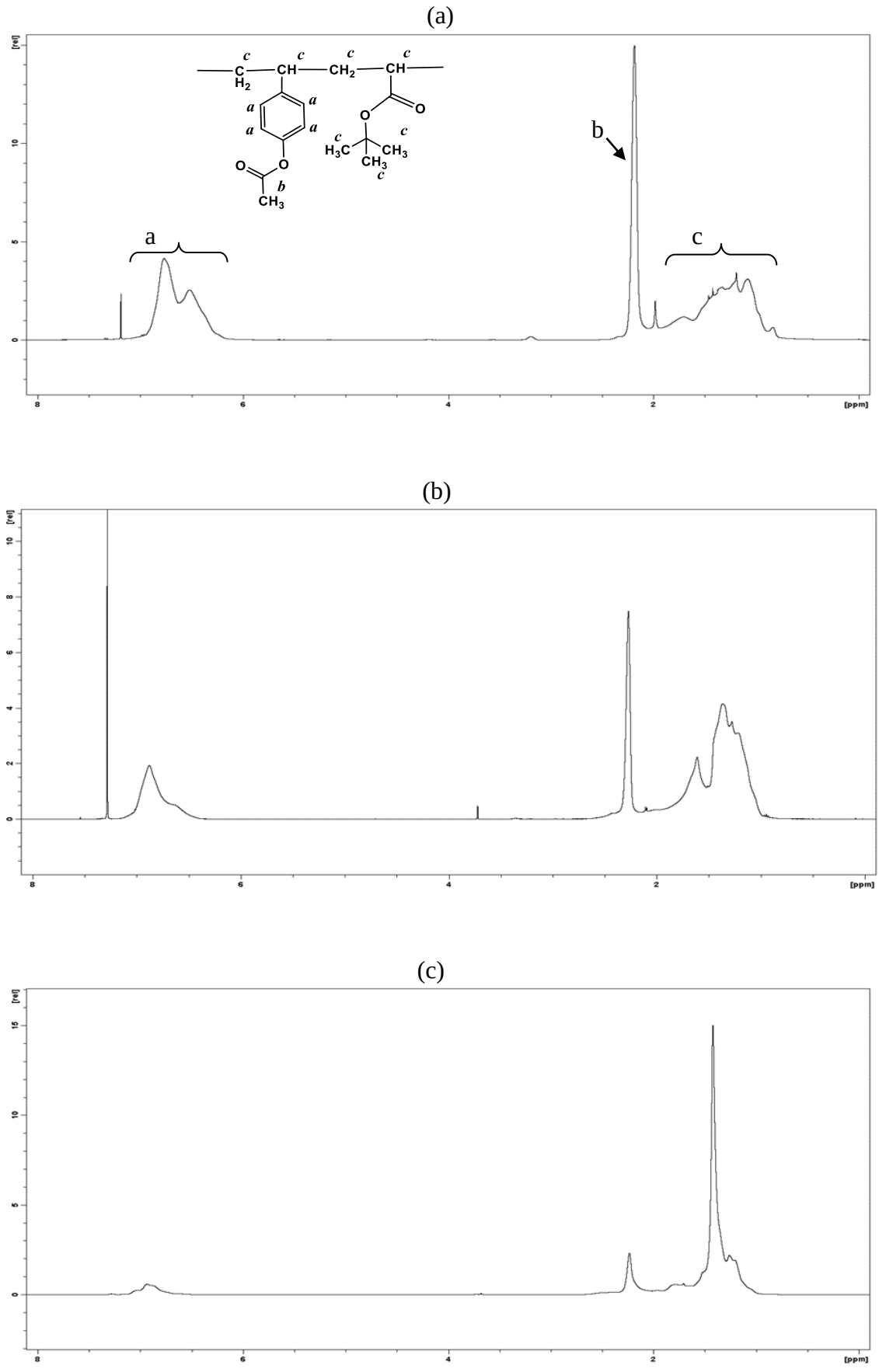

Figure-4.6: ^{1}H NMR spectra of purified (a) AOST-stat-tBA80; (b) AOST-stat-tBA50 and (c) AOST-stat-tBA20 copolymers synthesized by RAFT process.

4.5 Synthesis and Characterization of AOST-tBA block copolymers

AOST-tBA block copolymers with different copolymer compositions were synthesized using AOST homopolymer as the first block. The RAFT to initiator ratio was 10:1, and the polymerization reactions were stopped below 50% conversion in order to avoid formation of dead chains. The resulted copolymers were characterized using SEC and ^{1}H NMR. The molecular weight, molecular weight dispersity data for the first block and the block copolymers are listed in Table-4.6. The number at the end of the copolymer name indicates the composition of AOST in the copolymer characterized by ^{1}H NMR.

The copolymers formed are with narrow molecular weight distributions as shown by the SEC data, and also evident from the SEC molecular weight distribution plots. Figure-4.7 shows the molecular weight distribution comparison for the AOST homopolymer with the block copolymers. The molecular weight distribution plots of the homopolymer shift towards higher molecular weight region after chain extension. Figure-4.8 shows the comparative ^{1}H NMR plot for the AOST homopolymer and AOST-b-tBA copolymer. After the chain extension of the AOST homopolymers, the formation of the block copolymer is clear from the presence of tBA protons peak at around 1.4 ppm.

Table-4.6: Molecular weight and composition data for the AOST-block-tBA copolymers characterized by SEC and ^{1}H NMR.

Designation	Mn (AOST)	$Đ_M$ (AOST)	Mn (AOST-block-tBA)	$Đ_M$ (AOST-block-tBA)	AOST:tBA (SEC)	AOST:tBA (NMR)
AOST-block-tBA12	3200	1.09	17400	1.22	0.18	0.12
AOST-block-tBA45	9000	1.05	16900	1.16	0.53	0.45
AOST-block-tBA60	9000	1.05	13700	1.09	0.66	0.60

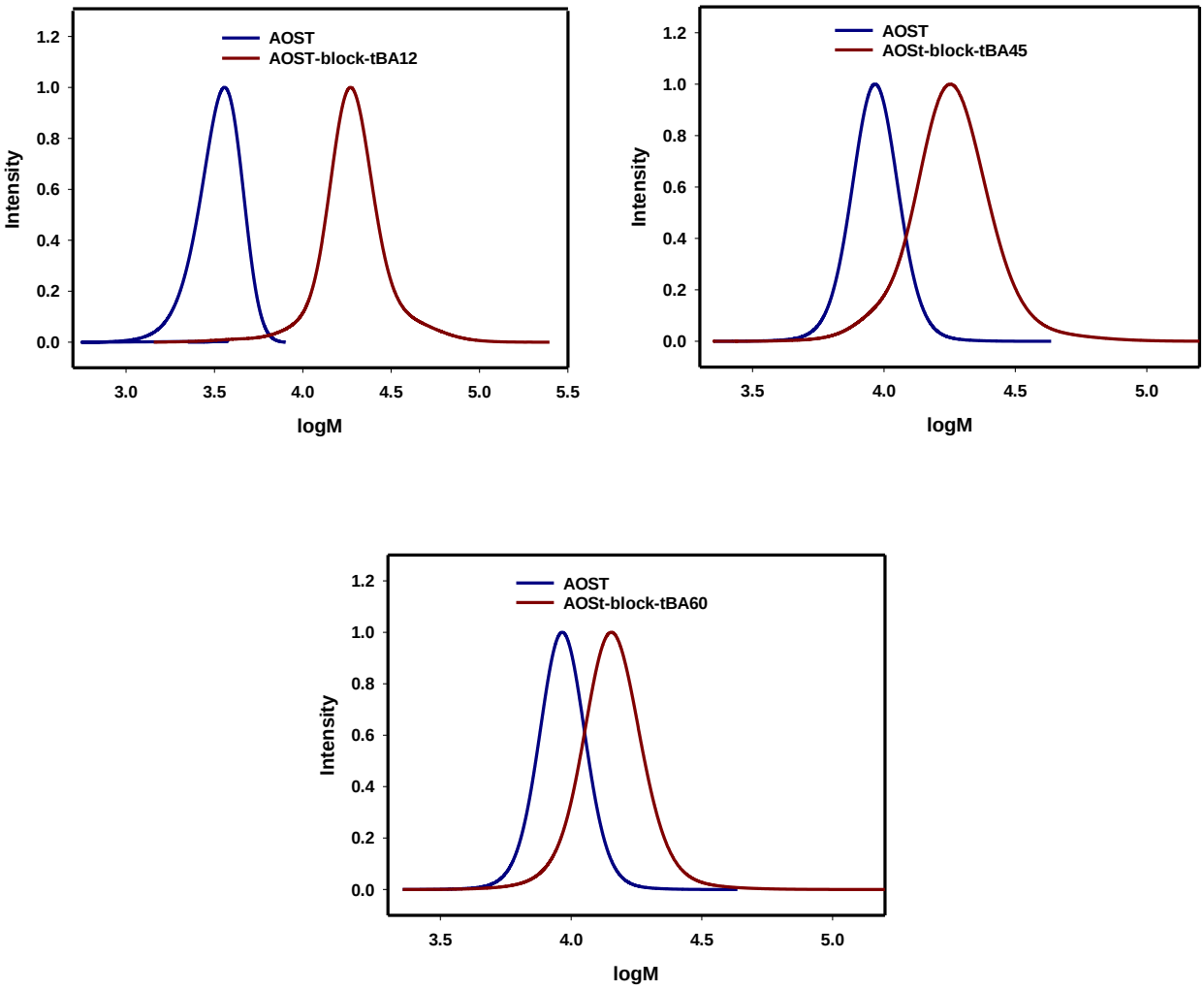

Figure-4.7: Comparison of AOST homopolymer with their corresponding block copolymers.

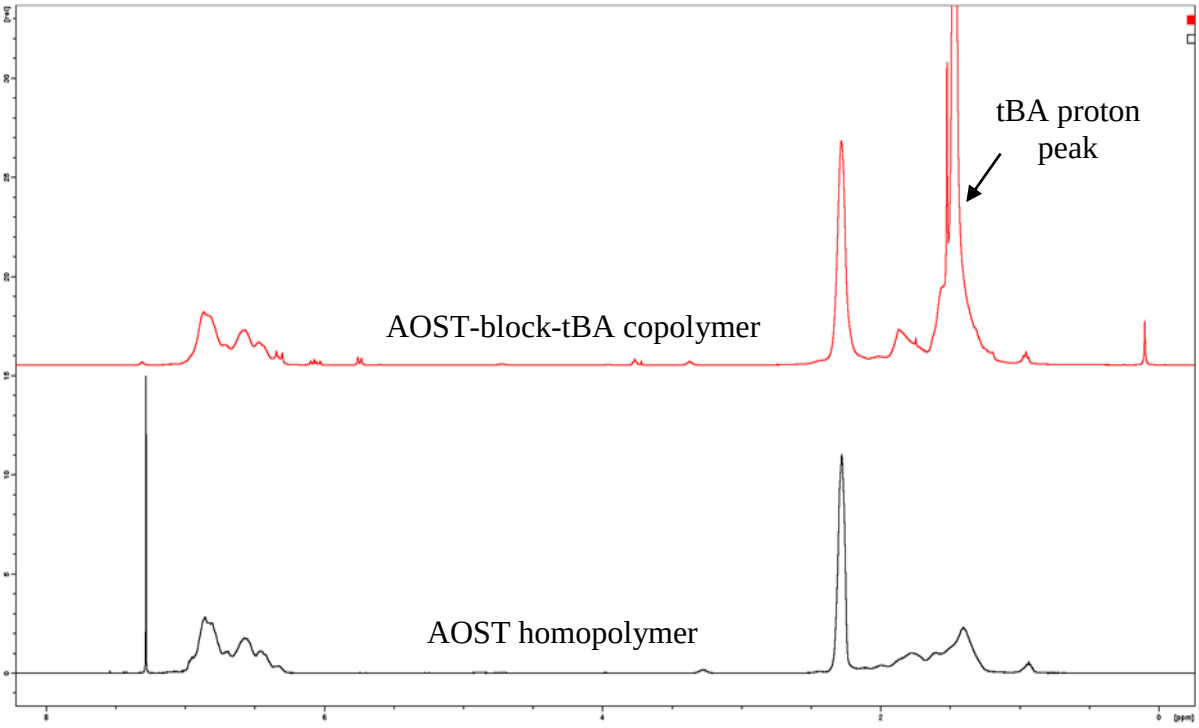

Figure-4.8: Comparative ^{1}H NMR of AOST homopolymer and AOST-block-tBA copolymer, shows the introduction of tBA proton peak at ~1.4 ppm after chain extension.

4.6 Synthesis and Characterization of AOST-tBA Gradient Copolymers

In addition to the conventional statistical and block copolymers, AOST-tBA forced gradient copolymers were synthesized using the continuous feeding method to produce copolymers with 50:50 composition. In a 20 mL vial, 39.6 mg (0.166 mmol) of PABTC and 28.5 mg (0.174 mmol) of AIBN was added to 2.528 g (0.016 mol) of AOST monomer, and 2.004 g of DMF was added as the solvent. In another vial, 1.106 g of dioxane was added to 1.860 g (0.015 mole) tBA. Both of the vials were sealed with rubber septa and degassed of oxygen with N_2 for 30 minutes.

To produce a gradient structure in the copolymer, the synthesis process was started by putting the vial containing AOST monomer in an oil bath at 70 ºC, and tBA monomer solution was added continuously to the system at 0.4 mL/hour using a syringe pump. Samples were collected from the reaction system at regular intervals, and characterized with ^{1}H NMR to monitor the progress of reaction. The individual monomer conversion and the overall copolymer conversion for the synthesis of AOST-grad-tBA copolymer are given in Table-4.7.

Table-4.7: Conversion data for the synthesis of AOST-grad-tBA copolymer by continuous feeding approach.

Reaction time	[H] from AOST	Conversion of styrene (%)	[H] from tBA	Conversion of tBA (%)	Overall conversion of tBA (%)	Overall copolymer conversion (%)
0 hour	59.86		16.40		0.00	0.00
2 hours	47.83	20.10	13.80	15.85	3.96	12.03
4 hours	41.64	30.44	14.17	13.60	6.80	18.62
6 hours	29.59	50.57	12.72	22.44	16.83	33.70
8 hours	16.00	73.27	10.23	37.62	37.62	55.45
10 hours	9.91	83.44	8.50	48.17	48.17	65.81
20 hours	0.88	98.53	4.04	75.37	75.37	86.95

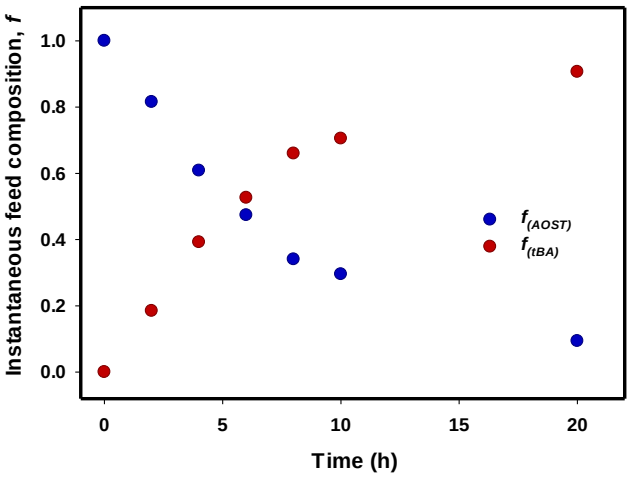

Figure-4.9: Instantaneous feed composition of AOST and tBA monomer for the synthesis of AOST-grad-tBA copolymer.

At the very beginning, the reaction system contained only AOST monomer. As the polymerization reaction progressed, and tBA monomer solution was gradually added to the system, the instantaneous composition of tBA increased with time while the opposite happened for AOST monomer. The instantaneous composition of AOST and tBA monomer in the reaction system characterized by ^{1}H NMR is shown in Figure-4.9 which shows an increase of instantaneous composition of tBA and decrease of instantaneous composition of AOST with polymerization time. The crude polymer solution collected from the reaction system at regular time interval were diluted by adding a small amount of THF, and then added to excess amount of methanol slowly to form a copolymer precipitate. The purified copolymers were collected and dried in a vacuum oven at room temperature to bring to a constant weight.

The molecular weight and the molecular weight dispersity data of the purified copolymers characterized by SEC is shown in Table-4.8. Molecular weight of the gradient copolymers were also determined from ^{1}H NMR by comparing the copolymer peaks to those of the RAFT end peaks. In both cases, the molecular weight of the copolymer gradually increases with copolymer conversion, but the values found from these two methods differ from each other at higher conversion. PtBA has been reported to form branching in radical polymerization [371] which could affect the molecular weight values determined by SEC due to the change in the hydrodynamic volume [372-374]. Therefore, copolymer molecular weights from SEC are significantly lower than those found from ^{1}H NMR, especially at higher conversions where probability of long chain branching is higher. The copolymer molecular weight and molecular weight dispersity of the AOST-tBA gradient copolymer plotted against copolymer conversion are given in Figure-4.10 which shows an increase in the molecular weight of the gradient copolymer with low molecular weight dispersity.

Table-4.8: Molecular weight, molecular weight dispersity and mole fraction composition of the gradient copolymers at different conversion characterized by SEC and ^{1}H NMR.

Overall Conversion (%)	M_n **(SEC)**	$Đ_M$ **(SEC)**	M_n **(^{1}H NMR)**	$F_{(AOST)}$:$F_{(tBA)}$
18.62	3800	1.15	3300	0.82 : 0.18
33.70	6300	1.16	5300	0.74 : 0.26
55.45	8800	1.20	9700	0.66 : 0.34
65.81	9900	1.24	14900	0.61 : 0.39
86.95	11800	1.39	21800	0.57 : 0.43

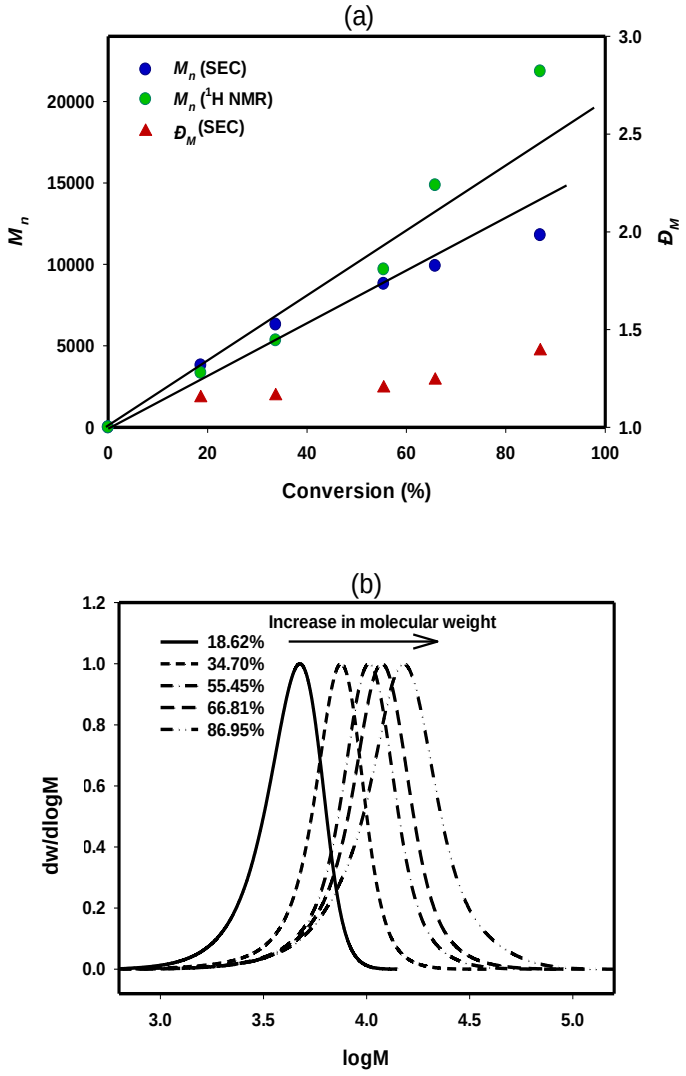

Figure-4.10: (a) The change of molecular weight and molecular weight dispersity, and (b) change in molecular weight distribution plot with copolymer conversion for AOST-grad-tBA copolymers.

The composition of the copolymer was characterized by ^{1}H NMR of the purified copolymers at different conversion. As Table-4.8 shows, the composition of AOST in the copolymer decreases with the increase in the copolymer conversion and the opposite happens for tBA composition. This is understandable from the change in the instantaneous composition of the monomers with copolymer conversion. In the initial periods, the reaction mixture is rich in AOST monomer, therefore the copolymer chains formed at the beginning of the reaction are also rich in AOST units. As AOST monomers are consumed with the progress in reaction, and tBA monomer was being added continuously to the system, the copolymer chains formed in the later part of the polymerization are rich in tBA units.

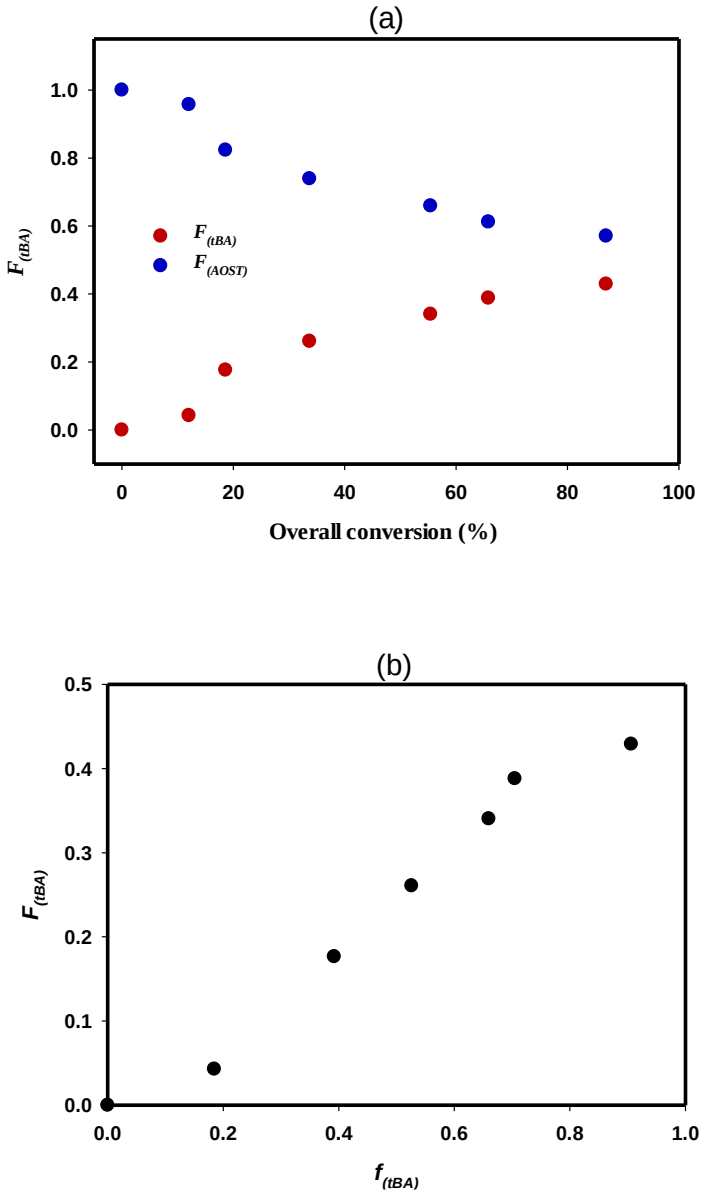

Figure-4.11: The change of composition of tBA in the copolymer with (a) overall copolymer conversion, and (b) instantaneous composition of tBA monomer.

The increase in the composition of tBA and decrease in the composition of AOST in the copolymer with the change in the copolymer composition is clearly shown in Figure-4.11 (a), and produces a AOST-grad-tBA copolymer with composition of 0.57:0.43 (AOST:tBA) at 87% overall copolymer conversion. The composition of tBA in the copolymer also gradually increases with instantaneous tBA composition as shown in Figure-4.11 (b).

4.7 Synthesis of HOST homopolymers and HOST-tBA copolymers

HOST homopolymers and copolymers of HOST were prepared by de-acetylation of AOST homo and copolymers through a hydrolysis process. There have been a number of reports discussing different approaches to remove the acetoxy group from AOST polymers [158, 353, 360, 361, 375-381]. Among many others, some commonly used reagents reported for selective hydrolysis of acetoxy groups are mixture of methanol and ammonium hydroxide [360], mixture of methane sulphonic acid and methanol [382], mixture of sodium methoxide and methanol [375], hydrazine hydrate [158, 353, 361, 381], sodium hydroxide [361] etc. at different temperatures. In this study, acetoxystyrene homopolymer and copolymers were hydrolysed using hydrazine hydrate to produce hydroxystyrene homopolymer and copolymers.

The acetoxy homo and copolymers were added to a flask containing 1,4-dioxane and hydrazine hydrate at 9 to 1 ratio, and the mixture was stirred continuously in a N_2 atmosphere at room temperature for 6 hours. The resulted hydroxystyrene copolymer solution was diluted by adding small amount of THF before precipitating and washing in excess water. The purified polymer was then dried in a vacuum oven at room temperature for 48 hours to bring to a constant weight.

Removal of the acetoxy group was confirmed by characterizing the homopolymer and copolymers by ^{1}H and quantitative ^{13}C NMR before and after the hydrolysis process. $CDCl_3$ was used as the NMR solvent for the polymers before hydrolysis, but due to insolubility of the hydroxystyrene polymers in $CDCl_3$, either DMSO-d6 or acetone-d6 was used instead for the polymers after hydrolysis. For quantitative NMR analysis, an approximately 10 wt% polymer solution was prepared.

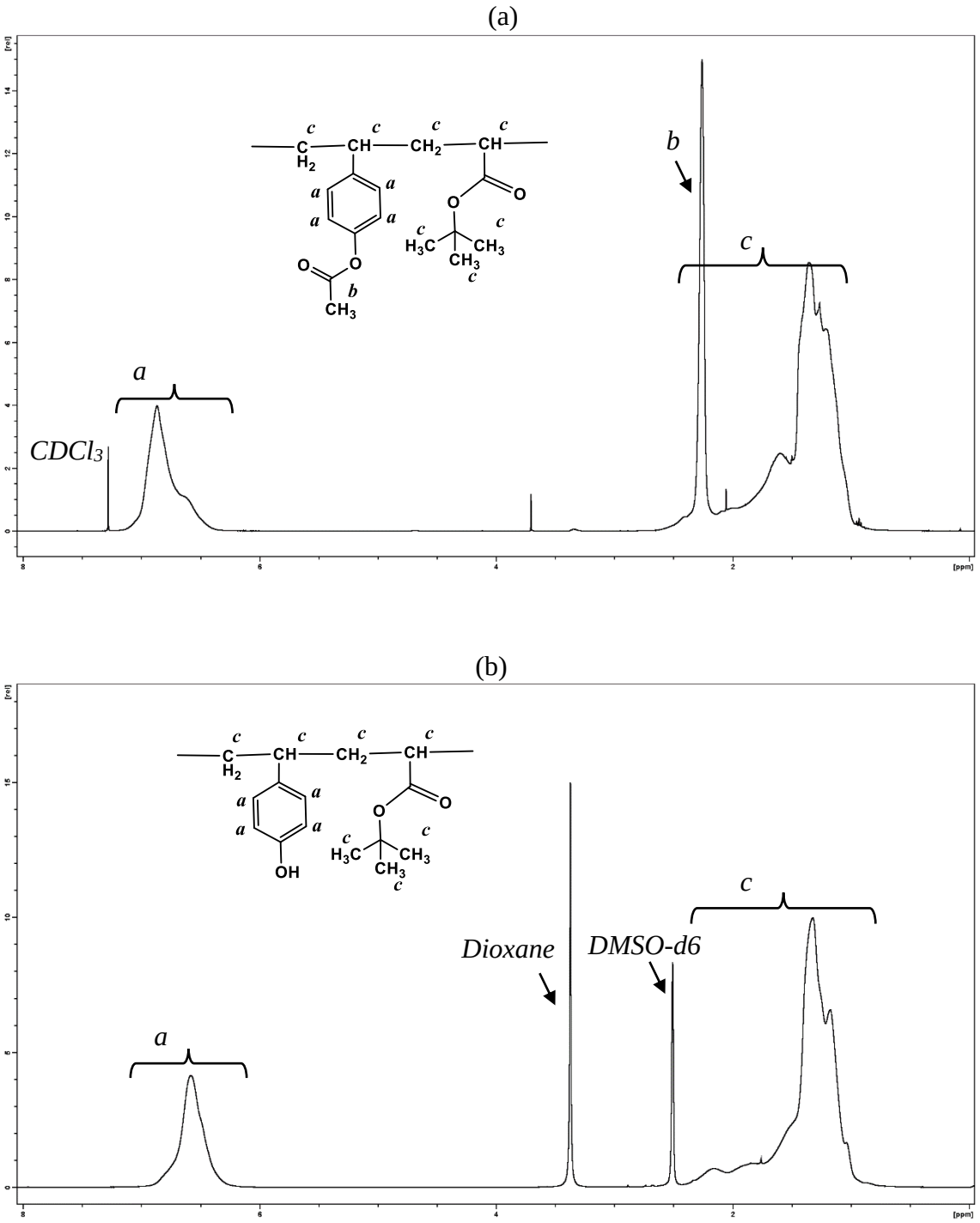

Figure-4.12: ^{1}H NMR of (a) AOST-stat-tBA and (b) HOST-stat-tBA copolymers showing peaks for corresponding protons.

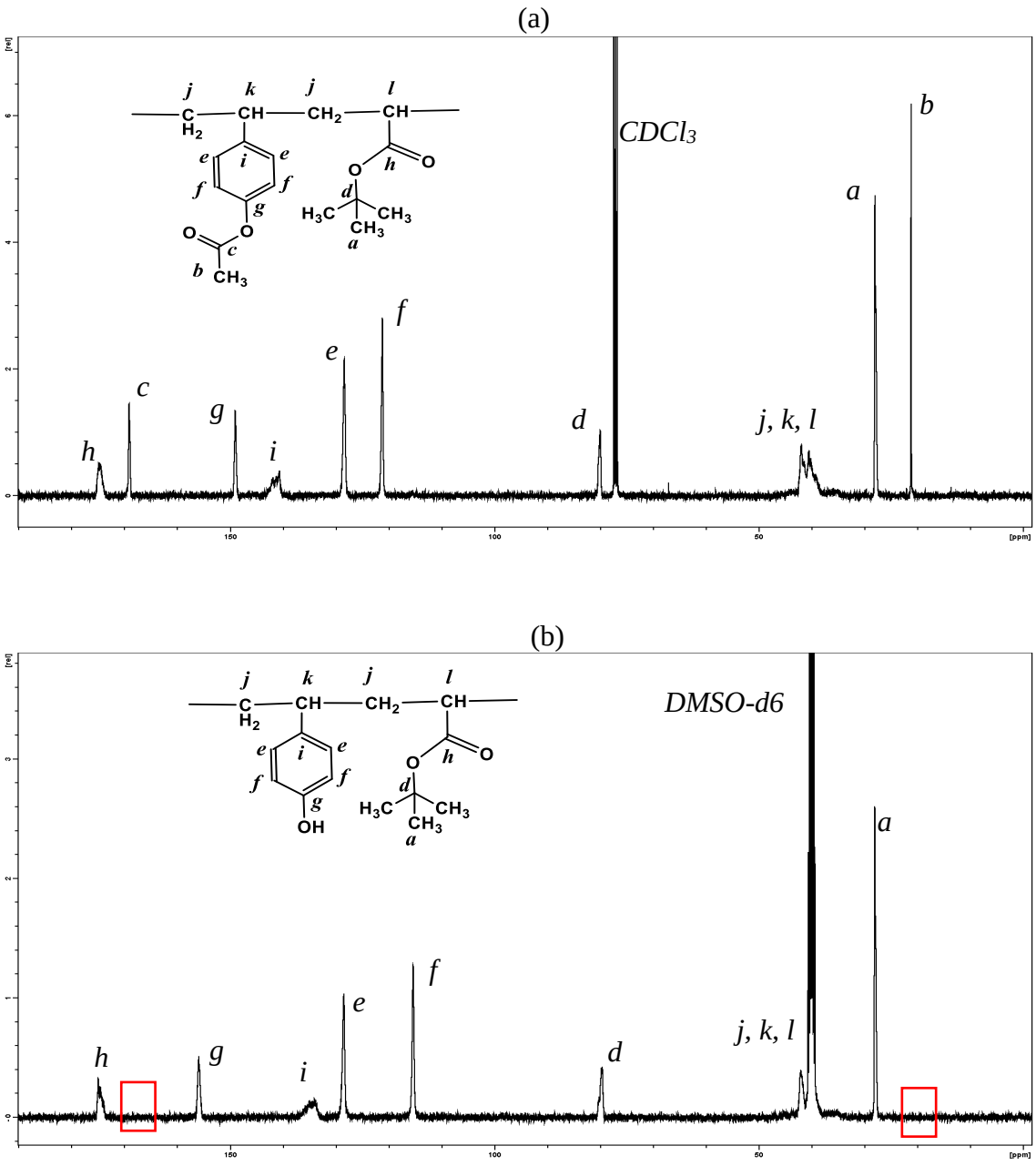

Figure-4.13: Quantitative ^{13}C NMR spectra for (a) AOST-stat-tBA50, and (b) and the hydrolysed product HOST-stat-tBA copolymer showing the corresponding C peaks. The red boxes show region of the peaks disappeared after hydrolysis.

Figure-4.12 and Figure-4.13 show a comparison of ^{1}H NMR and quantitative ^{13}C NMR spectra of AOST-stat-tBA50 copolymers before and after hydrolysis respectively. The ^{1}H NMR of AOST-stat-tBA50 copolymer shows peak for the methyl proton in the acetoxy group at around 2.3 ppm, which disappears after hydrolysis (Figure-4.12). The removal of acetoxy group through hydrolysis was further confirmed by quantitative ^{13}C NMR. No peaks for carbons 'b' and 'c' in acetoxy group at around 20 ppm and 170 ppm were found after the hydrolysis process as shown in Figure-4.13. By following the same procedure, the AOST homopolymer and all the AOST-stat-tBA, AOST-block-tBA, AOST-grad-tBA copolymers were hydrolysed to produce hydroxyl polymers, and characterized by ^{1}H and quantitative ^{13}C NMR to confirm their compositions.

4.8 Conclusions

In this chapter, the synthesis of PAOST, PtBA homopolymers and HOST-tBA copolymers using RAFT and CvRP methods has been discussed. AOST-tBA statistical copolymers with three different feed compositions were synthesized using PABTC RAFT agent and AIBN initiator. RAFT was found to be successful to produce AOST-stat-tBA copolymers with comparable molecular weight and narrow molecular weight dispersity as characterised by SEC studies. AOST-stat-tBA copolymers with three different feed ratios have also been synthesized by CvRP method, though the molecular weight dispersity was comparatively higher than those of the RAFT copolymers. The ratio of monomer to initiator was adjusted to achieve the copolymer molecular weights comparable to the RAFT copolymers. The compositions of the copolymers were determined using ^{1}H NMR and quantitative ^{13}C NMR studies.

In addition to the statistical copolymers, AOST-tBA gradient copolymers were synthesized using continuous feeding approach. The formation of the gradient structure was evident from the changes in the copolymer composition. With the addition of tBA monomer, as the polymerization progressed, the composition of AOST gradually decreased while the tBA composition increased to produce AOST-grad-tBA copolymers. Beside the statistical and gradient copolymers, AOST-tBA block copolymers have also been synthesized using the chain extension process. By adding tBA monomers to PAOST homopolymer, AOST-block-tBA copolymers were synthesized with compositions similar to those of the statistical and gradient copolymers so as to compare their properties.

Upon successful synthesis of the homopolymers and the copolymers, the acetoxy group from the AOST unit was hydrolysed to produce hydroxystyrene (HOST) homopolymer and copolymers. The acetoxy group was selectively hydrolysed by treating the polymer solution with hydrazine hydrate, and the complete removal of the acetoxy methyl group was confirmed using ^{1}H and quantitative ^{13}C NMR. The peak for the acetoxy methyl group was found to have completely disappeared with that of the t-butyl group remaining intact, to produce PHOST homopolymer, and HOST-tBA copolymers.

4.9 References

[158] Gray MK, Zhou H, Nguyen ST, Torkelson JM. Synthesis and glass transition behavior of high molecular weight styrene/4-acetoxystyrene and styrene/4-hydroxystyrene gradient copolymers made via nitroxide-mediated controlled radical polymerization. Macromolecules. 2004;37:5586-95.

[350] Frechet JMJ, Eichler E, Ito H, Willson CG. Poly(p-tert-butoxycarbonyloxystyrene): a convenient precursor to p-hydroxystyrene resins. Polymer. 1983;24:995-1000.

[351] Ito H, Dalby C, Pomerantz A, Sherwood M, Sato R, Sooriyakumaran R, et al. Monomer Reactivities and Kinetics in Radical Copolymerization of Hydroxystyrene Derivatives and tert-Butyl (Meth)acrylate. Macromolecules. 2000;33:5080-9.

[352] Choi K-W, Prabhu VM, Lavery KA, Lin EK, Wu W-l, Woodward JT, et al. Effect of photoacid generator concentration and developer strength on the patterning capabilities of a model EUV photoresist. Proc SPIE-Int Soc Opt Eng. 2007;6519:651943/1-/9.

[353] Arshady R, Kenner GW, Ledwith A. Phenolic resins for solid phase peptide synthesis. Copolymerization of styrene and p-acetoxystyrene. J Polym Sci, Polym Chem Ed. 1974;12:2017-25.

[354] Ito H, Willson CG, Frechet JMJ, Farrall MJ, Eichler E. Synthesis of poly(p-hydroxy-α-methylstyrene) by cationic polymerization and chemical modification. Macromolecules. 1983;16:510-17.

[355] Huang J, Li X, Guo Q. Interpolymer complexes and miscible blends of poly(p-vinylphenol) and poly(ethyleneimine). Eur Polym J. 1997;33:659-65.

[356] Xu Y, Graf J, Painter PC, Coleman MM. Miscibility windows for poly(styrene-co-vinylphenol) blends with poly(n-butyl methacrylate) and poly(n-hexyl methacrylate): a comparison of theoretical predictions with Fourier transform infrared experimental data. Polymer. 1991;32:3103-18.

[357] Xiang M, Jiang M, Zhang Y, Wu C, Feng L. Intermacromolecular Complexation due to Specific Interactions 4. The Hydrogen-Bonding Complex of Vinylphenol-Containing Copolymer and Vinylpyridine-Containing Copolymer. Macromolecules. 1997;30:2313-9.

[358] Zhao JQ, Pearce EM, Kwei TK. Binary and Ternary Blends of Polystyrene-block-Poly(p-hydroxystyrene). Macromolecules. 1997;30:7119-26.
[359] Long TE, Colby RH, Landry CJT, Landry MR, Long VK, Massa DJ, et al. Effect of compatibilizer architecture on the mechanical and morphological properties of polymer blends and composites. Polym Prepr (Am Chem Soc, Div Polym Chem). 1997;38:385-6.
[360] Barclay GG, Hawker CJ, Ito H, Orellana A, Malenfant PRL, Sinta RF. The "Living" Free Radical Synthesis of Poly(4-hydroxystyrene): Physical Properties and Dissolution Behavior. Macromolecules. 1998;31:1024-31.
[361] Chen X, Jankova K, Kops J, Batsberg W. Hydrolysis of 4-acetoxystyrene polymers prepared by atom transfer radical polymerization. J Polym Sci, Part A: Polym Chem. 1999;37:627-33.
[362] Ito H. Chemical Amplification Resists for Microlithography. Microlithography · Molecular Imprinting: -/-. Berlin, Heidelberg: Springer Berlin Heidelberg; 2005. p. 37-245.
[363] Sovish RC. Preparation and polymerization of p-vinylphenol. J Org Chem. 1959;24:1345-7.
[364] Sweat DP, Yu X, Kim M, Gopalan P. Synthesis of poly(4-hydroxystyrene)-based block copolymers containing acid-sensitive blocks by living anionic polymerization. J Polym Sci, Part A: Polym Chem. 2014;52:1458-68.
[365] Lee T-Y, Lin Y-J, Yu C-Y, Chang J-F. Well-defined diblock and triblock copolymers for KrF lithography. J Appl Polym Sci. 2010;118:3245-54.
[366] Guo Y, Hill DJT, Whittaker AK, Jack KS, Peng H. Terpolymerization of Styrenic Photoresist Polymers: Effect of RAFT Polymerization on the Compositional Heterogeneity. Macromolecules. 2015;48:3438-48.
[367] Thevarajah JJ, Van Leeuwen MP, Cottet H, Castignolles P, Gaborieau M. Determination of the distributions of degrees of acetylation of chitosan. Int J Biol Macromol. 2017;95:40-8.
[368] Thevarajah JJ, Sutton AT, Maniego AR, Whitty EG, Harrisson S, Cottet H, et al. Quantifying the Heterogeneity of Chemical Structures in Complex Charged Polymers through the Dispersity of Their Distributions of Electrophoretic Mobilities or of Compositions. Anal Chem (Washington, DC, U S). 2016;88:1674-81.
[369] Maier H, Malz F, Radke W. Characterization of the Chemical Composition Distribution of Poly(n-butyl acrylate-stat-acrylic acid)s. Macromol Chem Phys. 2015;216:228-34.
[370] Wood MR, Duncalf DJ, Rannard SP, Perrier S. Selective one-pot synthesis of trithiocarbonates, xanthates, and dithiocarbamates for use in RAFT/MADIX living radical polymerizations. Org Lett. 2006;8:553-6.
[371] Couvreur L, Piteau G, Castignolles P, Tonge M, Coutin B, Charleux B, et al. Pulsed-laser radical polymerization and propagation kinetic parameters of some alkyl acrylates. Macromol Symp. 2001;174:197-207.
[372] Gaborieau M, Castignolles P. Size-exclusion chromatography (SEC) of branched polymers and polysaccharides. Anal Bioanal Chem. 2011;399:1413-23.

[373] Junkers T, Schneider-Baumann M, Koo SSP, Castignolles P, Barner-Kowollik C. Determination of Propagation Rate Coefficients for Methyl and 2-Ethylhexyl Acrylate via High Frequency PLP-SEC under Consideration of the Impact of Chain Branching. Macromolecules (Washington, DC, U S). 2010;43:10427-34.
[374] Castignolles P. Transfer to Polymer and Long-Chain Branching in PLP-SEC of Acrylates. Macromol Rapid Commun. 2009;30:1995-2001.
[375] Sheehan MT, Sounik JR. Preparation of co- and terpolymers of p-hydroxystyrene and alkyl acrylates. Triquest, LP, USA . 1999. p. 39 pp.
[376] Vicari R. Process for the suspension polymerization of 4-acetoxystyrene and hydrolysis to 4-hydroxystyrene polymers. Google Patents; 1990.
[377] Choi S-J, Jung S-Y, Kim C-H, Park C-G, Han W-S, Koh Y-B, et al. Design and properties of new deep-UV positive photoresist. Proc SPIE-Int Soc Opt Eng. 1996;2724:323-31.
[378] Messerschmidt M, Millaruelo M, Komber H, Haeussler L, Voit B, Krause T, et al. Synthesis of Partially Protected Block Copolymers Based on 4-Hydroxystyrene Using NMRP and a Sequence of Polymer Analogous Reactions. Macromolecules. 2008;41:2821-31.
[379] Ito H. Chemical amplification resists for microlithography. Adv Polym Sci. 2005;172:37-245.
[380] Kanagasabapathy S, Sudalai A, Benicewicz BC. Reversible Addition-Fragmentation Chain-Transfer Polymerization for the Synthesis of Poly(4-acetoxystyrene) and Poly(4-acetoxystyrene)-block-polystyrene by Bulk, Solution and Emulsion Techniques. Macromolecular Rapid Communications. 2001;22:1076-80.
[381] Ledwith A, Rahnema M, Sen Gupta PK. Phenolic resins for solid-phase peptide synthesis. III. Copolymerization of acrylonitrile and p-acetoxystyrene and comparison of reactivity with styrene-based resins. J Polym Sci, Polym Chem Ed. 1980;18:2239-46.
[382] Gupta B. Selective hydrolysis of copolymers of p-acetoxystyrene and allyl esters of ethylenically unsaturated acids. Hoechst Celanese Corp., USA . 1989. p. 4 pp.

Chapter 5: Properties of Hydroxystyrene – t-Butylacrylate Copolymers

5.1 Thermal Properties

The thermal properties of copolymers are strongly dependent on the composition of the copolymer as well as on their chain structures. The relation between copolymer structure and thermal properties has been discussed in details in chapter-1, and have also been found to be true for styrene-acrylonitrile copolymer system as discussed in chapter-4. The thermal properties of AOST-tBA and HOST-tBA copolymers were studied using both TGA and DSC analysis, and discussed in the following sections.

A number of studies reported the thermal properties of AOST, HOST and tBA monomers using TGA and DSC techniques, and the T_g values were found to vary within a range depending on the polymer molecular weight [360, 383-390]. The ranges of reported T_g values are 112-125 ºC for AOST [383-388], 30-50 ºC for tBA [391, 392], and 150-190 for HOST [360, 385-388, 390] homopolymer. Though a much broader range of T_g (31-107 ºC) for tBA homopolymer is listed in polymer handbook which is noted as conflicting data [393]. This could be due to the branching in the tBA homo and copolymers prepared by radical polymerization. TGA data for AOST, tBA homopolymers, AOST-block-tBA copolymer, and comparison between the homopolymers and the copolymer are given in Figure-5.1. Approximately 4-5 mg of polymer sample was taken in an aluminium pan, and the sample was heated up to 500 ºC at 10 ºC per minute. As the TGA curves and derivatives of TGA curves show, AOST homopolymer starts degrading at temperature slightly higher than 350 ºC, whereas tBA degrades at around 230 ºC temperature which are in good agreement with the TGA data reported for the corresponding homopolymer [383, 390, 394-396]. TGA curve for the AOST-block-tBA50 copolymer shows the degradation of each block at temperatures similar to those of the homopolymers which is clear from the comparison of the TGA curves of the homopolymers with the block copolymer as given in Figure-5.1(d).

The DSC plots for copolymers with similar compositions but three different chain structures are shown in Figure-5.2. Statistical, block and gradient copolymers of AOST-tBA show very different properties in DSC analysis owing to their chain structures, despite having similar copolymer compositions. The DSC plot for AOST-stat-tBA50 copolymer shows a sharp transition at around 95 ºC, which is in between of two homopolymers' T_gs. On the other hand, AOST-block-tBA

copolymer gives two T_g values corresponding to each block, one of them is about 45 ºC belonging to tBA block, and the other one is at near 120 ºC belonging to AOST block.

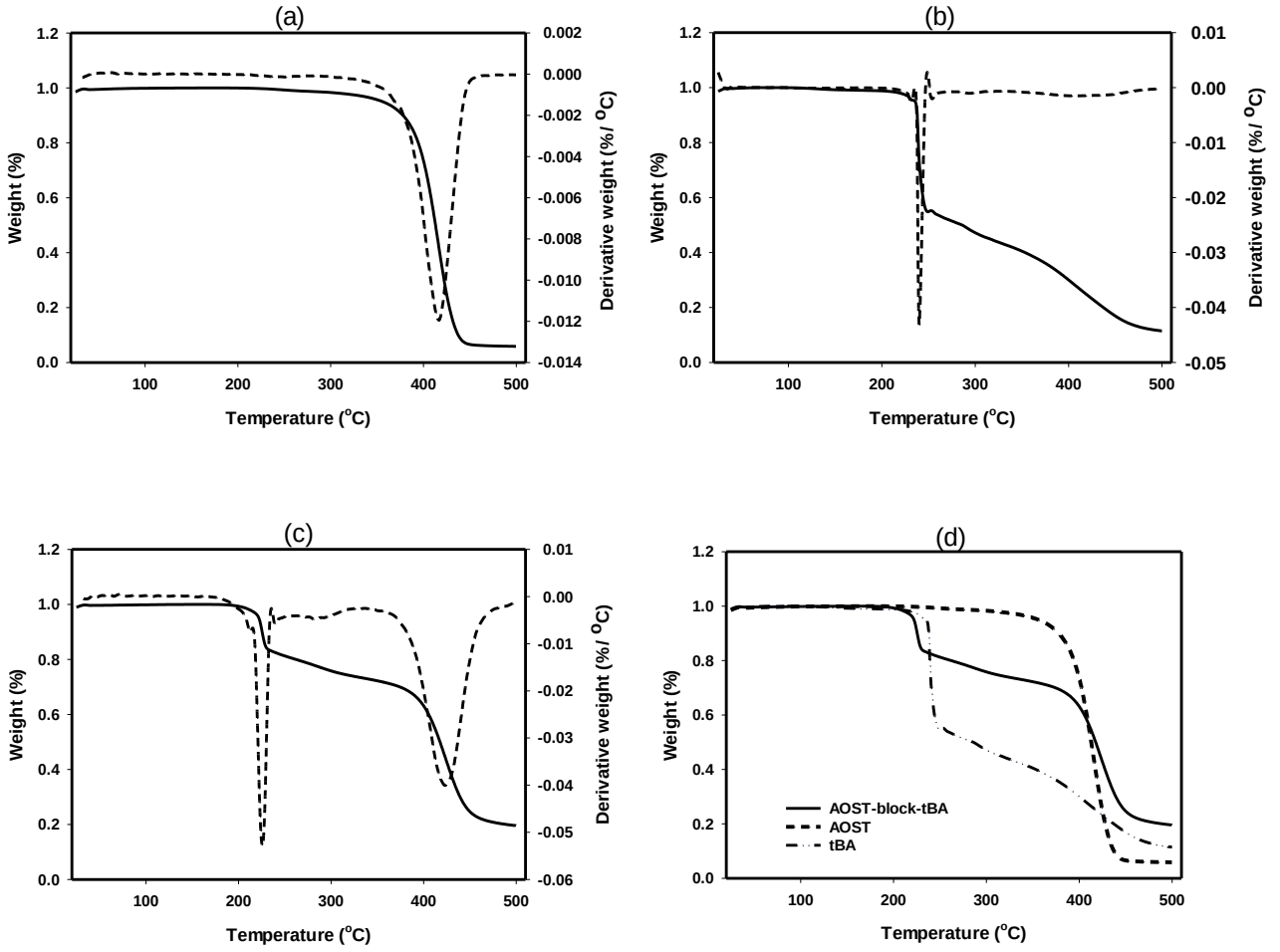

Figure-5.1: TGA curve and TGA derivative curve for (a) AOST homopolymer, (b) tBA homopolymer, (c) AOST-block-tBA copolymer, and (d) comparison of TGA curves for the homopolymers with the block copolymer.

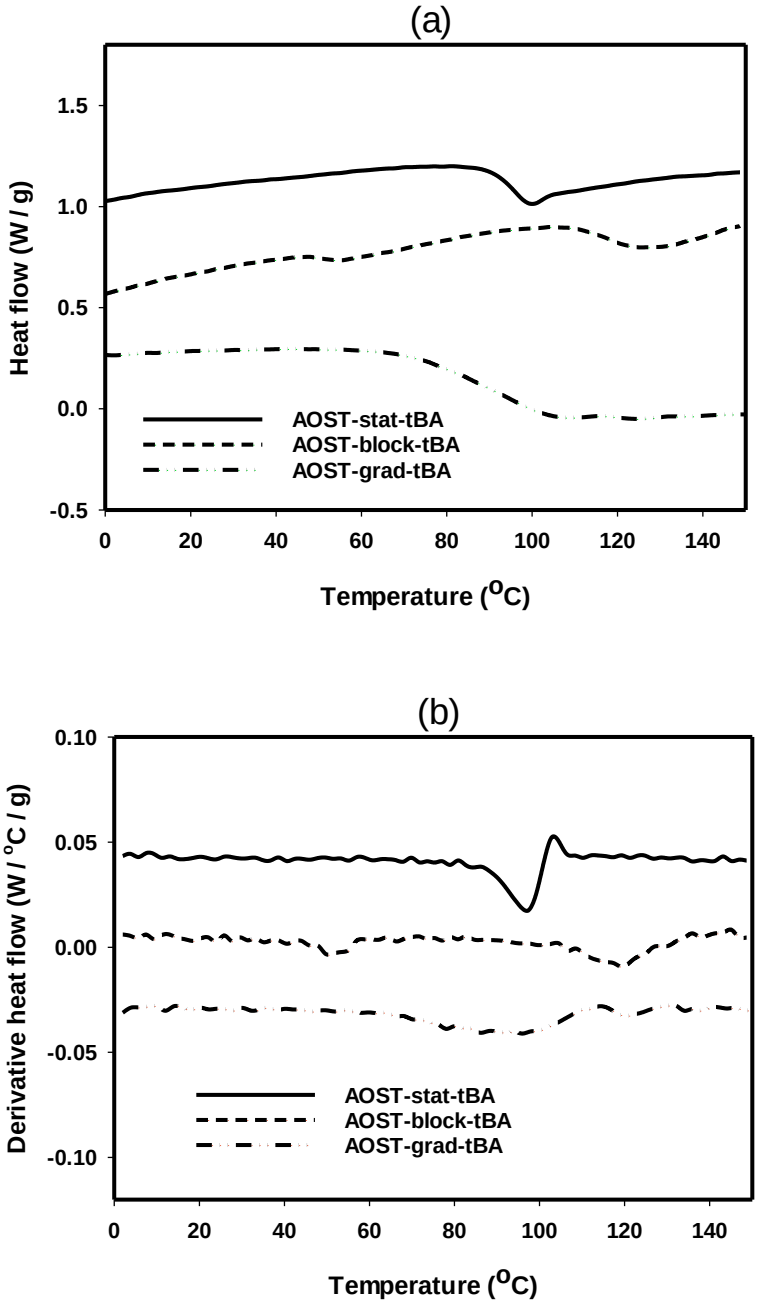

Figure-5.2: (a) Heat flow and (b) derivative heat flow for AOST-stat-tBA, AOST-block-tBA and AOST-grad-tBA copolymers.

The gradient copolymer (AOST-grad-tBA), however, shows very unique nature in DSC analysis. Unlike the statistical and block copolymers, AOST-tBA copolymer with gradient structure gives a single T_g which is unusually broad as shown in the DSC heat flow and derivative heat flow curves in Figure-5.2. This is in good agreement with the thermal behaviour reported for the gradient copolymers in the literature described in chapter-1, and also with the results found for St-AN copolymer system.

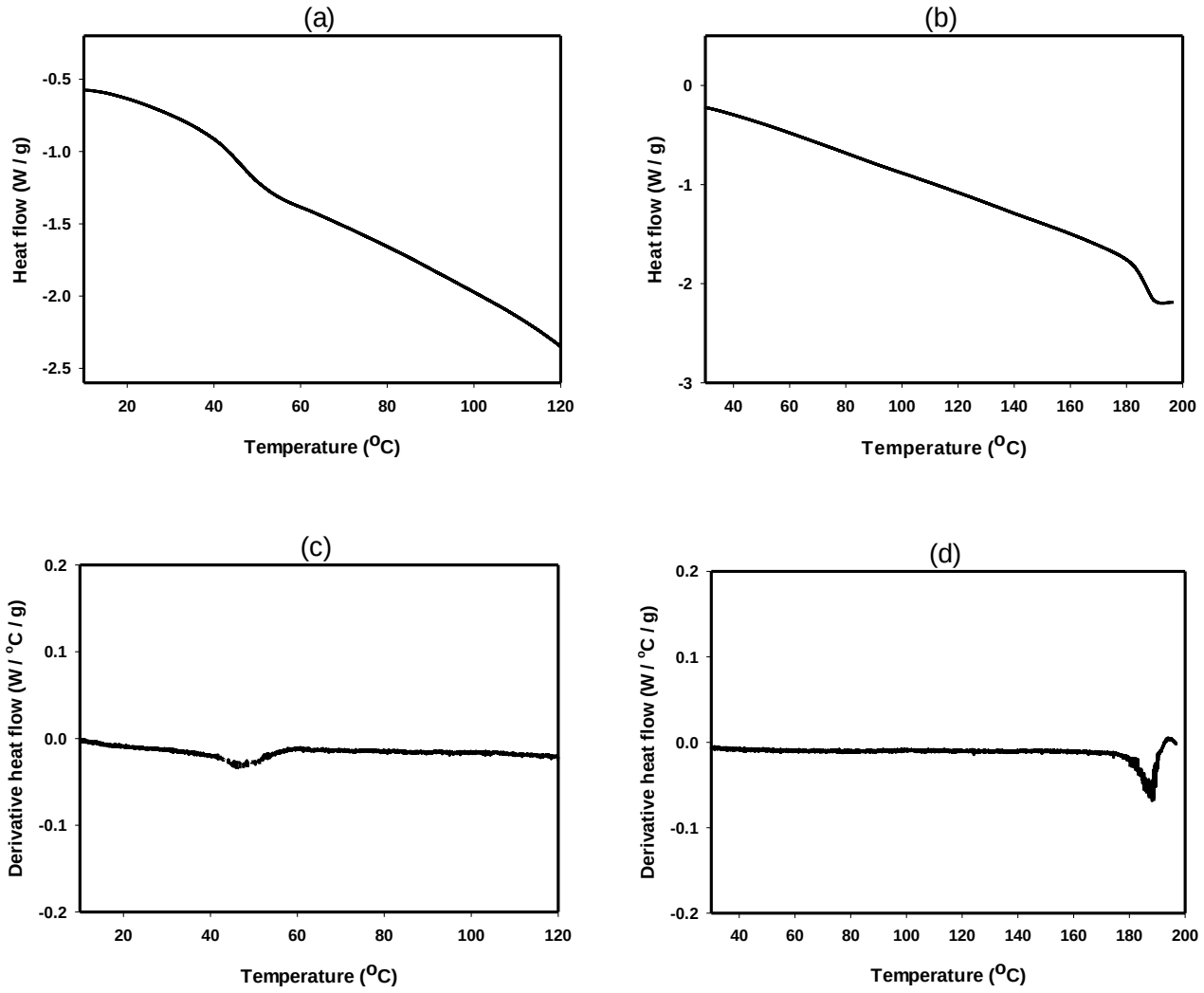

Figure-5.3: Heat flow (a), (b) and derivative heat flow (c), (d) for tBA and HOST homopolymer respectively, characterised by DSC analysis.

The thermal behaviour of the hydrolysed products HOST-tBA copolymers are very different to those of the AOST-tBA copolymers. This is due to the degradation of t-butyl group at low temperature, whereas T_g value of HOST comparatively high. The DSC heating curves and first derivative of DSC heating curves for PtBA and PHOST homopolymers are shown in Figure-5.3. The T_g values were found to be approximately 47 ºC and 188 ºC for PtBA and PHOST homopolymers respectively. A number of papers mention the thermal degradation of PtBA at temperatures as low as 150 ºC [397-401] (the degradation of PtBA will be discussed in detail in the next section with the help of FTIR studies). Therefore, the DSC curves for the HOST-tBA copolymers did not provide any meaningful information about the copolymer structure due to degradation of t-butyl group at low temperature.

5.2 Preparation of HOST-tBA copolymer thin films

Thin films of PHOST, PtBA homopolymers and HOST-tBA copolymers were prepared by spin coating of polymer solution on to silicon wafer. 3 wt% polymer solution was prepared using propylene glycol methyl ether acetate (PGMEA) as solvent, and the solution was passed through a PTFE 0.45 micron 13 mm filter to remove any insoluble particles. Prior to applying the polymer solution, the silicon wafer was cleaned by sonicating in isobutyl alcohol, methanol and acetone, for five minutes in each. The polymer solutions were spin coated for 60 s at 4000 rpm to achieve homogeneous homopolymer and copolymer thin films. Thickness data were collected using Filmtek to confirm the homogeneity of the films as shown in Figure-5.4. The thickness of the HOST-tBA copolymers were found to be approximately 100 nm with standard deviation less than 3 nm. The spin coated thin films were then kept in the vacuum oven for 48 hours at room temperature to get rid of any remaining solvent on the film surface.

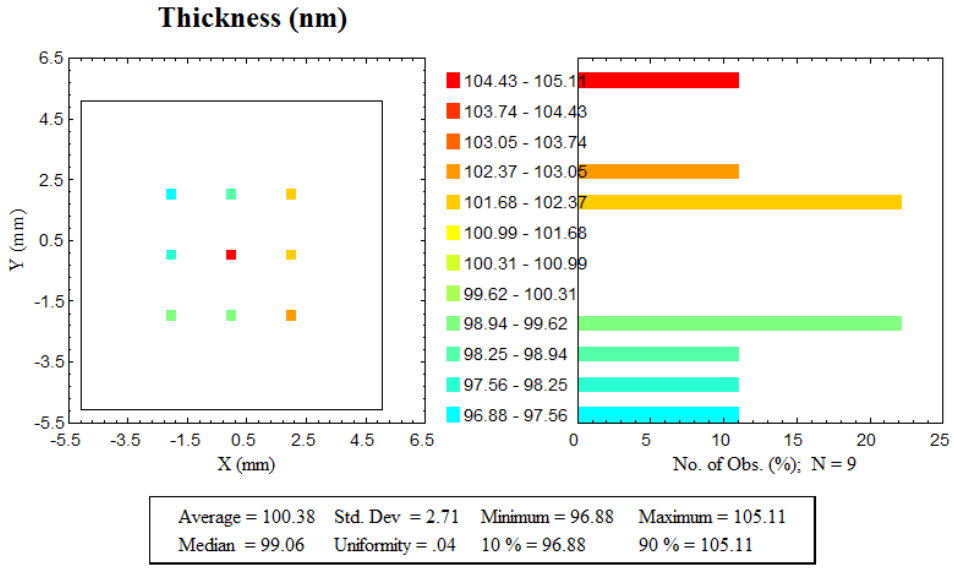

Figure-5.4: Thickness data for AOST-stat-tBA50 copolymer thin films on silicon wafer, collected by Filmtek.

5.3 GATR-FTIR studies of HOST-tBA copolymer thin films

The thin films of PHOST, PtBA homopolymers, and the HOST-tBA copolymers were characterized and studied using grazing angle attenuated total reflection – Fourier transform infrared (GATR-FTIR) spectroscopy. The FTIR data were collected using a Nicolet 5700 spectrometer and the background spectra were obtained on a cleaned silicon wafer. The data were collected on absorption mode with resolution 4 cm^{-1} and 256 scans for wavelength range 4000-400 cm^{-1}. Figure-5.5 shows the GATR-FTIR spectra for PHOST and PtBA homopolymers. The spectrum for PHOST shows the characteristic broad peak at around 3400 cm^{-1} for OH group, and another peak at around 1610 cm^{-1} for C=C in the benzene ring. On the other hand, PtBA gives characteristic peak for the carbonyl group at around 1725 cm^{-1}.

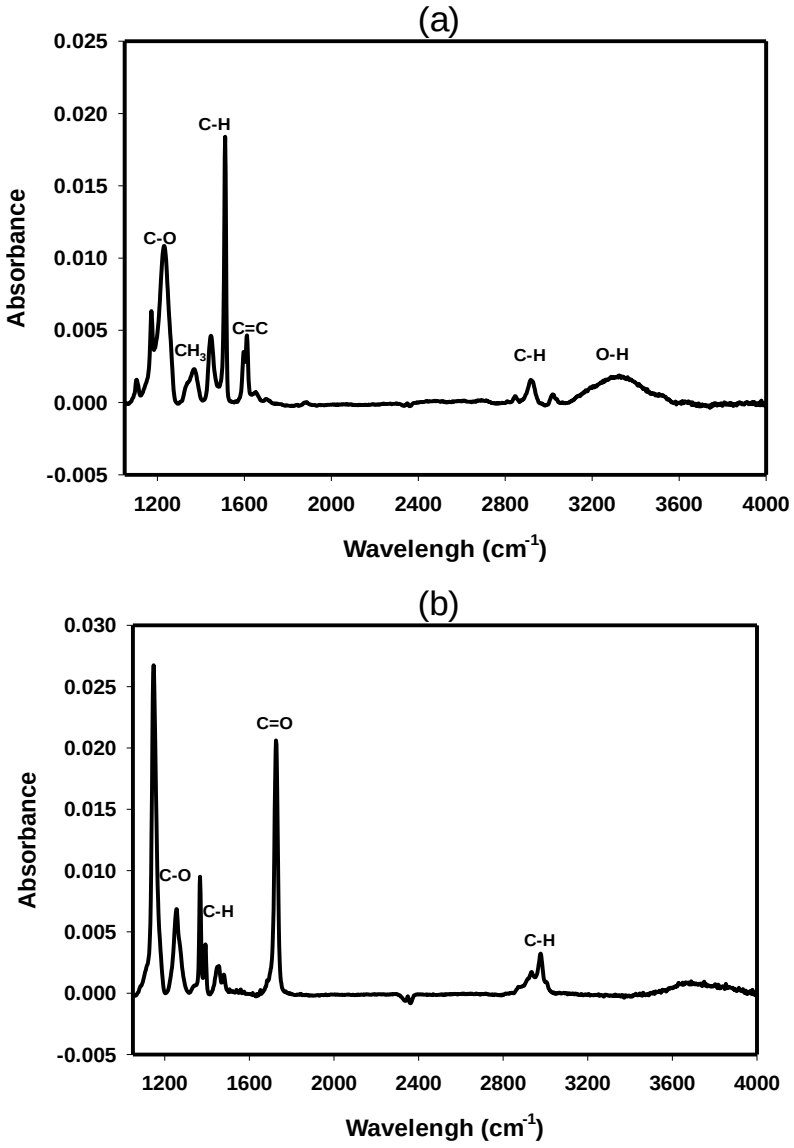

Figure-5.5: GATR-FTIR absorption spectra for (a) PHOST and (b) PtBA homopolymers showing the corresponding peaks.

Thermal degradation of homopolymer and copolymers of tBA were discussed in a number of studies [397-401]. At temperatures higher than 150 ºC, t-butyl acrylate has been reported to form anhydride, and shown with the help of FTIR spectra [402, 403]. The peak for the ester carbonyl group (1725 cm^{-1}) in the GATR-FTIR spectrum was reported to be shifted to 1752 and 1804 cm^{-1} due to the formation of anhydride as a result of the annealing process. This has been found true for PtBA homopolymer and HOSt-tBA copolymers in this study. Figure-5.6 shows the comparison of GATR-FTIR data of PtBA homopolymer before annealing, and also for PtBA thin film annealed at 150 ºC for two hours. The degradation of tBA group is clear from the change in the peaks from 1600 to 1850 cm^{-1} due to the formation of anhydride.

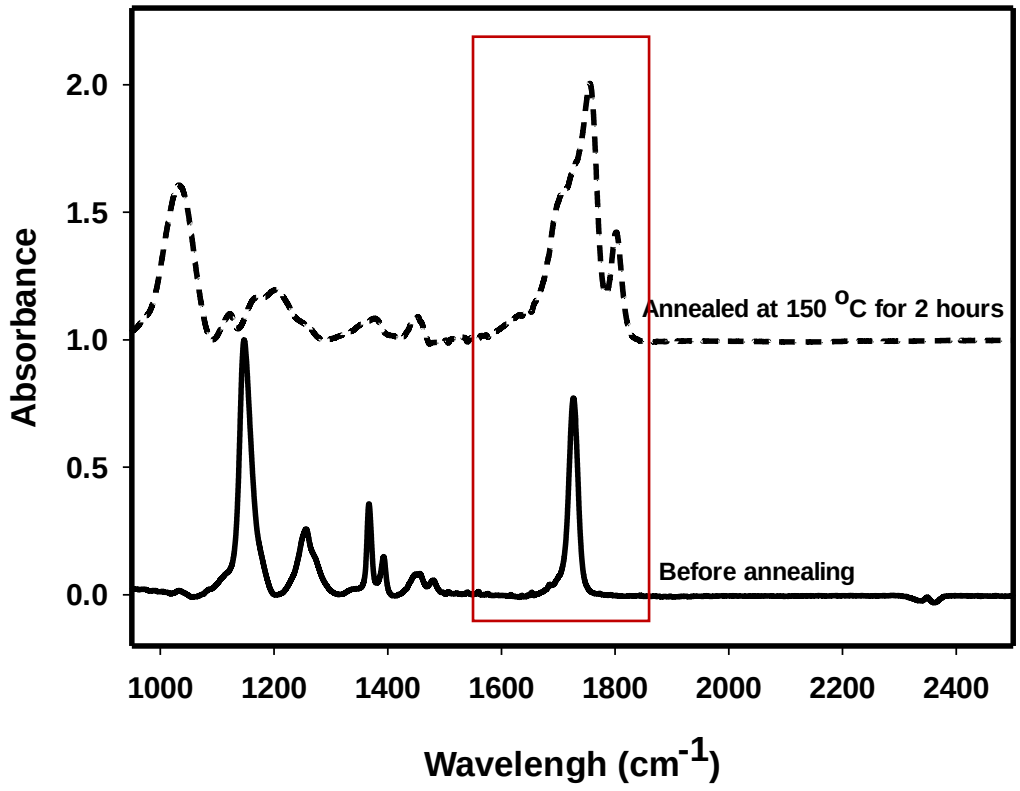

Figure-5.6: GATR-FTIR spectra of PtBA homopolymer before and after annealing process showing the change in the carbonyl peak.

The mechanism of thermal degradation of PtBA is well established, and involves two steps [402, 403]. In the first step, the elimination of the t-butyl group as alkene produces acrylic acid, and the second step involves dehydration of the produced carboxylic acid to give six-membered cyclic anhydride and water [402].

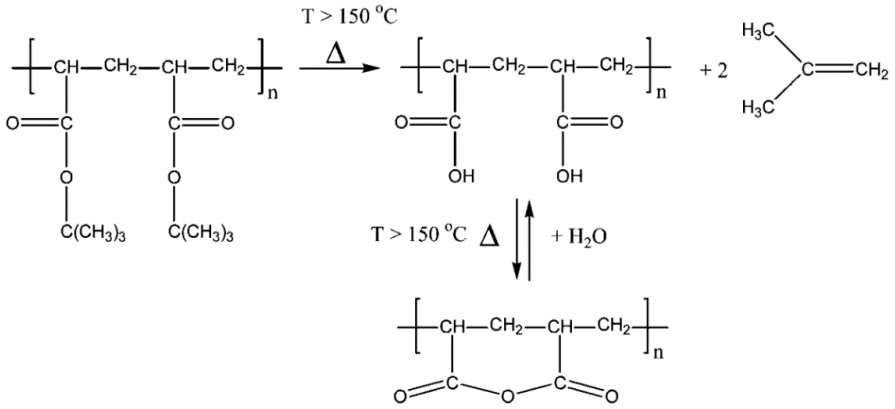

Figure-5.7: Mechanism of thermal degradation of PtBA [403].

The GATR-FTIR spectra of three different compositions of HOST-stat-tBA copolymers were compared to the PHOST and PtBA homopolymers in Figure-5.9. The intensity of the carbonyl peak at 1725 cm^{-1} increases with increasing tBA composition in the HOST-tBA copolymers. In contrary, the intensity of the unsaturated carbon (C=C) peak at 1610 cm^{-1} decreases due to the decrease in HOST composition in the copolymers. Interestingly, for the HOST-tBA copolymers, an extension to the carbonyl peak was noticed at 1698 cm^{-1}. Many papers have assigned this peak to the carbonyl group H-bonded to the OH group of the hydroxystyrene unit [404-409]. The presence of H-bonded carbonyl group peak was discussed in detail on many occasions for copolymer blends, specifically for blends containing PHOST (which is also known as 'poly(vinyl phenol)') copolymers such as blends of PHOST with poly(vinyl acetate) [404], poly(ethylene-vinyl acetate) [404], poly(*β*-propiolactone) [405], poly(vinyl alkyl ethers) [405], poly(ethylene oxide) [405], poly(*N*-vinyl pyrrolidone) [405], poly(n-alkyl methacrylates) [407], poly(2-ethoxyethyl methacrylate) [408] etc. The hydrogen bond could either be self-association/intra-association between the OH groups of PHOST or inter-association between OH group of PHOST and carbonyl group of PtBA [408, 410].

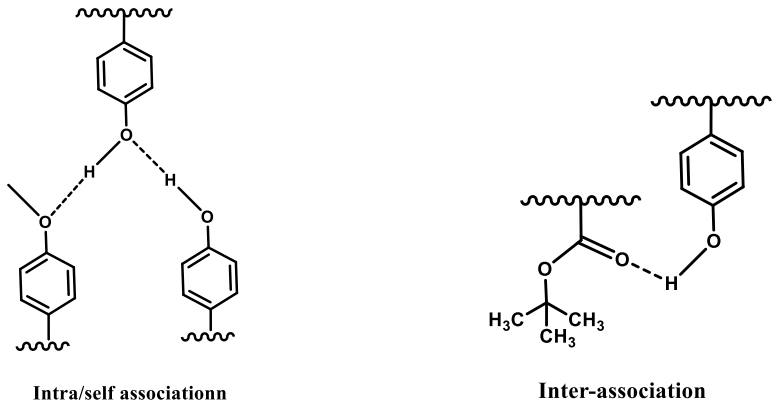

Figure-5.8: Hydrogen bonding between PHOST units, termed as intra/self-association, and hydrogen bonding between PHOST and PtBA units, termed as inter-association.

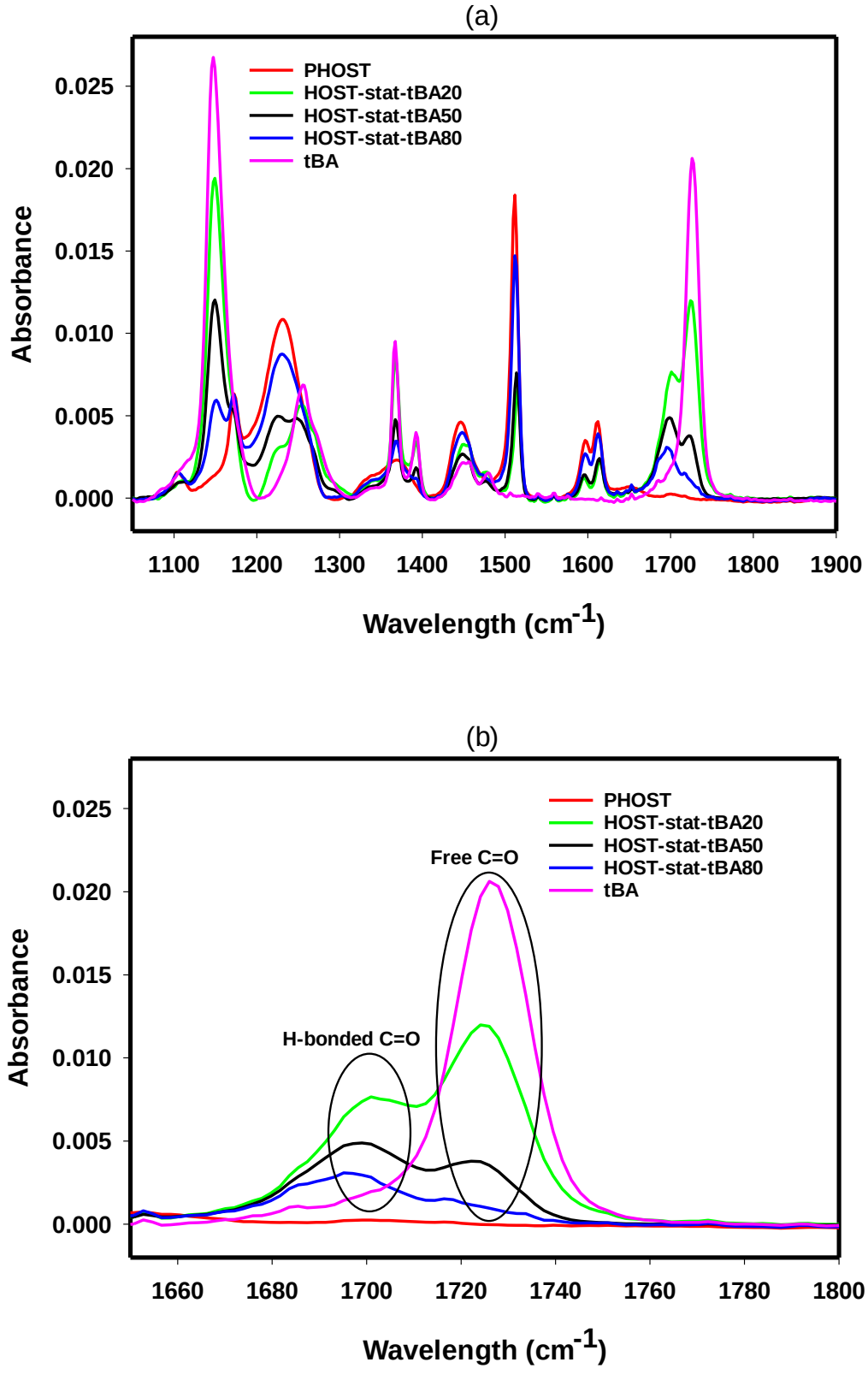

Figure-5.9: (a) GATR-FTIR spectra comparison of HOST-stat-tBA copolymers with those of the PHOST and PtBA homopolymers, (b) shows the comparison of the carbonyl peak region of the homopolymers and copolymers.

The two characteristic band for free carbonyl group and hydrogen bonded carbonyl group in the carbonyl stretching region of HOST-stat-tBA copolymers could be quantitatively analysed using peak-fitting software. Figure-5.10 shows the components of the carbonyl group peak for three different compositions of HOST-stat-tBA copolymers. It is clear from the ratio of the peak fitting plots that, the fraction of the hydrogen bonded carbonyl group increases with increasing composition of HOST in the copolymers. This is due to the availability of OH group to form hydrogen bond. For HOST-stat-tBA20 copolymers, due to low HOST fraction in the copolymer, there are not much OH group to form hydrogen bond. Whereas for HOST-stat-tBA80 copolymers, plenty of OH groups are available for hydrogen bond formation and therefore the fraction of hydrogen bonded carbonyl is very high compared to that of the free carbonyl group for this composition.

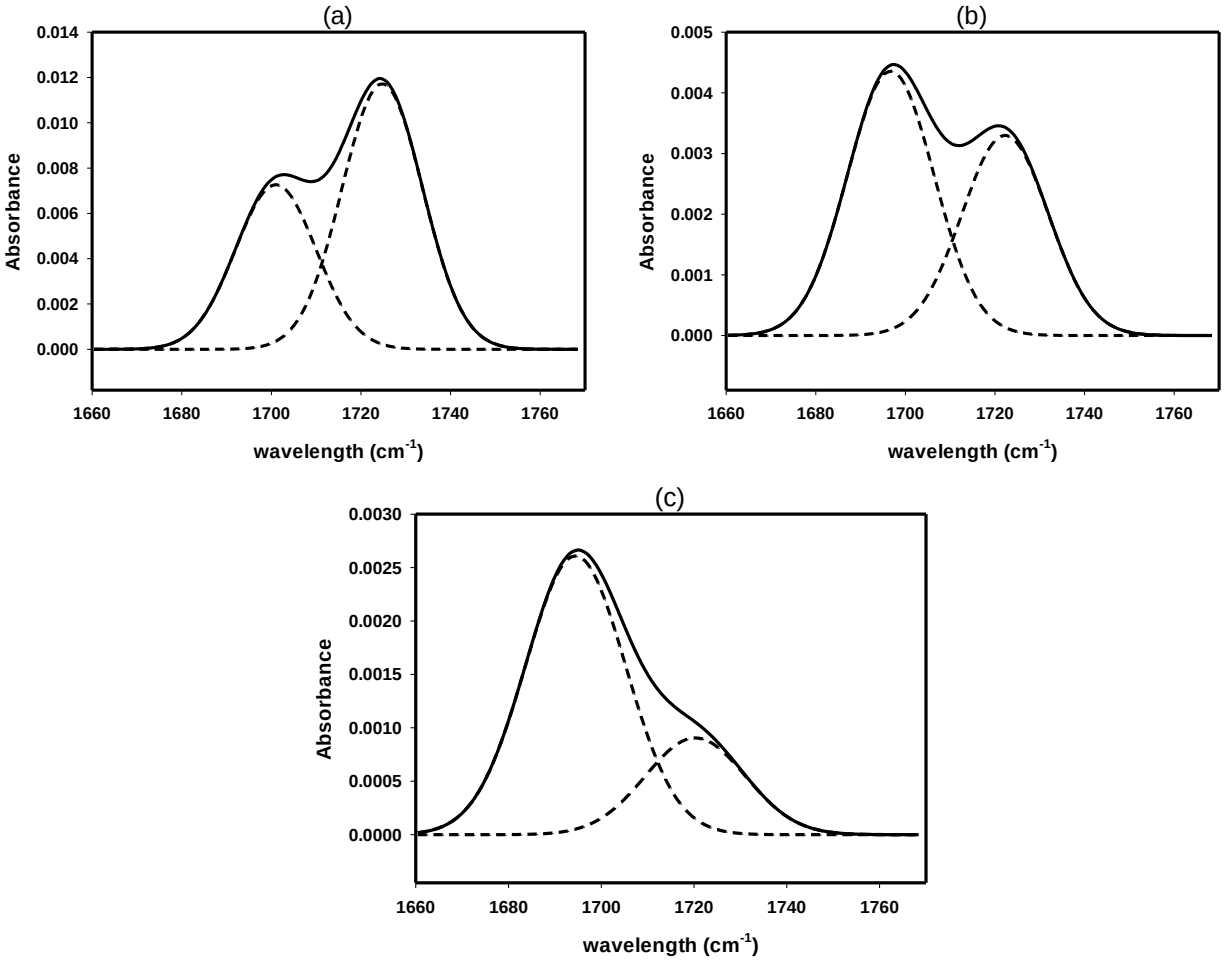

Figure-5.10: Carbonyl peak region in GATR-FTIR spectra for (a) HOST-stat-tBA20, (b) HOST-stat-tBA50 and (c) HOST-stat-tBA80 copolymers, showing the peaks for 'free' carbonyl group at 1725 cm^{-1}, and H-bonded carbonyl group at 1698 cm^{-1}.

Typical molar absorptivity ratio (due to the differences in the relative intensities between the hydrogen bonded and non-hydrogen bonded fractions) has been reported to fall within the range 1.2-1.5 [411]. Assuming the absorptivity ratio to be 1.5 for HOST-tBA system, the fractions of the free carbonyl and hydrogen bonded carbonyl groups were determined for HOST-stat-tBA copolymers, given in Table-5.1.

Table-5.1: Position, area and composition of the hydrogen bonded carbonyl and free carbonyl group peaks for HOST-stat-tBA copolymers.

Designation	**H-bonded carbonyl group**		**Free carbonyl group**		**H-bonded C=O: Free C=O**
	Peak position (cm^{-1})	**Peak area***	**Peak position (cm^{-1})**	**Peak area***	
HOST-stat-tBA80	1695.3	0.077	1722.5	0.018	74:26
HOST-stat-tBA50	1698.4	0.144	1725.2	0.090	52:48
HOST-stat-tBA20	1701.4	0.196	1725.8	0.211	38:62

* arbitrary unit

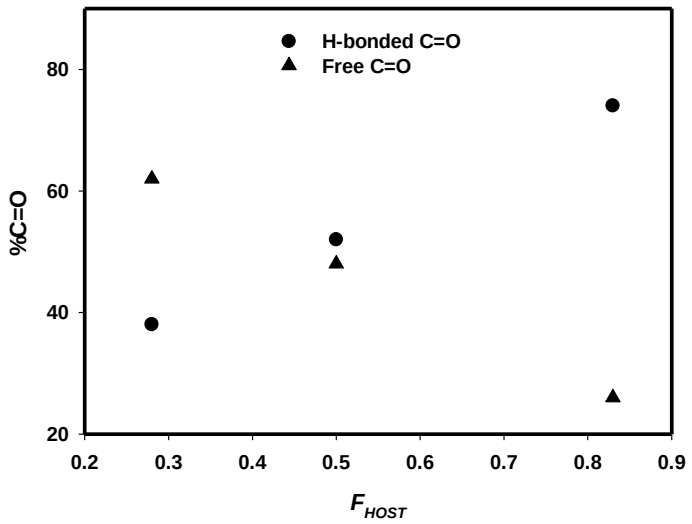

Figure-5.11: Change in the fraction of free carbonyl group and hydrogen bonded carbonyl group with HOST composition in HOST-stat-tBA copolymers.

The change in the fraction of hydrogen bonded carbonyl group and free carbonyl group against the HOST composition in the copolymer has been shown in Figure-5.11. With the increasing HOST composition, the fraction of hydrogen bonded carbonyl group is found to increase linearly, while the opposite happened to the free carbonyl fraction. However, the hydrogen bonding in the HOST-tBA copolymer not only depends on the copolymer composition, but also depends on the copolymer structure. The carbonyl stretching region in GATR-FTIR spectra for HOST-tBA statistical, gradient and block copolymers with similar copolymer composition is shown in Figure-5.12.

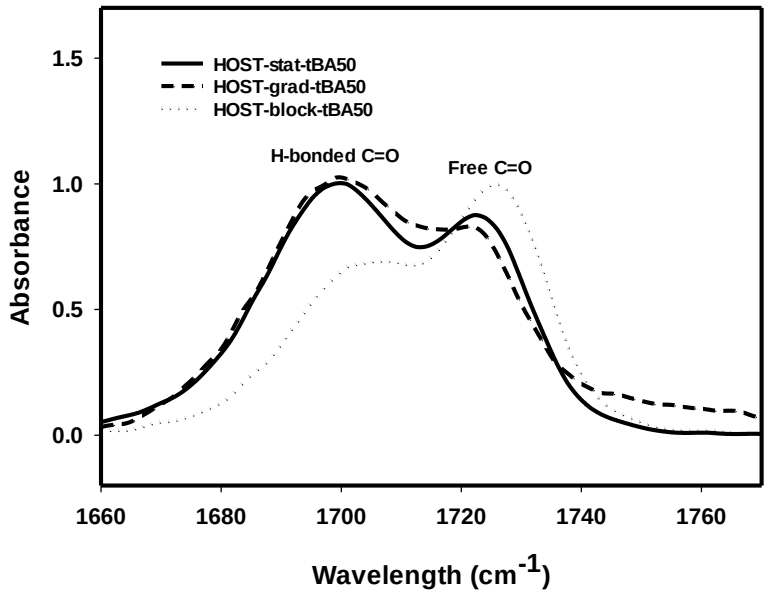

Figure-5.12: Comparison of the carbonyl stretching region of statistical, gradient and block HOST-tBA copolymers, showing the hydrogen bonded and free carbonyl bands.

The fractions of the hydrogen bonded carbonyl and free carbonyl bands were quantified using peak fitting software, and listed in Table-5.2. The hydrogen bonding was found to be maximum for statistical copolymer, and it was minimum for the block copolymer. In HOST-tBA statistical copolymers, there are enough HOST units containing OH group near to the carbonyl group to form hydrogen bonds. But it is not the case for the block copolymer, and hence has very low fraction of hydrogen bonded carbonyl group. HOST-grad-tBA copolymers, however has sequences of short blocks in the middle of the chain with longer blocks towards the ends of the chain. Therefore, the fraction of hydrogen bonded carbonyl group is less than the statistical copolymers, but greater than that of the block copolymers.

Table-5.2: Hydrogen bonded carbonyl and free carbonyl group bands for statistical, gradient and block HOST-tBA copolymers with similar compositions.

Designation	H-bonded carbonyl group		Free carbonyl group		H-bonded C=O: Free C=O
	Peak position (cm^{-1})	Peak area*	Peak position (cm^{-1})	Peak area*	
HOST-stat-tBA50	1698.4	0.144	1725.2	0.090	52:48
HOST-grad-tBA50	1696.7	22.90	1720.50	17.33	47:53
HOST-block-tBA50	1700.7	14.26	1725.2	21.69	30:70

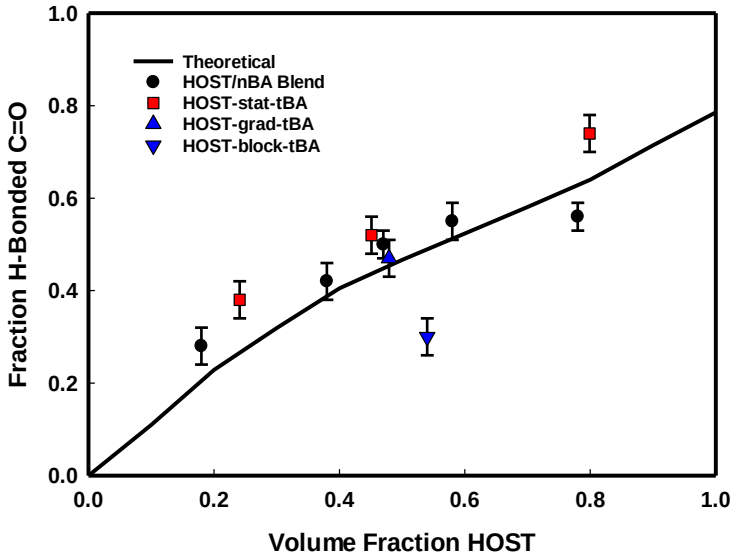

Figure-5.13: The comparison of the hydrogen bonded carbonyl group fraction of HOST-tBA statistical, gradient and block copolymer to the theoretical and experimental results reported by Coleman et al. [412] for PHOST/PnBA blends.

Coleman and co-workers [405, 407, 412] studied binary polymer blends of PHOST where the components interact through the formation of hydrogen bonds. Using an equation for the volume fractions of self-associating and non-self-associating species, they predicted the fraction of hydrogen bonded carbonyl group for several PHOST blends including PHOST/PnBA blend, and compared that to the experimentally determined data. They found very good agreement between the experimental hydrogen bonded carbonyl group fraction in the blend and the theoretical data. In this study, the plot for predicted hydrogen bonded carbonyl group has been generated for PHOST/PnBA blend using the data reported by Coleman et al. [412], and the data for HOST-tBA statistical, block and gradient copolymers have been compared as shown in Figure-5.13. The molar volume of tBA and nBA were found to be close (44.35 and 44.36 cm^3/mol respectively) as calculated from the data table given by Krevelen et al. [413] Therefore the predicted data for PHOST/PnBA and PHOST/PtBA are essentially same, and was used to compare the experimental data for PHOST-PtBA copolymer system. Reasonable agreement has been found for the statistical and gradient copolymers, but the fraction of hydrogen bonded carbonyl in the HOST-block-tBA copolymer was significantly lower than the prediction. This could be explained based on the fact that, due to the blocks being distinctly separate from each other, the carbonyl group does not have access to as many closely adjacent OH groups to form H bonds.

5.4 XPS Studies of HOST-tBA Copolymer Thin Films

X-ray photoelectron spectroscopy has been effectively used on many occasions to characterise the thin film surface of the copolymers or copolymer blends containing HOST and tBA units [414-417]. The PHOST, PtBA homopolymers, and the HOST-tBA copolymer thin films prepared by spin coating were characterised using the XPS technique to study the surface compositions.

The survey and high resolution XPS spectra for PHOST and PtBA homopolymers, and HOST-stat-tBA50 copolymer thin films have been given in Figure-5.14, Figure-5.15 and Figure-5.16 respectively. Both the homopolymers, and the copolymer show C 1s and O 1s peaks at binding energy around 285 eV and 532 eV respectively, though the ratio of C and O are different in the homopolymers and the copolymers.

The high resolution XPS spectra show the components of C 1s and O 1s peaks for the homopolymers and the copolymer. PHOST homopolymer contains both aliphatic and aromatic carbons, and also C-O, which are shown in high resolution C 1s and O 1s spectra for PHOST. Similarly, the components of C 1s (C-C/CH_2, C*COO, C-O, C=O) and O 1s (C=O*-O, C=O-O*) have been shown for PtBA in Figure-5.15. High resolution spectra of the HOST-tBA copolymers contain all the components from the homopolymers as shown in Figure-5.16.

The compositions of the HOST-tBA copolymer thin film surfaces were determined from XPS survey spectra, using the ratio of C and O in the copolymers. The survey spectra were collected with pass energy 160 eV at a 1.0 eV step size. For the high resolution spectra, the pass energy was 20 eV and the step size was 0.05 eV.

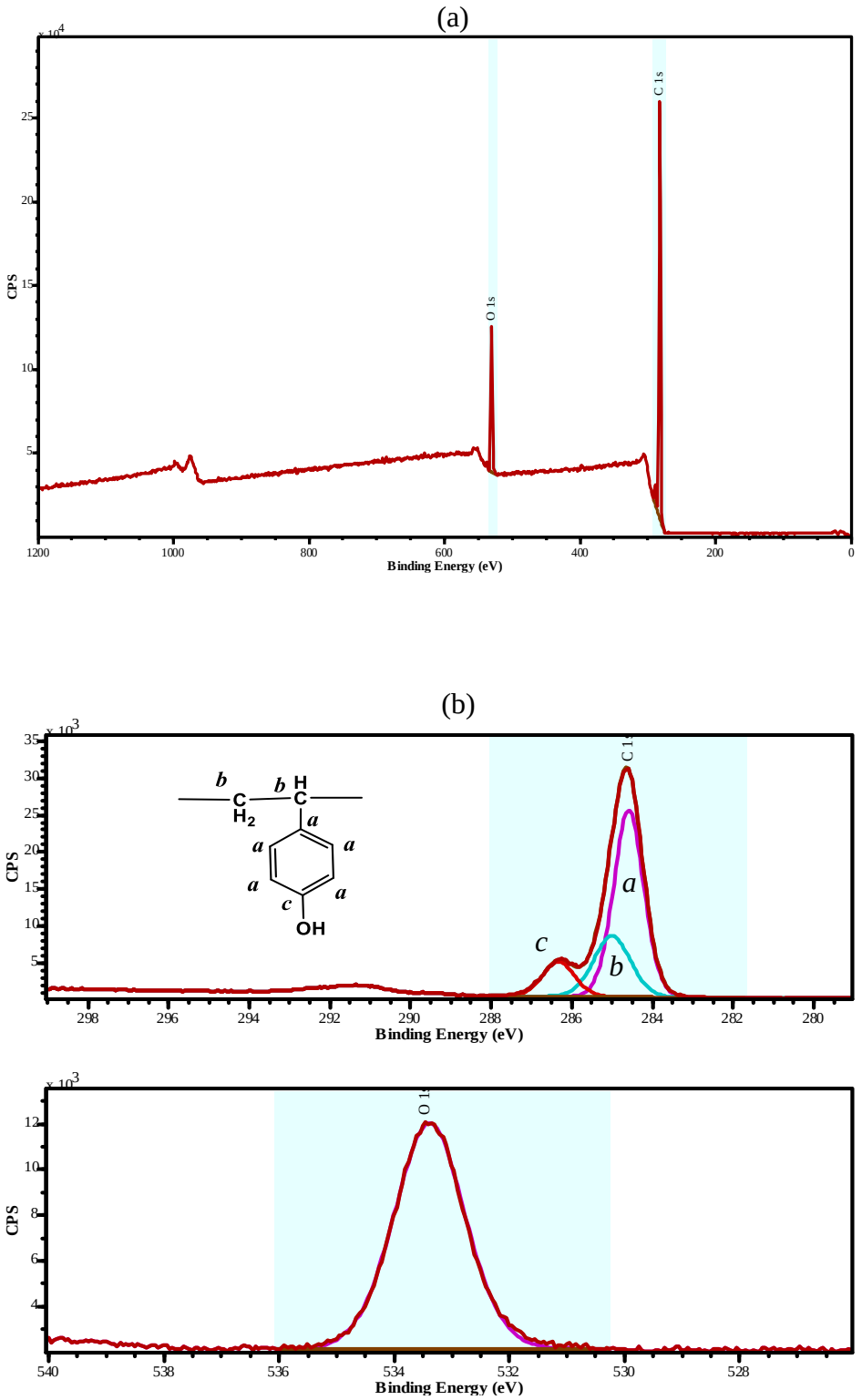

Figure-5.14: (a) Survey and (b) high resolution XPS spectra for PHOST homopolymer thin film.

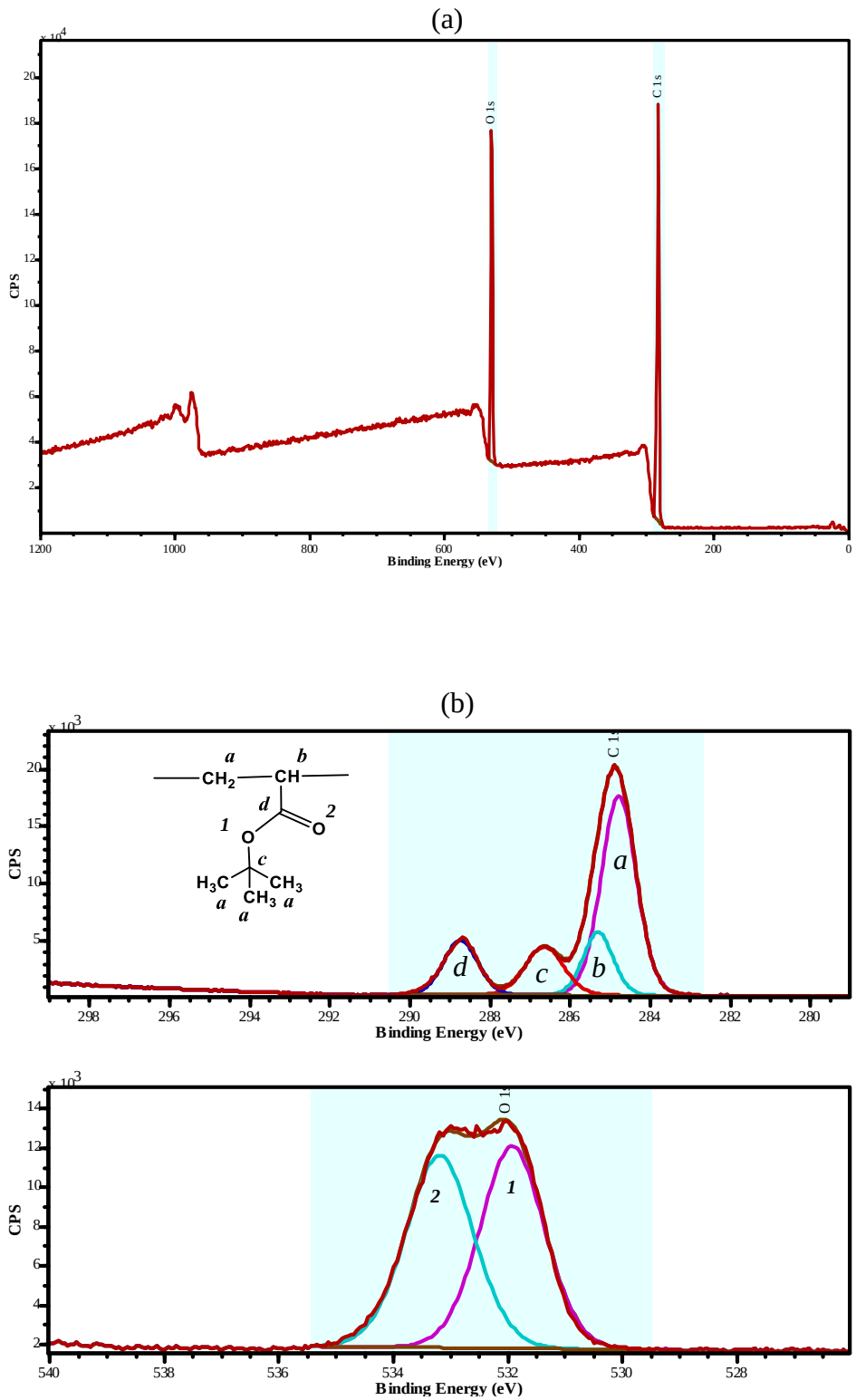

Figure-5.15: (a) Survey and (b) high resolution XPS spectra for PtBA homopolymer thin film.

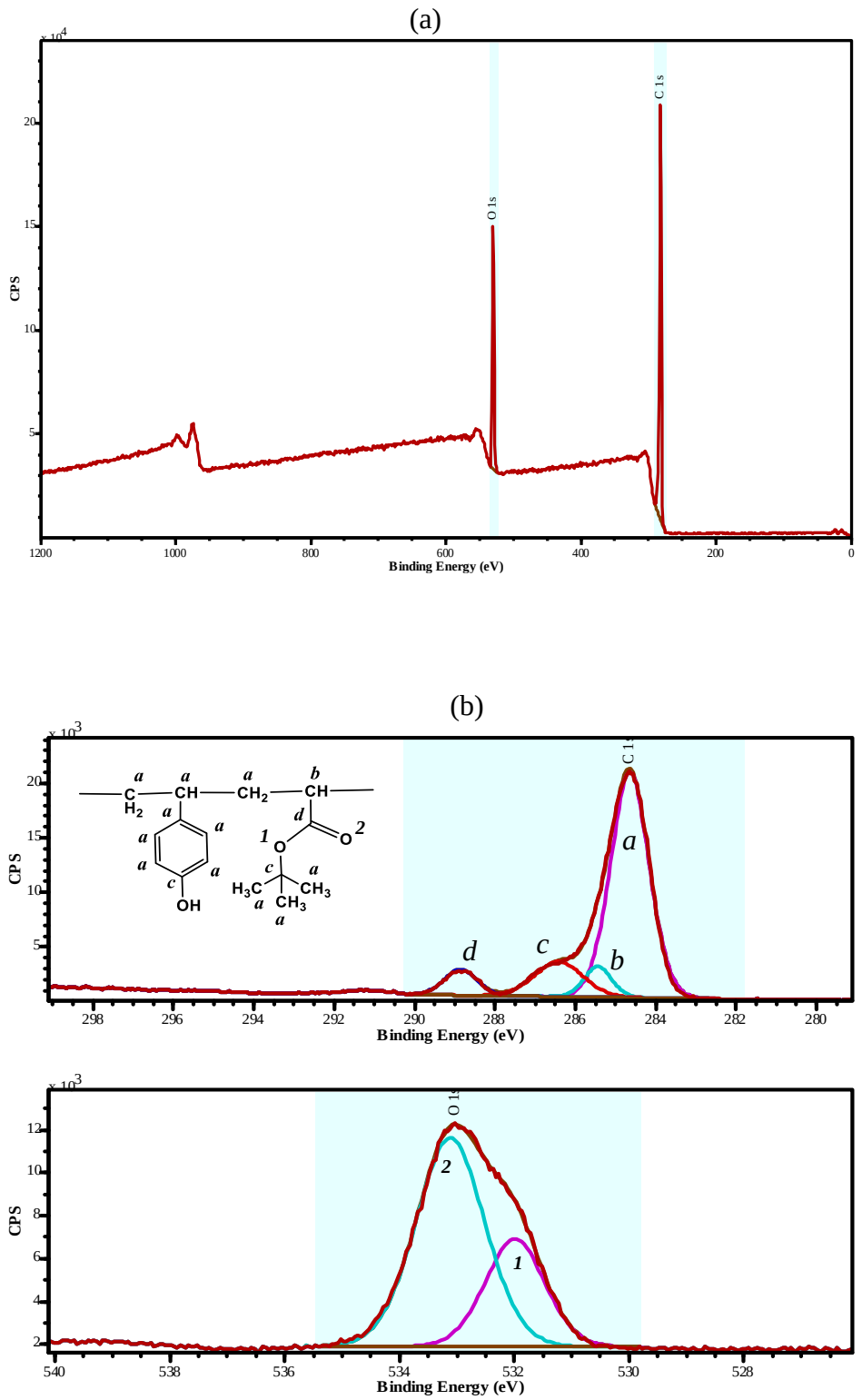

Figure-5.16: (a) Survey and (b) high resolution XPS spectra for HOST-stat-tBA50 copolymer thin film.

XPS survey spectra of the PHOST, PtBA homopolymer, and HOST-tBA copolymer thin films were used to calculate the C/O ratio on the polymer thin film surface. Figure-5.17 and Figure-5.18 show the C/O ratio of the copolymers on the thin films surface plotted against the expected C/O ratios. The expected C/O ratios of the copolymers were calculated using the copolymer composition determined by ^{13}C NMR. The error bars in the plot was calculated from six measurements for a single data.

The measured C/O vs expected C/O on the thin film surface of homopolymers, as well as statistical, block and gradient copolymers synthesized by RAFT method is shown in Figure-5.17. For both the un-annealed and annealed thin films, the measured C/O was found to increase with the expected C/O. Though, the measured C/O ratio for PtBA homopolymer and HOST-tBA copolymers with low expected C/O is slightly higher than the expected line, while XPS gives slightly lower C/O for PHOST homopolymer and HOST-tBA copolymer with high C/O value. However, the measured C/O for the block copolymer was significantly lower than the expected line.

The copolymer thin films were then annealed at 130 ºC temperature for 60 s, based on thermal degradation data in this study and temperature reported by Ito et al. [418] for same copolymer pair. XPS data collected annealed polymer thin films are given in Figure-5.17 (b). As Figure-5.17 (b) shows, the measured C/O value slightly increases for the block copolymer as a result of annealing, but decreases for HOST-tBA gradient copolymer. Other than that, no significant annealing effect has been noticed for the HOST-tBA copolymer thin films.

Figure-5.18 shows the comparison of the thin film surface composition for HOST-stat-tBA copolymers synthesized by RAFT and CvRP methods. The C/O value for the CvRP copolymers are slightly lower than those of the RAFT copolymer thin films with similar expected C/O values. After annealing the thin films at 130 ºC for 60 s, C/O values for the RAFT copolymers slightly decreases but an increase in the CvRP copolymers C/O values was noticed. However, the difference of the C/O values before and after annealing was very small to relate to the structural differences between the HOST-stat-tBA copolymers synthesized by the two different methods.

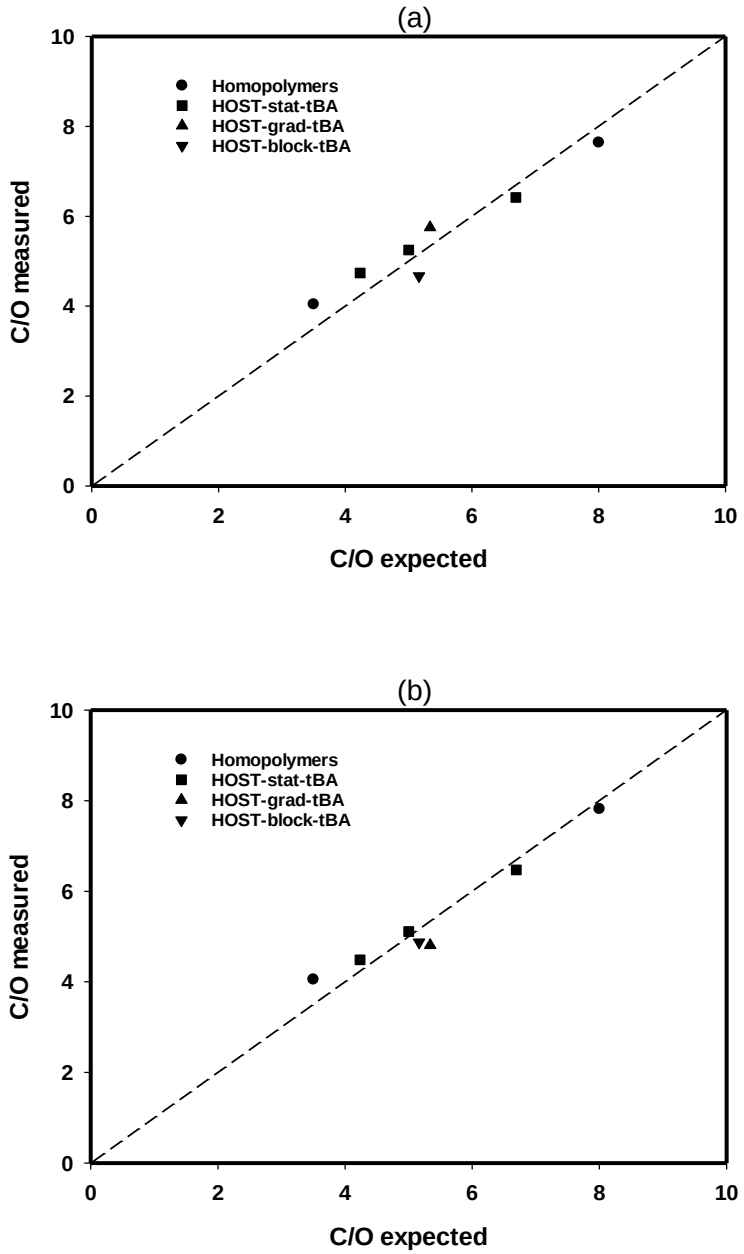

Figure-5.17: The measured C/O plotted against the expected C/O ratio for the homopolymers, HOST-tBA statistical, gradient and block copolymers synthesized by RAFT method (a) before annealing, and (b) after annealing at 130 ºC for 60 s.

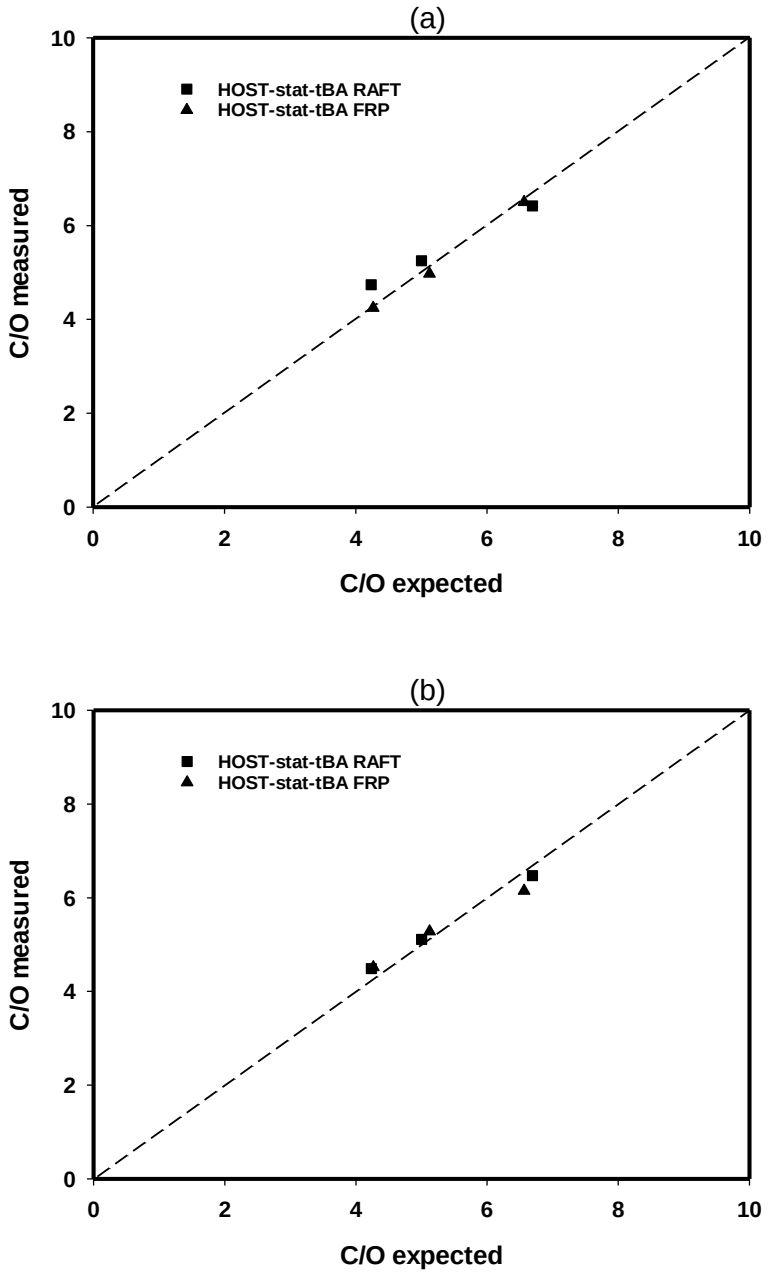

Figure-5.18: The measured C/O plotted against the expected C/O ratio for the HOST-stat-tBA copolymers synthesized by RAFT and CvRP methods (a) before annealing, and (b) after annealing at 130 ºC for 60 s.

5.5 Contact Angle and Surface Energy Studies of HOST-tBA Copolymer Thin Films

A number of studies reported the contact angle and surface free energy of copolymer thin films containing HOST [419-424] and tBA [415-417, 425] units. In this study, the surface free energies of PHOST, PtBA homopolymers and HOST-tBA copolymer thin films were determined by measuring the contact angles of water and diiodomethane on the thin film surface. The static contact angle of polymer thin films was measured using an OCA20 contact angle system at room temperature and the error was estimated from six measurement for a single data point. The dispersive and polar components of surface energy of water and diiodomethane is given in Table-5.3. The surface free energy was calculated from the dispersive and polar components by geometrical mean method.

Table-5.3: The geometric mean surface free energy components for water and diiodomethane [343].

Test liquid	Dispersive component, γ_L^d (mJ m^{-2})	Polar component, γ_L^p (mJ m^{-2})	Total surface free energy γ_L (mJ m^{-2})
Water	21.8	51.0	72.8
Diiodomethane	49.5	1.3	50.8

Contact angle of water and diiodomethane was measured on the as spin coated polymer thin films, and also after annealing the thin films at 130 ºC for 60 s. For PHOST homopolymer thin film, the contact angle for water and diiodomethane was found to be 65.8º and 31.6º respectively, while the values for PtBA were 85.5º and 49.5º. These contact angle values for the PHOST and PtBA homopolymers found in this experiment are in good agreement with the reported values [416, 417, 420, 421]. PtBA homopolymer thin films are more hydrophobic due to the presence of the t-butyl group, and the OH group makes PHOST more hydrophilic in nature.

The contact angle values for water and diiodomethane on the HOST-tBA copolymer thin films synthesized by RAFT and CvRP methods are listed in Table-5.4, and the surface energies are listed in Table-5.5, both before and after annealing process. The contact angles and the surface free energy are also plotted against the HOST composition in the copolymer in Figure-5.19 and Figure-5.20. Contact angle of water for both un-annealed and annealed copolymer thin films gradually decreases with increasing HOST compositions in HOST-tBA copolymers. The presence of HOST

units in the copolymer causes the hydrophilic nature, and hence causes the decrease in water contact angles.

Table-5.4: Static contact angle of water and diiodomethane on PHOST, PtBA homopolymers and their copolymer thin films, before and after annealing process.

Designation	F_{HOST} (**^{1}H NMR**)	**Contact angle (°)**			
		Water (θ_1)		**Diiodomethane (θ_2)**	
		Un-annealed	**Annealed**	**Un-annealed**	**Annealed**
PHOST RAFT	1.00	65.8	61.5	31.6	29.8
PtBA RAFT	0.00	85.5	83.5	49.5	48.8
HOST-stat-tBA20 RAFT	0.28	82.6	82.8	56.8	59.7
HOST-stat-tBA50 RAFT	0.50	80.3	78.6	58.4	58.3
HOST-stat-tBA80 RAFT	0.83	65.5	65.4	42.7	32.3
HOST-grad-tBA50 RAFT	0.58	69.6	65.4	57.2	56.4
HOST-block-tBA50 RAFT	0.54	84.5	83.6	55.4	56.8
HOST-stat-tBA20 CvRP	0.29	84.8	90.8	50.6	52.7
HOST-stat-tBA50 CvRP	0.53	73.6	73.6	57.3	56.7
HOST-stat-tBA80 CvRP	0.81	71.0	74.4	43.9	44.1

Table-5.5: Surface free energy of HOST-tBA copolymer thin films determined by geometrical mean method using the contact angles.

Designation	F_{HOST} (^{1}H NMR)	Surface energy of un-annealed thin films			Surface energy of annealed thin films		
		γ_S^d	γ_S^P	γ_S^{total}	γ_S^d	γ_S^P	γ_S^{total}
PHOST RAFT	1.00	38.13	9.92	48.05	38.16	12.18	50.34
PtBA RAFT	0.00	32.08	3.22	35.30	32.14	3.87	36.01
HOST-stat-tBA20 RAFT	0.28	27.10	5.52	32.63	25.36	5.97	31.33
HOST-stat-tBA50 RAFT	0.5	25.75	6.96	32.71	25.54	7.84	33.38
HOST-stat-tBA80 RAFT	0.83	32.47	12.14	44.62	37.73	10.26	47.99
HOST-grad-tBA50 RAFT	0.58	24.80	13.09	37.89	24.64	15.79	40.43
HOST-block-tBA50 RAFT	0.54	28.29	4.44	32.73	27.27	5.07	32.34
HOST-stat-tBA20 CvRP	0.29	31.29	3.62	34.90	31.07	1.91	32.98
HOST-stat-tBA50 CvRP	0.53	25.35	10.53	35.88	25.71	10.38	36.08
HOST-stat-tBA80 CvRP	0.81	32.75	9.09	41.84	33.24	7.28	40.52

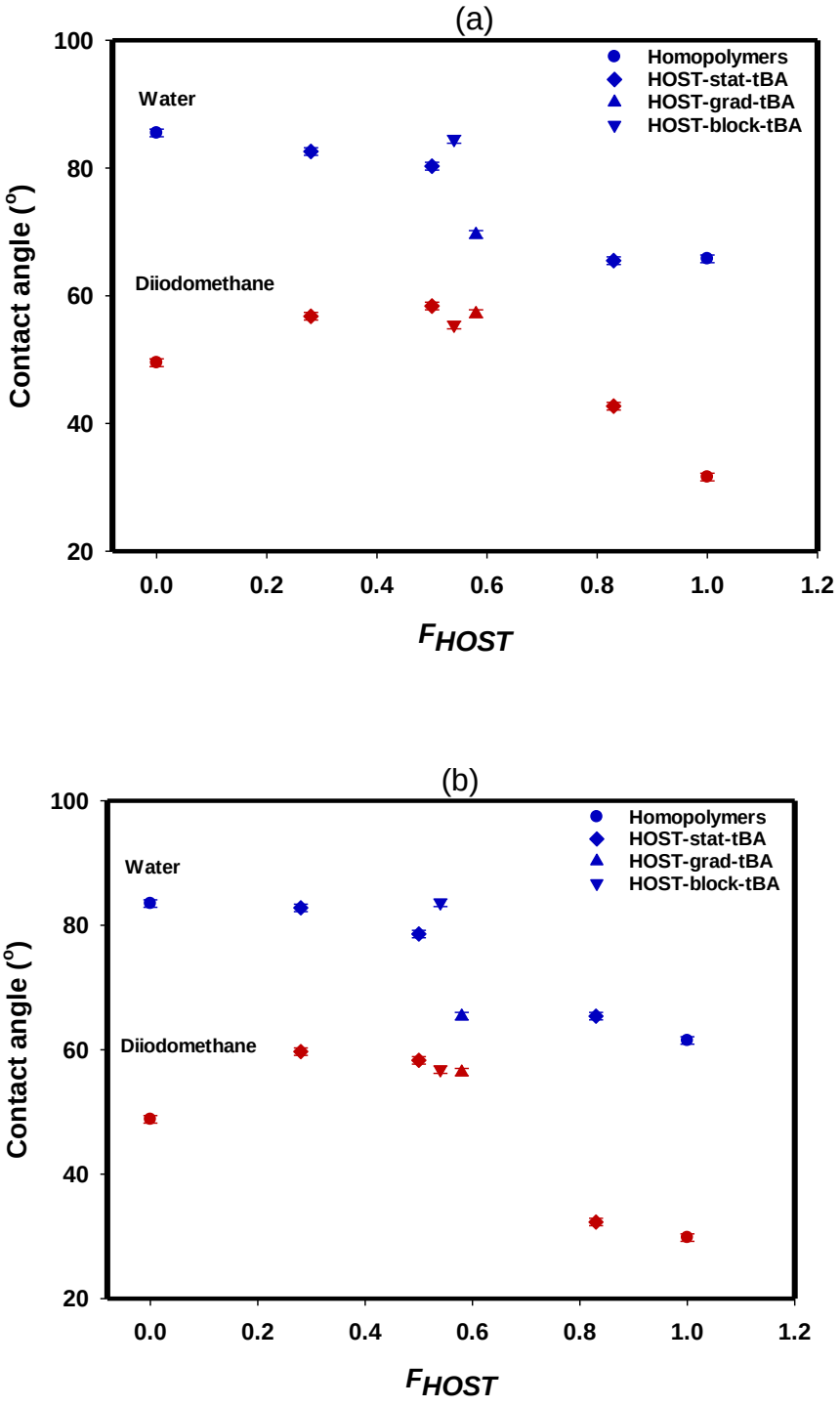

Figure-5.19: Contact angles of water (blue) and diiodomethane (red) on the thin films of HOST-tBA copolymers synthesized by RAFT method (a) before annealing and (b) after annealing the thin films at 130 ºC for 60 s.

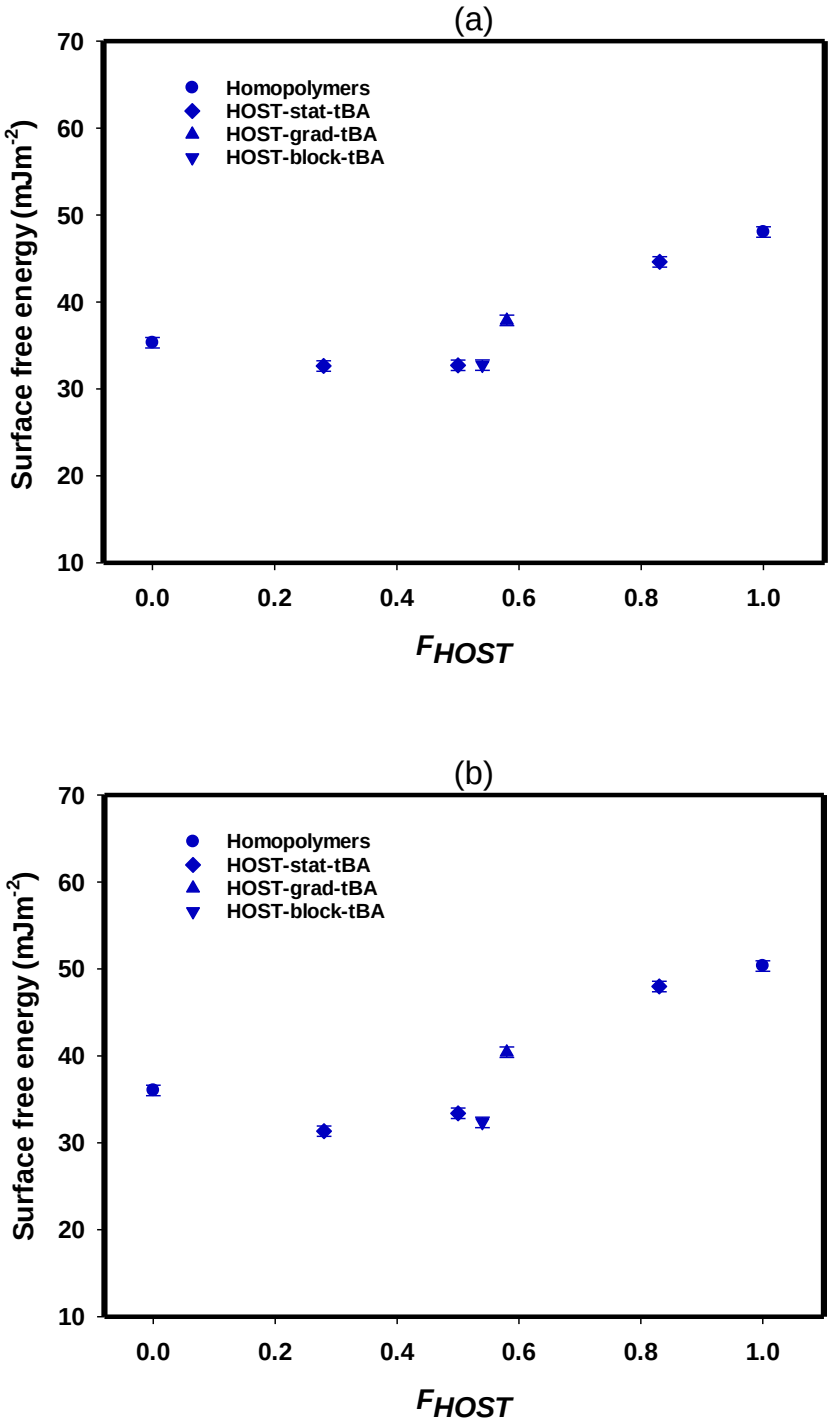

Figure-5.20: Surface free energy of HOST-tBA (RAFT) copolymer thin films (a) before annealing, and (b) after annealing at 130 ºC for 60 s.

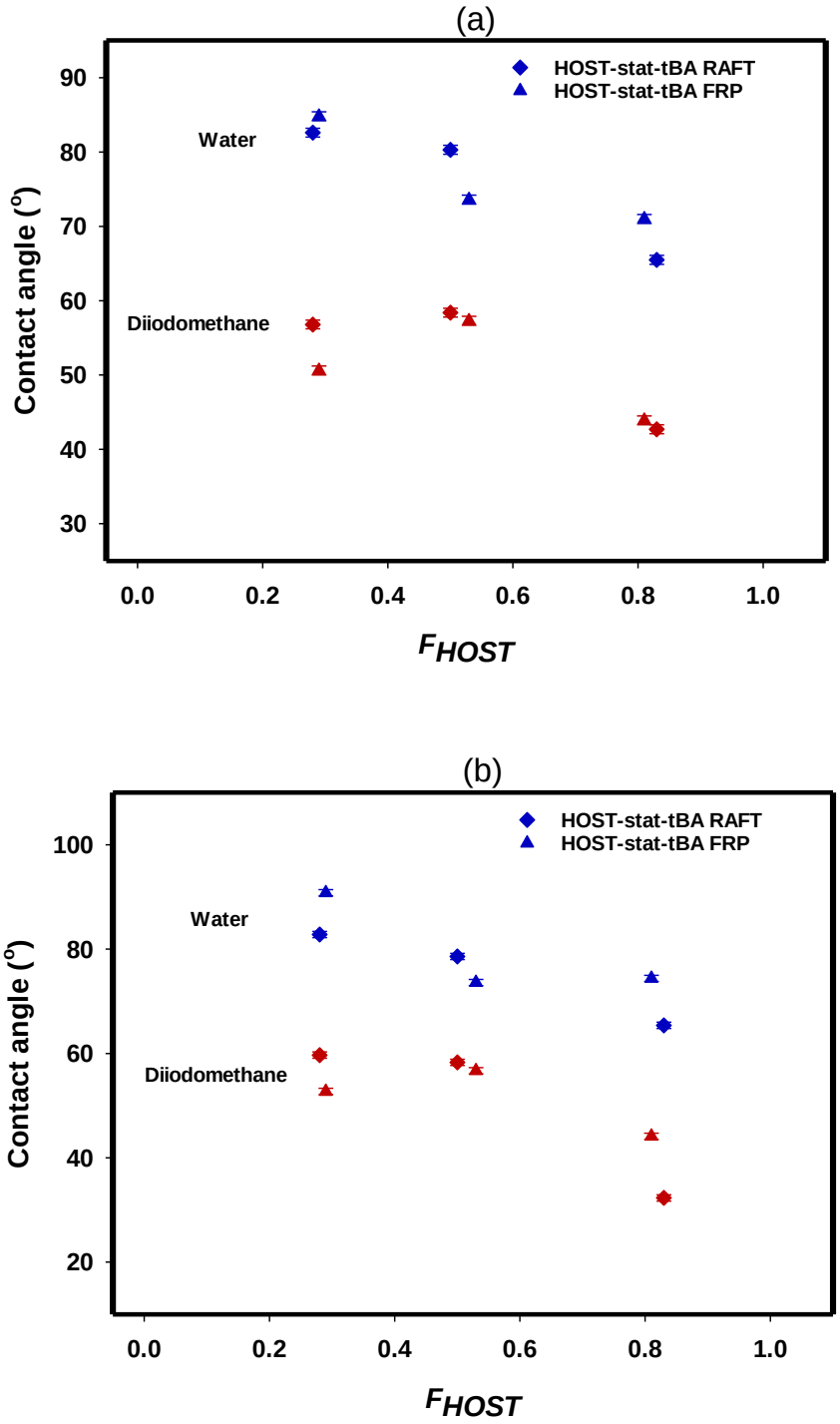

Figure-5.21: Comparison of the contact angles on HOST-tBA copolymer thin films synthesized by RAFT and CvRP method for water and diiodomethane (a) before annealing, and (b) after annealing.

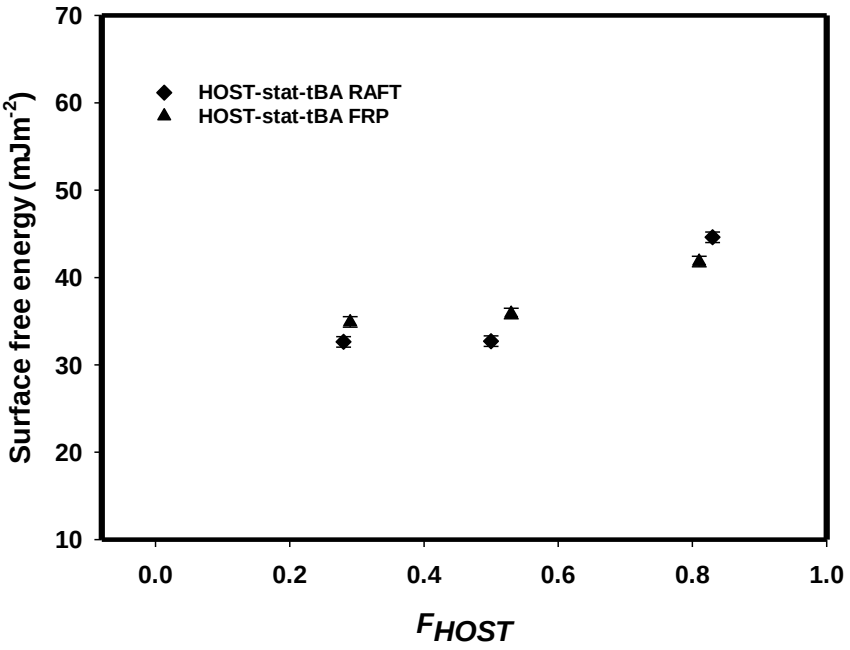

(b)

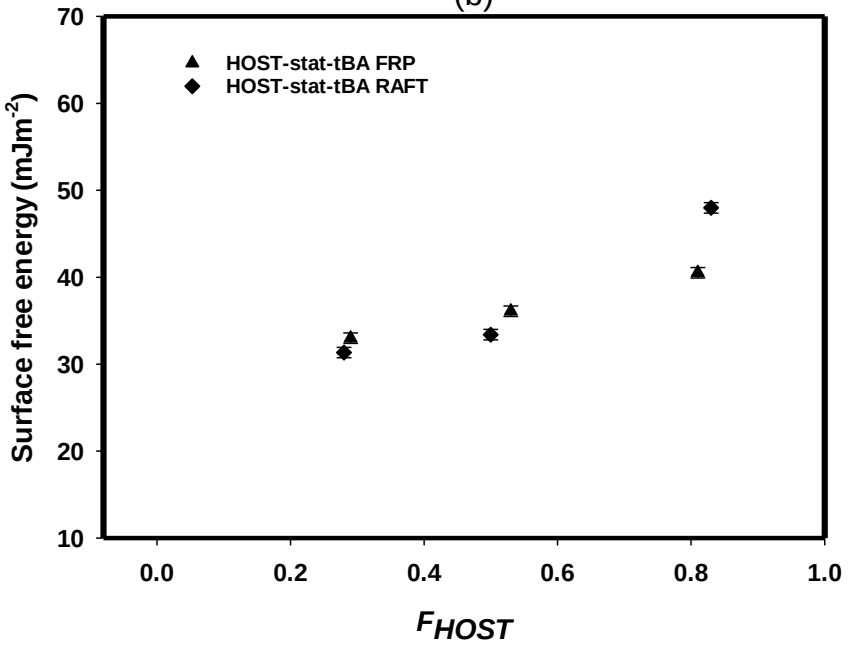

Figure-5.22: Surface energy comparison of the thin films of HOST-tBA copolymers synthesized by RAFT and CvRP method (a) before annealing, and (b) after annealing.

Contact angles for diiodomethane also decreases with the increasing HOST composition in the copolymers, though not as systematic as for that of water. Copolymers with more than 50% of tBA units show contact angle values higher than the PtBA homopolymer, and then decreases for higher HOST composition copolymers and PHOST homopolymers. Therefore, the surface free energy of the copolymers with high tBA composition are slightly lower than the homopolymer with low surface free energy, and then increases for the copolymers with higher HOST compositions.

If we look at the contact angles of the HOST-tBA statistical, gradient and block copolymers with comparable copolymer compositions (approximately 50:50), the block copolymer showed higher contact angle values than those of the statistical and gradient counterparts. This indicates the phase segregation of the block copolymer on thin film surface. Therefore, the hydrophobic tBA units show a tendency to move towards the air-thin film interface, and the hydrophilic unit, HOST moves towards the hydrophilic silicon wafer surface.

Figure-5.19 (b) and Figure-5.20 (b) show the contact angle and surface free energy of the HOST-tBA copolymer thin films after annealing them at 130 ºC temperature for 60 s. No noticeable change in the contact angle and surface free energy of the thin film surface was noticed as a result of annealing process. This could be due to the low annealing temperature, but at temperature higher than 130 ºC, tBA group starts degrading, and therefore would damage the copolymer structure.

The contact angle and surface energy of the thin films of HOST-stat-tBA copolymers prepared by RAFT and CvRP method are compared in Figure-5.21 and Figure-5.22. Both the RAFT and CvRP copolymer thin films show the similar trend of change in the contact angle and surface free energy values. There were slight random differences, but no significant difference in contact angle or surface free energy was found for the copolymer chains prepared by the RAFT and CvRP methods.

5.6 Conclusions

The properties of HOST-tBA copolymers, and their thin film surface properties have been studied in details in this chapter. The thermal properties of the un-hydrolysed copolymer (AOST-tBA) was characterised using TGA and DSC techniques. The statistical, gradient and block copolymer with similar copolymer exhibited characteristic glass transition values due to the sequence of the monomer segments in the copolymer. The statistical copolymer showed a sharp, single T_g in between to those of the homopolymers, while the block copolymer showed to T_g values corresponding to each homopolymer. In contrary, the gradient copolymer gives a single T_g which is unusually broad. This is due to the continuous change in the copolymer chain from one end to the other.

Interesting information have been observed from the GATR-FTIR spectra studies of the copolymer thin films. The thermal degradation of the t-butyl group was evident from the presence of the anhydride peak at wavelength 1650 cm^{-1} to 1850 cm^{-1}. Therefore, the copolymer thin films were annealed at temperature lower than 150 ºC to avoid thermal degradation of t-butyl group. GATR-FTIR spectra also provided very important information on the hydrogen bonding in HOST-tBA copolymers on the thin film surface. The hydrogen bonded and free carbonyl groups were quantified from the spectra using peak-fitting software. It was found that, the fraction of hydrogen bonded carbonyl group was strongly dependent on the composition of the copolymers, as well as on the orientation of the monomer units in the copolymer chains. Hydrogen bonded fraction in the block copolymer was significantly lower than those of the statistical and gradient copolymer. Due to two distinct blocks, not many HOST are available around the carbonyl group of tBA to form hydrogen bonding. The plot of the experimental fraction of hydrogen bonded carbonyl group against the volume fraction of HOST showed close agreement with the predicted data.

The composition of HOST-tBA copolymer thin film surface were studied using XPS studies, and the surface free energy of the polymer thin films were determined by contact angle measurements. The experimental C/O found from XPS survey data plotted against the predicted C/O, and no significant difference in the composition was observed for statistical, gradient and block structures in the HOST-tBA copolymers. No noticeable difference in the was found for the surface energy as well for the statistical, gradient and block structure, but the surface energy of HOST-tBA copolymer was found to be increased with the increasing composition of HOST.

5.7 References

[343] Adao MHVC, Saramago BJV, Fernandes AC. Estimation of the Surface Properties of Styrene-Acrylonitrile Random Copolymers from Contact Angle Measurements. J Colloid Interface Sci. 1999;217:94-106.

[360] Barclay GG, Hawker CJ, Ito H, Orellana A, Malenfant PRL, Sinta RF. The "Living" Free Radical Synthesis of Poly(4-hydroxystyrene): Physical Properties and Dissolution Behavior. Macromolecules. 1998;31:1024-31.

[383] Xu H, Yang B, Wang J, Guang S, Li C. Preparation, Thermal Properties, and Tg Increase Mechanism of Poly(acetoxystyrene-co-octavinyl-polyhedral oligomeric silsesquioxane) Hybrid Nanocomposites. Macromolecules. 2005;38:10455-60.

[384] Xu H, Kuo S-W, Huang C-F, Chang F-C. Poly(acetoxystyrene-co-isobutylstyryl POSS) nanocomposites: Characterization and molecular interaction. J Polym Res. 2002;9:239-44.

[385] Kuo S-W, Xu H, Huang C-F, Chang F-C. Significant glass-transition-temperature increase through hydrogen-bonded copolymers. J Polym Sci, Part B: Polym Phys. 2002;40:2313-23.

[386] Himuro S, Sakamoto N, Arichi S. Miscibility behavior of poly(4-hydroxystyrene) with poly(4-acetoxystyrene). Polym J (Tokyo). 1992;24:1371-6.

[387] Nakamura K, Hatakeyama T, Hatakeyama H. Differential scanning calorimetric studies on the glass transition temperature of poly(hydroxystyrene) derivatives containing sorbed water. Polymer. 1981;22:473-6.

[388] Nakamura K, Hatakeyama T, Hatakeyama H. Effect of substituent groups on hydrogen bonding of polyhydroxystyrene derivatives. Polym J (Tokyo). 1983;15:361-6.

[389] Zhu KJ, Kwei TK, Pearce EM. Thermostability of poly(p-hydroxystyrene) blends with poly(vinylpyrrolidone) and poly(ethyloxazoline). J Appl Polym Sci. 1989;37:573-8.

[390] Sheen Y-C, Lu C-H, Huang C-F, Kuo S-W, Chang F-C. Synthesis and characterization of amorphous octakis-functionalized polyhedral oligomeric silsesquioxanes for polymer nanocomposites. Polymer. 2008;49:4017-24.

[391] Liu W, Nakano T, Okamoto Y. Polymerization of t-butyl acrylate using organoaluminum complexes and correlation between main-chain tacticity and glass transition temperature of the obtained polymers. Polymer. 2000;41:4467-72.

[392] Connal LA, Vestberg R, Gurr PA, Hawker CJ, Qiao GG. Patterning on Nonplanar Substrates: Flexible Honeycomb Films from a Range of Self-assembling Star Copolymers. Langmuir. 2008;24:556-62.

[393] Brandrup J, Immergut EH, Editors. Polymer Handbook, Fourth Edition: Wiley; 1998.

[394] Wang W-W, Jiang L, Ren W-Y, Zhang C-M, Man C-Z, Nguyen T-P, et al. The crystallinity, thermal properties and microscopic morphology of di-block copolymers of L-lactide and several acrylates. RSC Adv. 2016;6:31934-46.

[395] Kopchick JG, Storey RF, Jarrett WL, Mauritz KA. Morphology of poly[(t-butyl acrylate)-b-styrene-b-isobutylene-b-styrene-b-(t-butyl acrylate)] pentablock terpolymers and their thermal conversion to the acrylic acid form. Polymer. 2008;49:5045-52.
[396] Mahdavi H, Mahmoudian M, Shikhhasani F. Nanofiltration membranes based on blend of polysulfone-g-poly(tert-butyl acrylate) copolymer and polysulfone. Polym Sci, Ser B. 2014;56:494-503.
[397] Schaefgen JR, Sarasohn IM. Observations on the thermolytic decomposition of poly(tert-butyl acrylate). Journal of Polymer Science. 1962;58:1049-61.
[398] Özlem S, Hacaloglu J. Thermal degradation of poly(n-butyl methacrylate), poly(n-butyl acrylate) and poly(t-butyl acrylate). Journal of Analytical and Applied Pyrolysis. 2013;104:161-9.
[399] Davis KA, Matyjaszewski K. Atom Transfer Radical Polymerization of tert-Butyl Acrylate and Preparation of Block Copolymers. Macromolecules. 2000;33:4039-47.
[400] Litmanovich AD, Cherkezyan VO. Intermolecular effects in macromolecular reactions—1. Decomposition of poly(t-butyl acrylate_. European Polymer Journal. 1984;20:1041-4.
[401] La Y-H, Stoykovich MP, Park S-M, Nealey PF. Directed Assembly of Cylinder-Forming Block Copolymers into Patterned Structures to Fabricate Arrays of Spherical Domains and Nanoparticles. Chemistry of Materials. 2007;19:4538-44.
[402] Fernandez-Garcia M, de la Fuente JL, Cerrada ML, Madruga EL. Preparation of poly(tert-butyl acrylate-g-styrene) as precursors of amphiphilic graft copolymers. 1. Kinetic study and thermal properties. Polymer. 2002;43:3173-9.
[403] Duvigneau J, Schoenherr H, Vancso GJ. Atomic Force Microscopy Based Thermal Lithography of Poly(tert-butyl acrylate) Block Copolymer Films for Bioconjugation. Langmuir. 2008;24:10825-32.
[404] Moskala EJ, Howe SE, Painter PC, Coleman MM. On the role of intermolecular hydrogen bonding in miscible polymer blends. Macromolecules. 1984;17:1671-8.
[405] Moskala EJ, Varnell DF, Coleman MM. Concerning the miscibility of poly(vinyl phenol) blends - Fourier-transform IR study. Polymer. 1985;26:228-34.
[406] Coleman MM, Lee JY, Serman CJ, Wang Z, Painter PC. Poly(ethylene-co-methacrylic acid)-polyether blends. Polymer. 1989;30:1298-307.
[407] Serman CJ, Painter PC, Coleman MM. Studies of the phase behavior of poly(vinyl phenol)-poly(n-alkyl methacrylate) blends. Polymer. 1991;32:1049-58.
[408] Hill DJT, Whittaker AK, Wong KW. Miscibility and Specific Interactions in Blends of Poly(4-vinylphenol) and Poly(2-ethoxyethyl methacrylate). Macromolecules. 1999;32:5285-91.
[409] Kuo S-W. Hydrogen-bonding in polymer blends. J Polym Res. 2008;15:459-86.
[410] Li D, Brisson J. Hydrogen bonds in poly(methyl methacrylate)-poly(4-vinyl phenol) blends: 1. Quantitative analysis using FTi.r. spectroscopy. Polymer. 1998;39:793-800.
[411] Coleman MM, Graf JF, Painter PC. Specific interactions and the miscibility of polymer blends : practical guides for predicting & designing miscible polymer mixtures / Michael M. Coleman,

John F. Graf, Paul C. Painter. Lancaster, Pa., U.S.A.: Lancaster, Pa., U.S.A. : Technomic Pub. Co.; 1991.
[412] Coleman MM, Lichkus AM, Painter PC. Thermodynamics of hydrogen bonding in polymer blends. 3. Experimental studies of blends involving poly(4-vinylphenol). Macromolecules. 1989;22:586-95.
[413] Van Krevelen DW, Te Nijenhuis K. Chapter 4 - Volumetric Properties. Properties of Polymers (Fourth Edition). Amsterdam: Elsevier; 2009. p. 71-108.
[414] Chilkoti A, Castner DG, Ratner BD, Briggs D. Surface characterization of a poly(styrene/p-hydroxystyrene) copolymer series using x-ray photoelectron spectroscopy, static secondary ion mass spectrometry, and chemical derivatization techniques. J Vac Sci Technol, A. 1990;8:2274-82.
[415] Wang P, Koberstein JT. Morphology of immiscible polymer blend thin films prepared by spin-coating. Macromolecules. 2004;37:5671-81.
[416] Pan F, Wang P, Lee K, Wu A, Turro NJ, Koberstein JT. Photochemical Modification and Patterning of Polymer Surfaces by Surface Adsorption of Photoactive Block Copolymers. Langmuir. 2005;21:3605-12.
[417] Feng CL, Vancso GJ, Schoenherr H. Interfacial Reactions in Confinement: Kinetics and Temperature Dependence of the Surface Hydrolysis of Polystyrene-block-poly(tert-butyl acrylate) Thin Films. Langmuir. 2005;21:2356-63.
[418] Ito H, Alexander D-F, Breyta G. Dissolution Kinetics and FAG Interaction of Phenolic Resins in Chemically Amplified Resists. Journal of Photopolymer Science and Technology. 1997;10:397-407.
[419] Majumdar D, Ratner BD. Synthesis, bulk characterization, and surface characterization of p-hydroxystyrene/styrene copolymers. J Polym Sci, Part A: Polym Chem. 1988;26:1991-2002.
[420] Jacobasch HJ, Grundke K, Augsburg A, Gietzelt T, Schneider S. Wetting of solids by liquids with low and high viscosity. Prog Colloid Polym Sci. 1997;105:44-54.
[421] Augsburg A, Grundtke K, Poeschel K, Jacobasch HJ, Neumann AW. Determination of contact angles and solid surface tensions of poly(4-X-styrene) films. Acta Polym. 1998;49:417-26.
[422] Tate RS, Fryer DS, Pasqualini S, Montague MF, de Pablo JJ, Nealey PF. Extraordinary elevation of the glass transition temperature of thin polymer films grafted to silicon oxide substrates. J Chem Phys. 2001;115:9982-90.
[423] Messerschmidt M, Millaruelo M, Choinska R, Jehnichen D, Voit B. Thin Film Nanostructures Prepared via Self-Assembly of Partly Labile Protected Block Copolymers for Hybrid Patterning Strategies. Macromolecules. 2009;42:156-63.
[424] Yoshioka H, Izumi C, Shida M, Yamaguchi K, Kobayashi M. Repeatable adhesion by proton donor-acceptor interaction of polymer brushes. Polymer. 2017;119:167-75.
[425] Walters KB, Hirt DE. Grafting of end-functionalized poly(tert-butyl acrylate) to poly(ethylene-co-acrylic acid) film. Polymer. 2006;47:6567-74.

Chapter 6: Conclusions

The field of CvRP has experienced enormous development over the past two-three decades. In particular, the invention of controlled radical polymerization techniques such as ATRP, NMP, RAFT provide the freedom to design and prepare homo and copolymers with precise control over molecular weight, molecular weight dispersity, and the distribution of monomer units in the copolymer chains, for a wide range of monomer pairs. These advances in the polymerization techniques have allowed the introduction of 'gradient copolymers', a novel class of copolymers with unique structure compared with conventional statistical and block copolymers. In this study, two different monomer pairs (styrene-acrylonitrile and hydroxystyrene – t-butyl acrylate) have been used to synthesize statistical, block and gradient copolymers using RAFT method. Copolymers of both of the monomer pairs have also been synthesized using the conventional CvRP method. The dependence of various properties of the copolymers on their chain structures has been studied.

The kinetics of RAFT polymerization of styrene – acrylonitrile (St-AN) copolymerization in bulk have been studied in detail using the CPDB RAFT agent. Assuming the terminal model for copolymerization, reactivity ratios St (r_{St}) and AN (r_{AN}) were determined for nine different monomer feed compositions. Considering the higher proportion of monomer as the polymerization solvent, a solvent effect on the reactivity ratios is proposed based on bootstrap model. No significant differences have been observed between the reactivity ratios determined in this study for the RAFT method and the reactivity ratios determined for the CvRP method for same feed compositions. A computer program 'REACT' was employed to predict the copolymer compositions and triad distributions for four different monomer feed compositions (St:AN = 10:90; 20:80; 60:40; 80:20) using the experimental reactivity ratios for RAFT method. The experimental compositions and triad distributions determined by ^{1}H and ^{13}C NMR were found to be in well agreement with the results predicted by REACT. For 60% St feed composition, purely St-AN statistical copolymers were formed, while for the three other feed compositions, the copolymer chains were found to be gradient in nature as found from the composition and triad distributions. In addition to the spontaneous gradients, St-AN forced gradient copolymers have been synthesized using the continuous feeding approach. In addition, St-AN block copolymers were prepared using a chain extension technique by the RAFT method. Similar to the RAFT method, St-AN copolymers for four different feed monomer compositions have also been synthesized by the CvRP method.

Acetoxystyrene – t-butyl acrylate (HOST-tBA) statistical copolymers for three different monomer feed compositions, forced gradient and block copolymers were synthesized by the RAFT method using PABTC RAFT agent. AOST-tBA statistical copolymers have also been synthesized using the CvRP method, and copolymer molecular weights were achieved similar to those of the RAFT copolymers by adjusting the ratio of monomer to initiator. HOST-tBA copolymers were obtained from the AOST-tBA copolymers by hydrolysing the acetoxy groups using hydrazine hydrate.

The thermal properties of both of the copolymer systems was studied using TGA and DSC techniques. In both cases, a unique broad T_g was found for the gradient copolymers due to the compositional gradient in the chain structures. Statistical copolymers, on the other hand, gave one sharp T_g, while two T_gs were observed for each blocks in the block copolymers. The surface properties of the copolymer thin films have also been found to be directly dependent on the composition as well as on the chain structure of the copolymers. Both the XPS and surface free energy studies suggests strong phase segregation on the thin film surface for St-AN copolymers, but no such phase segregation for the statistical copolymers. On the other hand, due to the continuous drift in composition, St-AN gradient copolymers showed significant phase segregation, but not as pronounced as the block copolymers. However, the properties of the HOST-tBA copolymer system was not as dependent on the chain structures as those of the St-AN copolymer system. The comparison of the properties of the copolymers synthesized by the RAFT and CvRP methods also does not suggest any significant differences in this study. This is mainly due to the presence of hydrogen bonding in HOST-tBA copolymer thin films.

An important observation was the formation of hydrogen bonding in HOST-tBA copolymers as characterised by GATR-FTIR spectroscopy. A new peak was observed at slightly lower wavenumbers than the usual carbonyl peak position, and assigned to the hydrogen bonded carbonyl group. The fraction of hydrogen bonded carbonyl group was quantified from GATR-FTIR studies, and was found to be directly dependent on the copolymer compositions and chain structures. The fraction of hydrogen bonded carbonyl groups was maximum for the statistical copolymers due to the availability of OH groups adjacent to the carbonyl groups, and minimum for the block copolymers due to their blocky structure. However, the fraction of hydrogen bonded carbonyl groups of the gradient copolymers was intermediate those of the statistical and block copolymers, as the gradient copolymer combined statistical segments in the middle of the chains and blocky segments at the ends of the copolymer chains.

This study has shown that, like the uniqueness of the structure, the properties of the gradient copolymers are also unique, and very different to those of the corresponding conventional statistical and block copolymers. By changing the rate of addition of the monomers in the continuous feeding approach, different degrees of gradient could be achieved in the copolymer structure. However, it is very important to characterize and determine the chemical composition distribution with enough accuracy in order to achieve the required gradient in the copolymer structure to fine-tune the properties. Based on the correlation between the copolymer chain structure and their properties found in this study, the use of gradient copolymers with varying degree of compositional gradient in addition to the conventional statistical and block copolymers as photoresist materials could provide the relation between the copolymer chain structure and LER. Therefore, in continuation of this thesis, future work would involve finding effective methods to determine the chemical composition distribution successfully, and use of gradient copolymers as photoresist materials to evaluate the effect of chemical composition distribution of copolymers on LER.